Final Technical Report

DOE Award Number: DE-FC36-04GO14230

Project Period: January 1, 2004 through June 30, 2102

Principal Investigator: Diran Apelian
WPI/ Metal Processing Institute
100 Institute Road
Worcester, MA 01609-2280
(508) 831-5992: dapelian@wpi.edu

Recipient Organization: Worcester Polytechnic Institute
100 Institute Road
Worcester, MA 01609-2280

Business Contact: Research Administration
100 Institute Road
Worcester, MA 01609-2280
Director of Sponsored Research: Francois Lemire
(508) 831-5811: flemire@wpi.edu
Operations Director at MPI: Carol Garofoli
(508) 831-5592: garofoli@wpi.edu

Date of Report: August 15, 2012

ACKNOWLEDGEMENT, DISCLAIMER, AND PROPRIETARY DATA NOTICE

Acknowledgment:
This report is based upon work supported by the U. S. Department of Energy under Award No. DE-FC36-04GO14230.

Disclaimer:
Any findings, opinions, and conclusions or recommendations expressed in this report are those of the author(s) and do not necessarily reflect the views of the Department of Energy.

Proprietary Data Notice:
None

TABLE OF CONTENTS

List of Acronyms

SSM	**Semi-Solid Metal**
SoD	**Slurry on Demand**
CRP	**Continuous Rheoconversion Process**
MHD	**Magnetohydrodynamic**
ACRC	**Advanced Casting Research Center**
MPI	**Metal Processing Institute**

List of Figures

List of Tables

Executive Summary

Semi-solid metal (SSM) processing has emerged as an attractive method for near-net-shape manufacturing due to the distinct advantages it holds over conventional near-net-shape forming technologies. These advantages include lower cycle time, increased die life, reduced porosity, reduced solidification shrinkage, improved mechanical properties, etc. SSM processing techniques can not only produce the complex dimensional details (e.g. thin-walled sections) associated with conventional high-pressure die castings, but also can produce high integrity castings currently attainable only with squeeze and low-pressure permanent mold casting processes. There are two primary semi-solid processing routes, (a) thixocasting and (b) rheocasting. In the thixocasting route, one starts from a non-dendritic solid precursor material that is specially prepared by a primary aluminum manufacturer, using continuous casting methods. Upon reheating this material into the mushy (a.k.a. "two-phase") zone, a thixotropic slurry is formed, which becomes the feed for the casting operation. In the rheocasting route (a.k.a. "slurry-on-demand" or "SoD"), one starts from the liquid state, and the thixotropic slurry is formed directly from the melt via careful thermal management of the system; the slurry is subsequently fed into the die cavity. Of these two routes, rheocasting is favored in that there is no premium added to the billet cost, and the scrap recycling issues are alleviated.

The CRP™ is a process where the molten metal flows through a reactor prior to casting. The role of the reactor is to ensure that copious nucleation takes place and that the nuclei are well distributed throughout the system prior to entering the casting cavity. The CRP™ has been successfully applied in hyper-eutectic Al-Si alloys (i.e., 390 alloy) where two liquids of equal or different compositions and temperatures are mixed in the reactor and creating a SSM slurry. The process has been mostly used for hypo-eutectic Al-Si alloys (i.e., 356, 357, etc.) where a single melt passes through the reactor. In addition, the CRP™ was designed to be flexible for thixocasting or rheocasting applications as well as batch or continuous casting. Variable heat extraction rates can be obtained by controlling either the superheat of the melt, the temperature of the channel system, or the temperature of the reactor.

This program had four main objectives all of which were focused on a mechanistic understanding of the process in order to be able to scale it up, to develop it into a robust process,and for SSM processing to be commercially used.

Introduction

SSM has been proven to be a more energy efficient technology than liquid metal casting. Accordingly, very large energy savings can be realized via SSM production. In recent years, the driving force to reduce process cost has led to the development of rheocasting (also termed slurry-on-demand, SoD) method. Among a few emerging SoD processes, the continuous rheoconversion process (CRP) developed by the research team at WPI has been proven to be highly effective for the manufacture of high quality semi-solid feedstock under both thixocasting and rheocasting conditions. Other advantages of CRP include process simplicity, a wide processing window, and the feasibility of recycling scrap metal. The CRP has distinct advantages over other emerging SoD processes, and shows great potential for commercial applications. In this program, we addressed technical issues such as the fundamental understanding of the operative mechanisms behind the CRP, the optimization of the CRP for industrial applications,

as well as scale-up issues i.e., metal throughput, heat/cooling system design for mass production, etc. Meanwhile, other critical issues related to semi-solid processing such as SSM alloy development, SSM heat treatment optimization were also addressed. With the success of this program, the economics and energy efficiency of SSM has substantially improved.

The main objectives of the project were to:

1) **Optimize the continuous rheoconversion process (CRP) developed by the research team at WPI and scale up the CRP for commercial applications through collaborations with ACRC Consortium Members. The consortium is the largest industry-university alliance in N. America with close to 30 corporate members. For more details see: www.wpi.edu/+mpi;**

2) **Develop optimum alloys for SSM/CRP processes;**

3) **Establish optimum heat treatment schedules for various commercial SSM alloys;**

4) **Develop a comprehensive constitutive mathematical model that includes the internal microstructural dynamics of SSM slurries and allows better simulation of die filling during the production of SSM parts.**

In addition, within the context of the research program is the transfer of the technology developed to the industrial sector through appropriate workshops, seminars, presentations at scientific societies' conferences, as well as publications in the open literature.

Each of the above four project objectives are further reviewed and discussed in this final report by reporting out the salient and most important results; this is done by presenting peer-reviewed publications focusing on each of these four objectives of the program. This is not only a credible way of presenting the outcomes of this program, but it also demonstrates the dissemination and transfer of this technology to the market place.

Context and Background

Semi-solid metal (SSM) processing has emerged as an attractive method for near-net-shape manufacture due to the distinct advantages it holds over conventional near-net-shape forming technologies. These advantages include lower cycle time, increased die life, reduced porosity, reduced solidification shrinkage, improved mechanical properties, etc. SSM processing techniques can not only produce the complex dimensional details (e.g. thin-walled sections) associated with conventional high-pressure die castings, but also can produce high integrity castings currently attainable only with squeeze and low-pressure permanent mold casting. There are two primary semi-solid processing routes, (a) thixocasting and (b) rheocasting. In the thixocasting route, one starts from a non-dendritic solid precursor material that is specially prepared by a primary aluminum manufacturer, using continuous casting methods. Upon reheating this material into the mushy (a.k.a. "two-phase") zone, a thixotropic slurry is formed, which becomes the feed for the casting operation. In the rheocasting route (a.k.a. "slurry-on-demand" or "SoD"), one starts from the liquid state, and the thixotropic slurry is formed directly

from the melt via careful thermal management of the system; the slurry is subsequently fed into the die cavity. Of these two routes, rheocasting is favored in that there is no premium added to the billet cost, and the scrap recycling issues are alleviated

In the early days of SSM development, it was thought that one had to cool the liquid down into the two-phase region, and to shear off and break the dendrites (i.e. melt agitation via mechanical or, later on, magnetohydrodynamic - MHD - stirring) and thus producing a slurry. However, during the last few years, work sponsored at ACRC – MPI by the Department of Energy [1], as well as work by the research team at MIT [2] led to the discovery that one did not need to break off dendrites to produce the semi-solid structure of globular primary alpha phase. Instead, if the temperature of the melt was such that one could produce many nuclei ("copious nucleation"), and if the nuclei did not grow past a certain point (i.e. suppression of dendritic growth), nor melt back into the bulk liquid, then one could produce a slurry with the ideal semi-solid structure directly from the melt. This concept is the genesis of commercial processes and methodologies to generate semi-solid slurries from the liquid state. The concept relies on *controlled nucleation and growth*, as opposed to the previous theory, in which a dendritic structure is modified into a globular structure via shear forces.

The driving force to reduce process cost has led to the development of several rheocasting (also termed slurry-on-demand) processes. These include UBE's New Rheocasting (NRC) [3], Idra-Prince's Semi-Solid Rheocasting (SSR) [4], THT Presses' Sub-Liquidus Casting (SLC^{TM}) [5], and Alcan's Swirl Enthalpy Equilibration Device (SEED) [6], as well as the Continuous Rheoconversion Process (CRP^{TM}) [7, 8], developed by ACRC/MPI.

The CRP^{TM} is a process where the molten metal flows through a reactor prior to casting. The role of the reactor is to ensure that copious nucleation takes place and that the nuclei are well distributed throughout the system prior to entering the casting cavity. The CRP^{TM} has been successfully applied in hyper-eutectic Al-Si alloys (i.e., 390 alloy) where two liquids of equal or different compositions and temperatures are mixed in the reactor and creating a SSM slurry [9]. The process has been mostly used for hypo-eutectic Al-Si alloys (i.e., 356, 357, etc.) where a single melt passes through the reactor. In addition, the CRP^{TM} was designed to be flexible for thixocasting or rheocasting applications as well as batch or continuous casting. Variable heat extraction rates can be obtained by controlling either the superheat of the melt, the temperature of the channel system, or the temperature of the reactor.

The work of Findon [7] demonstrated that the CRP^{TM} is a robust process, which can consistently generate near-ideal semi-solid structures for grain refined and non-grain refined A356 type alloys within a large process window. The recent work of Pan and Findon [8] has shown that the CRP^{TM} is also highly effective for the manufacture of high quality semi-solid feedstock of other commercial alloy systems, including hypereutectic aluminum-silicon (390), aluminum-copper (A206), wrought aluminum alloys, as well as Mg alloys.

Results and Discussion

For each of the four objectives of the program, we present our final report through the salient publications. These are peer reviewed and have been published and disseminated.

1) Optimize the continuous rheoconversion process (CRP) and scale up for commercial applications - ***See Appendix A*** (which contains six manuscripts and one patent, **A.1** through **A.7**).

A brief summary is given here for Objective 1:

The most salient development and pivotal impact of this work is that previous to this project, the notion has been that one needed to physically shear the dendrites to form a semi-solid slurry. We have shown that one needs to nucleate "baby" dendrites and have them be distributed throughout, without having the "baby" dendrites grow (via thermal management). This is a huge innovation in that it eradicated the notion of rheocasting billets that were specially made, but rather now one can start with molten metal and through the rheo-conversion reactor can obtain a semi solid structure with a globular (and non-dendritic) structure. Appendices A.1 through A.6 are peer reviewed published papers that document the body of work laying the fundamental understanding of the process such that it can be scaled up commercially.

A.1 M. Findon and D. Apelian, "The Continuous Rheoconversion Process for Semi-Solid Slurry Production", AFS Transactions, Vol. 112, June 2004, pp 04- 056.

A.2 Q.Y. Pan, M. Findon and D. Apelian, "The Continuous Rheoconversion Process (CRP): A Novel SSM Approach", Paper # 2-4 in the Proceedings of the Eighth International Conference on Semi-Solid Processing of Metals and Alloys, Limasol, Cyprus, September 2004; published by NADCA, Wheeling, Illinois.

A.3 Q.Y. Pan, D. Apelian, and P. Hogan, "The Continuous Rheoconversion Process (CRPTM): Optimization & Industrial Applications", 3rd International Conference on High Tech Die Casting, Vicenza, Italy, 21-22 September 2006, paper 53, published in the CD-ROM of the conference proceedings by the Italian Association of Metallurgy (AIM), Milan, 2006; the paper also published in "Metallurgical Science and Technology", 2006, Vol. 24, n. 2, pp. 9-18 (2006), edited by Teksid Aluminum.

A.4 Q.Y. Pan, S. Wiesner, D. Apelian, "Application of the Continuous Rheoconversion Process (CRP) to Low Temperature HPDC-Part I: Microstructure, in the Proceedings of 9th International S2P, Busan, Korea, September 11-13, 2006, in Solid State Phenomena Vols. 116-117 (2006) pp. 402-405 Trans Tech Publications, Switzerland.

A.5 Q.Y. Pan, P. Hogan, D. Apelian, and M.M.Makhlouf, "The Continuous Rheoconversion Process (CRP™)", in the Proceedings of LMT – Light Metals Technology 2007, September 2007, Saint-Sauveur, Québec, CA, published by CANMET.

A.6 John L. Jorstad, Q. Y. Pan, Diran Apelian, " Interaction of Key Variables During Rheocasting: Effects of Fraction Solid and Flow Velocity on Performance", NADCA Transactions 2007.

A.7 A. M. de Figueredo, D. Apelian, M. Findon, and N. Saddock, "Alloy Substantially Free of Dendrites and Method of Forming the Same", US Patent No. 7,513,962, April 7, 2009.

2) Develop optimum alloys for SSM/CRP processes – ***See Appendix B*** (which contains five manuscripts, B1 through B5).

A brief summary is given here for Objective 2:

As has always been the case, a new process is developed, and yet the alloys that take advantage of the process or leverage the attributes of the process are not materialized. In other words, a new process is always used to cast existing alloys, versus asking the question, what opportunity windows open up with this new process. The objective her e(objective 2) was to probe alloy system that take advantage of the process, as well as to address the hyper-eutectic and hypo-eutectic alloys of the Al-Si system. In Appendix B, paper B.5 documents the alloys that are novel and which take advantage of the rheoconversion process.

B.1 Q.Y. Pan, M. Arsenault, D. Apelian and M.M. Makhlouf, "SSM Processing of AlB2 Grain Refined Al-Si Alloys", AFS Transactions, Vol. 112, June 2004, pp 04-053.

B.2 D. Saha and D. Apelian, "Semi Solid Processing of Hypereutectic Alloys", AFS Transactions, Vol. 112, June 2004, pp 04-057.

B.3 Q.Y. Pan, L. Wang, D. Apelian and M.M. Makhlouf , "Optimization of 380 Alloy for Semi-Solid Processing", NADCA Transactions, #T05-143 (2005).

B.4 S. Wiesner, Q.Y. Pan, D. Apelian, "Application of the Continuous Rheoconversion Process (CRPTM) to Low Temperature HPDC-Part II: Alloy Development & Validation", in the Proceedings of 9th International S2P, Busan, Korea, September 11-13, 2006, in Solid State Phenomena Vols. 116-117 (2006) pp 64-67, Trans Tech Publications, Switzerland.

B.5 Q.Y. Pan, P. Hogan, and D. Apelian, "Optimization of Commercial Alloys for Semi-Solid Processing", NADCA Transactions (2006).

3) Establish optimum heat treatment schedules for various commercial SSM alloys-
See *Appendix C* (One manuscript)

A brief summary is given here for Objective 3:
With Rheoconversion, the resultant microstructure is dramatically different than conventionally cast microstructures. In this objective we showed that there are benefits associated in heat treatment of semi-solid structures. The diffusion distances are smaller and the kinetics of heat treatment enable shorter and more efficient heat treatment processes. The paper in Appendix C, was selected as the Best Paper of the Congress in 2005.

C.1 B. Dewhirst, J.L. Jorstad, and D. Apelian, "Effect of Artificial Aging on Microstructure and Tensile Properties of Semi-Solid Processed A356 Castings", NADCA Transactions, #T05-063 (2005) - Selected as the Best Paper of the Congress. The paper was also published in Die Casting Engineer, May 2005, published by NADCA, pp 38-44, 2005

4) Develop a comprehensive constitutive mathematical model – See *Appendix D*
(one manuscript, D1).

A brief summary is given here for Objective 4:
As in all process development, a model is needed to be able to simulate the process in order to have a basis for scaling up. The empirical approach of what the effect of certain process variables are on the resultant microstructure cannot solely be carried out experimentally. We developed a model that enabled us to pinpoint the optimum operating window for rheoconversion. Paper D. 1 presents and discusses the model

D.1 Q. Xu, D. Apelian, M.M. Makhlouf, "Numerical Modeling and Computer Simulation of the Continuous Rheoconversion Process", NADCA Congress Transactions, April 2009.

In addition, the results that emanated from this program are documented in a series of papers and patents that were presented and published. The complete set is shown in ***Appendix E*** - attached.

Benefits Assessment
SSM technology, and particularly the CRP technology have the potential (over a period of 10 years) of having 25% of the die casting and permanent mold Aluminum market. Accordingly, the following facts can be summarized:

Conventional Current Technology
Amount of Al consumed: 1.6 X 10^6 Tons (die casting + permanent mold)
Amount of Energy consumed: 27.3 x Btu/ton

Total Energy consumed: 43.68 x 10^{12} Btu

SSM Technology (assumptions)
SSM technology uses 80% of the energy used in conventional technology (and brings in a 20% savings). This is based on a conservative heat balance where the entering liquid into the die cavity is already 20% frozen and the remaining 80% is liquid. This assumption will change to a more favorable number if the slurry that enters the die casting cavity is 40% solid, and 60% liquid. Assuming the latter, then the energy savings would be 40% rather than 20%

The energy metrics below are conservative, in that we only capture the energy reduction of not reheating thixocast billets, and providing a slurry ready process that can be used directly in die casting operations. Thus we capture a 20% savings of energy usage.

One could expand on the energy savings by taking into account reduction in scrap, which we are not incorporating to be conservative in our calculations.

Proposed Technology
Over a period of 10 years, SSM technology will capture 24% of the market
[25% (year 10) - 1% (year 1), yielding 24%].

24% of the market, 1.6 X 10^6 Tons, is 0.38 x 106 Tons of Al.
Energy used by SSM technology (80% of 27.3 x 10^6 Btu/ton) is 21.84 x 10^6 Btu/ton.

Thus, the usage by the proposed technology is 8.3 x 10^{12} Btu.
The savings we anticipate is 2.1 x 10^{12} Btu.

Commercialization
The CRP process has been validated industrially and has had commercial success. The patent (see A.7) is owned by WPI, and managed by the WPI Technology licensing office. The following companies have adopted their practices to incorporate SSM processing technologies and also have made use of the concepts of CRP to enhance nucleation: Aluminium Rheinfelden, Mercury Marine, Nemak, Premier Tool & Die Cast, THT Pressses, and Buhler.

Accomplishments
Appendix E documents the outcomes from this program and the extensive dissemination that transpired. In addition to these publications, it must be noted that the program greatly benefitted from the meetings with the industrial sector every 6 months. The ACRC consortium at WPI – the Advanced Casting Research Center was the venue for presentation of results and obtaining feedback from industry partners.

One patent was granted for the CRP process, and this is a major accomplishment. The patent is not licensed yet, but the prospects are high as interest is high by industrial sector.

As can be noted from the publications, we had the opportunity to graduate several graduate students: B. J. Bernard, Matt Findon, Pat Hogan, Deepak Saha, Mark Arsenault, Brian Dewhirst, and had several Post-Docs, Q. Pan, A. de Figueredo, and Research Professor, Q. Xu and Y. Li.

See http://www.wpi.edu/Academics/Research/MPI/
See: Completed Research Projects

Patents: CRP patent received.
Title: "Alloy Substantially Free of Dendrites and Methods of Forming the Same"
Patent No: US 7,513,962 B2
Date of Patent: April 7, 2009

Conclusions
This work that has been carried out over 7 years plus has categorically confirmed the viability of SSM processing by copious nucleation and distribution of nuclei to attain non-dendritic cast structures. The results obtained in the laboratory as well as in commercial trials have demonstrated the benefits of SSM processing from energy savings as well as a resultant cast structure that is far superior to conventional castings.

The challenge remains within the market dynamics of the industry for adoption of the technology by the majority of casters. With all the benefits of SSM and the CRP process, the industry is slow to adopt it. This has been due to a slow market need for such developments as well as a recession that has impacted the auto industry's ability to adopt new innovations. However, this scenario is changing and the environment seems to be much more receptive today. With the increasing need and demand for thin cast components, it is envisioned that CRP/SSM processing is the preferred route to manufacture such configurations.

Recommendations
It is the strong recommendation of the team at WPI that this work has opened many more "doors" that need to be pursued. Specifically:

- SSM/CRP to produce nanostructured metals
- SSM/CRP to make thin castings in the range of less than 2-3 mm
- There is a need to study the effect of composition on viscosity of liquid metals as well as the effect of shear.

References

1. DOE Report number DE-FC07-98ID13618

2. M.C. Flemings, “Semi-Solid Processing – The Rheocasting Story”, Test Tube to Factory Floor: Implementing Technical Innovations, from the Proceedings of the Spring Symposium May 22, 2002 published by Metal Processing Institute, Worcester Polytechnic Institute, Worcester MA 01609 (2003).

3. UBE Industries Ltd., *Method and apparatus for shaping semisolid materials*, in *European Patent EP 0 745 694 A1*. 1996. p. 117.

4. J.A. Yurko, R.A. Martinez, and M.C. Flemings, "SSRTM: The Spheroidal Growth Route To Semi-Solid Forming", in 8th International Conference on Semi-Solid Processing of Alloys and Composites, 2004, Limassol, Cyprus.

5. J.L. Jorstad, "SSM Processes - An Overview", in 8th International Conference on Semi-Solid Processing of Alloys and Composities, 2004, Limassol, Cyprus.

6. D. Doutre, J. Langlais, and S. Roy, "The SEED Process for Semi-Solid Forming", in 8th International Conference on Semi-Solid Processing of Alloys and Composites, 2004, Limassol, Cyprus.

7. M. Findon, “Semi-Solid Slurry Formation via Liquid Metal Mixing”, M.Sc., Thesis,Worcester Polytechnic Institute, 2003.

8. Q.Y. Pan, M. Findon, and D. Apelian, "The Continuous Rheoconversion Process (CRP): A Novel SSM Approach", in 8th International Conference on Semi-Solid Processing of Alloys and Composites, 2004, Limassol, Cyprus.

Appendices:

Appendix A: Continuous rheo-conversion process (CRP)
Appendix B: Alloy Development for SSM/CRP processes
Appendix C: Heat Treatment of SSM Alloys
Appendix D: Simulation and Modeling of CRP process
Appendix E: Compendium of Publications on SSM emanating from Program

APPENDIX A

The Continuous Rheoconversion Process for Semi-Solid Slurry Production

M. Findon and D. Apelian
Advanced Casting Research Center
Metal Processing Institute, WPI, Worcester, MA, USA

ABSTRACT

Slurry-on-demand semi-solid metal (SSM) processing methods have been developed since the mid 90's since they alleviate many of the issues associated with thixocasting processes. The objective of this work was to study the mechanisms of nucleating primary particles during the early stages of solidification, and to distribute them throughout the bulk. A process named "Continuous Rheoconversion Process" (CRP) was developed, which mixes two aluminum alloy melts within a static reactor, and simultaneously inducing convection and rapid cooling. Work to date (with Al-Si-Mg alloys) using the CRP process has shown that globular semi-solid microstructures with negligible entrapped liquid can be produced. Even in the absence of melt inoculants, α-Al particle sizes of 60μm are attainable. By varying slurry analysis methods it was found that these structures can be obtained consistently for both thixocasting and rheocasting applications, which is an important advantage in terms of process flexibility. Other advantages of the CRP include overall process simplicity, a wide processing temperature range, and ability to incorporate scrap metal easily. A review of recent SSM processes is presented, the experimental apparatus is briefly described, and the important experimental results are discussed.

INTRODUCTION

Semi-solid metal (SSM) processing is a promising technology that resulted from groundbreaking findings in the early 1970's at the Massachusetts Institute of Technology (Flemings, 1991). Since the initial discovery, several casting processes have been developed to exploit the advantages offered by SSM. However, incorporating SSM into a die casting operation is challenging (i.e., billet reheating; temperature control; re-use of scrap, etc.), and thus it has for the most part been confined to a niche area of near-net shape manufacturing. In the recent past, since the mid 90's, much interest and work has been carried out to address the impedances to commercialize SSM processing.

The main property of semi-solid metal ("slurry") that renders it superior to conventional casting processes is the non-turbulent (a.k.a. "laminar" or "thixotropic") flow behavior that results when one enters the "two-phase" field of solid plus liquid (Flemings, 1991). Specifically, shearing of semi-solid slurry leads to a marked decrease in viscosity, so that a partially frozen alloy can be made to flow like a non-Newtonian fluid. Thixotropic flow behavior arises from the ideal SSM microstructure of small, spherical α-Al particles suspended in a liquid matrix. In all semi-solid processes, it is imperative that this microstructure be produced consistently. Moreover, a uniform distribution of this microstructure throughout a volume of slurry is essential for production of high-quality components.

Since the early days of SSM process development in the 1970's, many techniques have been devised to cast near-net-shape components with semi-solid slurries (de Figueredo and Apelian, 2001). Most of these processes are known as "thixocasting," in which the semi-solid material is obtained by reheating specially prepared feedstock material. Precursor metal for thixocasting does not contain the conventional dendritic microstructure; instead it is comprised of fine, equiaxed primary α-Al particles. Upon reheating, the semi-solid microstructure is obtained, and the material can be used as feed in the casting operation. The other approach to semi-solid processing is called "rheocasting," wherein the slurry is formed directly from the molten state. Also known as "slurry-on-demand" or SoD, rheocasting is the preferred route for the development of new SSM processes, since it alleviates the cost of specially produced feedstock.

The motivation for this work stems from the desire within the SSM community to develop a *continuous* slurry-on-demand approach. This paper documents the findings from our work with a new slurry-making technique developed at WPI. The "Continuous Rheoconversion Process (CRP)" mixes two separate aluminum melts within a reactor, resulting in semi-solid slurries having highly globular particle morphologies. The melt streams undergo forced convection while nuclei are being formed in very high numbers. A thorough microstructural investigation is presented in order to characterize and ultimately scale up this novel solidification process.

BACKGROUND

This section presents a timeline of the major SSM processing routes that have been developed over the last thirty years. General processing aspects of SSM will be described, including thixotropic behavior and the differences between thixocasting and rheocasting. Examples of semi-solid methodologies will be presented in detail.

During the course of his PhD research (Spencer, 1971), Spencer documented the initial findings that led to the discovery of semi-solid processing. By solidifying a partially solidified alloy within a Couette-type viscometer and applying shear, he found that non-dendritic structures could be produced. The flow behavior of the semi-solid material was quite different from that of liquid metal; it was non turbulent, quiescent, and non-Newtonian. These are interesting attributes from a casting standpoint, since laminar flow (i.e., a stable metal flow front) in a die circumvents the typical defects observed in conventionally cast components. Several other advantages soon became apparent as well, including longer tool life, less solidification shrinkage, and a cleaner final product free of oxides and entrapped mold gases.

Following the initial discovery, a number of processes were designed to take advantage of the unique behavior of semi-solid metal slurries. From the very beginning, the processes that were being developed all devised novel ways to produce the thixotropic microstructure through some method of vigorous agitation during solidification. It was hypothesized that the induced agitation broke up dendrite arms, which then ripened and spheroidized to form a non-dendritic structure (Flemings, 1991). It soon became apparent that there were two routes for processing semi-solid metal, i.e. two different ways to arrive at the desired point within the solid-liquid, two-phase region. The first route starts from the solid state ("thixocasting"), and the second starts from the liquid state ("rheocasting"). Figure 1 schematically illustrates these two avenues for semi-solid metal formation.

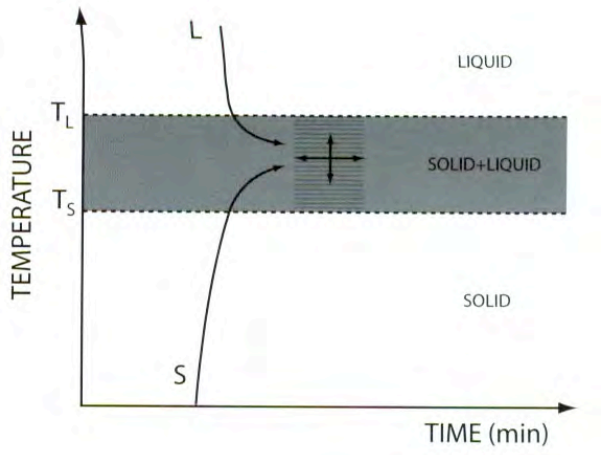

Figure 1: Schematic of the two major semi-solid processing approaches (de Figueredo and Apelian, 2001).

Thixocasting processes start out with a solid precursor material ("feedstock") that has been specially prepared by a billet manufacturer, and then supplied to the casting facility (de Figueredo and Apelian, 2001). Feedstock metal has an equiaxed, non-dendritic microstructure. Small amounts or "slugs" of this alloy are reheated into the semi-solid temperature range, leading to a slurry having a thixotropic structure. In most applications, the slug is subsequently placed directly into a shot sleeve of a die casting apparatus, and the part is formed.

During the initial years of SSM process development, mechanical stirring was used in various ways to break up dendrites and produce thixotropic metal structures (Flemings, 1991). The combination of rapid heat extraction and vigorous melt agitation was affected by using different sizes, shapes, and velocities of stirring rods. Various researchers addressed the evolution of the "stircast" structure during the mid eighties (Doherty, et. al., 1984; Molenaar, et. al., 1986). Although "stircast" methods worked well in that they effectively produced the desired metal structures, erosion of the stirrer became the "weak link" of the process. Focus was placed on the development of "passive" agitation techniques to mitigate stirrer erosion and ensure impurity-free castings (Kirkwood, 1994).

The first highly effective passive method for producing SSM feedstock for thixocasting applications was the Magnetohydrodynamic (MHD) casting process (de Figueredo and Apelian, 2001). In this approach, the solidifying melt is not agitated by a mechanical stirrer, but by alternating electromagnetic fields. Induction coils are placed around a crucible to induce these forces. The crucible is equipped with a cooling system to initiate freezing in the alloy while the melt is exposed

to the electromagnetic forces. Upon cooling down to ambient temperature, the alloy has an equiaxed, non-dendritic microstructure. The MHD stirring process works remarkably well and is widely used commercially today. Figure 2 presents a semi-solid microstructure typically obtained with the MHD process.

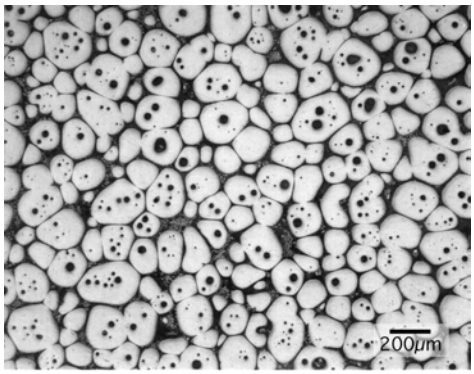

Figure 2: SSM structure of alloy A356 obtained using the MHD process (de Figueredo and Apelian, 2001).

Thixoforming processes comprise the majority of industrial semi-solid applications used today. The main reason for this is the convenience of not requiring melting equipment within the SSM casting facility. However, there are also some disadvantages to thixocasting that may outweigh its benefits. Since billet makers must produce the feedstock material as a service to the SSM caster, there is a premium that the caster must absorb (Jorstad, 2001). Furthermore, in thixocasting processes, scrap metal must be sent back to the billet manufacturer and cannot be recycled. Most importantly, process control is somewhat difficult in thixocasting, because solid fraction (and corresponding viscosity) is sensitive to temperature gradients in the reheated material. Thus, narrow temperature ranges must be achieved consistently for successful operations.

Current industrial drive is towards the development of new rheocasting ('slurry-on-demand') techniques wherein the semi-solid slurry is produced directly from the liquid metal by controlling the solidification path within its freezing range. The development of ideal one-step rheocasting applications is highly preferable to the current two- or three-step applications associated with most thixocasting methods (Apelian, 2000). As such, a major goal is to develop a continuous rheocasting process. Thixocasting approaches are inherently batch processes, in which only small amounts of slurry can be produced during each forming operation. This places limits on the sizes and shapes of parts produced in this manner. A continuous process would circumvent these hindrances, and could be used for a broader variety of applications.

Earlier work in the 1980's that resulted in equiaxed cast structures without breaking up dendrites made use of copious nucleation by casting melts with low superheats. The most popular of these processes was the Microcast-X or "MX" process (de Figueredo and Apelian, 2001). In this process, a superalloy melt with a small degree of superheat was poured into a colder mold having a high heat transfer coefficient. Copious nucleation of the primary phase occurred along the wall of this mold, and fluid flow dispersed these nuclei throughout the bulk of the solidifying melt. This method resulted in significant grain refinement, leading to non-dendritic microstructures. Figure 3 shows such a microstructure obtained with this method.

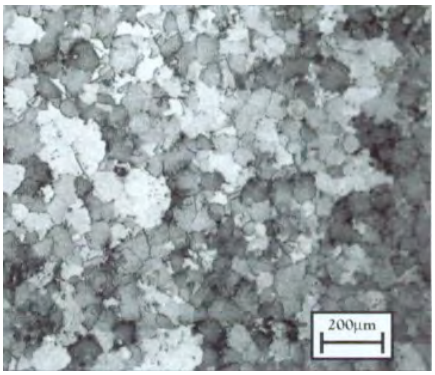

Figure 3: Structure of alloy MarM247 produced by the Microcast-X process (de Figueredo and Apelian, 2001).

Although reheating of the sample shown in Figure 3 would result in an SSM structure, this method was not exclusively developed for rheocasting applications. Rather, the developers of the process were striving for improved properties in superalloys via grain refinement (de Figueredo and Apelian, 2001). Nevertheless, this is an important consideration when one traces casting developments wherein high nucleation rates were operative. Processes analogous to this such as liquidus casting or low temperature pouring also rely on this mechanism for the production of equiaxed structures (Wang, et. al., 2002; Xia and Tausig, 1998). Another casting approach developed in the late 1980's at Southwire Corporation by Chia (de Figueredo and Apelian, 2001) gave rise to a pseudo-SSM structure; equiaxed and fine grain sized copper bars were cast via the Properzi process. Similar to low-temperature pouring, the bars were cast with only 2-4 degrees of superheat. Liquid flow provided convection for seed dispersal, and the low superheat ensured that the seeds did not remelt, but survived in the bulk liquid as grain refining agents.

In the mid-1990's UBE Industries, Ltd. of Japan introduced the new rheocasting (NRC) process (UBE Industries, Ltd., 1996), which paved the way for a new class of cost-effective, simple, and highly effective rheocasting applications. The developers of this technique did not break up dendrites; instead dendritic growth was suppressed from the beginning of solidification. Figure 4 lists the major steps of the NRC process.

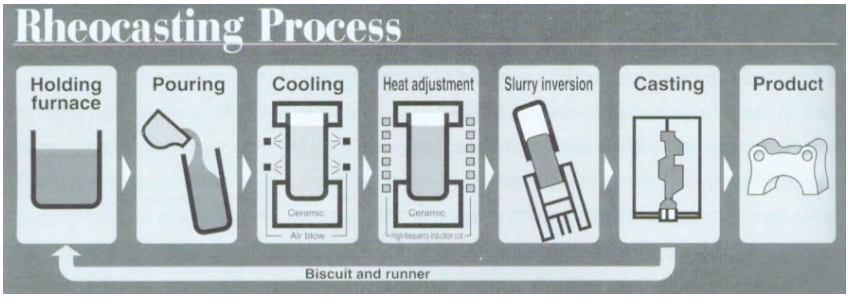

Figure 4: General steps involved in UBE's new rheocasting (NRC) process (de Figueredo and Apelian, 2001).

As shown in Figure 4, the first step in the process involves achieving adequate control over the temperature of the liquid alloy. Similar to previous liquidus casting techniques, the temperature is kept close to the liquidus. The liquid is poured along a cooling slope or "jig" to induce nucleation, and then along the side of an insulating vessel. Fluid flow within this vessel provides forced convection, dispersing the nuclei throughout the bulk where they can act as further nucleation sites. Next, air is blasted against the sides of the crucible, and heat transfer is allowed to occur only through the sides of the vessel. As the resulting slurry cools through the SSM range, the heat content in the vessel is adjusted with heaters to arrive at the desired solid fraction. When the slurry is ready for processing, the vessel is inverted, the metal drops into a shot cavity, and the component is formed. Figure 5 is a microstructure of SSM material obtained with the UBE process.

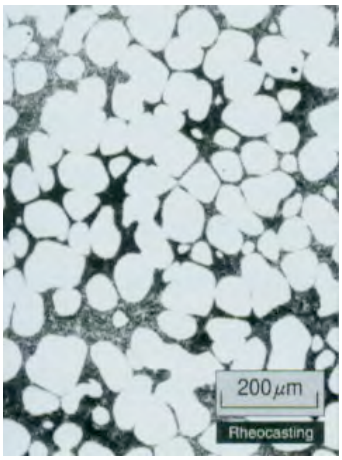

Figure 5: Typical microstructure of an Al-Si-Cu alloy obtained with the UBE process (de Figueredo and Apelian, 2001).

The UBE patent (UBE Industries, Ltd., 1996) extends the solidification ideas outlined above to several other potential SSM processing routes. Hence, each of the techniques listed in the patent follows the general procedure outlined above. That is, heat extraction and forced convection are induced in order to spheroidize the primary particles and obtain thixotropic slurry structures. The NRC process is used solely for rheocasting or SoD applications, but it is a batch process, not a continuous one. Since relatively small vessels are used, only one shot per vessel is attainable. Nonetheless it has been successfully implemented in industrial settings.

A similar process has been reported from the Chiba Institute of Technology (Motegi, et. al., 2002). Here, an inclined plate is utilized to nucleate α-Al from an aluminum melt with varying levels of superheat. The flow of liquid along the plate disperses the nuclei throughout the bulk liquid, resulting in a high level of grain refinement in the solidified samples. Wrought Aluminum alloy (Al-1.63%Si-0.54%Mg) was produced for thixocasting applications. Average particle size in the most refined samples is about 60μm.

In the recent past, through the SSM consortium established at WPI, colleagues at MIT developed a new slurry-on-demand process, the Semi-Solid Rheocasting (SSR) process (de Figueredo and Apelian, 2001; Martinez, et. al., 2001; Flemings, et. al., 2000). The three basic steps in this process, illustrated in Figure 6, are as follows: (1) the melt experiences a short period of agitation as it cools through its liquidus, (2) localized heat extraction is effected by the rotating "cold finger," and (3) the low solid fraction slurry is cooled slowly to a desired solid fraction.

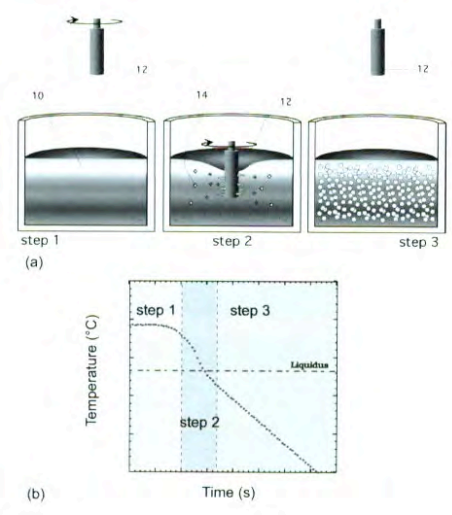

Figure 6: (a) Illustration of the steps involved in the SSR process (b) Typical thermal history of SSR-processed slurry (de Figueredo and Apelian, 2001).

The SSR process results in highly globularized semi-solid slurries, as seen in Figure 7. The combined stirring and cooling of the melt causes the primary-phase particles to grow non-dendritically, as in the UBE process. Figure 6a is closely drawn to scale, which implies that the amount of slurry per run that can be created in the laboratory-scale version of the apparatus limits the process to batch-type applications. To scale it up, the licensing rights to the SSR process were acquired by IdraPrince Inc. (a subsidiary of IdraPresse, SpA), and commercialization of the technique is currently being carried out (Yurko, et. al., 2002).

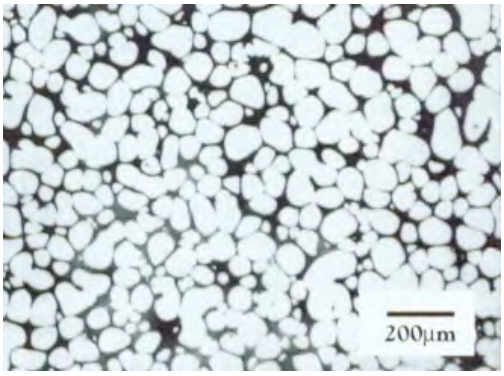

Figure 7: Microstructure of an A356 alloy slurry produced using the SSR process (de Figueredo and Apelian, 2001).

In addition to the processes described above, other successful rheocasting processes have been developed over the years in which different approaches to attain an SSM structure have been used. In one such technique, known as the SLC® (sub-liquidus casting) process, melt agitation is not induced; instead, the process relies on close control over temperature in an undercooled melt to attain SSM structures (Jorstad, et. al., 2002). This process was developed by THT Presses, Inc., and is currently used as a low-cost alternative to conventional SSM processes such as MHD stirring. Figure 8 is a microstructure produced with the SLC process and analyzed at ACRC/ MPI.

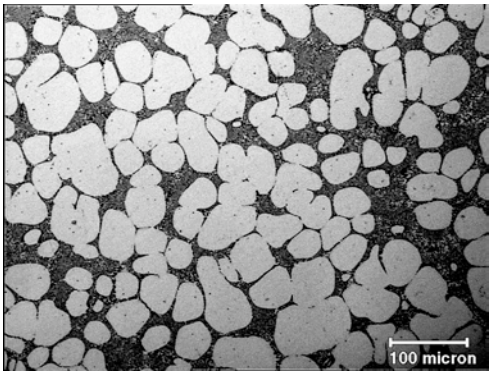

Figure 8: SSM microstructure obtained with the SLC process (Pan, 2003). Alloy: A356.

In another method, melt agitation is not attained with mechanical means, but with a passive mixing technique. The process was developed at the Fiat Research Center in Orbassano, Italy, in the mid-1980's (Antona and Moschini, 1986). A "static mixer" is employed, comprised of a series of alternating right-hand and left-hand helicals made of a material with a high conductivity. As a result, high levels of shear are induced in the alloy melt as heat is extracted by the helicals. The process works quite well and results in slurries having low viscosities at relatively high solid fractions. However, the equipment associated with the process is rather complicated, since two separate electromagnetic pumps are required to induce melt flow (Antona and Moschini, 1986). Though this may not be cost-competitive for wider-ranging rheocasting applications, the concept of passive melt agitation is still a promising one for the development of simpler, less expensive slurry-making processes.

The presentation of the above semi-solid processing technologies has laid the groundwork for the introduction of a new approach to continuous rheocasting. It has been shown that the most effective processes for the production of the thixotropic microstructure combine copious nucleation with forced convection to achieve non-dendritic, spherical particle morphologies. Moreover, the previously held belief that dendrites need to be broken off in the two-phase range to produce a SSM structure is no longer valid. Instead, creating "broken dendrites", or nuclei, at the onset of solidification, and ensuring that they survive, and by restraining their growth, SSM structures are attained. The current need in SSM processing is to devise a relatively simple, easy-to-implement, flexible process that can be used for a wide variety of processing applications. Such a process should use novel and relatively simple methods of melt agitation to avoid the problems associated with the previously discussed approaches.

EXPERIMENTAL

APPARATUS

The CRP is a relatively simple process that takes two liquids, held at a particular level of superheat, and passively mixes them together within a reactor that provides forced convection and rapid heat extraction. In terms of commercial applicability, the projected advantages of the process include process simplicity, flexibility, tight control over SSM structure evolution, fast adjustment of solid fraction, and incorporation of scrap metal for recycling. The term "flexibility" refers to the ability of the process to be used for both thixocasting and rheocasting applications. The schematic diagram, Figure 9 illustrates the concept of a "tortuous path" to induce forced convection.

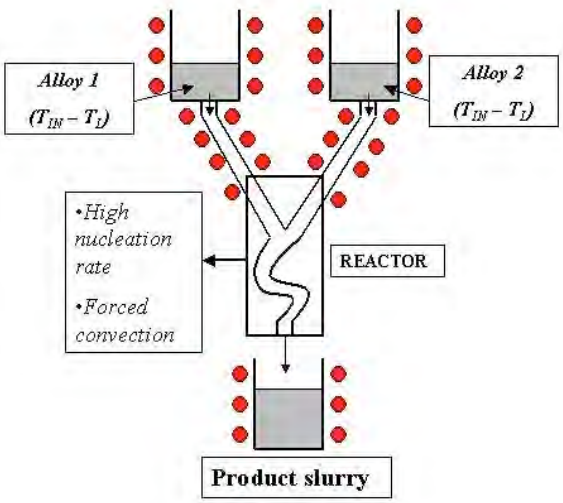

Figure 9: Early schematic of the Continuous Rheoconversion Process (CRP).

The major characteristics of the CRP apparatus include independent temperature control of each precursor alloy melt, a heated channel system to transport the melts without any heat loss, and a reactor to (a) provide copious nucleation and (b) induce forced convection in the melts as they flow through it. The reactor can be preheated to vary its level of heat extraction. The above diagram is intended to provide the reader with the basic variables inherent to the device. These parameters include but are not limited to independent control over the heat content of the melts, the chemical composition of each melt, and the rate at which heat is extracted from the "product melt" within the reactor. Figure 10 is a photograph of the CRP apparatus.

It was important to ensure that the preliminary reactor effectively mixed the melt streams, and that convection forces were in place. Therefore a similitude experiment was carried out in which two water streams containing different colored dyes were mixed within the preliminary reactor. Plexiglas® was placed over the face of the reactor and the experiment was recorded with a video camera. Based on this experiment, it was determined that adequate mixing took place within the reactor. It is thus reasonable to state that molten aluminum flowing through the reactor experiences forced convection due to interaction of the two liquids streams.

Figure 10: Photograph of the CRP apparatus.

PROCESS VARIABLES

The independent variables are those that can be changed by applying different experimental conditions, whereas the dependent variables are dictated *by* the imposed conditions. In this study, there are only two dependent variables: (a) the microstructure of the samples obtained in any given experiment and (b) the temperature of the low solid fraction slurry that exits the mixing reactor. If further testing were done, such as rheological measurements or mechanical testing of cast samples, then these too would be dependent variables that could be correlated to the imposed conditions of an experiment.

On the other hand, there are several independent variables that can be varied due to the design of the CRP apparatus. The most important is the heat content in the precursor melts. Since the two furnaces independently control each melt, this variable is tightly controlled. Another independent variable is melt chemistry. Separate starting vessels make available the option of using alloys of different compositions. For example, one could mix a melt containing grain-refining additions with one containing no grain refiners. The heat extracting capability of the reactor is an independent variable, since the reactor can be preheated prior to melt mixing. The degree of heat extraction corresponds to the nucleation rate induced in the solidifying melt stream. The temperature of the receiving crucible is also an independent variable, and can be varied to observe the effect of cooling rate on the structural evolution in the collected slurry. Finally, when the receiving crucible is preheated, the cooling rate of the slurry can be controlled by varying the crucible temperature. Other sample collection methods to be described shortly can also affect cooling rate, which directly impacts the microstructural evolution.

There are also a few independent variables that were not explored in this study. The first is velocity of the melts as they flow into the reactor. Since the lengths of the melt transport tubes (and the angles at which they are bent) were kept constant, velocity was not varied. This variable warrants further attention, since slower melt velocities may lead to variations in the level of forced convection. Also, since only two reactor designs were used, the inner channel design was not changed appreciably. In future studies, different reactor designs will be employed to address variation of forced convection. Finally, in all experiments, the temperatures of the two precursor melts were kept equal to influence uniform temperature fields within the reactor. When two different alloy systems are used in the CRP, their temperature difference (due to different liquidus points) becomes another potential variable.

ALLOYS USED

The three alloys used were A356.2 (with no grain refiners), A356.2 (with TiB_2 grain refiners), and SiBloy®, which contains permanent grain refiners in the form of AlB_2 particles. Table 1 gives the chemical compositions and liquidus temperatures of each of these alloys. Chemical compositions were obtained with a Spectromax® spectrographic analysis machine. Liquidus temperatures were determined with the derivative method on data collected in cooling experiments using calibrated thermocouples.

Table 1: Chemical compositions (wt%) and liquidus temperatures (^{O}C) of the alloys used

	T_L	Si	Fe	Mn	Mg	Ti	Sr	V	B	Al
A356.2 (NGR) - without GR	616.2	6.82	0.07	0	0.324	<0.002	<0.001	0.006	0.001	Bal.
A356.2 (GR) – with GR	615.5	6.87	0.06	0	0.36	0.11	<0.001	0.008	0.0005	Bal.
SiBloy®	616.0	6.83	0.08	0.02	0.291	0.003	0	0.001	0.016	Bal.

The first stock of A356.2 alloy had a negligible Ti content, and thus was absent of grain refinement. This alloy was used solely in the thixocasting experiments. A second supply of A356.2 alloy had TiB_2 ("TiBor") grain refiners present. The third alloy used, SiBloy®, is a permanently grain refined alloy containing AlB_2 particles in the molten state. SiBloy® was only used for one experiment in order to compare its grain refinement to that of A356.2 with TiBor. The grain-refined alloys were used only in the rheocasting experiments. A batch of A356.2 with no titanium was prepared for the final experiment, in which slurry structures from grain-refined and non-grain-refined alloys were compared.

SLURRY COLLECTION METHOD

Two methods of slurry collection and analysis were followed. In the first method, the slurry was solidified in air within a clay-graphite crucible, after which small samples were reheated into the SSM range and quenched. This is termed the thixocasting set, and its purpose was to verify exploratory findings, as well as to study the microstructural evolution of the as-solidified samples upon reheating.

In the second method, the product slurry did not solidify to give a thixocast sample, but rather simulated the "slurry-on-demand" method. In these experiments, which comprise the rheocasting set, the slurry was collected and quenched into water at various temperatures within the two-phase range of the alloy. Three distinct methods of collecting the rheocast slurry were used in the rheocasting set of experiments. In the first method (the results of which are not presented here), slurry was quenched immediately into water without entering a crucible. In the second technique, a heated receiving crucible was employed from which small amounts of the slurry were removed (scooped out) at various times and quenched in water. In the third approach the entire slurry crucible was quenched in water at a single temperature in the two-phase field. By changing the temperature of the receiving crucible, the cooling rates of the received slurry were varied. Figure 11 is a schematic that illustrates the solidification paths induced in these two sets of experiments. Figure 12 is a flow chart that shows the steps involved in two of the three sample collection methods.

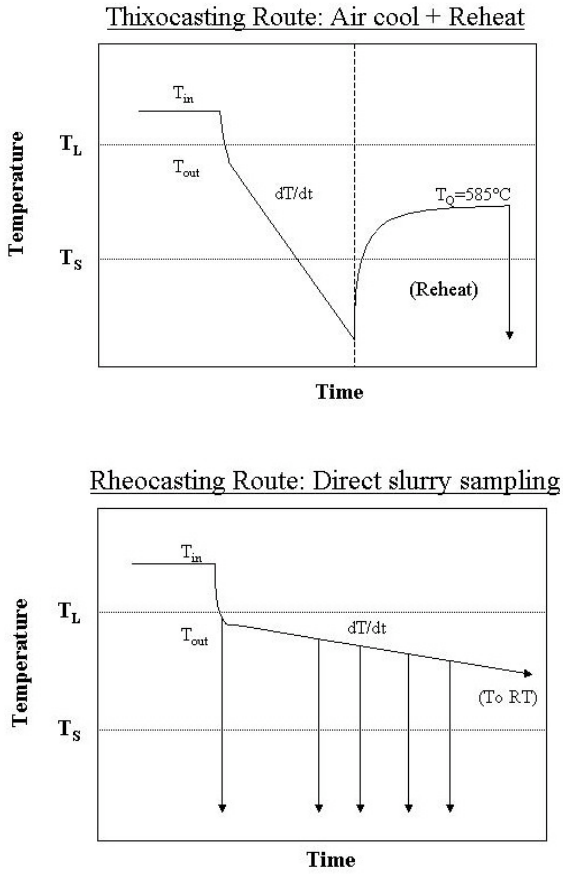

Figure 11: Schematic diagrams detailing the solidification paths undergone in the two experimental phases. Arrows indicate quenching of slurry.

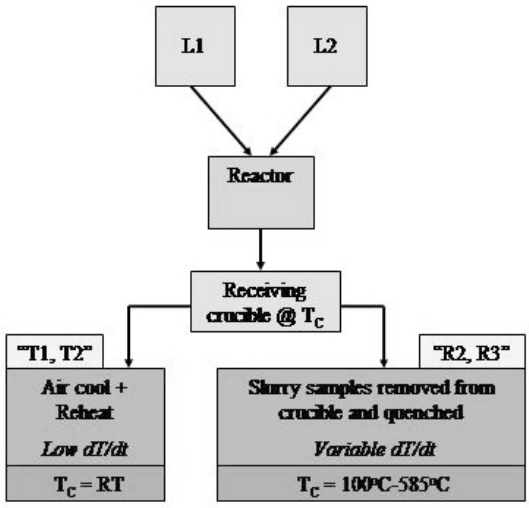

Figure 12: A flow chart illustrating two of the three sample collection methods.

RESULTS AND DISCUSSION

THIXOCASTING ROUTE

In the first set of experiments, a thixocasting approach was followed. Here, "as-solidified" samples were reheated to the semi-solid state and quenched. Two variables were investigated in these experiments: superheat of the melts prior to mixing ("T1" experiments) and temperature of the reactor ("T2" experiments).

Variable: Superheat

Results from two superheat-variable experiments are presented in this section. Table 2 gives the conditions and thermal results of the experiments.

Table 2: Conditions and thermal results for the T1 (superheat-variable) experiments

Experiment	T_{in} [^{o}C]	T_{in}-T_{L} (Superheat) [^{o}C]	T_{out} (approx.) [^{O}C]	$T_{reactor}$ [^{o}C]	dT/dt (in crucible)[^{o}C/sec]	Sampling method
T1-2	625	9	611-613	30	-1.10	Air cool; reheat
T1-4	660	44	615-617	30	-0.85	Air cool; reheat

Figures 13 and 14 exhibit the representative micrographs from the experiments described above. To the left are the as-solidified structures; at the right are the structures obtained after reheating to 585^{o}C and holding for 10 minutes, followed by immediately quenching into water.

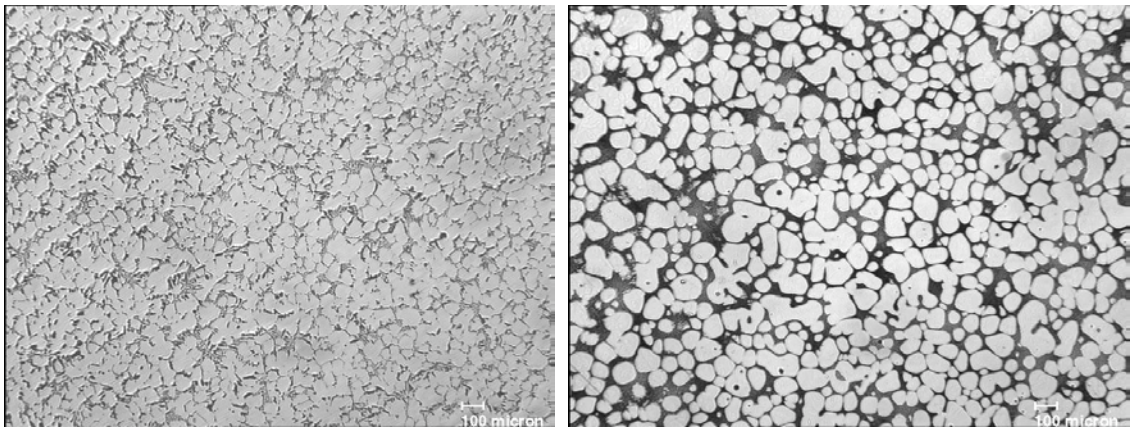

Figure 13: (a) As-solidified and (b) reheated microstructures from experiment T1-2. Residence time of reheated slug in SSM range: 38 minutes.

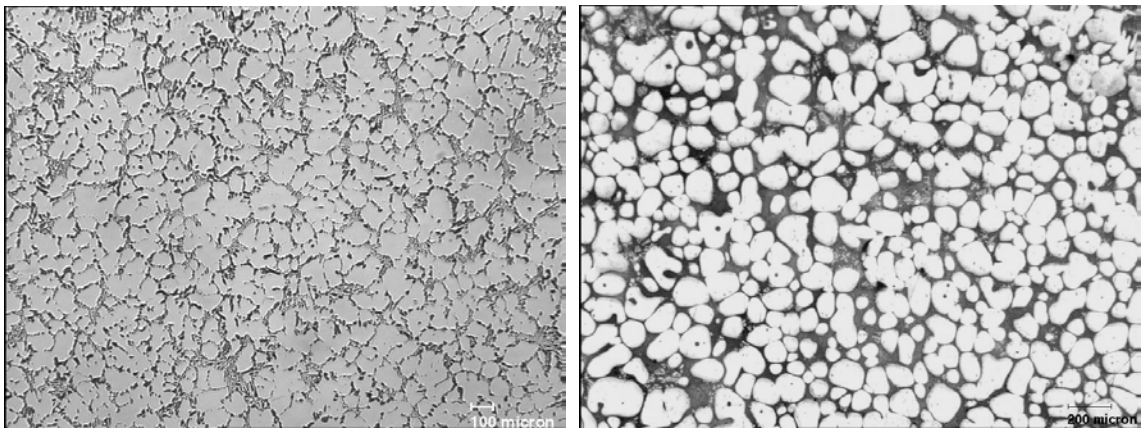

Figure 14 (a) As-solidified and (b) reheated microstructures from experiment T1-4. Residence time of reheated slug in SSM range: 18 minutes.

The above Figures show the effect of raising the superheat of the precursor melts on the resultant microstructures. Each of the above microstructures is highly refined compared to typical as-received ingots. The reheated samples show globular α-Al particles distributed in a liquid matrix, with very little entrapped liquid. It is clear that the entrapped liquid in these samples results from coarsening of irregular (i.e. semi-dendritic) particles during reheating. In Figures 13 and 14 most of the particles have a spherical morphology, but a small portion of them is irregular in shape. Irregularly shaped particles are seen in all results from this study, and their origins are likely related to dendritic growth within the reactor. Although to a limited extent, small dendrites inevitably grow in some parts of the flowing liquid; collisions of these particles may account for the observed shapes. Also evident in the micrographs is an appreciable level of particle agglomeration, which is common characteristic of the structures obtained with the current reactor.

Table 3: Image analysis results for the T1 experiments

Experiment	Avg. Particle Diameter, As-solidified (μm)	Avg. Particle Diameter, reheated (μm)	Avg. Shape Factor, reheated	Number of particles analyzed
T1-2	65.2	92.1	0.86	547
T1-4	90.1	101.2	0.87	378

Table 3 summarizes the image analysis results for the micrographs shown. Increasing the superheat clearly results in larger particle size in both the as-solidified and reheated samples. Shape factor data show that increasing superheat does not affect the morphologies of the analyzed particles. Shape factor was determined from the relationship,

$$\text{Shape Factor} = (4\pi * \text{Area}) / \text{Perimeter}^2 \qquad \textbf{Equation 1}$$

A shape factor value of one corresponds to a perfectly spherical particle, whereas values close to zero indicate dendrites or very irregularly shaped particles. In the reheated samples (and slurry samples shown later), only the more spherical particles were analyzed in order to avoid confusion arising from numerical contributions of irregular particles. This was achieved by defining a classification scheme in the analysis program in which particles with very low shape factor values were excluded. Finally, the number of particles analyzed gives an indirect quantification of the degree of particle irregularity in the samples. Although the micrographs chosen may not portray the exact fraction of irregular particles in the entire sample, it is noteworthy that this value decreases for increasing superheat.

In Figure 13, the most uniform as-solidified structure is observed, with the highest level of grain refinement and non-dendritic morphology. Figure 14 has a larger overall particle size, and shows the highest number of irregular particles. Even at this high superheat, the particles are for the most part non-dendritic. Despite the higher fraction of irregular particles, the reheated structure indicates a predominantly globular morphology. This may be due to the long residence times of the reheated samples in the SSM range. Longer residence times lead to coarsening of the particles; therefore initially irregular particles may become more spherical due to the driving force for these particles to reduce surface area. This also explains why for each experiment the particles in the reheated samples are larger than in the as-solidified ones.

It is concluded from this set of experiments that globular structures can be obtained by mixing alloy melts having relatively high superheats. This indicates that the reactor is able to extract very large amounts of heat in a small amount of time. Therefore it is not necessary to have a precursor liquid very close to the liquidus temperature in order to obtain thixotropic structures with CRP. Finally, in both the as-solidified and reheated samples, there is a clear trend of (a) increasing particle size with increasing superheat and (b) increasing level of particle irregularity (or tendency to grow dendritically) with increasing superheat.

Variable: Reactor temperature

Table 4 shows the conditions and thermal results for two variable reactor temperature experiments. In T2-5 and T2-6, the superheat was kept the same while the temperature of the reactor was varied.

Table 4: Conditions and thermal results for selected T2 (variable reactor temperature) experiments

Experiment	T_{in} [^{o}C]	T_{in}-T_L [^{o}C]	$T_{reactor}$ [^{o}C]	T_{out} (approx.) [^{o}C]	dT/dt (in crucible) [^{o}C/sec]	Collection method
T2-5	640	24	315	614.3	-0.84	Air cool; reheat to 585^{o}C
T2-6	640	24	500	616.4	-0.74	Air cool; reheat to 585^{o}C

The temperature of the reactor was increased in order to decrease its heat extraction capability. The purpose was to vary the processing conditions to give a wide range of particle morphologies, as well as to establish relationships between the variables and the resultant microstructures. In doing so, the limits of the reactor's heat extraction capability were gauged. Figures 15 and 16 show the results from the experiments listed above.

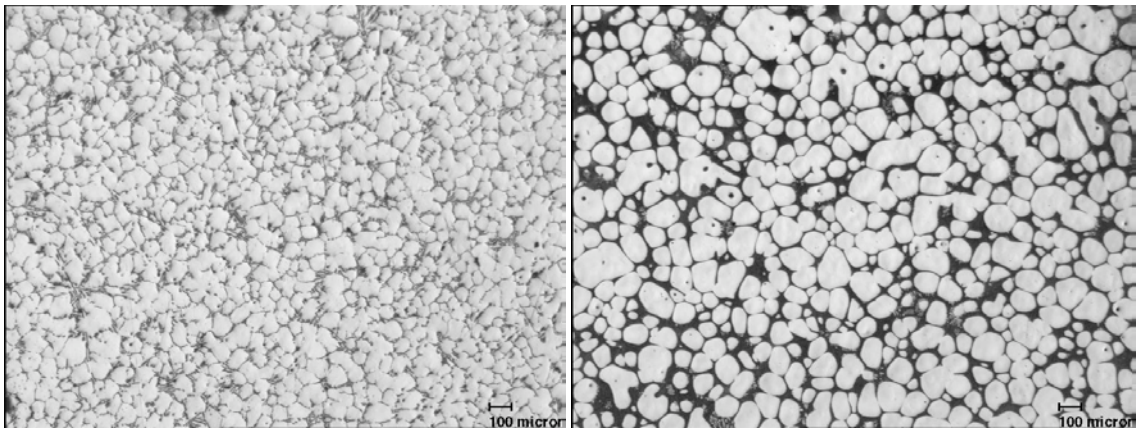

Figure 15: (a) As-solidified and (b) reheated microstructures from experiment T2-5. Residence time of reheated slug in SSM range: 25 minutes.

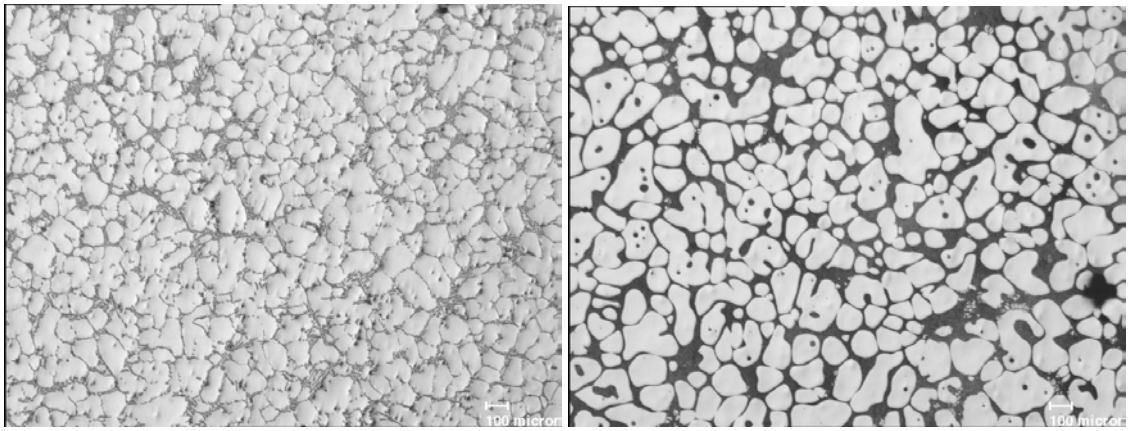

Figure 16: (a) As-solidified and (b) reheated microstructures from experiment T2-6. Residence time of reheated slug in SSM range: 16 minutes.

In the reheated samples, it is observed that these two reactor temperatures lead to highly globular structures of similar particle size. In the first experiment, the product slurry exited the reactor at a temperature just below the liquidus temperature of the alloy, resulting in a very low solid fraction, highly fluid slurry. Previous work at MIT with the SSR process (Martinez, et. al., 2001) suggested that as long as this condition is met (i.e. forming a very low solid fraction rather than cooling the alloy several degrees below the liquidus), then non-dendritic structures result. In other words, all of the particles seen in any given sample must form at or just below the liquidus temperature; therefore it is only necessary to cool the liquid to a one or two degrees below this temperature. The above results show that this reasoning pertains to the CRP as well.

Table 5: Image analysis results for the T2 experiments

Experiment	Avg. Particle Diameter, As-solidified (μm)	Avg. Particle Diameter, reheated (μm)	Avg. Shape Factor, reheated	Number of particles analyzed
T2-5	76.8	98.5	0.90	387
T2-6	105.3	116.7	0.71	235

Table 5 lists the image analysis results for the T2 experiments. In the above Table, and throughout this section, the term "average" in relation to shape factor values refers to the mean value taken from the entire data set of all particles analyzed by the classification scheme. It is clear from the micrographs that particle shape irregularity reaches a maximum when the reactor temperature is highest. Numerically, shape factor values change noticeably in experiment T2-6. Also, the number of particles analyzed drops in T2-6, which suggests that more irregular particles were excluded by the classification scheme. Moreover, in T2-6 the presence of non-spherical particles in both the as-solidified and reheated samples is more evident than in the previous experiments. The exiting slurry was just above the liquidus temperature of the alloy, as shown in Table 4, therefore the thermal conditions of the reactor led to a lower level of nucleation. The decrease in nucleation rate led to a larger particle size in T2-6, since grain growth was promoted by the presence of fewer particles. On reheating, a higher amount of liquid was entrapped by the coarsening particles, as seen in Figure 16.

It is concluded from these experiments that the goal of forming a distinct range of particle morphologies was met by heating the reactor to various temperatures. Particle size increased and shape factor decreased when the reactor was not able to extract heat. A higher reactor temperature led to more dendritic morphologies, whereas lower reactor temperatures produced spherical, thixotropic slurry structures. The extent to which the metal is cooled below its liquidus temperature dictates how globular the overall structure becomes.

RHEOCASTING ROUTE

Slurry quenched at various SSM temperatures

In the rheocasting set of experiments, a heated receiving crucible allowed for the direct sampling of semi-solid slurry produced by the CRP. Three different methods of slurry collection were followed. First, slurry was immediately quenched into water without the presence of a receiving crucible; second, several samples of slurry were collected and quenched at various points while cooled slowly through the two-phase range; and finally, the entire slurry-containing receiving crucible was quenched at one temperature in the semi-solid temperature range.

In these experiments, slurry samples were quenched at various temperatures within the SSM range. In the first experiment, a very slow cooling rate though the SSM range occurred due to a high receiving crucible temperature. In the other three experiments, the cooling rate was higher, and was kept nearly constant. In these higher cooling rate experiments, the variable of grain refinement additions was also investigated. Table 6 lists the conditions and thermal results of the experiments to be presented. For each of these experiments, the reactor was kept at room temperature.

Table 6: Conditions and thermal results for the R2 experiments

Experiment	T_{in} [^{o}C]	T_{out} [^{o}C]	$T_{crucible}$ [^{o}C]	dT/dt (in crucible) [^{o}C/sec]	Total residence time in SSM range (min)	Slurry temp. [^{o}C]	Alloy
R2-5	625	614	450	-0.22	2.8	610, 600, 590, As-solidified	A356.2 w/ TiB_2
R2-7	625	614	450	-0.18	3.6	600, 590, 580, As-solidified	Non-grain-refined A356.2

Figures 17 and 18 compare the results from experiments R2-5 and R2-7. In R2-5, A356.2 (with TiB_2) was used, whereas in R2-7, non-grain-refined A356.2 alloy was used. The purpose of these experiments was twofold: first, to compare the presence of two different kinds of grain refiners to the non-grain-refiner-containing A356.2 alloy; and secondly, to study the effect of a higher cooling rate through the semi-solid temperature range.

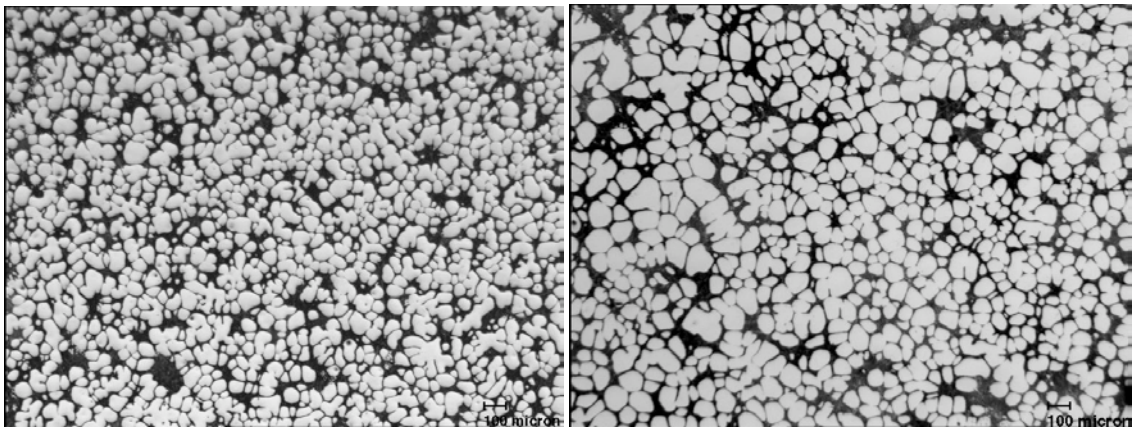

Figure 17: Slurries obtained using grain refined A356.2 (above left) and non-grain refined A356.2 (right). Samples quenched at 590°C (2.3min and 2.8min after collection, respectively).

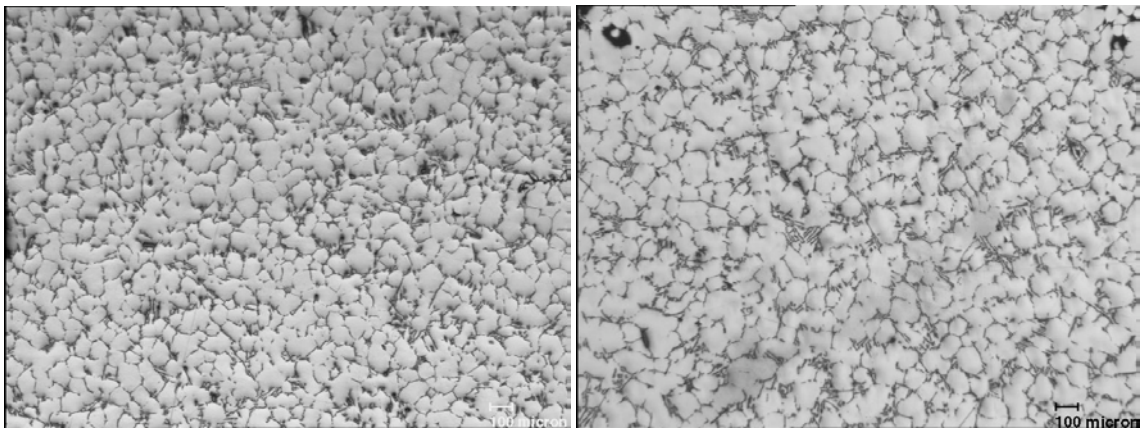

Figure 18: Slurries obtained using grain refined A356.2 (left) and non-grain refined A356.2 (right). As-solidified structures.

The above Figures show that the presence of grain refiners in an alloy processed with the CRP only modifies the resultant structures to a small degree. The two types of grain refiners used both lead to a similar particle size. The Figures also clearly indicate that when a non-grain refined alloy is used, the average particle size becomes slightly coarser; however, they still have highly refined structures in comparison to most commercial SSM processes. It should be noted that the cooling rate of the slurry after exiting the reactor in experiment R2-7 was slightly lower than in experiment R2-5, which may have also contributed to this observed trend.

The structures shown above indicate that the level of nucleation obtained with the reactor with *no inoculants present* is sufficient for the formation of equiaxed, non-dendritic structures. The results also indicate that when inoculants are present prior to mixing within the reactor, even finer structures can be produced. Quantitative verification of these statements is presented in Table 7, which shows the general trend of increasing particle size in the three experiments.

Table 7: Image analysis results for experiments R2-5 through R2-7

Sample	Avg. Particle Diameter (μm)	Avg. Shape Factor	Number of particles analyzed
GR A356.2 - 590^{o}C	55.3	0.88	127
GR A356.2 - As-solidified	66.4	-	203
NGR A356.2 - 590^{o}C	67.9	0.90	458
NGR A356.2 - As-solidified	81.0	-	167

Slurry quenched at a single SSM temperature

In these experiments, the entire slurry-containing crucible was quenched into water at a single temperature in the SSM range. The volume of slurry quenched here is much larger than the volumes of "slugs" reheated in the thixocasting set. The effect of a higher cooling rate than the ones in the R2 experiments was investigated. Table 8 lists the conditions and thermal results for the R3 experiments.

Table 8: Conditions and thermal results for selected R3 experiments

Experiment	T_{in} [^{o}C]	T_{out} [^{o}C]	$T_{crucible}$ [^{o}C]	dT/dt (in crucible) [^{o}C/sec]	Total residence time in SSM range (min)	Slurry temp. [^{o}C]	Comment
R3-1	625	613	100	-0.70	0.5	588	A356.2 w/ GR

Among the rheocasting experiments, experiment R3-1 underwent the highest cooling rate through the SSM range; thus its residence time within the two-phase field was the lowest. This explains the small particle size observed below in Figure 19.

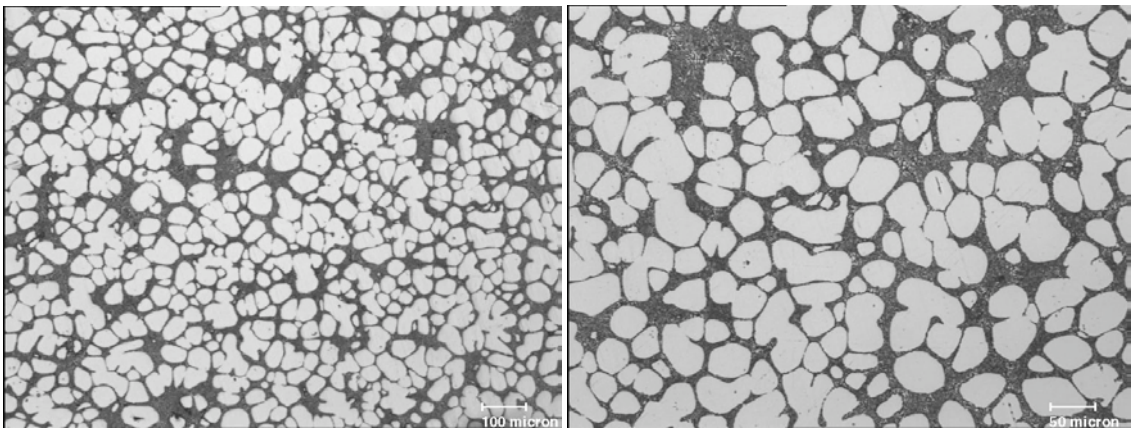

Figure 19: Microstructures from experiment R3-1; 50X (left), 100X (right).

Figure 19 shows the most refined microstructure obtained in this study, with primary particles in the range of 30-50μm in diameter. The majority of the particles have a spherical shape. This is an important result because it shows that when a suitable receptacle temperature is chosen, the cooling rate through the two-phase field can be optimized, thus limiting grain growth and forming better SSM structures.

Table 9: Image analysis results for the R3-1 experiment

Experiment	Avg. Particle Diameter (μm)	Avg. Shape Factor	Number of particles analyzed
R3-1	35.2	0.83	155

CONCLUSIONS

An apparatus for the controlled mixing of two liquids, the Continuous Rheoconversion Process, has been shown to consistently form non-dendritic semi-solid slurries under a variety of imposed conditions. The process involves the flow of molten aluminum through a static mixing reactor that gives forced convection and copious nucleation of the primary phase. The heat extraction capability of the reactor is high enough to ensure the formation of equiaxed structures even with high superheats in the precursor melts. The combination of forced convection and copious nucleation promotes the formation of small, non-dendritic primary α-Al particles.

The first phase of experiments (the thixocasting route) varied the heat transfer conditions within the reactor by changing the melt superheat and reactor temperature, and thus produced a wide range of morphologies. Thixotropic slurry structures were obtained by reheating these samples. The second phase of experiments (the rheocasting route) showed that by optimizing the cooling rate through the two-phase field, the microstructural evolution of the produced slurries led to even better-refined structures. Results from the rheocasting approach give direct evidence that the CRP is a suitable precursor device for an industrial slurry-making apparatus. Furthermore, it has been shown that very fine structures can be obtained even when using an alloy containing no grain refining agents. When proper process conditions are chosen, primary particle sizes on the order of 50 microns and shape factor values of 0.90 are attainable. The important conclusions found in this work are summarized below:

- Increasing superheat in the pre-mixed melts leads to larger and more irregular primary particles; highly refined structures are obtained for superheats approaching 45^{o}C.
- Increasing the temperature of the reactor leads to lower heat extraction of the liquid flowing through it; thus, more dendritic morphologies occur at high reactor temperatures.
- Slurries quenched at various temperatures in the two-phase field yield highly thixotropic structures, especially when the cooling rate through the SSM range is optimized; grain refining agents only lower particle size by a few microns, suggesting that sufficient nucleation occurs in a non-grain-refined alloy within the reactor.

The results from this work indicate that this process is highly effective for slurry-making applications, and thus may help in the development of new rheocasting approaches for semi-solid forming. Future work will address modeling and optimization of the mixing reactor; rheoconversion of different alloy systems such as hypereutectic aluminum, wrought aluminum, and magnesium; and the proposal of scale-up concepts of the Continuous Rheoconversion Process for industrial applications.

REFERENCES

Antona, P.L. and Moschini, R, "New Foundry Process for the Production of Light Metals in the Semi-Liquid, Doughy State," *Metallurgical Science and Technology,* Vol. 4, Issue 2, pp.49-58 (1986).

Apelian, D., "A Roadmap for Semi-Solid Processing," *Proceedings of the 6th International Conference on Semi-Solid Processing of Alloys and Composites,* Turino, Italy, pp.47-54 (2000).

de Figueredo, A. and Apelian, D., *Science and Technology of Semi-Solid Metal Processing,* Chapter 2, edited by A. de Figueredo, published by NADCA, Rosemont, IL (2001).

Doherty, R.D., Lee, H., and Feest, E.A., "Microstructure of Stir-cast Metals," *Materials Science and Engineering,* Vol. 65, pp.181-189 (1984).

Flemings, M.C., "Behavior of Metal Alloys in the Semisolid State," *Metallurgical Transactions,* Vol. 22A, pp.957-981 (1991).

Flemings, M.C., Martinez-Ayers, R.A., de Figueredo, A.M., and Yurko, J.A.: *United States Patent US 2002/0096231 A1,* (July 25, 2002).

Jorstad, J., *Science and Technology of Semi-Solid Metal Processing,* Chapter 4, edited by A. de Figueredo, published by NADCA, Rosemont, IL (2001).

Jorstad, J., Thieman, M., and Kamm, R., "SLC®, the Newest and Most Economical Approach to Semi-Solid Metal (SSM) Casting," *Proceedings of the 7th International Conference on Semi-Solid Processing of Alloys and Composites,* Tsukuba, Japan, pp.701-706 (2002).

Kirkwood, D.H., "Semisolid Metal Processing," *International Materials Reviews,* Vol. 39, No. 5, pp.173-189 (1994).

Martinez, R.A., Yurko, J.A., de Figueredo, A.M., and Flemings, M.C., "Efficient Formation of Structures Suitable for Semi-Solid Forming," *NADCA Transactions,* pp.47-54 (2001).

Molenaar, J.M.M., Katgerman, L., Kool, W.H., and Smeulders, R.J., "The Structure of Stircast Al-6Cu," *Journal of Materials Science,* Vol. 21, pp.389-394 (1986).

Motegi, T., Tanabe, F., and Sugiura, E., "Continuous Casting of Semisolid Aluminum Alloys," *Materials Science Forums,* Vol. 396-402, pp.203-208 (2002).

Pan, Q.Y., Unpublished research, Worcester Polytechnic Institute (2003).

Spencer, D.B., Ph.D. Thesis, Massachusetts Institute of Technology, Cambridge, MA (1971).

UBE Industries, Ltd.: *European Patent EP 0 745 694 A1* (1996).

Wang, H., Davidson, C.J., Taylor, J.A., and St. John, D.H., "Semisolid Casting of AlSi7Mg0.35 Alloy Produced by Low-Temperature Pouring," *Materials Science Forums,* Vol. 396-402, pp.143-148 (2002).

Xia, K. and Tausig, G., "Liquidus Casting of a Wrought Aluminum Alloy 2618 for Thixoforming," *Materials Science and Engineering,* Vol. A246, pp.1-10 (1998).

Yurko, J.A., Martinez, R.A., and Flemings, M.C., "Development of the Semi-Solid Rheocasting (SSR) Process," *Proceedings of the 7th International Conference on Semi-Solid Processing of Alloys and Composites,* Tsukuba, Japan, pp.659-664 (2002).

The Continuous Rheoconversion Process (CRP): *A Novel SSM Approach*

Q.Y. Pan, M. Findon*, and D. Apelian

Advanced Casting Research Center (ACRC)
Metal Processing Institute (MPI)
WPI, Worcester, Massachusetts, USA

*Madison-Kipp Corporation
Madison, Wisconsin, USA

Keywords: Semi-solid processing, slurry-on-demand, liquid mixing, rheocasting, thixocasting, modeling and simulation.

Abstract

Semi-solid metal (SSM) processing is an attractive manufacturing scheme due to the superior quality associated with semi-solid castings. In recent years, the driving force to reduce process cost has led to the development of a few novel rheocasting (also termed slurry-on-demand) processes. These include UBE's new rheocasting (NRC) process (UBE Industries, Ltd., 1996), the semi-solid rheocasting (SSR) process (MIT/WPI, 2000); the SLC® (sub-liquidus casting) process (THT Presses, Inc., 2002), etc. This paper presents an overview of a novel SSM process that has been developed recently at MPI/WPI. The process, termed the "Continuous Rheoconversion Process" (CRP), is a passive liquid mixing technique in which the nucleation and growth of the primary phase are controlled using a specially designed "reactor." The reactor provides heat extraction, copious nucleation, and forced convection during the initial stage of solidification, leading to the formation of thixotropic structures. Experimental results with various commercial aluminum alloys indicate that the CRP is highly effective for the manufacture of high quality semi-solid feedstock for both thixocasting and rheocasting applications. Other advantages include process simplicity, a wide processing window, and the feasibility of recycling scrap metal within the process flowstream. Salient results from validation experiments, as well as numerical simulations, are reviewed and discussed.

1. Introduction

Semi-solid metal (SSM) processing has emerged as an attractive method for near-net-shape manufacturing due to the distinct advantages it holds over traditional near-net-shape forming technologies. These advantages include lower cycle time, increased die life, reduced porosity, reduced solidification shrinkage, improved mechanical properties, etc. SSM processing techniques can not only produce the complex dimensional details (e.g. thin-walled sections) associated with conventional high-pressure die casting, but also can produce high integrity castings currently attainable only with squeeze and low-pressure permanent mold casting. There are two primary semi-solid processing routes, (a) thixocasting and (b) rheocasting. In the thixocasting route, one starts from a solid precursor material that is specially prepared by a primary aluminum manufacturer, using continuous casting methods. Upon reheating this material into the mushy (a.k.a. "two-phase") zone, a thixotropic slurry is formed, which becomes the feed for the casting operation. In the rheocasting route (a.k.a. "slurry-on-demand" or "SoD"), one starts from the liquid state, and the thixotropic slurry is formed directly from the melt via

special thermal treatments; the slurry is subsequently fed into the die cavity. Of these two routes, rheocasting is favored in that there is no premium added to the billet cost, and the scrap recycling issues are alleviated

In the early days of SSM development, it was thought that one had to cool the liquid down into the two-phase region, form dendrites, and then shear off and break the dendrites (i.e. melt agitation via mechanical or, later on, magnetohydrodynamic [MHD] stirring) in order to produce a slurry. However, during the last few years, work sponsored at ACRC – MPI by the Department of Energy [1], as well as work by the research team at MIT [2] led to the discovery that one did not need to break off dendrites to produce the semi-solid structure of globular primary alpha phase. Instead, if the temperature of the melt was such that one could produce many nuclei ("copious nucleation"), and if the nuclei did not grow past a certain point (i.e. suppression of dendritic growth), nor melt back into the bulk liquid, then one could produce a slurry with the ideal semi-solid structure directly from the melt. This "recipe" has become the new methodology for generating semi-solid slurries from the liquid state; it is a *controlled nucleation and growth* phenomenon, as opposed to the previous theory, in which a dendritic structure was modified by shear forces to result in the preferred globular structure.

In recent years, the driving force to reduce process cost has led to the development of a few promising rheocasting methods. These include UBE's new rheocasting (NRC) process (UBE Industries, Ltd., 1996) [3]; the semi-solid rheocasting (SSR) process (MIT/WPI, 2000) [4]; the SLC® (sub-liquidus casting) process (THT Presses, Inc., 2002) [5]; the "Continuous Rheoconversion Process" (CRP) (WPI, 2002) [6], etc. In essence, all of the above-mentioned processes utilize the same fundamental concept: nucleation and dispersion of the nuclei to achieve the semi-solid structure as the alloy melt is cooled below the liquidus temperature.

The attractive advantages of SSM motivated our research towards the development of a new process, wherein the advantages of SSM are realized and with the caveat that the "new process" can be incorporated into existing die casting machines without significant levels of retrofitting and infrastructure changes. This paper presents an overview of a novel semi-solid process that has been developed at MPI/WPI. The process is termed the Continuous Rheoconversion Process (CRP), and is a passive liquid mixing technique that utilizes the above-described recipe. Presented below are the concept, representative microstructures, operative mechanisms, and modeling results of the CRP.

2. CRP: *Concept & Apparatus*

The CRP is a simple process in which two melts (either of the same alloy, or two different alloys), held at a particular level of superheat, are passively mixed within a reactor. The reactor provides heat extraction and forced convection during the initial stage of solidification, leading to the formation of thixotropic structures. Figure 1 illustrates the concept of the CRP process. The advantages of the CRP include process simplicity, flexibility, tight control over SSM structure evolution, fast adjustment of solid fraction, and incorporation of scrap metal for recycling. The term "flexibility" refers to the ability of the process to be viable for both thixocasting and rheocasting applications.

Figure 2 is a photograph of the CRP apparatus. The major characteristics of the CRP apparatus include independent temperature control of each precursor alloy melt, a heated channel system to transport the two melts, and a reactor that enables two phenomena to occur: (a) copious nucleation within the melt, and (b) forced convection of the two streams as they flow through the reactor. The reactor can be preheated to vary the level of heat extraction. Important parameters include the superheat and chemical

composition of the melts, the heat extracting rate of the reactor, and the temperature of the receiving reservoir.

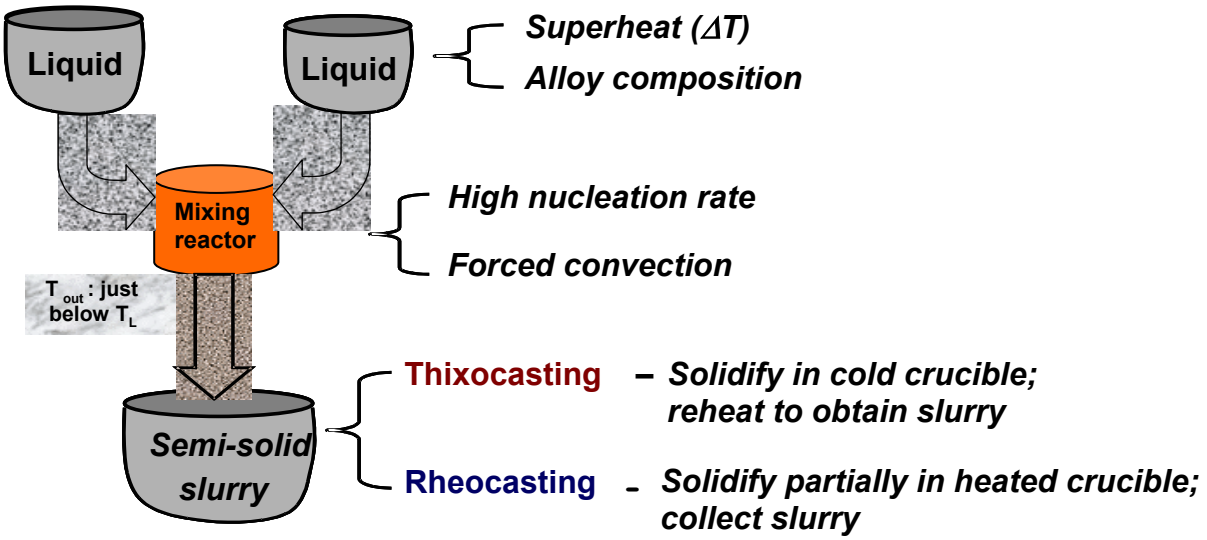

Figure 1: Conceptual schematic of the Continuous Rheoconversion Process (CRP).

Figure 2: Photograph of the CRP apparatus.

3. CRP: *SSM Structures*

The CRP is a flexible process in that it can be used for both the thixocasting and rheocasting routes. As shown in Figure 3, in the thixocasting route, the slurry is solidified in air within a clay-graphite crucible, after which small "slugs" from the solidified sample are reheated into the two-phase range and quenched for microstructure analysis. In the rheocasting or slurry-on-demand route, the slurry is collected and quenched into water at various temperatures within the two-phase range of the alloy.

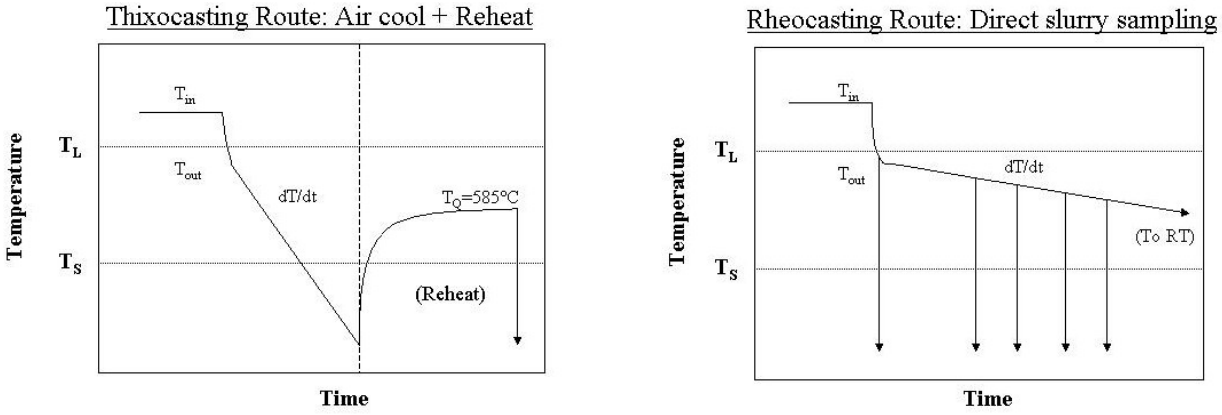

Figure 3: Schematic showing the solidification paths of the CRP's thixocasting and rheocasting routes. Arrows indicate water quenching of slurry.

Figure 4 exhibits typical semi-solid structures of an A356 alloy (without grain refinement) obtained by mixing two low-superheat melts with the same initial temperature (superheat: 9°C). Whereas Figure 5 shows typical semi-solid structures of the same alloy obtained by mixing two high-superheat melts (superheat: 44°C). From Figures 4 and 5, one can see that under both conditions, a globular, near-ideal semi-solid structure can be obtained. This indicates that the reactor is able to extract a very large amount of heat in a small amount of time. Thus the CRP has a large processing window, and therefore excellent process control (in terms of thermal management).

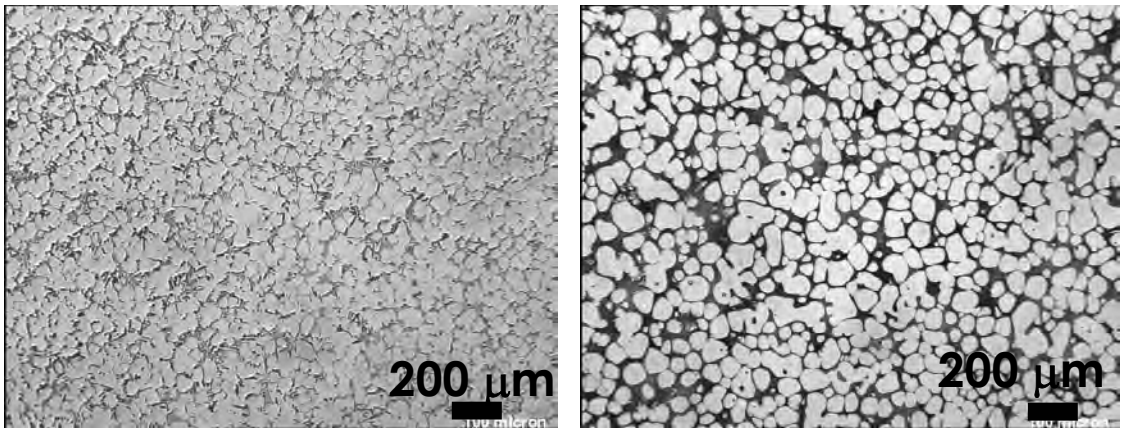

Figure 4: Microstructures of an A356 alloy obtained by mixing two low-superheat melts (superheat: 9°C): (a) As-solidified (left); (b) Reheated to 585°C and water quenched (right).

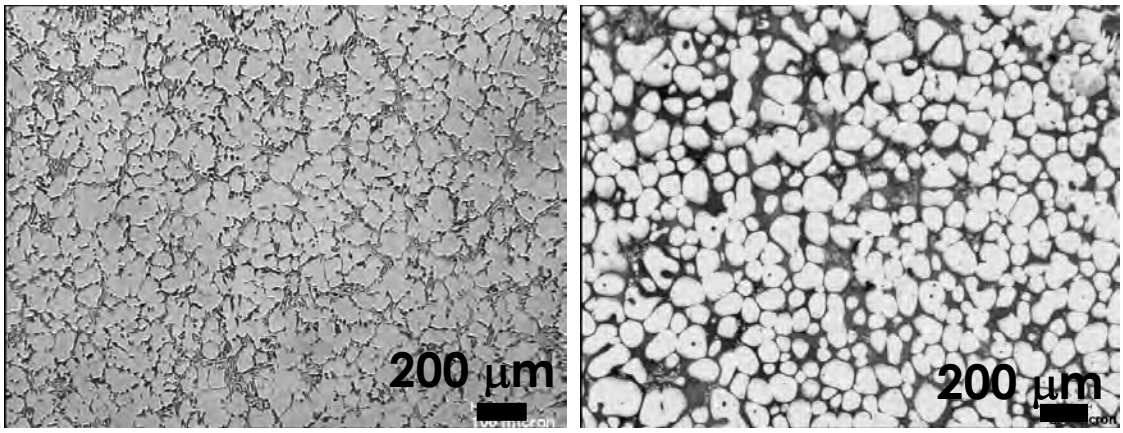

Figure 5: Microstructures of an A356 alloy obtained by mixing two high-superheat melts (superheat: 44°C): (a) As-solidified (left); (b) Reheated to 585°C and water quenched (right).

Figures 6 and 7 illustrate typical semi-solid structures of TiB_2 grain-refined A356 alloys obtained under different rheocasting conditions. Figure 6 compares semi-solid microstructures of A356 alloy slurries sampled at two different temperatures (605°C vs. 585°C). The successful use of this sampling method was an important indicator that the CRP can indeed generate slurries with near-ideal semi-solid microstructures directly from the molten state; i.e., the rheocasting route can be effectively followed with the CRP. The Figures document the gradual change in morphology of a slurry batch that is cooled very slowly through the two-phase temperature range. Figure 7 compares semi-solid structures of A356 alloy slurries with and without grain refinement. From Figure 7, one can see that grain refinement does not significantly change the resultant semi-solid structures. The presence of grain refiners in an alloy only improves the resultant structures to a small degree, suggesting that the level of nucleation provided by the reactor itself is sufficient for the formation of high quality semi-solid structures.

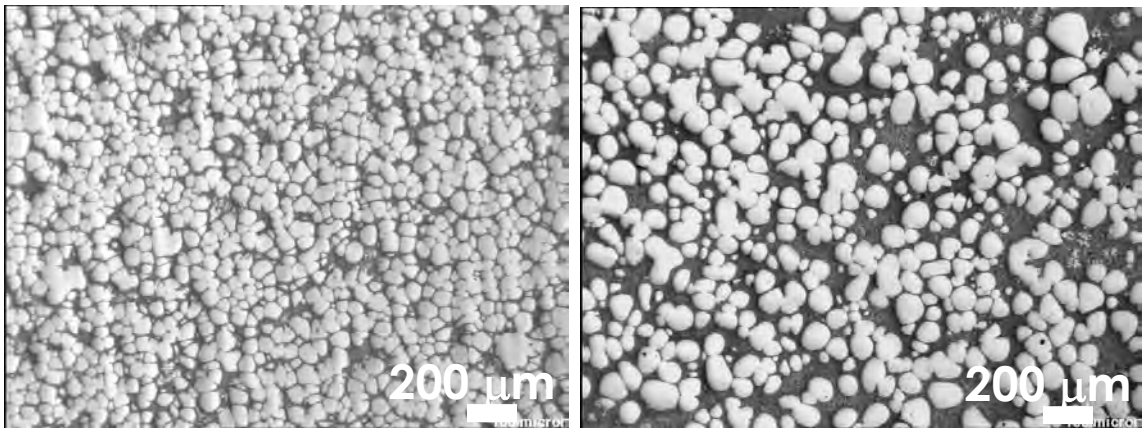

Figure 6: Microstructures of grain-refined A356 slurries sampled at two different temperatures in the two-phase region, (a) 605°C (left), and (b) 585°C (right).

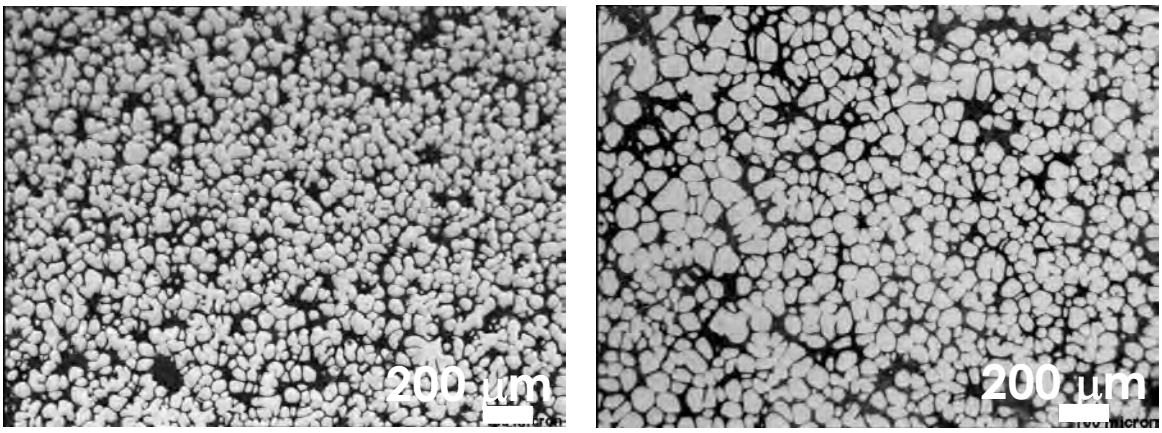

Figure 7: A comparison of semi-solid structures of TiB_2 grain refined A356 slurry (left); and A356 slurry without grain refinement (right). Samples quenched at 590°C.

In addition to Al-Si foundry alloys, we have processed a variety of other alloy systems using the CRP, including hypereutectic alloy 390, wrought alloys, Al-Cu alloys etc. It has been found that the CRP can consistently produce high quality semi-solid structures even for those alloys that are not "castable," or which are known for their poor castability. Figure 8 shows such a structure from an A206 alloy (Al-4.5wt%Cu). Experimental results pointed out that the CRP can improve the castability of the alloy significantly. The reason for this is that the CRP changes the morphology of the primary phase from coarse dendrites to fine globules, which eliminates the feeding problem during solidification that is associated with traditional casting methods. Therefore, this alloy is actually "castable" using the CRP, and this holds true for various other wrought alloys as well.

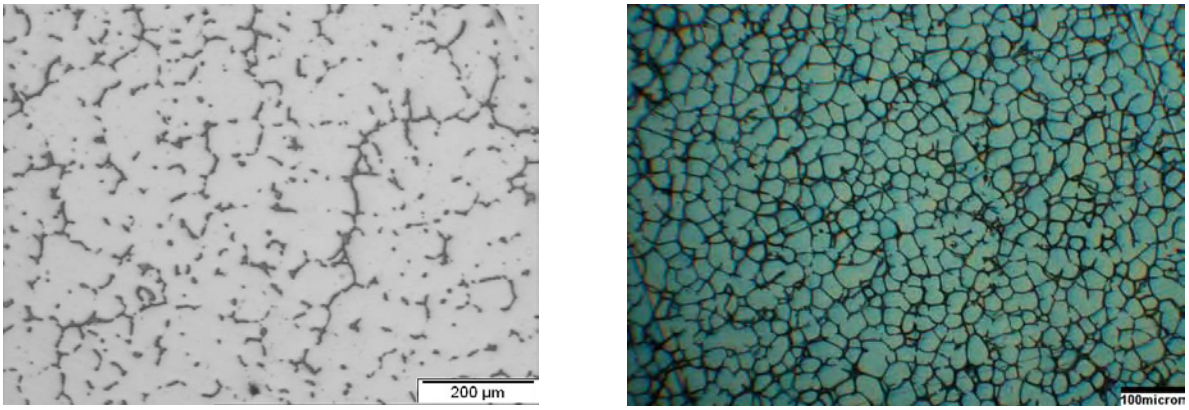

Figure 8: Microstructures of an A206 alloy: (a) Air-cooled from the liquid state (left), (b) As-solidified structure obtained with the CRP (right).

4. CRP: *Operative Mechanisms*

High nucleation rate combined with forced convection leads to (a) copious nucleation of the primary phase, (b) dispersal of these nuclei throughout the bulk liquid, and (c) survival of these nuclei via homogeneous temperature fields. These are the operative mechanisms for the CRP; the net result is total suppression of dendritic growth of the primary aluminum phase. The high heat extraction capability of the reactor combined with forced convection (via mixing) ensures the formation of thixotropic structures even with appreciable superheats in the precursor melts. The high level of grain refinement observed in the as-solidified samples can be explained by highly potent nucleation events within this reactor, while the uniformity of these structures throughout the samples indicates that these nuclei were dispersed effectively by the fluid flow in the reactor.

5. CRP: *Reactor Optimization*

As mentioned earlier, the reactor provides rapid heat extraction, copious nucleation, and forced convection during the initial stage of solidification, leading to the formation of thixotropic structures. Obviously, the reactor plays a crucial role in structure formation in the CRP. To optimize the reactor design for the ultimate purpose of scaling up the CRP to an industrial level, the reactor was modeled using commercial simulation and computational tools. In addition, fluid flow experiments in plexiglass models were conducted to verify these concepts.

Figure 9 shows the flow pattern of two liquids as they flow through a reactor. Modeling results show that the angles α and β are important. To ensure a certain amount of mixing/convection in the reactor, the value of α and β has to be less than 90°. By analyzing the temperature profile and fluid flows in the reactor, we found that the high heat extraction capability of the reactor ensures the formation of a plurality of nuclei at the inner walls of the reactor, and subsequently, the nuclei are swept away and dispersed uniformly into the slurry due to the mixing action. Figure 10 shows a reactor with a different geometry. Simulation results suggest that by increasing the number of the paths/channels in the reactor, the nucleation rate as well as level of mixing/convection can be maximized. Fluid flow experiments in plexiglass models have verified the flow patterns in these reactors. Currently, we are conducting simulation experiments with transparent alloys (succinonitrile-water [SCN] system) to reproduce the nucleation phenomena in the reactors, and to further validate the modeling results. The reactor will then be fully optimized and scaled up for industrial applications.

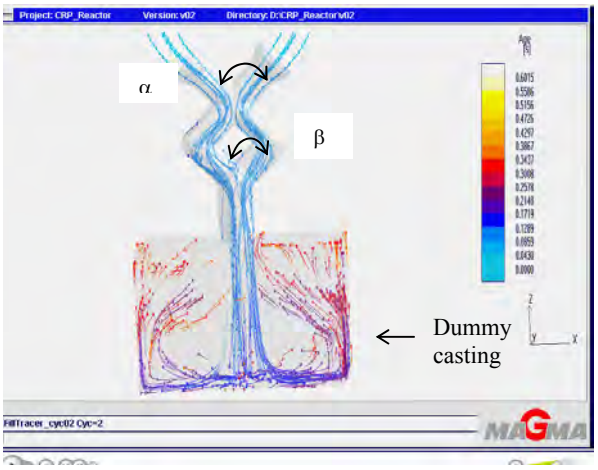

Figure 9: Flow pattern in a mixing reactor.

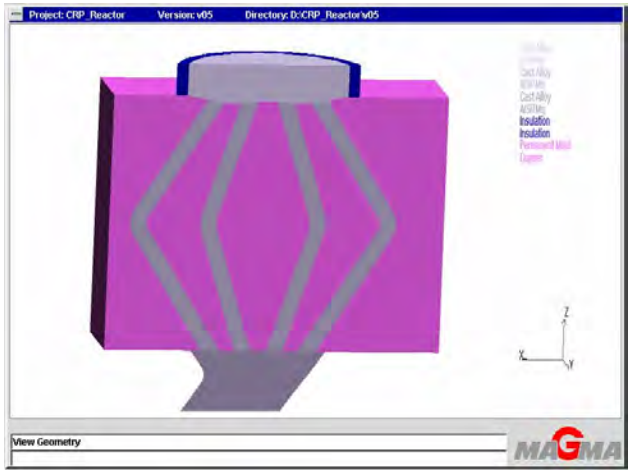

Figure 10: Alternate (untested) reactor design.

6. Conclusions

The CRP has been shown to consistently generate near-ideal semi-solid structures for a variety of alloys for both thixocasting and rheocasting applications. The process involves the flow of molten metal through a specially designed "reactor" that provides forced convection and copious nucleation, leading to the formation of the desired thixotropic structure. The results with various commercial aluminum alloys indicate that the CRP is highly effective for the manufacture of high quality semi-solid feedstock. Currently, the process is being optimized for industrial applications.

Acknowledgements

The authors are grateful to the ACRC Consortium members for their engagement and active participation in our work on SSM processing. This work was supported by the Department of Energy, Contract No. DE-FC36-02ID1432.

References

1. DOE Report number DE-FC07-98ID13618
2. M.C. Flemings, "Semi-Solid Processing – The Rheocasting Story", Test Tube to Factory Floor: Implementing Technical Innovations, from the Proceedings of the Spring Symposium May 22, 2002 published by Metal Processing Institute, Worcester Polytechnic Institute, Worcester MA 01609 (2003).
3. UBE Industries, Ltd.: *European Patent EP 0 745 694 A1* (1996).
4. J.A. Yurko, R.A. Martinez, and M.C. Flemings, "Development of the Semi-Solid Rheocasting (SSR) Process," *Proceedings of the 7th International Conference on Semi-Solid Processing of Alloys and Composites,* Tsukuba, Japan, pp.659-664 (2002).
5. J. Jorstad, M. Thieman, and R. Kamm, "SLC®, the Newest and Most Economical Approach to Semi-Solid Metal (SSM) Casting," *Proceedings of the 7th International Conference on Semi-Solid Processing of Alloys and Composites,* Tsukuba, Japan, pp.701-706 (2002).
6. M. Findon, "Semi-Solid Slurry Formation via Liquid Metal Mixing", M.Sc. Thesis, Worcester Polytechnic Institute, 2003.

THE CONTINUOUS RHEOCONVERSION PROCESS (CRP™): OPTIMIZATION & INDUSTRIAL APPLICATIONS

Q.Y. Pan, D. Apelian, and P. Hogan

Advanced Casting Research Center (ACRC) - Metal Processing Institute (MPI) - WPI, Worcester, MA 01609 USA

Abstract

Semi-solid metal (SSM) processing has emerged as a preferred manufacturing scheme due to the superior quality associated with semi-solid castings. In recent years, the driving force to reduce process cost requires the development of robust, commercially viable rheocasting (also termed slurry-on-demand (SoD)) processes. The continuous rheoconversion process (CRP™) is a novel SoD process that was developed at MPI/WPI. The process is based on a passive liquid mixing technique in which the nucleation and growth of the primary phase are controlled using a specially designed "reactor". The reactor provides heat extraction, copious nucleation, and forced convection during the initial stage of solidification, thus leading to the formation of globular structures. This paper presents our recent work on the optimization of the CRP™ for industrial applications. Specifically, we will discuss critical issues of optimizing and simplifying the process to retrofit most die casting facilities. Salient results from simulations and several industrial trials that have been carried out with ACRC Consortium Members are reviewed and discussed.

Riassunto

Il processo di produzione di getti metallici via semi-solido (SSM) ha acquisito crescente importanza grazie alle superiori qualità dei prodotti ottenuti. Negli ultimi anni, la spinta alla riduzione dei costi di produzione ha portato allo sviluppo di processi reologici (altresì chiamati processi slurry-on-demand (SoD)) tecnologicamente robusti e commercialmente abbordabili. Il processo di reoconversione continua (CRP™) consiste in un nuovo processo SoD sviluppato al MPI/WPI. Il processo si basa su una tecnica di miscelazione liquida passiva durante la quale la enucleazione e la crescita della fase primaria viene controllata in un reattore di concezione speciale. Il reattore provvede alla estrazione del calore, ad una enucleazione copiosa e alla convezione forzata durante le fasi iniziali di solidificazione, portando così alla formazione di strutture globulari. In questo lavoro illustriamo le nostre più recenti ricerche sull'ottimizzazione del CRP™ per applicazioni industriali. Nello specifico, discuteremo degli aspetti critici di ottimizzazione e semplificazione del processo che devono essere affrontati nelle realtà di produzione industriale. Verranno anche discussi i principali risultati derivati dalle simulazioni and alcuni test industriali condotti presso strutture del consorzio ACRC.

KEYWORDS

Semi-Solid Processing; The Continuous Rheoconversion Process (CRP™); Modelling, Optimization; Industrial Application.

INTRODUCTION

Semi-solid metal (SSM) processing has emerged as an attractive method for near-net-shape manufacturing due to the distinct advantages it holds over conventional near-net-shape forming technologies. These advantages include lower cycle time, increased die life, reduced porosity, reduced solidification shrinkage, improved mechanical properties, etc. SSM processing techniques can not only produce the complex dimensional details (e.g. thin-walled sections) associated with conventional high-pressure die castings, but also can produce high integrity castings currently attainable only with squeeze and low-pressure permanent mold casting. There are two primary semi-solid processing routes, (a) thixocasting and (b) rheocasting. In the thixocasting route, one starts from a non-dendritic solid precursor material that is specially prepared by a primary aluminum manufacturer, using continuous casting methods. Upon reheating this material into the mushy (a.k.a. "two-phase") zone, a thixotropic slurry is formed, which becomes the feed for the casting operation. In the rheocasting route (a.k.a. "slurry-on-demand" or "SoD"), one starts from the liquid state, and the thixotropic slurry is formed directly from the melt via careful thermal management of the system; the slurry is subsequently fed into the die cavity. Of these two routes, rheocasting is favored in that there is no premium added to the billet cost, and the scrap recycling issues are alleviated.

In the early days of SSM development, it was thought that one had to cool the liquid down into the two-phase region, and to shear off and break the dendrites (i.e. melt agitation via mechanical or, later on, magnetohydrodynamic [MHD] stirring) and thus producing a slurry. However, during the last few years, work sponsored at ACRC – MPI by the Department of Energy [1], as well as work by the research team at MIT [2] led to the discovery that one did not need to break off dendrites to produce the semi-solid structure of globular primary alpha phase. Instead, if the temperature of the melt was such that one could produce many nuclei ("copious nucleation"), and if the nuclei did not grow past a certain point (i.e. suppression of dendritic growth), nor melt back into the bulk liquid, then one could produce a slurry with the ideal semi-solid structure directly from the melt. This concept is the genesis of commercial processes and methodologies to generate semi-solid slurries from the liquid state. The concept relies on *controlled nucleation and growth*, as opposed to the previous theory, in which a dendritic structure is modified into a globular structure via shear forces.

The driving force to reduce process cost has led to the development of several rheocasting (also termed slurry-on-demand) processes. These include UBE's New Rheocasting (NRC) [3], Idra-Prince's Semi-Solid Rheocasting (SSR) [4], THT Presses' Sub-Liquidus Casting (SLC™) [5], and Alcan's Swirl Enthalpy Equilibration Device (SEED) [6], as well as the Continuous Rheoconversion Process (CRP™) [7, 8], developed by ACRC/MPI.

The CRP™ is a process where the molten metal flows through a reactor prior to casting. The role of the reactor is to ensure that copious nucleation takes place and that the nuclei are well distributed throughout the system prior to entering the casting cavity. The CRP™ has been successfully applied in hyper-eutectic Al-Si alloys (i.e., 390 alloy) where two liquids of equal or different compositions and temperatures are mixed in the reactor and creating a SSM slurry [9]. The process has been mostly used for hypo-eutectic Al-Si alloys (i.e., 356, 357, etc.) where a single melt passes through the reactor. In addition, the CRP™ was designed to be flexible for thixocasting or rheocasting applications as well as batch or continuous casting. Variable heat extraction rates can be obtained by controlling either the superheat of the melt, the temperature of the channel system, or the temperature of the reactor.

The work of Findon [7] demonstrated that the CRP™ is a robust process, which can consistently generate near-ideal semi-solid structures for grain refined and non-grain refined A356 type alloys within a large process window. The recent work of Pan and Findon [8] has shown that the CRP™ is also highly effective for the manufacture of high quality semi-solid feedstock of other commercial alloy systems, including hypereutectic aluminum-silicon (390), aluminum-copper (A206), wrought aluminum alloys, as well as Mg alloys.

The CRP™ has shown great potential for commercial applications. In order to optimize/scale-up the CRP™ for use by industry, several questions/challenges still remain such as:

- What is the optimal design for the reactor?
- How critical is the heat extraction/forced convection in the formation of SSM structures? and furthermore
- How to retrofit most existing die casting facilities?

These questions/challenges are the theme of this work. In this paper, we present our recent work on the optimization of the CRP™ for industrial applications.

1. OPTIMIZATION OF THE CRP™ REACTOR DESIGN

To retrofit most die casting facilities, the CRP™ reactor has been simplified in such a way that only one melt is involved wherein both nucleation and mixing takes place simultaneously within the reactor. Moreover, to enhance the control of melt nucleation and to conveniently adjust slurry fraction solid, a cooling system is incorporated into the reactor. Based on experimental data generated from preliminary trials, finite element and finite volume models were created in order to optimize the CRP™ reactor design. Some salient results from the modeling effort are briefly described in this section.

1.1 FLUID FLOW OPTIMIZATION

Finite volume models were created and analyzed in commercially available FLUENT software in order to study the flow conditions and patterns in the reactor. Past and current successful designs were modeled in an effort to identify the critical aspects of the flow of the molten metal, and to optimize the reactor design. The optimization efforts were intended to result in new reactor designs which would incorporate the critical flow parameters but eliminate any excess features or flow disorder which inhibited the ease of introduction into industrial settings.

Three-dimensional models of the reactors were created in Pro/Engineer software and meshed with 4 node tetrahedral elements in GAMBIT, meshing software which is included with Fluent. The solver was formulated to use the well known SIMPLE pressure-velocity coupling along with the standard K-ε turbulence model.

Figure 1 displays visual outputs of the turbulence intensity values in two reactor designs. Analysis of the various reactors revealed that the current reactor induces less turbulence than several past designs, and is effective in producing SSM structures as previous reactors. Therefore, further efforts focus on the optimization of the cooling system and some potential issues found from the preliminary trials, such as the possibility of splashing of the melt or trapping of gases upon pouring.

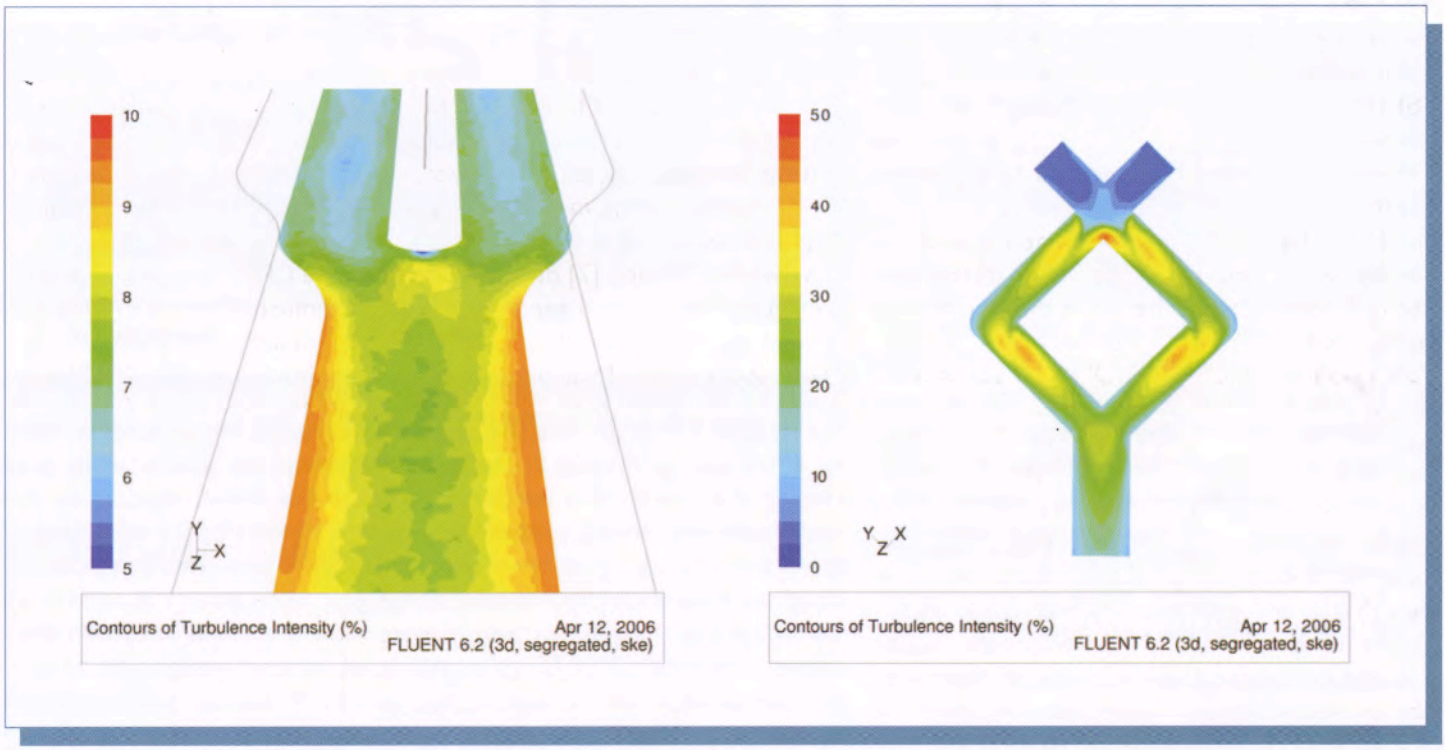

Fig. 1: Levels of turbulence intensity generated by CRP™ reactors. Current design (left) and past design (right). Note the differing scales.

1.2 COOLING CHANNEL OPTIMIZATION

The cooling system of the reactor, consisting of water channels running along the long axis of the reactor, is critical for the successful functioning of the reactor. Moreover, nearly the same amount of enthalpy must be extracted from the melt with each subsequent pour. The cooling channels must be able to extract heat from the reactor in a manner that will allow for a stable temperature profile throughout the reactor over a period of time during which castings are being made. The letter "C" in CRP™ stands for *continuous*, and to have a robust process, the above factors must be attended to and addressed.

Two separate two-dimensional finite element models were created and meshed in commercially available ANSYS software in order to determine the optimal configuration of cooling channels in the reactor. The first cross-section was taken in the upper region of the reactor, where the melt is poured, and where there are two flow channels. The second cross-section was taken in the lower region of the reactor, where the two flow channels converge into one, with the convergence acting as a means to homogenize the melt. The best configuration should work well in both regions of the reactor.

Convection coefficients for the transfer of heat from the flowing melt to the reactor, from the reactor to the cooling water, and from the reactor to the ambient air were estimated used Nusselt correlations for the relevant flow regimes. These

coefficients are quantified in Table 1. Contact time between the melt and the reactor was estimated to be 10 seconds, with a length of time from 1 to 2 minutes between each pour.

A measure for quantifying the success of each channel configuration and conditions was created in order to determine the optimal conditions in an objective fashion. The temperature at the surface of the flow channel in the reactor was monitored at three locations: At the bottom of the flow channel, at the highest point on the flow channel which is in contact with the melt, and at a point in the middle of these two locations. Melt does not entirely fill the channels during each pour however. For the purposes of the study, the assumption was made that only the bottom third of the channel was full of metal. This means that although the flow channels have a radius of 0.75", the depth of the flowing metal was assumed to be 0.25". This affected the amount of reactor surface in contact with the flowing melt, and therefore the amount of heat extracted. At each point in time during the 1-2 minutes between pours, the average temperature of the three points was calculated, as well as the maximum difference between the temperatures at any of the three points. The conditions for optimized configuration of cooling channels are as follows.

TABLE 1: HEAT TRANSFER COEFFICIENTS USED IN COOLING CHANNEL OPTIMIZATION

Flow Regime	h (W/m^2-K)
Melt to Reactor (Upper Region)	25,000
Melt to Reactor (Lower Region)	27,750
Reactor to Cooling Water	Variable depending on flow rate, channel diameter. Dittus-Boelter correlation used.
Reactor to Air	5 [10]

1) Minimize the difference in temperature between any two points during the cooling cycle. Initial exploratory simulations found that any temperature gradient present after a single pour will become more severe as subsequent cycles have passed.
2) Return the reactor close to its original temperature for the next pour.

The optimal configuration was found to be a configuration of three channels in a staggered arrangement. The current two channel design tends to allow for a hot spot to develop in the upper corners of the reactor while over cooling the center to a temperature below the initial value. Using the optimized three channel configuration reactor allowed for the minimization of hot spots. Figure 2 gives the configurations of the optimized three channel design vs. the present two channel design.

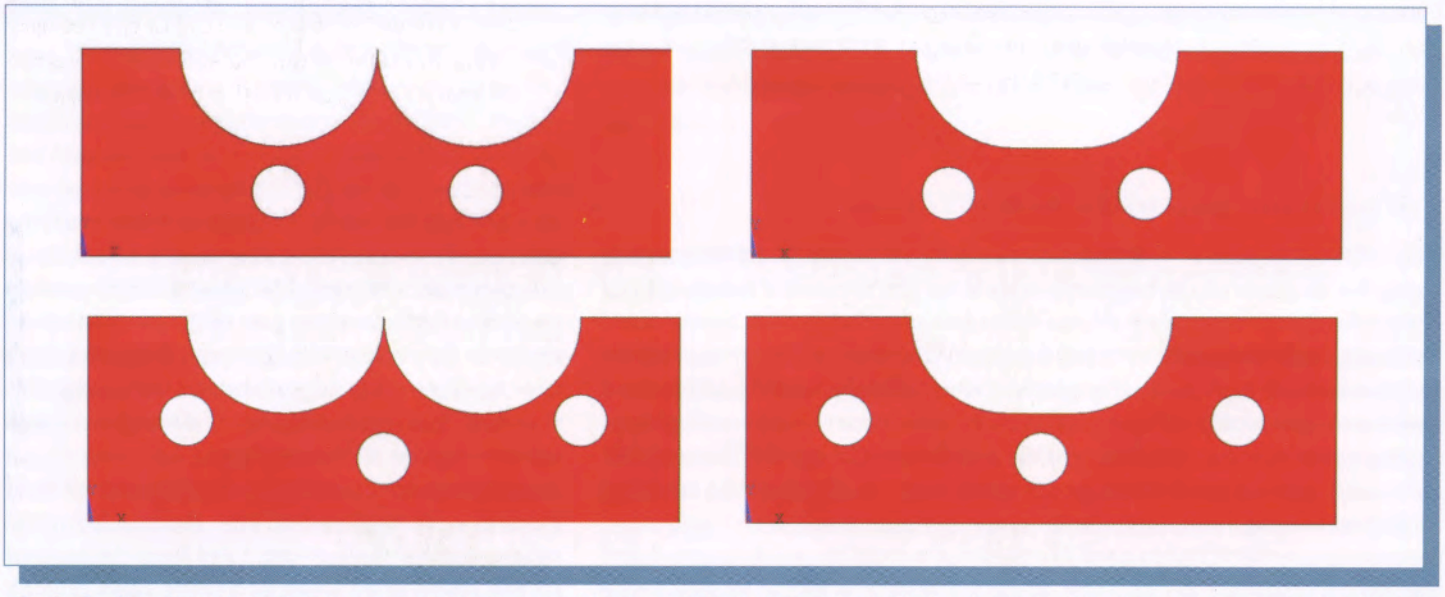

Fig. 2: Cooling channel configuration, current (two channels) and optimized (three channels); the picture on left shows upper part of the channel, and the one on right illustrates bottom part of the channel.

2. INDUSTRIAL APPLICATIONS:

As part of the campaign to optimize and scale up the CRP™ for industrial applications, we carried out several β trials at ACRC Consortium member facilities. One such trial was the application of the CRP™ to low temperature high pressure die casting (HPDC), and another trial was a marriage of the CRP™ and the Sub-Liquidus Casting (SLC™) process. This section gives some salient results obtained from the β trials.

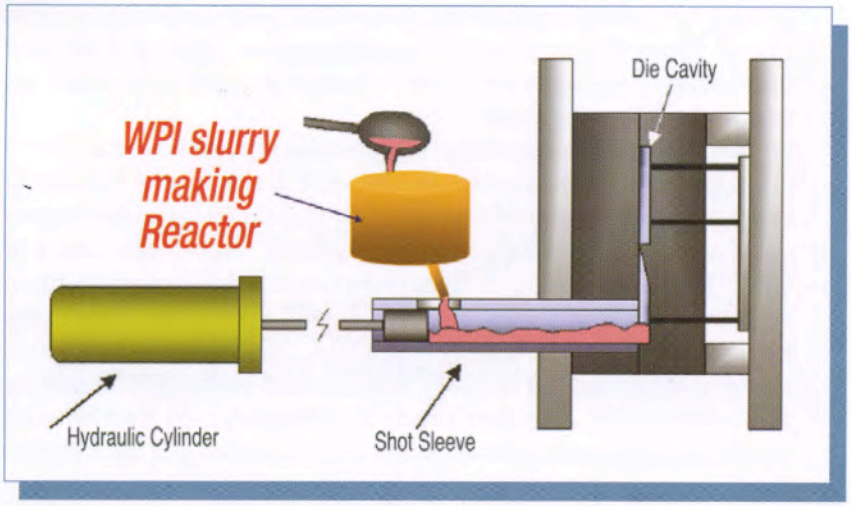

Fig. 3: CRP™ concept implemented within a typical die casting setting.

2.1 APPLICATION OF THE CRP™ TO LOW TEMPERATURE HPDC

As illustrated in Figure 3, the CRP™ reactor was mounted directly above the shot sleeve of a 840T Bühler die casting machine (Evolution 84 D). During each run, a dosing furnace was used to pump melt from the holding furnace to the inlet of the reactor; subsequently, the melt flowed through the reactor (where copious nucleation and mixing take place) and then into the shot sleeve. The slurry fraction solid can be adjusted by changing the temperature and flow rate of the cooling water.

Two different alloys were used in the trials: commercial 383 alloy, and a modified/optimized 383 alloy. For comparison, all CRP™ and conventional die castings (auto component; weighing 5.1 kg) were cast under the same conditions. The degassed alloy melt was transferred to the holding furnace, which was set at 650°C. The dosing furnace was employed to pump a constant volume of melt from the holding furnace either directly to the shot sleeve or to the inlet of the reactor. The melt then flowed through the reactor and then into the shot sleeve.

2.1.1 RESULTS AND ANALYSES

Experimental results show that CRP™ reactor can significantly shorten cycle time (thus process cost for mass production) due to the fact that the reactor can reduce the melt temperature by 50-80°C, depending on the cooling capacity applied. Moreover, microstructure analysis points out that compared to conventional liquid die castings, CRP™ processed castings have finer eutectic and smaller intermetallic phases, which is beneficial for casting quality. Given below are some typical microstructures obtained from various castings.

Figure 4 shows the microstructure of 383 alloy as a function of processing method (CRP™ vs. conventional HPDC). From Figure 4, one can see that:

- CRP™ processed castings have more primary alpha globules (SSM structure) than standard die castings. The fraction solid of the primary alpha phase is about 10%, and the average primary alpha particle size is about 40μm.

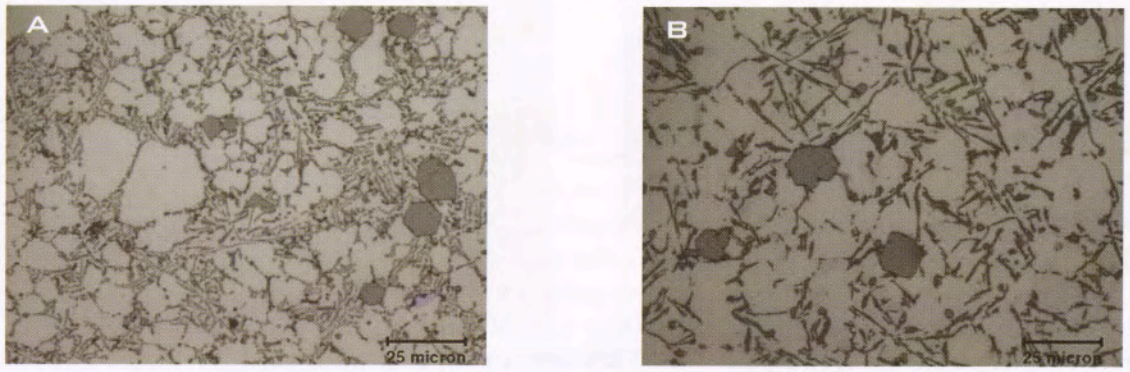

Fig. 4: Microstructures of CRP™ processed 383 castings (a) vs. HPDC 383 castings (b).

- The eutectic Si in the CRP™ processed castings is much finer than in conventional die castings. The reason is that for CRP™, the solidification journey starts from a semi-solid slurry (although the fraction solid of the slurry is low ~10%), where part of the solidification latent heat has already been released. Moreover, the solid α phase in the slurry can serve as a "reservoir" to absorb the heat released from the surrounding liquid during subsequent solidification, thus leading to a relatively high cooling rate. As a result, a finer eutectic is formed in CRP™ processed castings.
- Two types of Fe-bearing intermetallic phases are observed. One is needle-like β (AlFeSi) phase, and the other is polyhedral or star-like Fe-bearing phase. EDX analysis shows that the polyhedral or star-like Fe-bearing phase contains Al, Fe, Mn, Cr, Si, etc. Also, due to a relatively high cooling rate, smaller polyhedral crystals are seen in CRP™ processed castings. Image analysis points out that the size of Fe-bearing polyhedral crystals in CRP™ processed castings is in the range of 5-10μm vs. 10-18μm in conventional die castings.

To improve the SSM processability of 383 alloy, extensive thermodynamic simulations have been conducted to tailor/optimize 383 alloy composition to render the alloy SSM friendly. Specifically, we found that the content of Si and Ni has a significant effect on the SSM process window. Increasing Ni content or decreasing Si content can open up the process window remarkably. Detailed simulation results are given in Ref. [11]. Based on our simulation results, a modified 383 alloy was prepared and cast. Figure 5 shows the microstructure of CRP™ processed castings vs. conventional liquid high pressure die castings. It can be seen that:

- As found in 383, the CRP™ processed castings have much more primary alpha globules (SSM structure) than conventional liquid die castings. Image analysis shows that the fraction solid of the primary alpha phase in the CRP™ processed castings is about 25% with an average particle size of 35μm. Conventional die castings contain both globular and dendritic primary alpha phase. Some coarse primary alpha dendrites can be clearly seen in Figure 5(b).
- Observations on eutectic Si and intermetallic phases show that CRP™ processed castings have much finer eutectic Si and smaller Fe-bearing intermetallic phases than conventional die castings. Image analysis points out that the size of the Fe-bearing polydedral intermetallic phase in CRP™ processed castings falls in a range between 5-10μm vs. 10-20μm in conventional die castings. These observations further confirm the findings in 383 alloy.
- In addition, the modified 383 alloy shows a much better SSM formability than standard 383 alloy, particularly at a relatively high fraction solid range. Detailed experimental results are presented and discussed in Ref. [11].

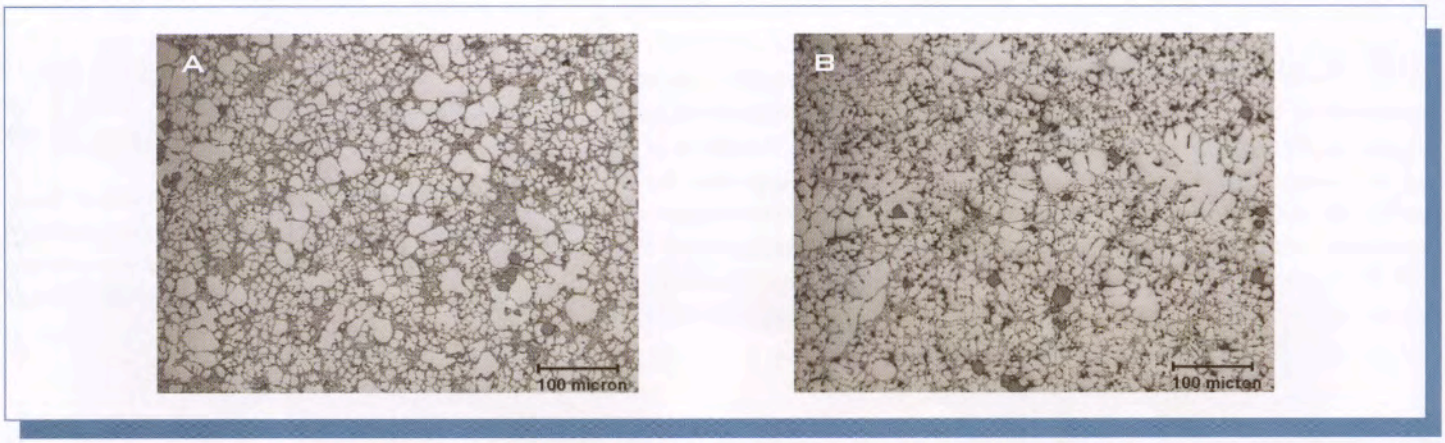

Fig. 5: Microstructures of modified 383 alloy castings processed via CRP™ (a) vs. HPDC (b).

2.2 A MARRIAGE OF THE CRP™ AND SLC™ PROCESSES

The Sub Liquidus Casting Process (SLC™) was introduced by THT Presses, Inc. in 2000, and was described at the NADCA congress in 2002 [12]. Unique features of the process include 1) a vertical shot orientation, 2) a shot diameter to depth ratio of at least two 3) a gate plate through which the rheocasting slurry passes into the die cavity and 4) a dovetail feature in the head of the piston to facilitate separating cast parts from biscuits during part ejection. For the SLC™ process, degassed, and *well-grain-refined* melt is introduced into the shot sleeve at a temperature only a few degrees above liquidus. The alpha phase initially forms as tiny rosette grains that then spheroidize and ripen into a globular slurry having a fraction solid of about 0.5 as it cools to near the eutectic temperature (for A356 alloy, approximately 575 °C). That slurry is then injected through the gate plate and into the die; the gate plate concept provides a universe of opportunities for positioning gates to minimize both flow distances and solidification shrinkage feeding distances. The large shot diameter, short

shot stroke feature and gate plate make the THT equipment well suited to a slurry form of semi-solid processing.

The CRP™ plus SLC™ was an attractive combination because SLC™ depends on excellent grain refinement of slurry for timely slurry development and CRP™, while easily *initiating* the desirable semi-solid globular alpha structure, depends on the casting process to actually form slurry of a significant fraction solid for injection into the die.

A CRP™ reactor (Figures 6) was adapted to use with a 400T press at THT in Dayton, OH. The reactor was fitted with rollers to facilitate movement into position to pour melt over it and into the shot sleeve of the casting machine, and then quickly retract it to allow closing the tool for casting.

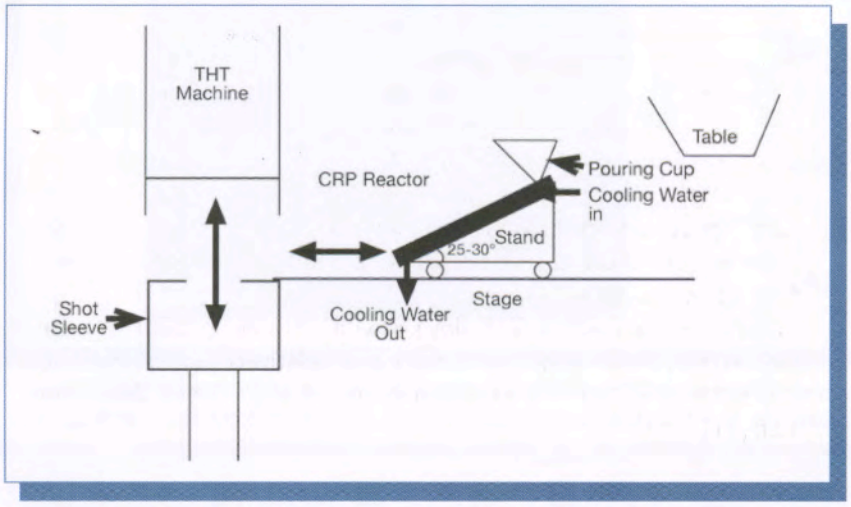

Fig. 6: Schematic of CRP™ reactor adapted to the THT casting machine.

The eight-cavity casting tool and resulting cast bars (re-assembled to a biscuit with gate posts to illustrate the gating scheme) are shown in Figure 7. The tool is H-13 steel. Each cavity has a single ingate measuring 1.61 cm^2, the area used when calculating gate flow velocities appropriate for semi-solid (2 m/s) versus squeeze casting (0.5 m/s).

A356 alloy for the trial was prepared by melting pure aluminum, and Al-Si, Al-Mg master alloys, so as to guarantee absence of any chemical grain refiner. Experimental procedures involved: 1) melting pure metals and master alloys (no grain refiners and no Sr modifiers), rotary degassing with Ar-0.5%Cl and adjusting temperature of the melt to 640-660 °C; 2) pouring melt over the CRP™ reactor and into the shot sleeve of the THT machine; 3) withdrawing CRP™ unit, and closing the tool and making the shot. The total seconds from pouring melt over the CRP™ reactor to achieve a slurry fraction solid between 0.4 and 0.5 was about 27 seconds. For the squeeze casting variation, melt was ladled directly into the shot sleeve and the die was closed and the shot made in the shortest possible time (~ 7 seconds). A second set of experiments was repeated after adding 150ppm Sr to the melt for eutectic modification.

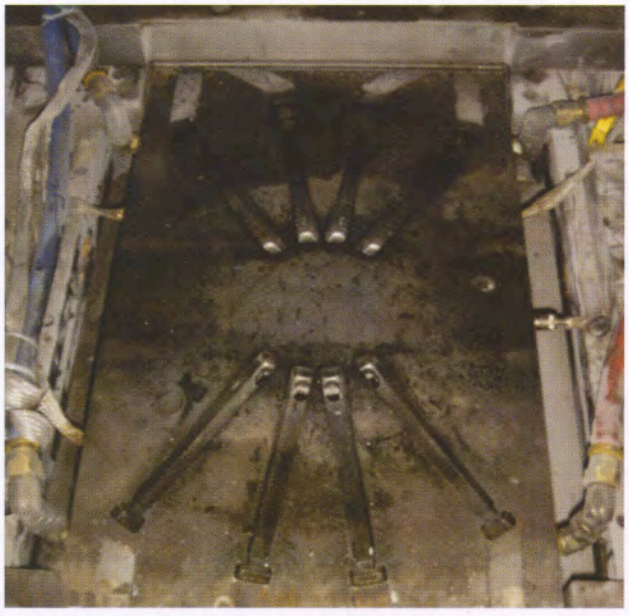

Fig. 7: Photo of the tool (an 8-cavity rectangular bar die) and actual casting with gate posts and ingates.

Tensile properties of the A356 alloy were evaluated after heat treatment both in T5 and T6 conditions. The heat treatment for T6 was: solutionized at 540 °C/4 hrs, and aged at 170 °C/4 hrs in a conventional furnace; the T5 treatment consisted of aging at 170 °C/4 hrs.

Figure 8 gives typical microstructures of CRP™/SLC™ processed castings vs. liquid squeeze castings. It can seen that the CRP™/SLC™ castings have a fine and uniform globular alpha structure, whereas liquid squeeze castings from the same melt show a (albeit mixed coarse and fine) dendritic structure. The mixed coarse and fine dendrites in the squeeze casting are likely a result of the minimum time required to shuttle the lower die into position, close the tool and inject metal (about 7 seconds in total) being sufficient to allow partial solidification to take place in the shot sleeve (relatively slow solidification) while the balance takes place in the die (very rapid solidification).

Figure 9 illustrates the effect of Sr modification on the microstructures of

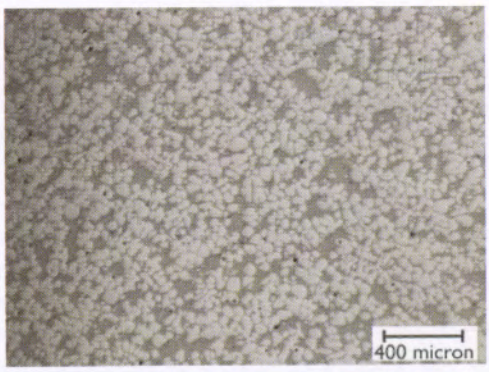

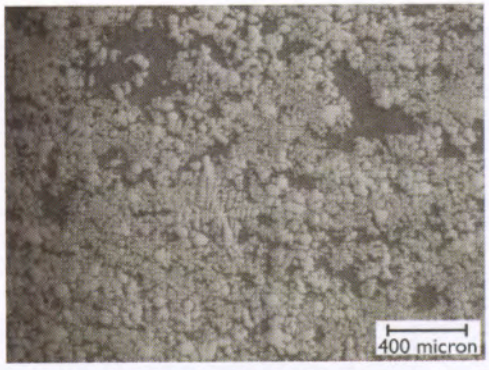

Fig. 8: A356 alloy with no chemical grain refinement and no Sr-modification, SLC™ cast after passing melt over the CRP™ reactor (left) versus liquid squeeze cast without use of the CRP™ reactor (right); note the very fine globular structures, a result of the CRP™ reactor + development of a high fraction solid during SLC™ casting versus the mixed alpha coarse cells and tiny dendrites in the squeeze casting..

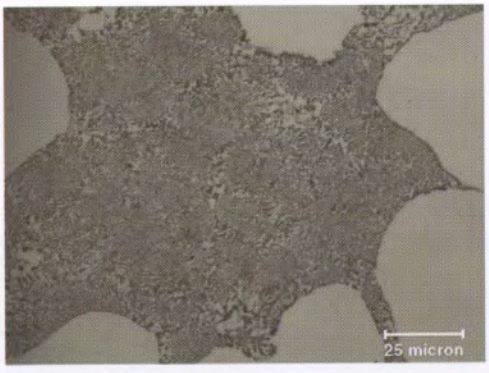

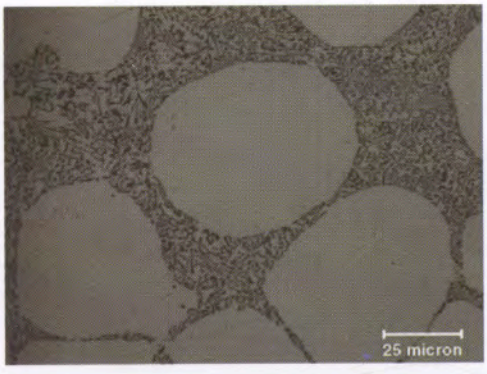

Fig. 9: Comparing Sr-modified CRP™/SLC™ cast Al-Si eutectic structure (left) to that of un-modified eutectic (right). Although the Sr-modified eutectic is somewhat finer, CRP™/SLC™ processing itself provides a fine eutectic even without modification.

CRP™/SLC™ processed castings vs. liquid squeeze castings. It is quite clear that Sr modification has little influence on the morphology and fineness of CRP™/SLC™ rheocast Al-Si eutectic (semi-solid processing alone results in a fine eutectic structure, without need for Sr modification). The liquid squeeze casting from the same melts, on the other hand, benefited significantly from Sr modification. Resulting tensile properties are summarized in Figure 10. There are several notable trends:

- A356 CRP™/SLC™ castings have slightly higher strength and ductility than liquid squeeze castings.
- Sr modification does not show significant influence on mechanical properties of A356 CRP™/SLC™ castings; however it does show noticeable effect on mechanical properties of A356 liquid squeeze castings. Sr modification improves mechanical properties of liquid squeeze castings (particularly ductility) to some extent.

Contrary to previous findings regarding SLC™ and other semi-solid casting

routes [9], there is a certain amount of ductility loss for T-5 heat treated castings as compared to F temper.

In summary, the CRP™ can provide the copious nucleation needed for SLC™ slurry to develop in a timely manner, and SLC™ has provided the means for CRP™ to evolve from mere nuclei to ideal semi-solid slurry. The combination of CRP™ and SLC™ has worked well to produce excellent globular alpha phase together with a fine and uniform Al-Si eutectic. The β trial has proven that the CRP™/SLC™ combination is a valuable marriage of two unique processes.

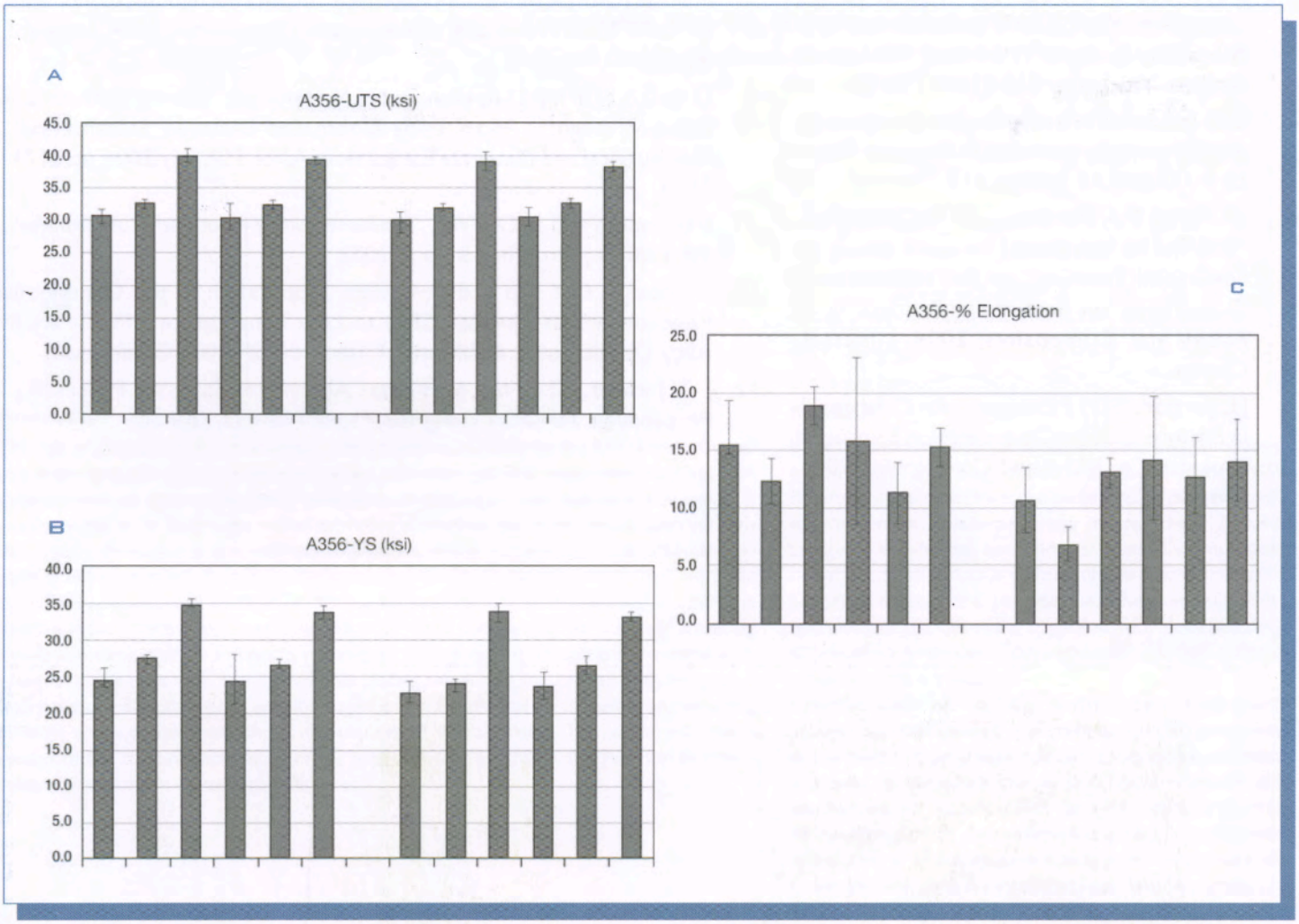

Fig. 10: Comparing mechanical properties of A356 castings processed via CRP™/SLC™ vs. liquid squeeze cast under F, T5 and T6 conditions.

CONCLUDING REMARKS

The CRP™ has been scaled up successfully for industrial applications. Numerous industrial β trials point out that the optimized CRP™ reactor can easily retrofit most die casting facilities to make SSM parts. The simplicity, robustness, as well as the low cost nature of the CRP™ makes the process commercially viable for semi-solid processing.

REFERENCES

1. DOE Report number DE-FC07-98ID13618
2. M.C. Flemings, "Semi-Solid Processing – The Rheocasting Story", Test Tube to Factory Floor: Implementing Technical Innovations, from the Proceedings of the Spring Symposium May 22, 2002 published by Metal Processing Institute, Worcester Polytechnic Institute, Worcester MA 01609 (2003).
3. UBE Industries Ltd., *Method and apparatus for shaping semisolid materials*, in *European Patent EP 0 745 694 A1*. 1996. p. 117.
4. J.A. Yurko, R.A. Martinez, and M.C. Flemings, "SSR™: The Spheroidal Growth Route to Semi-Solid Forming", in 8th International Conference on Semi-Solid Processing of Alloys and Composites, 2004, Limassol, Cyprus.
5. J.L. Jorstad, "SSM Processes - An Overview", in 8th International Conference on Semi-Solid Processing of Alloys and Composities, 2004, Limassol, Cyprus.
6. D. Doutre, J. Langlais, and S. Roy, "The SEED Process for Semi-Solid Forming", in 8th International Conference on Semi-Solid Processing of Alloys and Composites, 2004, Limassol, Cyprus.
7. M. Findon, *"Semi-Solid Slurry Formation via Liquid Metal Mixing"*, M.Sc., Thesis, Worcester Polytechnic Institute, 2003.
8. Q.Y. Pan, M. Findon, and D. Apelian, "The Continuous Rheoconversion Process (CRP): A Novel SSM Approach", in 8th International Conference on Semi-Solid Processing of Alloys and Composites, 2004, Limassol, Cyprus.
9. D. Saha, S. Shankar, D. Apelian, and M.M. Makhlouf, "Casting of Aluminum Based Wrought Alloys using Controlled Diffusion Solidification", Metallurgical and Materials Transactions A, Vol. 35A, July 2004, pp. 2174-2180.
10. F. Incropera and D. DeWitt, *"Fundamentals of Heat and Mass Transfer"*, 5th Edition. John Wiley & Sons, 2002.
11. S. Wiesner, Q.Y. Pan and D. Apelian, "Application of the Continuous Rheoconversion Process (CRP) to Low Temperature HPDC-Part II: Alloy Development & Validation", (the 9th S2P 2006 Conference).
12. J. L. Jorstad, "SLC, the Low-Cost Alternative for SSM Processing" Proceedings, NADCA Congress, Paper T02-052, (2002).

Solid State Phenomena Vols. 116-117 (2006) pp 402-405
Online available since 2006/Oct/15 at www.scientific.net

doi:10.4028/www.scientific.net/SSP.116-117.402

Application of the Continuous Rheoconversion Process (CRP) to Low Temperature HPDC-Part I: Microstructure

Qingue Pan[1,a], Stuart Wiesner[2,b] and Diran Apelian[1,c]

[1]Advanced Casting Research Center (ACRC), Metal Processing Institute (MPI), WPI, Worcester, MA 01609, USA

[2]Bühler Druckguss AG CH-9240, Uzwil, Switzerland

[a]qypan@wpi.edu, [b]stuart.wiesner@buhlergroup.com, [c]dapelian@wpi.edu

Keywords: Semi-Solid Processing, The Continuous Rheoconversion Process, Microstructure

Abstract: The continuous rheoconversion process (CRP) is a novel slurry-on-demand process that was developed at MPI/WPI in 2002. The process is based on a passive liquid mixing technique in which the nucleation and growth of the primary phase are controlled using a specially designed "reactor". The reactor provides heat extraction, copious nucleation, and forced convection during the initial stage of solidification, thus leading to the formation of globular structures. This paper presents our recent work on the scale-up of the CRP for industrial applications. Specifically, we demonstrate an important application of the CRP to low temperature (low fraction solid) HPDC. In Part I of this paper, we present salient results on microstructural characterization of CRP processed castings vs. conventional die castings.

Introduction

Semi-solid metal (SSM) processing has emerged as a preferred manufacturing method due to the superior quality associated with semi-solid castings. In recent years, the driving force to reduce process cost has necessitated the development of new rheocasting (also termed slurry-on-demand) processes. The continuous rheoconversion process (CRP) is a novel, low-cost rheocasting process that was developed at MPI/WPI in 2002 [1-3]. The process is based on a passive liquid mixing technique in which the nucleation and growth of the primary phase are controlled using a specially designed "reactor". The reactor provides heat extraction, copious nucleation, and forced convection during the initial stage of solidification, thus leading to the formation of globular structures. Experimental results with various commercial aluminium alloys indicated that the CRP is highly effective for the manufacture of high quality semi-solid feedstock [1-3]. Other advantages include process simplicity, a wide process window, and the feasibility of recycling scrap metal within the process flowstream, etc.

Recently the CRP has been scaled up for industrial applications. To retrofit most die casting facilities, the reactor has been optimized and simplified in such a way that only one melt is involved wherein both nucleation and mixing takes place simultaneously within the reactor. Moreover, to enhance the control of melt nucleation and to conveniently adjust slurry fraction solid, an optimized cooling system is incorporated into the reactor (as illustrated in Figure 1). This paper demonstrates an important application of the CRP to low temperature (low fraction solid) HPDC. In Part I, we present salient results on characterizing the microstructure of various CRP processed castings vs. conventional liquid die castings. In Part II, we present alloy optimization results obtained through thermodynamic simulations, as well as validation of the results via industrial Beta trials.

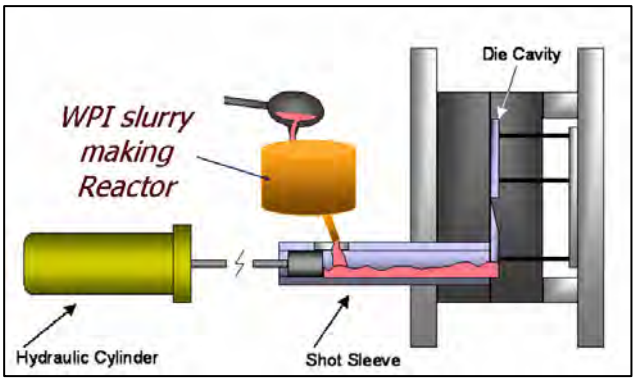

Figure 1: CRP concept implemented within a typical die casting setting.

Experimental

Materials: Two different alloys were used in this study: commercial 383 alloy, and a modified/optimized 383 alloy.

Die/Casting: Two different types of castings weighing 900 g and 5.1 kg, respectively were chosen for the experiments. The 900g casting was obtained using a so called "fluidity die", which was designed for die filling studies. The snake-like die has a thickness of 8 mm near the gate, and the thickness decreases step by step to 1 mm near the vents. The thickness of the gate is 2 mm. The other casting weighing 5.1 kg was an auto component.

CRP Reactor: The CRP reactor was mounted right above the shot sleeve of a 840T Bühler die casting machine (Evolution 84 D). During each run, a dosing furnace was used to pump melt from the holding furnace to the inlet of the reactor; subsequently, the melt flowed through the reactor (where copious nucleation and mixing takes place) and then into the shot sleeve. The slurry fraction solid can be adjusted by changing the temperature and flow rate of the cooling water.

Die Casting Operation: For comparison, all CRP and conventional die castings were cast under the same conditions. The degassed alloy melt was transferred to the holding furnace, which was set at 650°C. The dosing furnace was employed to pump a constant volume of melt from the holding furnace either directly to the shot sleeve or to the inlet of the reactor. The melt then flowed through the reactor and then into the shot sleeve.

Microstructure Characterization: All metallographic samples were prepared using standard procedures. Microstructure characterization was performed using optical microscopy, image analysis (microGOP2000/S) and SEM. To reveal microstructural details, images with different magnifications were taken for all samples examined.

Results and Analyses

In this section, we compare various microstructures of CRP processed castings with those that were conventionally die cast with liquid metal.

383 Alloy

Figure 2 shows the microstructure of 383 alloy as a function of processing method (CRP vs. conventional HPDC). From Figure 2, one can see that

- CRP processed castings have more primary alpha globules (SSM structure) than standard die castings. The fraction solid of the primary alpha phase is about 10%, and the average primary alpha particle size is about 40μm.

- The eutectic Si in the CRP processed castings is much finer than in conventional die castings. The reason is that for CRP, the solidification journey starts from a semi-solid slurry (although the fraction solid of the slurry is low ~10%), where part of the solidification latent heat has already been released. Moreover, the solid α phase in the slurry can serve as a "reservoir" to absorb the heat released from the surrounding liquid during subsequent solidification, thus leading to a relatively high cooling rate. As a result, a finer eutectic is formed in CRP processed castings.

- Two types of Fe-bearing intermetallic phases are observed. One is needle-like β (AlFeSi) phase, and the other is polyhedral or star-like Fe-bearing phase. EDX analysis shows that the polyhedral or star-like Fe-bearing phase contains Al, Fe, Mn, Cr, Si, etc. Also, due to a relatively high cooling rate, smaller polyhedral crystals are seen in CRP processed castings. Image analysis points out that the size of Fe-bearing polyhedral crystals in CRP processed castings is in the range of 5-10μm vs. 10-18μm in conventional die castings.

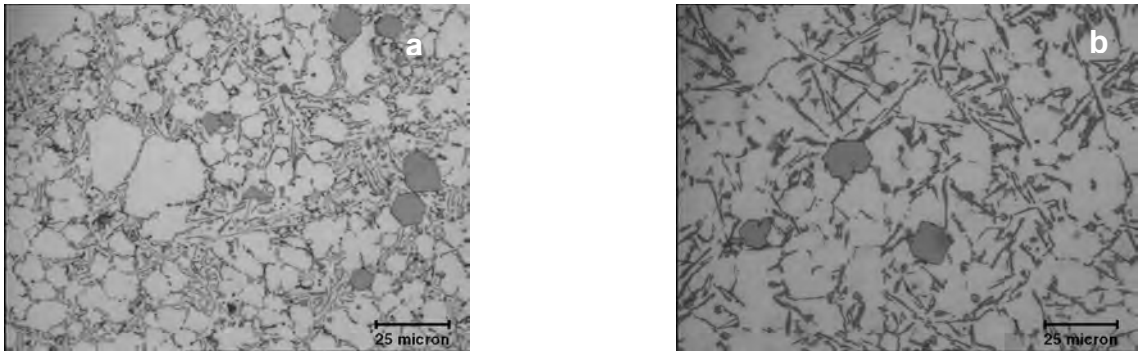

Figure 2: Microstructures of CRP processed 383 castings (a) vs. HPDC 383 castings (b).

Modified 383 Alloy

To improve the SSM processability of 383 alloy, extensive thermodynamic simulations have been conducted to tailor/optimize 383 alloy composition to render the alloy SSM friendly. Specifically, we found that the content of Si and Ni has a significant effect on the SSM process window. Increasing Ni content or decreasing Si content can open up the process window remarkably. Detailed simulation results are given in Part II of this paper [4]. Based on our simulation results, a modified 383 alloy was made. Figure 3 gives the microstructure of CRP processed castings vs. conventional liquid die castings. It can be seen that:

- As found in 383, the CRP processed castings have much more primary alpha globules (SSM structure) than conventional liquid die castings. Image analysis shows that the fraction solid of the primary alpha phase in the CRP processed castings is about 25% with an average particle size of 35μm. Conventional die castings contain both globular and dendritic primary alpha phase. Some coarse primary alpha dendrites can be clearly seen in Figure 3(b).

- Observations on eutectic Si and intermetallic phases show that CRP processed castings have much finer eutectic Si and smaller Fe-bearing intermetallic phases than conventional die

castings. Image analysis points out that the size of the Fe-bearing polydedral intermetallic phase in CRP processed castings falls in a range between 5-10μm vs. 10-20μm in conventional die castings. These observations further confirm the findings in 383 alloy.

- In addition, the modified 383 alloy shows a much better SSM formability than standard 383 alloy, particularly at a relatively high fraction solid range. Detailed experimental results are presented and discussed in the companion paper (Part II) [4].

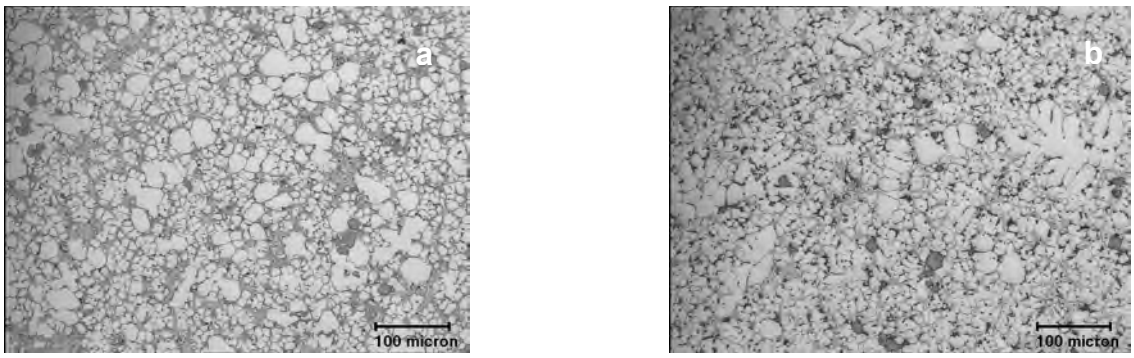

Figure 3: Microstructures of modified 383 alloy castings processed via CRP (a) vs. HPDC (b).

Concluding Remarks

This paper has demonstrated an important application of CRP to low temperature (low fraction solid) HPDC. Microstructure analysis points out that as compared to conventional liquid die castings, CRP processed castings have finer eutectic and smaller intermetallic phases, which is beneficial for casting quality. The simplicity as well as the flexibility of the CRP makes the process commercially viable for semi-solid processing.

References

[1] D. Apelian et al.: Energy Efficient Near-net Shape Manufacturing: semi-solid processing routes, in the Proceedings of The MPMD Fourth Global Innovations Symposium: Energy Efficient Manufacturing Processes, Edited by I. Anderson, T. Marechaux, and C. Cockrill, published by TMS (The Minerals, Metals & Materials Society, 2003), pp. 55-62

[2] M. Findon: Semi-Solid Slurry Formation via Liquid Metal Mixing, M.Sc. Thesis, Worcester Polytechnic Institute (2003)

[3] Q.Y. Pan, M. Findon and D. Apelian: The Continuous Rheoconversion Process (CRP): A Novel SSM Approach, in the Proceedings of the Eighth International Conference on Semi-Solid Processing of Metals and Alloys, Limasol, Cyprus, September 2004 (published by NADCA, Wheeling, Illinois)

[4] S. Wiesner, Q.Y. Pan and D. Apelian: Application of the Continuous Rheoconversion Process (CRP) to Low Temperature HPDC-Part II: Alloy Development & Validation (the 9th S2P 2006 Conference)

Semi-Solid Processing of Alloys and Composites
10.4028/www.scientific.net/SSP.116-117

Application of the Continuous Rheoconversion Process (CRP) to Low Temperature HPDC-Part I: Microstructure

10.4028/www.scientific.net/SSP.116-117.402

DOI References

[4] S. Wiesner, Q.Y. Pan and D. Apelian: Application of the Continuous Rheoconversion Process (CRP) to Low Temperature HPDC-Part II: Alloy Development & Validation (the 9 th S2P 2006 Conference)
doi:10.4028/www.scientific.net/SSP.116-117.64

THE CONTINUOUS RHEOCONVERSION PROCESS (CRP™)

Q.Y. Pan, P. Hogan, D. Apelian, and M.M.Makhlouf

Advanced Casting Research Center (ACRC)
Metal Processing Institute (MPI)
WPI, Worcester, MA 01609 USA

Abstract

Semi-solid metal (SSM) processing has emerged as a preferred manufacturing scheme due to the superior quality associated with semi-solid castings. In recent years, the driving force to reduce process cost requires the development of robust, commercially viable rheocasting (also termed slurry-on-demand (SoD)) processes. The continuous rheoconversion process (CRP™) is a novel SoD process that was developed at MPI/WPI. The process is based on a passive liquid mixing technique in which the nucleation and growth of the primary phase are controlled using a specially designed "reactor". The reactor provides heat extraction, copious nucleation, and forced convection during the initial stage of solidification, thus leading to the formation of globular structures. This paper gives an overview regarding the development of the CRP™. Specifically, critical issues of optimizing and simplifying the process for commercial applications are discussed. Salient results from several industrial trials that have been carried out with Consortium Members of our casting consortium (ACRC) are reviewed.

Keywords: Semi-solid processing; the Continuous Rheoconversion Process (CRP™); Industrial application.

Introduction

Semi-solid metal (SSM) processing has emerged as an attractive method for near-net-shape manufacturing due to the distinct advantages it holds over conventional near-net-shape forming technologies. These advantages include lower cycle time, increased die life, reduced porosity, reduced solidification shrinkage, improved mechanical properties, etc. SSM processing techniques can not only produce the complex dimensional details (e.g. thin-walled sections) associated with conventional high-pressure die castings, but also can produce high integrity castings currently attainable only with squeeze and low-pressure permanent mold casting processes. There are two primary semi-solid processing routes, (a) thixocasting and (b) rheocasting. In the thixocasting route, one starts from a non-dendritic solid precursor material that is specially prepared by a primary aluminum manufacturer, using continuous casting methods. Upon reheating this material into the mushy (a.k.a. "two-phase") zone, a thixotropic slurry is formed, which becomes the feed for the casting operation. In the rheocasting route (a.k.a. "slurry-on-demand" or "SoD"), one starts from the liquid state, and the thixotropic slurry is formed directly from the melt via careful thermal management of the system; the slurry is subsequently fed into the die cavity. Of these two routes, rheocasting is favored in that there is no premium added to the billet cost, and the scrap recycling issues are alleviated

In the early days of SSM development, it was thought that one had to cool the liquid down into the two-phase region, and to shear off and break the dendrites (i.e. melt agitation via mechanical or, later on, magnetohydrodynamic [MHD] stirring) and thus producing a slurry. However, during the last few years, work sponsored at ACRC/MPI by the Department of Energy [1], as well as work by the research team at MIT [2] led to the discovery that one did not need to break off dendrites to produce the semi-solid structure of globular primary alpha phase. Instead, if the temperature of the melt was such that one could produce many nuclei ("copious nucleation"), and if the nuclei did not grow past a certain point (i.e. suppression of dendritic growth), nor melt back into the bulk liquid, then one could produce a slurry with the ideal semi-solid structure directly from the melt. This concept is the genesis of commercial processes and methodologies to generate semi-solid slurries from the liquid state. The concept relies on

controlled nucleation and growth, as opposed to the previous theory, in which a dendritic structure is modified into a globular structure via shear forces.

The driving force to reduce process cost has led to the development of several rheocasting (also termed slurry-on-demand) processes. These include UBE's New Rheocasting (NRC) [3], Idra-Prince's Semi-Solid Rheocasting (SSR) [4], THT Presses' Sub-Liquidus Casting (SLCTM) [5], and Alcan's Swirl Enthalpy Equilibration Device (SEED) [6], as well as the Continuous Rheoconversion Process (CRP^{TM}) [7, 8], developed by ACRC/MPI.

The CRP^{TM} is a process where the molten metal flows through a reactor prior to casting. The role of the reactor is to ensure that copious nucleation takes place and that the nuclei are well distributed throughout the system prior to entering the casting cavity. The CRP^{TM} has been successfully applied in hyper-eutectic Al-Si alloys (i.e., 390 alloy) where two liquids of equal or different compositions and temperatures are mixed in the reactor and creating a SSM slurry [9]. The process has been mostly used for hypo-eutectic Al-Si alloys (i.e., 356, 357, etc.) where a single melt passes through the reactor. In addition, the CRP^{TM} was designed to be flexible for thixocasting or rheocasting applications as well as batch or continuous casting. Variable heat extraction rates can be obtained by controlling either the superheat of the melt, the temperature of the channel system, or the temperature of the reactor.

The work of Findon [7] demonstrated that the CRP^{TM} is a robust process, which can consistently generate near-ideal semi-solid structures for grain refined and non-grain refined A356 type alloys within a large process window. The recent work of Pan and Findon [8] has shown that the CRP^{TM} is also highly effective for the manufacture of high quality semi-solid feedstock of other commercial alloy systems, including hypereutectic aluminum-silicon (390), aluminum-copper (A206), wrought aluminum alloys, as well as Mg alloys.

The CRP^{TM} has shown great potential for commercial applications. In order to optimize/scale-up the CRP^{TM} for use by industry, several questions/challenges still remain such as:

- What is the optimal design for the reactor?
- How critical is the heat extraction/forced convection in the formation of SSM structures? and furthermore
- How to retrofit most existing die casting facilities?

These questions/challenges are the theme of this work. In this paper, we present our recent work on the optimization of the CRP^{TM} for industrial applications.

1 Optimization of the CRP^{TM} Reactor Design

To retrofit most die casting facilities, the CRP^{TM} reactor has been simplified in such a way that only one melt is involved wherein both nucleation and mixing takes place simultaneously within the reactor. Moreover, to enhance the control of melt nucleation and to conveniently adjust slurry fraction solid, a cooling system is incorporated into the reactor. Based on experimental data generated from preliminary trials, finite element and finite volume models were created in order to optimize the CRP^{TM} reactor design. Some salient results from the modeling effort are briefly described in this section.

1.1 Fluid Flow Optimization

Finite volume models were created and analyzed in commercially available FLUENT software in order to study the flow conditions and patterns in the reactor. Past and current successful designs were modeled in an effort to identify the critical aspects of the flow of the molten metal, and to optimize the reactor design. The optimization efforts were intended to result in new reactor designs which would incorporate the critical flow parameters but eliminate any excess features or flow disorder which inhibited the ease of introduction into industrial settings.

Three-dimensional models of the reactors were created in Pro/Engineer software and meshed with 4 node tetrahedral elements in GAMBIT, meshing software which is included with Fluent. The solver was formulated to use the well known SIMPLE pressure-velocity coupling along with the standard κ-ε turbulence model.

Figure 1 displays visual outputs of the turbulence intensity values in two reactor designs. Analysis of the various reactors

revealed that the current reactor induces less turbulence than several past designs, and is effective in producing SSM structures as previous reactors. Therefore, further efforts focus on the optimization of the cooling system and some potential issues found from the preliminary trials, such as the possibility of splashing of the melt or trapping of gases upon pouring.

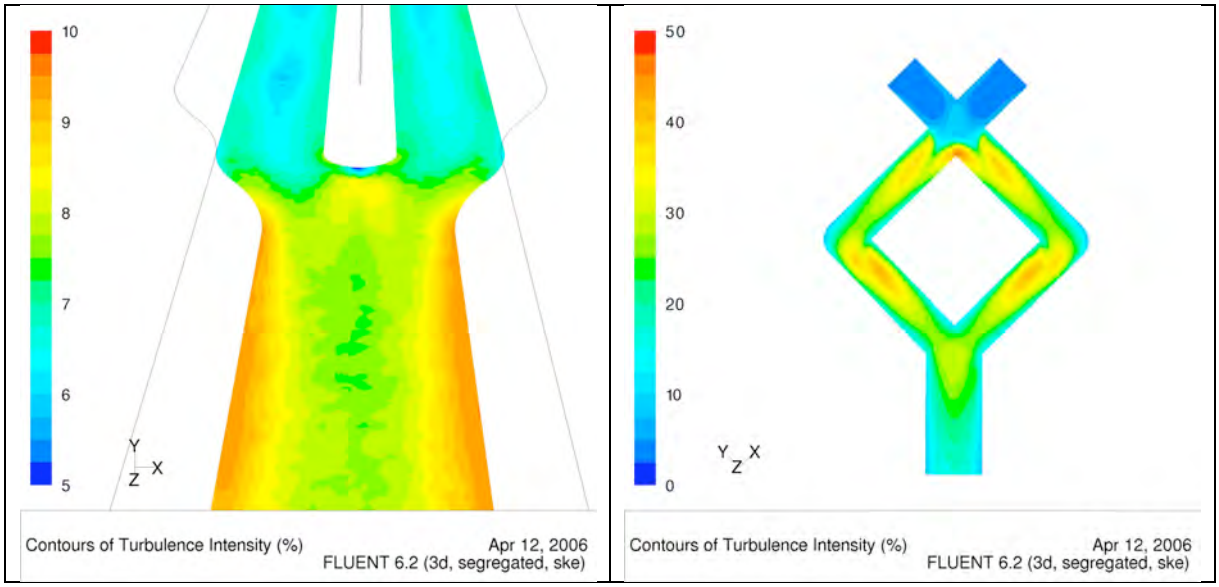

Figure 1: Levels of turbulence intensity generated by CRP™ reactors. Current design (left) and past design (right). Note the differing scales.

1.2 Cooling Channel Optimization

The cooling system of the reactor, consisting of water channels running along the long axis of the reactor, is critical for the successful functioning of the reactor. Moreover, nearly the same amount of enthalpy must be extracted from the melt with each subsequent pour. The cooling channels must be able to extract heat from the reactor in a manner that will allow for a stable temperature profile throughout the reactor over a period of time during which castings are being made. The letter "C" in CRP™ stands for *continuous*, and to have a robust process, the above factors must be attended to and addressed.

Two separate two-dimensional finite element models were created and meshed in commercially available ANSYS software in order to determine the optimal configuration of cooling channels in the reactor. The first cross-section was taken in the upper region of the reactor, where the melt is poured, and where there are two flow channels. The second cross-section was taken in the lower region of the reactor, where the two flow channels converge into one, with the convergence acting as a means to homogenize the melt. The best configuration should work well in both regions of the reactor.

Convection coefficients for the transfer of heat from the flowing melt to the reactor, from the reactor to the cooling water, and from the reactor to the ambient air were estimated used Nusselt correlations for the relevant flow regimes. These coefficients are quantified in Table 1. Contact time between the melt and the reactor was estimated to be 10 seconds, with a length of time from 1 to 2 minutes between each pour.

A measure for quantifying the success of each channel configuration and conditions was created in order to determine the optimal conditions in an objective fashion. The temperature at the surface of the flow channel in the reactor was monitored at three locations: At the bottom of the flow channel, at the highest point on the flow channel which is in contact with the melt, and at a point in the middle of these two locations. Melt does not entirely fill the channels during each pour however. For the purposes of the study, the assumption was made that only the bottom third of the channel was full of metal. This means that although the flow channels have a radius of 0.75", the depth of the flowing metal was assumed to be 0.25". This affected the amount of reactor surface in contact with the flowing melt, and therefore the amount of heat

extracted.

Table 1: Heat transfer coefficients used in cooling channel optimization.

Flow Regime	h (W/m^2-K)
Melt to Reactor (Upper Region)	25,000
Melt to Reactor (Lower Region)	27,750
Reactor to Cooling Water	Variable depending on flow rate, channel diameter. Dittus-Boelter correlation used.
Reactor to Air	5 [10]

At each point in time during the 1-2 minutes between pours, the average temperature of the three points was calculated, as well as the maximum difference between the temperatures at any of the three points. The conditions for optimized configuration of cooling channels are as follows.

1) Minimize the difference in temperature between any two points during the cooling cycle. Initial exploratory simulations found that any temperature gradient present after a single pour will become more severe as subsequent cycles have passed.
2) Return the reactor close to its original temperature for the next pour.

The optimal configuration was found to be a configuration of three channels in a staggered arrangement. The current two channel design tends to allow for a hot spot to develop in the upper corners of the reactor while over cooling the center to a temperature below the initial value. Using the optimized three channel configuration reactor allowed for the minimization of hot spots. Figure 2 gives the configurations of the optimized three channel design vs. the present two channel design.

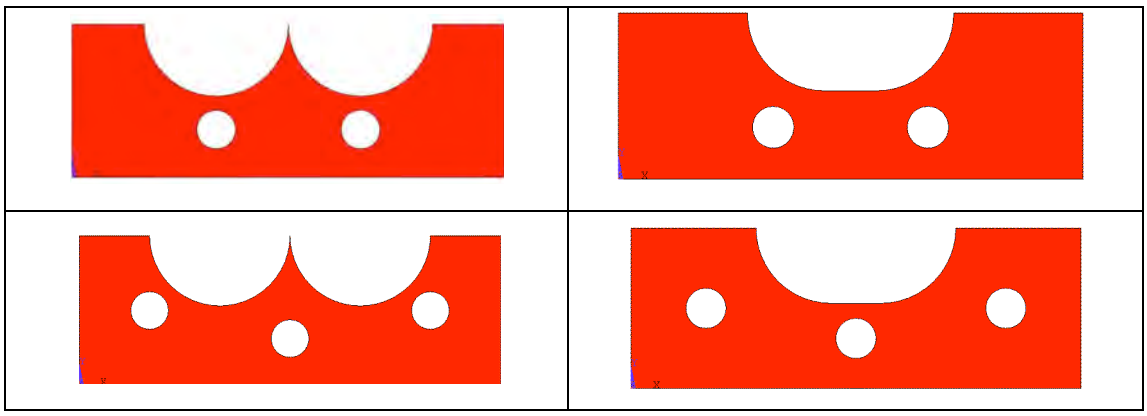

Figure 2: Cooling channel configuration, current (two channels) and optimized (three channels); the picture on left shows upper part of the channel, and the one on right illustrates bottom part of the channel.

2 Industrial Applications:

As part of the campaign to optimize and scale up the CRP™ for industrial applications, we carried out several Beta trials at ACRC Consortium member facilities. One such trial was the application of the CRP™ to low temperature high pressure die casting (HPDC), and another trial was a marriage of the CRP™ and the Sub-Liquidus Casting (SLC™) process. This section gives some salient results obtained from these trials.

2.1 Application of the CRP™ to Low Temperature HPDC

As illustrated in Figure 3, the CRP™ reactor was mounted directly above the shot sleeve of a 840T Bühler die casting machine (Evolution 84 D). During each run, a dosing furnace was used to pump melt from the holding furnace to the inlet of the reactor; subsequently, the melt flowed through the reactor (where copious nucleation and mixing takes place) and then into the shot sleeve. The slurry fraction solid can be adjusted by changing the temperature and flow rate of the cooling water.

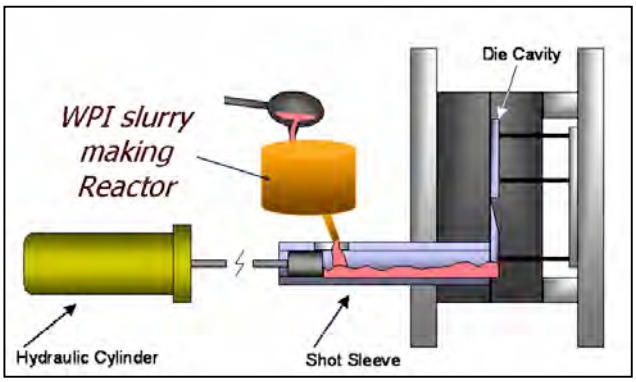

Figure 3: CRP™ concept implemented within a typical die casting setting.

Two different alloys were used in the trials: commercial 383 alloy, and a modified/optimized 383 alloy. For comparison, all CRP™ and conventional die castings (auto component; weighing 5.1 kg) were cast under the same conditions. The degassed alloy melt was transferred to the holding furnace, which was set at 650°C. The dosing furnace was employed to pump a constant volume of melt from the holding furnace either directly to the shot sleeve or to the inlet of the reactor. The melt then flowed through the reactor and then into the shot sleeve.

2.1.1 Results and Analyses

Experimental results show that CRP™ reactor can significantly shorten cycle time (thus process cost for mass production) due to the fact that the reactor can reduce the melt temperature by 50-80°C, depending on the cooling capacity applied. Moreover, microstructure analysis points out that compared to conventional liquid die castings, CRP™ processed castings have finer eutectic and smaller intermetallic phases, which is beneficial for casting quality. Given below are some typical microstructures obtained from various castings.

Figure 4 shows the microstructure of 383 alloy as a function of processing method (CRP™ vs. conventional HPDC). From Figure 4, one can see that:

- CRP™ processed castings have more primary alpha globules (SSM structure) than standard die castings. The fraction solid of the primary alpha phase is about 10%, and the average primary alpha particle size is about 40μm.

- The eutectic Si in the CRP™ processed castings is much finer than in conventional die castings. The reason is that for CRP™, the solidification journey starts from a semi-solid slurry (although the fraction solid of the slurry is low ~10%), where part of the solidification latent heat has already been released. Moreover, the solid α phase in the slurry can serve as a "reservoir" to absorb the heat released from the surrounding liquid during subsequent solidification, thus leading to a relatively high cooling rate. As a result, a finer eutectic is formed in CRP™ processed castings.

- Two types of Fe-bearing intermetallic phases are observed. One is needle-like β (AlFeSi) phase, and the other is polyhedral or star-like Fe-bearing phase. EDX analysis shows that the polyhedral or star-like Fe-bearing phase contains Al, Fe, Mn, Cr, Si, etc. Also, due to a relatively high cooling

rate, smaller polyhedral crystals are seen in CRP^{TM} processed castings. Image analysis points out that the size of Fe-bearing polyhedral crystals in CRP^{TM} processed castings is in the range of 5-10μm vs. 10-18μm in conventional die castings.

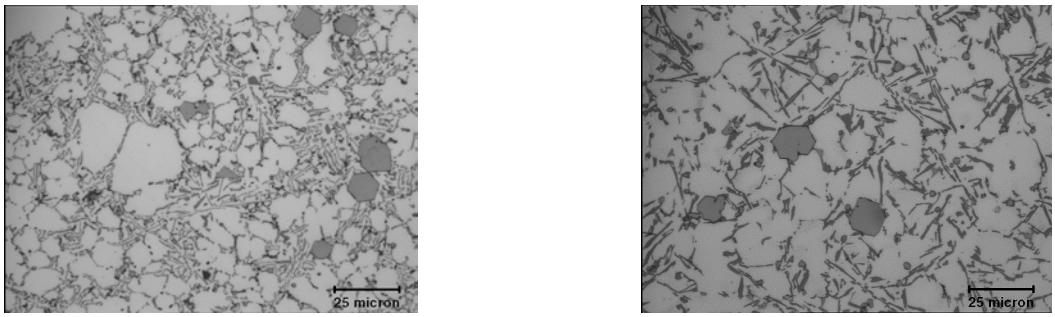

Figure 4: Microstructures of CRP^{TM} processed 383 castings (a) vs. HPDC 383 castings (b).

To improve the SSM processability of 383 alloy, extensive thermodynamic simulations have been conducted to tailor/optimize 383 alloy composition to render the alloy SSM friendly. Specifically, we found that the content of Si and Ni has a significant effect on the SSM process window. Increasing Ni content or decreasing Si content can open up the process window remarkably. Detailed simulation results are given in Ref. [9]. Based on our simulation results, a modified 383 alloy was prepared and cast. Figure 5 shows the microstructure of CRP^{TM} processed castings vs. conventional liquid die castings. It can be seen that:

- As found in 383, the CRP^{TM} processed castings have much more primary alpha globules (SSM structure) than conventional liquid die castings. Image analysis shows that the fraction solid of the primary alpha phase in the CRP^{TM} processed castings is about 25% with an average particle size of 35μm. Conventional die castings contain both globular and dendritic primary alpha phase. Some coarse primary alpha dendrites can be clearly seen in Figure 5(b).
- Observations on eutectic Si and intermetallic phases show that CRP^{TM} processed castings have much finer eutectic Si and smaller Fe-bearing intermetallic phases than conventional die castings. Image analysis points out that the size of the Fe-bearing polydedral intermetallic phase in CRP^{TM} processed castings falls in a range between 5-10μm vs. 10-20μm in conventional die castings. These observations further confirm the findings in 383 alloy.
- In addition, the modified 383 alloy shows a much better SSM formability than standard 383 alloy, particularly at a relatively high fraction solid range. Detailed experimental results are presented and discussed in Ref. [11].

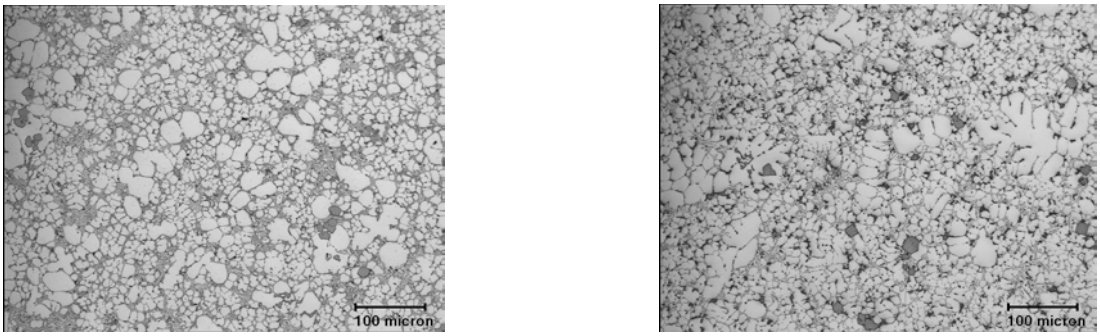

Figure 5: Microstructures of modified 383 alloy castings processed via CRP^{TM} (a) vs. HPDC (b).

2.2 A Marriage of the CRP™ and SLC™ Processes

The Sub Liquidus Casting Process (SLC™) was introduced by THT Presses, Inc. in 2000, and was described at the NADCA congress in 2002 [12]. Unique features of the process include 1) a vertical shot orientation, 2) a shot diameter to depth ratio of at least two to one, 3) a gate plate through which the rheocasting slurry passes into the die cavity and 4) a dovetail feature in the head of the piston to facilitate separating cast parts from biscuits during part ejection. For the SLC™ process, degassed, and *well-grain-refined* melt is introduced into the shot sleeve at a temperature only a few degrees above liquidus. The alpha phase initially forms as tiny rosette grains that then spheroidize and ripen into a globular slurry having a fraction solid of about 0.5 as it cools to near the eutectic temperature (for A356 alloy, approximately 575° C). That slurry is then injected through the gate plate and into the die; the gate plate concept provides a universe of opportunities for positioning gates to minimize both flow distances and solidification shrinkage feeding distances. The large shot diameter, short shot stroke feature and gate plate make the THT equipment well suited to a slurry form of semi-solid processing.

The CRP™ plus SLC™ is an attractive combination because SLC™ depends on excellent grain refinement of slurry for timely slurry development and CRP™, while easily *initiating* the desirable semi-solid globular alpha structure, depends on the casting process to actually form slurry of a significant fraction solid for injection into the die.

A CRP™ reactor (Figures 6) was adapted to use with a 400T press at THT in Dayton, OH. The reactor was fitted with rollers to facilitate movement into position to pour melt over it and into the shot sleeve of the casting machine, and then quickly retract it to allow closing the tool for casting.

The eight-cavity casting tool and resulting cast bars (re-assembled to a biscuit with gate posts to illustrate the gating scheme) are shown in Figure 7. The tool is H-13 steel. Each cavity has a single ingate measuring 1.61 cm^2, the area used when calculating gate flow velocities appropriate for semi-solid (2 m/s) versus squeeze casting (0.5 m/s).

A356 alloy for the trial was prepared by melting pure aluminum, and Al-Si, Al-Mg master alloys, so as to guarantee absence of any chemical grain refiner. Experimental procedures involved: 1) melting pure metals and master alloys (no grain refiners and no Sr modifiers), rotary degassing with Ar-0.5%Cl and adjusting temperature of the melt to 640-660 °C; 2) pouring melt over the CRP™ reactor and into the shot sleeve of the THT machine; 3) withdrawing CRP™ unit, and closing the tool and making the shot. The total seconds from pouring melt over the CRP™ reactor to achieve a slurry fraction solid between 0.4 and 0.5 was about 27 seconds. For the squeeze casting variation, melt was ladled directly into the shot sleeve and the die was closed and the shot made in the shortest possible time (~ 7 seconds). A second set of experiments was repeated after adding 150ppm Sr to the melt for eutectic modification.

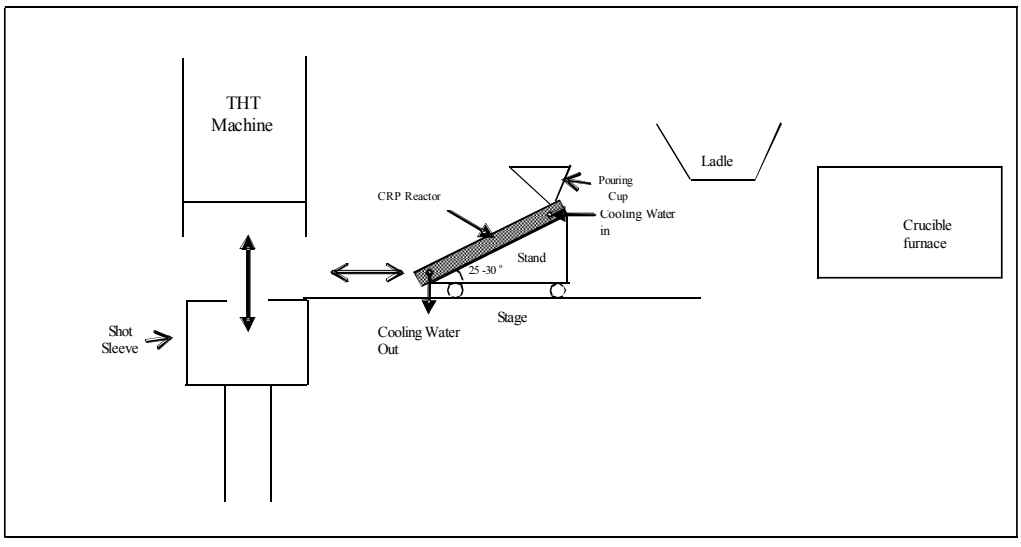

Figure 6: Schematic of CRP™ reactor adapted to the THT casting machine.

Figure 7: Photo of the tool (an 8-cavity rectangular bar die) and actual casting with gate posts and ingates.

Tensile properties of the A356 alloy were evaluated after heat treatment both in T5 and T6 conditions. The heat treatment for T6 was: solutionized at 540 °C/4 hrs, and aged at 170 °C/4 hrs in a conventional furnace; the T5 treatment consisted of aging at 170 °C/4 hrs.

Figure 8 gives typical microstructures of CRP™/SLC™ processed castings vs. liquid squeeze castings. It can seen that the CRP™/SLC™ castings have a fine and uniform globular alpha structure, whereas liquid squeeze castings from the same melt show a (albeit mixed coarse and fine) dendritic structure. The mixed coarse and fine dendrites in the squeeze casting are likely a result of the minimum time required to shuttle the lower die into position, close the tool and inject metal (about 7 seconds in total) being sufficient to allow partial solidification to take place in the shot sleeve (relatively slow solidification) while the balance takes place in the die (very rapid solidification).

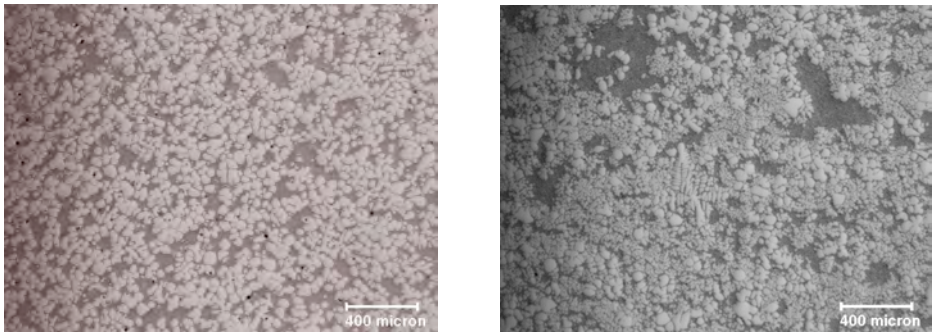

Figure 8: A356 alloy with no chemical grain refinement and no Sr-modification, SLC™ cast after passing melt over the CRP™ reactor (left) versus liquid squeeze cast without use of the CRP™ reactor (right). Note the very fine globular structures, a result of the CRP™ reactor + development of a high fraction solid during SLC™ casting versus the mixed alpha coarse cells and tiny dendrites observed in squeeze casting.

Figure 9 illustrates the effect of Sr modification on the microstructures of CRP™/SLC™ processed castings vs. liquid squeeze castings. It is quite clear that Sr modification has little influence on the morphology and fineness of CRP™/SLC™ rheocast Al-Si eutectic (semi-solid processing alone results in a fine eutectic structure, without need for Sr modification). The liquid squeeze casting from the same melts, on the other hand, benefited significantly from Sr modification.

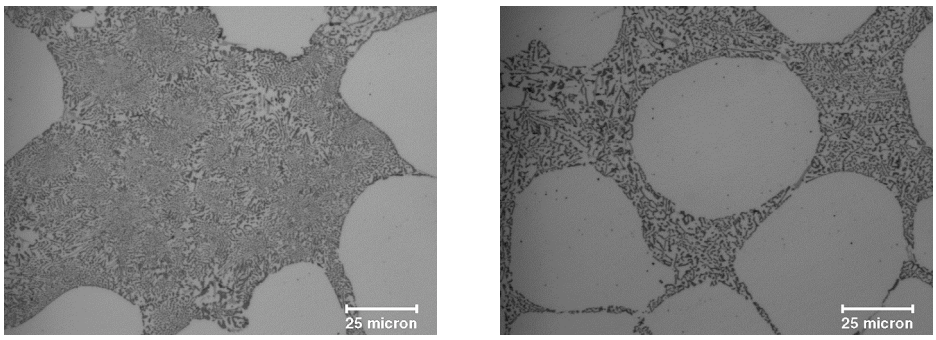

Figure 9: Comparing Sr-modified CRP™/SLC™ cast Al-Si eutectic structure (left) to that of un-modified eutectic (right). Although the Sr-modified eutectic is somewhat finer, CRP™/SLC™ processing itself provides a fine eutectic even without modification.

Resulting tensile properties are summarized in Figure 10. There are several notable trends:

- A356 CRP™/SLC™ castings have higher strength and ductility than liquid squeeze castings.
- Sr modification does not show significant influence on mechanical properties of A356 CRP™/SLC™ castings; however it does show noticeable effect on mechanical properties of A356 liquid squeeze castings. Sr modification improves mechanical properties of liquid squeeze castings (particularly ductility) to some extent.
- Contrary to previous findings regarding SLC™ and other semi-solid casting routes [9], there is a certain amount of ductility loss for T-5 heat treated castings as compared to F temper.

In summary, the CRP™ can provide the copious nucleation needed for SLC™ slurry to develop in a timely manner, and SLC™ provides the means for CRP™ to evolve from mere nuclei to ideal semi-solid slurry. The combination of CRP™ and SLC™ has worked well to produce excellent globular alpha phase together with a fine and uniform Al-Si eutectic. The Beta trial has proven that the CRP™/SLC™ combination is a valuable marriage of two unique processes.

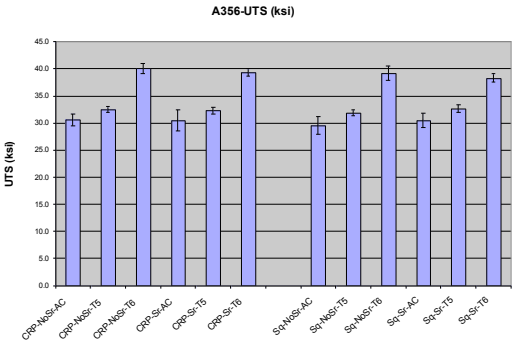

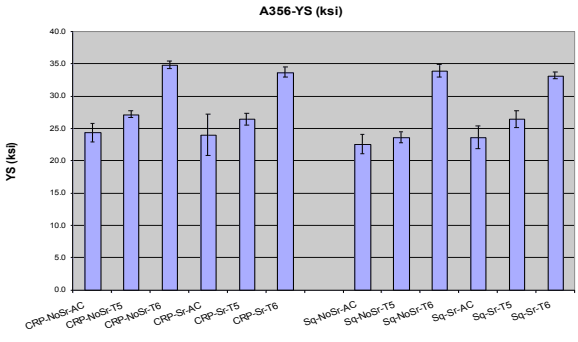

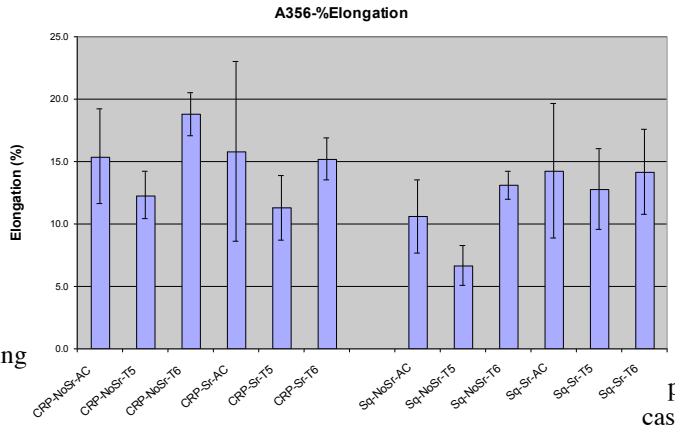

Figure10: Comparing mechanical properties of A356 castings processed via CRP™/SLC™ vs. liquid squeeze cast under F, T5 and T6 conditions.

Concluding Remarks

The CRP™ has been scaled up successfully for industrial applications. Numerous industrial Beta trials point out that the optimized CRP™ reactor can easily retrofit most die casting facilities to make SSM parts. The simplicity, robustness, as well as the low cost nature of the CRP™ makes the process commercially viable for semi-solid processing.

References

[1] DOE Report number DE-FC07-98ID13618

[2] M.C. Flemings, "Semi-Solid Processing – The Rheocasting Story", Test Tube to Factory Floor: Implementing Technical Innovations, from the Proceedings of the Spring Symposium May 22, 2002 published by Metal Processing Institute, Worcester Polytechnic Institute, Worcester MA 01609 (2003).

[3] UBE Industries Ltd., *Method and apparatus for shaping semisolid materials*, in *European Patent EP 0 745 694 A1*. 1996. p. 117.

[4] J.A. Yurko, R.A. Martinez, and M.C. Flemings, "SSR™: The Spheroidal Growth Route to Semi-Solid Forming", in 8th International Conference on Semi-Solid Processing of Alloys and Composites, 2004, Limassol, Cyprus.

[5] J.L. Jorstad, "SSM Processes - An Overview", in 8th International Conference on Semi-Solid Processing of Alloys and Composities, 2004, Limassol, Cyprus.

[6] D. Doutre, J. Langlais, and S. Roy, "The SEED Process for Semi-Solid Forming", in 8th International Conference on Semi-Solid Processing of Alloys and Composites, 2004, Limassol, Cyprus.

[7] M. Findon, *"Semi-Solid Slurry Formation via Liquid Metal Mixing"*, M.Sc., Thesis, Worcester Polytechnic Institute, 2003.

[8] Q.Y. Pan, M. Findon, and D. Apelian, "The Continuous Rheoconversion Process (CRP): A Novel SSM Approach", in 8th International Conference on Semi-Solid Processing of Alloys and Composites, 2004, Limassol, Cyprus.

[9] D. Saha, S. Shankar, D. Apelian, and M.M. Makhlouf, "Casting of Aluminum Based Wrought Alloys using Controlled Diffusion Solidification", Metallurgical and Materials Transactions A, Vol. 35A, July 2004, pp. 2174-2180.

[10] F. Incropera and D. DeWitt, *"Fundamentals of Heat and Mass Transfer"*, 5th Edition. John Wiley & Sons, 2002.

[11] S. Wiesner, Q.Y. Pan and D. Apelian, "Application of the Continuous Rheoconversion Process (CRP) to Low Temperature HPDC-Part II: Alloy Development & Validation", (the 9th S2P 2006 Conference).

[12] J. L. Jorstad, “SLC, the Low-Cost Alternative for SSM Processing” Proceedings, NADCA Congress, Paper T02-052, (2002).

111th METALCASTING CONGRESS
May 15–18, 2007 • Houston, Texas
NADCA

Interaction of Key Variables During Rheocasting: Effects of Fraction Solid and Flow Velocity on Performance

John L. Jorstad
J L J Technologies, Inc.

Q. Y. Pan & Diran Apelian
Advanced Casting Research Center, MPI, Worcester Polytechnic Institute (WPI)

ABSTRACT

The thixocasting (billet) route for semi solid processing naturally drove practitioners to process at near-maximum fractions of solid; anything less resulted in run-off, billet instability and handling issues. Rheocasting (the slurry route) has no such natural driver; slurry is contained during its formation and therefore does not require a particular fraction solid for handling; rheocasting can accommodate the full range from almost no solid to the maximum feasible for a given alloy (~0.5). Since rheocasting, for economic reasons, is now becoming the more popular semi solid processing route, there is need to better understand the effects of both fraction solid and flow velocity (the two must be interdependent) on microstructures, part integrity and properties so as to intelligently select processing variables. A study was therefore devised to test effects of fraction solid during rheocasting, over a range from 0 (squeeze casting) to 0.5 (maximum solid for A356 alloy), in combination with flow velocities ranging from 0.5 to 5 meters per second; the results and their comparison with modeled expectations are discussed herein.

INTRODUCTION

The two primary semi solid processing routes are Thixocasting, which uses solid pre-cast billet as feedstock, and Rheocasting, which employs liquid melt as its feedstock. During rheocasting, slurry is formed directly from a melt and is then injected into the die cavity. While thixocasting has a long history for "commercial" SSM, rheocasting is rapidly growing in popularity because it provides greater flexibility in alloy selection and sourcing, and process offal and run-around can be recycled into product without first being reprocessed into billet; rheocasting is becoming the low-cost SSM processing alternative.

Thixocasting and rheocasting differ significantly regarding their natural approach to fraction solid: Thixocasting re-heats solid billet into the semi solid temperature range; if heating continues beyond that required for a fraction solid of ~0.5, excessive eutectic run-off can occur and the billet becomes too soft and fragile for easy handling. Rheocasting, on the other hand cools molten alloy into the semi solid temperature range, meaning that the slurry must first be contained, thus handling and eutectic run-off are non-issues and slurry need not therefore be especially sensitive to fraction solid.

Thus, a need for greater understanding regarding the importance of fraction solid: Since rheocasting is now becoming the more popular processing route, there is need to better understand the effect of fraction solid and its interaction with flow velocity (the two must be interdependent) in defining microstructures, part integrity and properties so as to intelligently select processing variables.

Recent studies: Two studies were devised to test the effects of fraction solid on performance. One, reported during the special TMS John Campbell symposium in 2005 (Jorstad, et al, 2005), served to demonstrate that partially-solidified melts having significant fractions of solid (in that case, approximately 50%) can flow at velocities exceeding 2 meters/second while

still maintaining a stable free-surface flow front and relatively defect-free castings. The other, reported at the 9th International Conference on Semi Solid Processing of Alloys and Composites in Busan, Korea (Jorstad et al, 2006), tested the effects of fraction solid over a range from 0 (squeeze casting) to 0.5 (fully semi solid) in combination with flow velocities ranging from 0.5 to 5 meters per second on casting integrity, microstructure and properties, and indicated that higher fractions of solid allow higher flow rates without turbulence-related defects.

Confirms modeling: The results of both above studies tend to confirm (and are supported by) theoretical models of semi solid processing; those theoretical considerations are described here-in.

First, the Experimental Study, as Reported in Busan

Of the two studies noted above, the second was the more complete in terms of variables studied and results examined.

Experiment matrix: The casting matrix is shown in Table 1. Vg is the flow velocity (m/s) through ingates into each bar cavity. Casting temperature T is the slurry temperature required for each fraction solid according to the Fs versus T curve shown in Fig. 1.

Table 1. Casting matrix

f_s	T (°C)	V_g (m/s)
0	>650	0.5, 1.0, 1.5 & 2.0
0.2	598	0.5, 1.0, 1.5, 2.0 & 3.0
0.3	590	1.0, 2.0, 3.0 & 4.0
0.4	582	1.0, 2.0, 3.0 & 4.0
0.5	575	3.0, 4.0 & 5.0

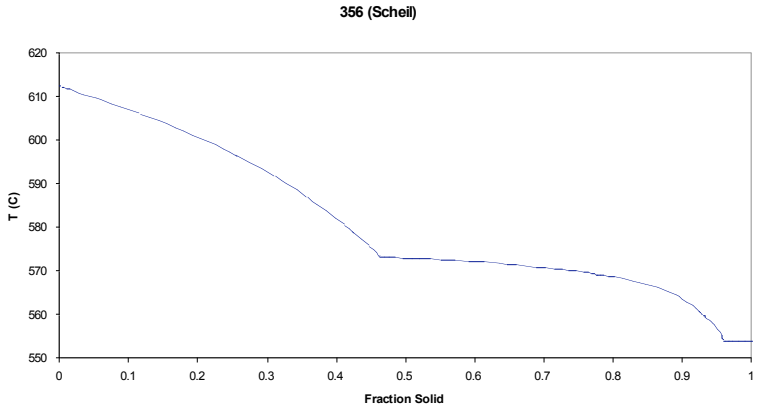

Fig. 1. A356 alloy fraction solid versus temperature.

The rheocasting process - Sub Liquidus Casting (SLC™): The SLC™ process was used to rheocast experimental cast bars. SLC™ was introduced by THT Presses, Inc. in 2000, and was described at previous NADCA Congress (Jorstad, et al, 2002). Using the SLC™ process, degassed, modified and well-grain-refined melt was introduced into the shot sleeve at a temperature only a few degrees above liquidus. The alpha phase initially formed as tiny rosette grains that then spheroidized and ripened into globular slurry having the targeted fraction solid f_s as it cooled toward the eutectic temperature (for A356 alloy, approximately 575° C). Slurry was then injected through the gate plate directly into the die cavity. Vertical shot orientation, large shot diameter/short shot stroke and gate plate features make the THT equipment well suited to a slurry (rheocasting) form of semi-solid processing.

The alloy: A356 alloy for the trial was re-melted ingot plus scrap parts previously made from pre-alloyed ingot. The composition (%) was: Si 7.49, Fe 0.19, Cu 0.01, Mn 0.01, Mg 0.31 (somewhat to the low side), Zn 0.02, Ti 0.013 and Sr 0.012.

The die: An eight-cavity H-13 steel die was employed; resulting cast bars (re-assembled to a biscuit with gate posts to illustrate the gating scheme) are shown in Fig. 2. Each test bar cavity had a single ingate measuring 1.61 cm2, the area used when calculating gate flow velocities for both semi-solid (0.5 to 5 m/s) and squeeze casting (0.5 to 2 m/s).

The process sequence: 1) A356 alloy ingot and/or old parts were melted, 1.5:1::Ti:B and Sr master alloys were added. Subsequently, the melt was degassed with Ar-0.5%Cl and the temperature adjusted to 625-630 ºC. 2) Thus-prepared melt was ladled into the shot sleeve of the THT machine. 3) Cooling in the shot sleeve was monitored using thermocouples for enough cycles to establish the total cooling time needed to bring slurry into the temperature range required for each fs; thereafter, the slurry cooling cycle was controlled only by that pre-determined time. 4) The lower die was shuttled over the shot sleeve, the tool closed and the shot was made.

Figure 2. Cast bars, reassembled on gating.

The total seconds from start-of-pour to reaching a slurry fraction solid ranged between 9 seconds (0.2 f_s) and 27 seconds (0.5 f_s). Total shot-to-shot cycle time was generally just over 1 minute.

For the squeeze casting variations (f_s 0), melt at ~700 ºC was ladled directly into the shot sleeve, the die closed and the shot made in the shortest possible time (< 7 seconds).

Heat treatment. Bars were heat treated to the T6 temper (solution heat treated at 540 °C for four hours, quenched in hot water and precipitation aged at 170 °C for four hours). All bars were x-rayed before heat treatment, and T-6 bars were inspected for blisters immediately following solution heat treatment. Bars were then machined into 9mm round sub-size tensile specimens per ASTM B 557M and tested.

EXPERIMENTAL RESULTS

Radiographic defect examination: Radiographic examination took place immediately following casting; results are summarized in Table 2. Clearly, based on this inspection technique alone, a larger solid fraction (f_s) in semi solid slurry allows a higher flow rate before gross turbulence-related defects are encountered. Examples of typical x-ray defect severity levels are depicted in Fig. 3.

Table 2. Number of radiographic-defective bars out of 24 total

	0.5 M/s	1.0 M/s	1.5 M/s	2.0 M/s	3.0 M/s	4.0 M/s	5.0 M/s
f_s 0	0	2	10	16	-	-	-
f_s 0.2	0	0	2	12	15	24	-
f_s 0.3	-	0	0	6	10	18	-
f_s 0.4	-	0	0	0	2	8	-
f_s 0.5	-	-	-	0	0	1	12

All fractions of solid (f_s) resulted in x-ray defect-free bars at the lowest flow velocity – 0.5 m/s. The squeeze castings (f_s 0) remained defect free except for minute indications in a single bar at a flow velocity of 1.0 m/s, but exhibited numerous defects at 1.5 m/s. As f_s increased, the velocity at which slurry could flow without becoming unstable and turbulent also increased until, at f_s 0.5, flow velocities up to 4 m/s caused no x-ray defects.

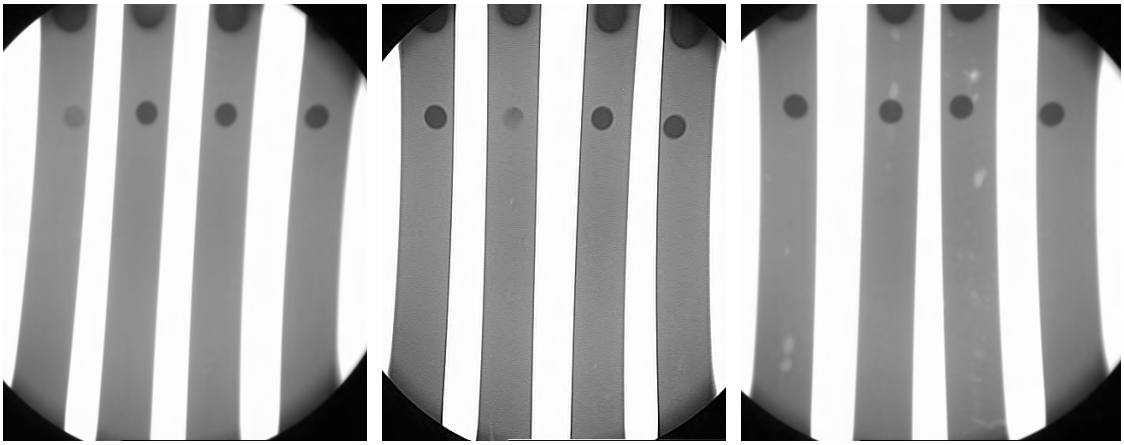

Fig. 3. Defect-free example (left), typical of f_s 0 at 0.5 m/s flow velocity, f_s 0.2 at up to 1.0 m/s, f_s 0.3 at up to 1.5 m/s, f_s 0.4 at up to 2.0 m/s and f_s 0.5 at up to 3.0 m/s; minute indications (center), typical of f_s 0 at 1.0 m/s, f_s 0.2 at 1.5 m/s, f_s 0.3 at 2.0 m/s, f_s 0.4 at 3.0 m/s and f_s 0.5 at 4.0 m/s; gross indications (right), typical of f_s 0 at 1.5 m/s, f_s 0.2 at 2.0 m/s, f_s 0.3 at 3.0 m/s, f_s 0.4 at 4.0 m/s and f_s 0.5 at 5.0 m/s.

These results were as should be expected, according to semi solid models of the effects of increasing viscosity (the result of increasing fraction solid) on the boundary flow conditions between stable and turbulent flow. This will be discussed in detail following the complete results of the experiments.

Blister Examination: The occurrence of blisters following T-6 solution heat treatment was another clear indication of turbulence during cavity fill, although die lube and lube practice can also be associated with blisters following elevated temperature exposure. Table 3 compiles the count of blistered bars out of all those solution heat treated, and shows a trend similar to that seen during x-ray examination; that is, the greater the fraction solid f_s the faster slurry could seemingly flow without resulting in T-6 blisters.

In each case, the first V_g where blisters were encountered tended to produce tiny surface blisters, which are often associated with lube and lube practice, whereas increasingly higher V_g produced larger and deeper blisters, more often an indication of turbulent entrapment of cavity gasses.

Table 3. Number of blistered bars out of 15 after T-6 (solution) heat treatment

	0.5 m/s	1.0 m/s	1.5 m/s	2.0 m/s	3.0 m/s	4.0 m/s	5.0 m/s
f_s 0	**0**	**1**	**4**	**3**			
f_s 0.2	**0**	**0**	**1**	**1**	**3**		
f_s 0.3		**0**	**0**	**0**	**2**		
f_s 0.4		**0**	**0**	**0**	**1**	**2**	
f_s 0.5				**0**	**0**	**1**	**4**

Microstructure Evaluation: Effects of f_s and V_g on microstructure are illustrated in Figs. 4-6. In general, larger fractions of solid resulted in more globular alpha phase and higher flow velocities resulted in more uniform alpha globule size. Neither fraction solid nor flow velocity had a significant effect on the Al-Si eutectic structure, which was in all cases well modified.

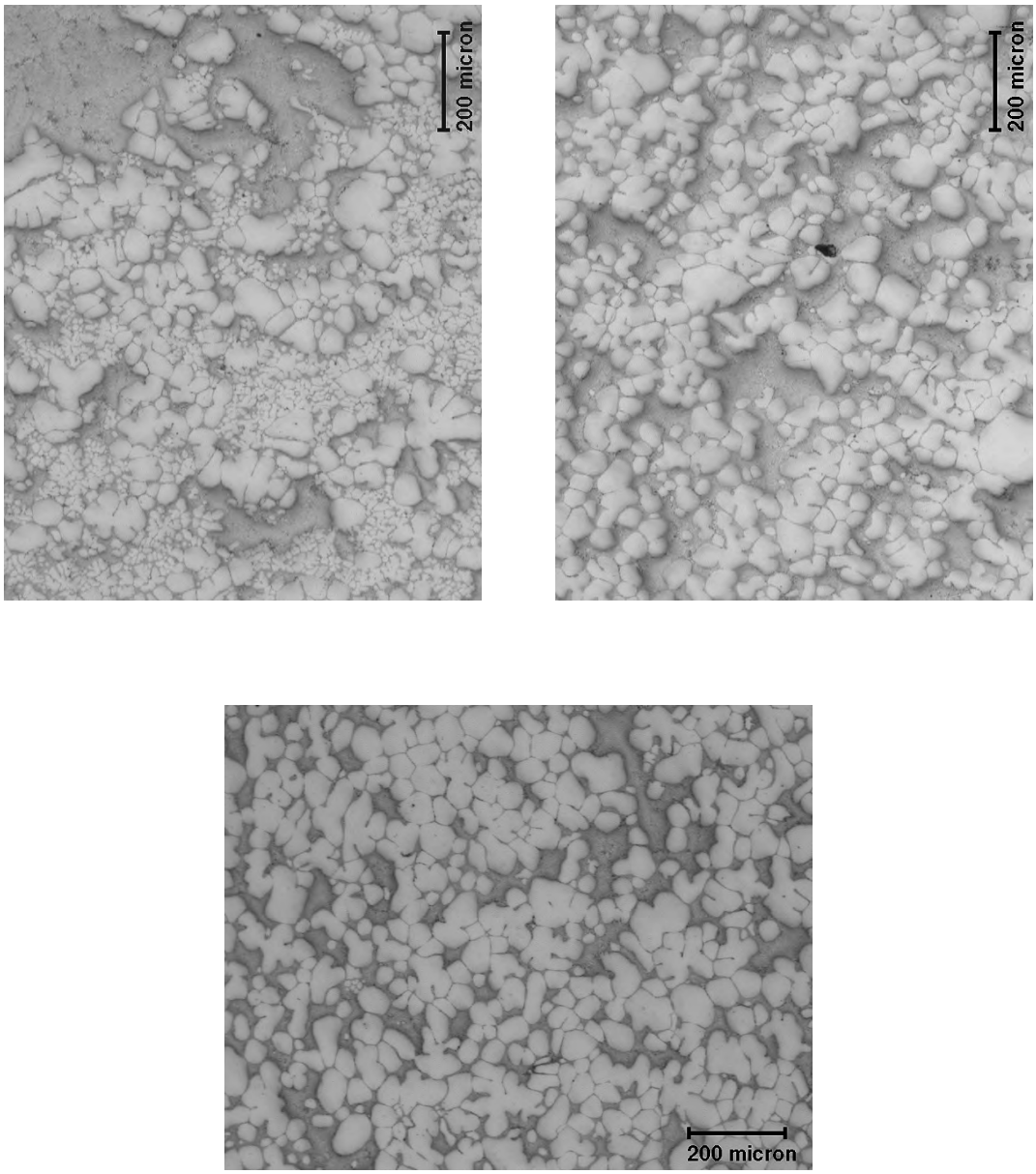

Fig. 4. Illustrates the effect of fraction solid f_s on the alpha structure; squeeze cast, ~0 f_s (above, left), rheocast 0.3 f_s (above, right) and 0.5 f_s (below, center). The alpha structure became more uniformly globular as f_s increased.

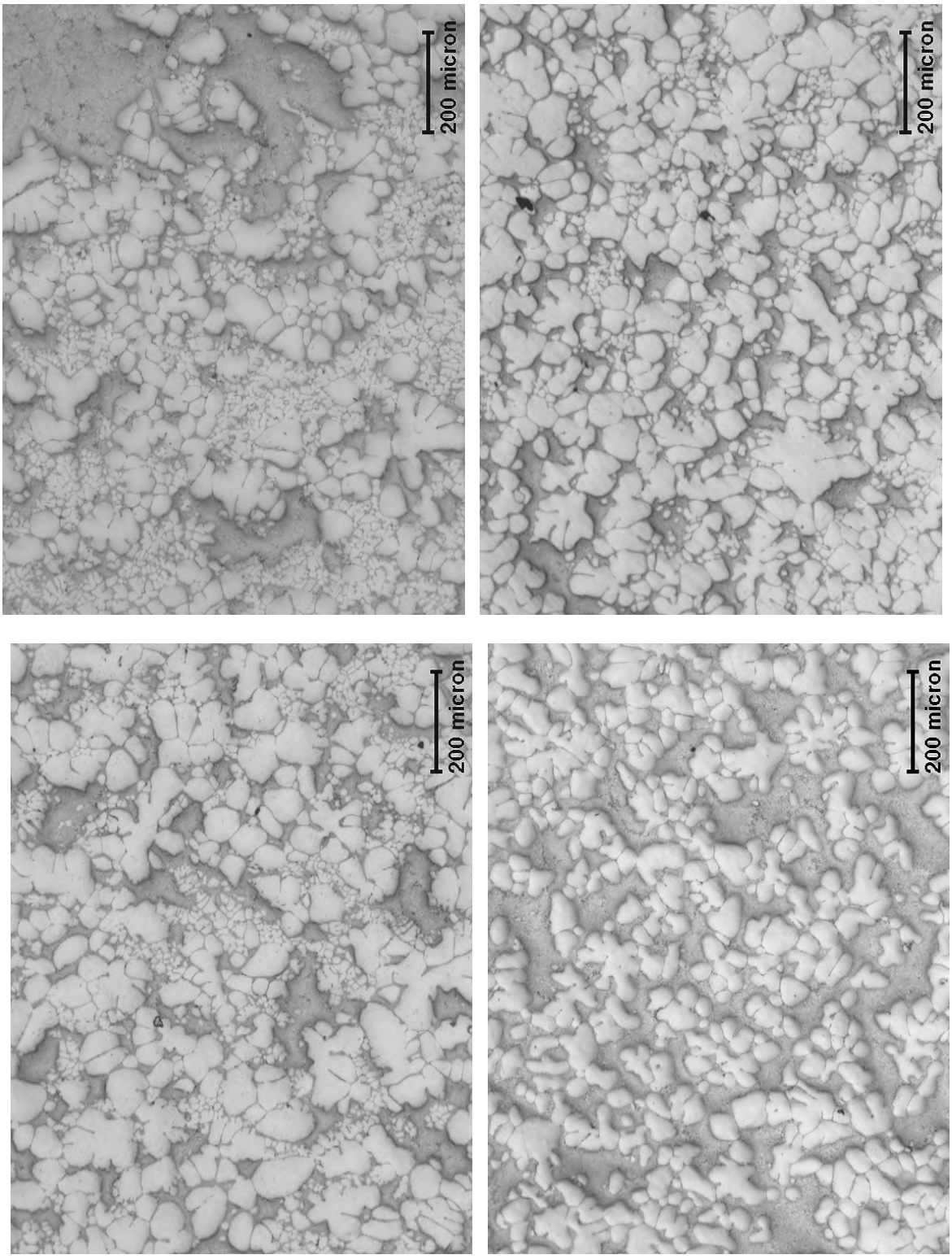

Fig. 5, Illustrates the effect of V_g on the alpha structure; squeeze cast, ~0 f_s, at 0.5 m/s V_g versus 2.0 m/s (above left pair) and rheocast 0.2 f_s at 0.5 m/s V_g versus 4.0 m/s (right pair). The alpha structure became somewhat more uniform in size as V_g increased.

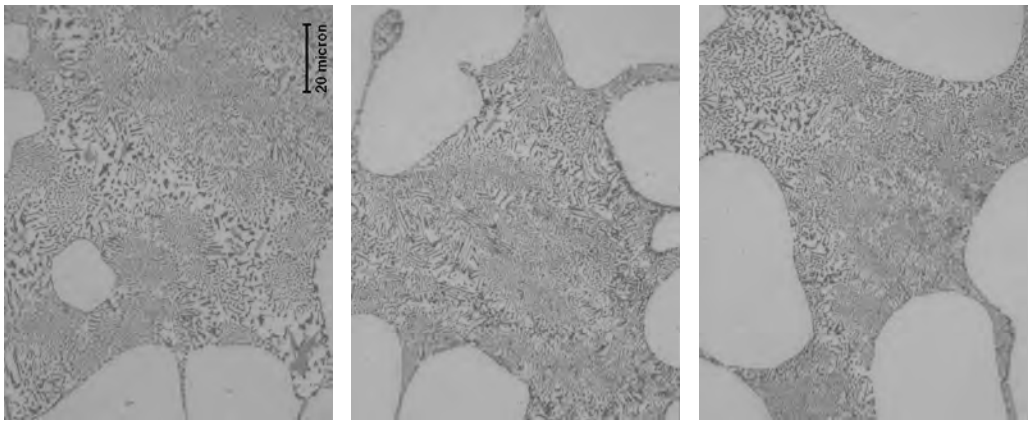

Fig. 6. Illustrates the lack of effect of either f_s or V_g on the Al-Si eutectic structure; squeeze cast, ~0 f_s at 1.0 m/s V_g (left) versus rheocast 0.3 f_s at 2.0 m/s V_g (center) versus 0.5 f_s at 4.0 m/s; the eutectic is well modified and remains relatively unchanged at all values of f_s and V_g.

Tensile Property Evaluation: The broad range of variables was expected to produce both good and poor quality bars; property data related to defective bars was omitted and the assessment shown in Fig. 7 is based only on the averages from good bars in each set (legitimate microstructure effects).

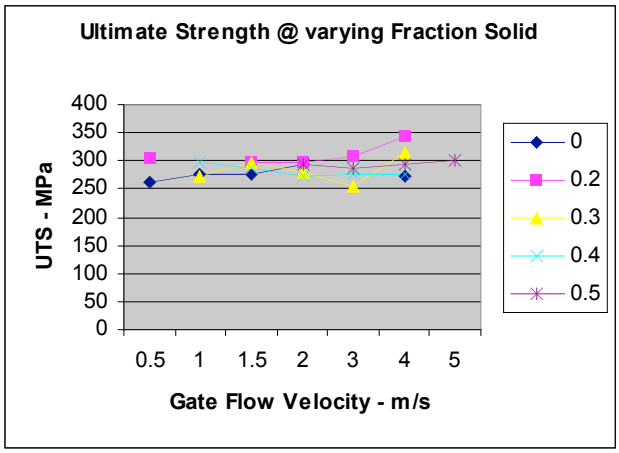

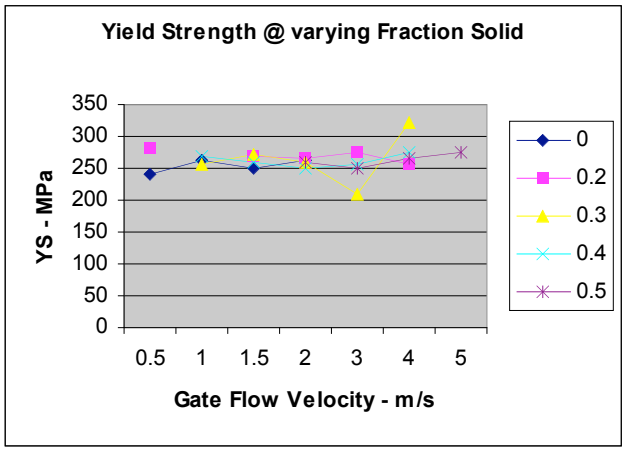

Fig. 7a (left) and 7b (right). Effects of fraction solid and gate velocity on tensile properties; UTS 7(a), YS 7 (b).

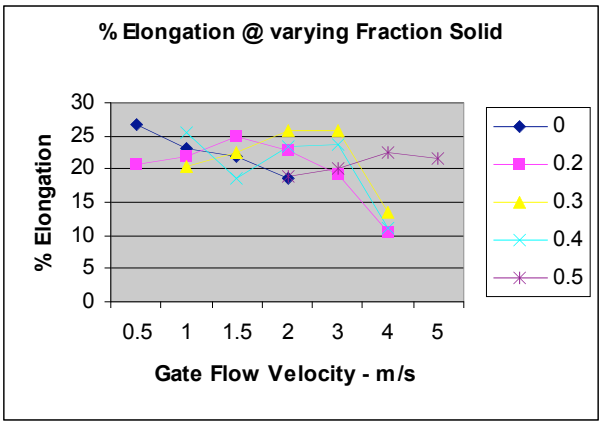

Fig. 7c. Effects of fraction solid and gate velocity on % elongation.

While both strength and especially ductility were good, there is no clear trend relating strength to either f_s or V_g. Ductility, on the other hand, seemed to legitimately suffer at the highest values of V_g combined with the lower values of f_s. Values for clearly defective bars had been omitted; still, tiny oxides that did not appreciably reduce strength may have been a result of the highest flow velocities combined with the lower fractions of solid, thus adversely impacting ductility. Still, the highest fraction solid retained good ductility even at high flow velocities.

THEORETICAL BASIS FOR FLOW BEHAVIOR

The results presented clearly indicate that:

1. Larger fractions of solid provided more stable flow, thus accommodating higher flow velocities without creating x-ray visible defects and/or blisters following solution heat treatment.

2. Higher flow velocities caused turbulence-type defects, depending however on fraction solid; the greater the fraction of solid, the faster slurry could flow before becoming unstable.

Results can be plotted and smoothed as illustrated in Fig 8, indicating trends that can be explained by the theoretical understanding of SSM flow behavior.

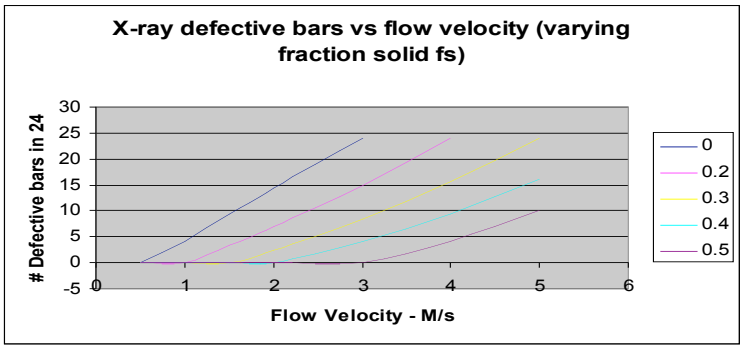

Fig. 8. Flow -related defects with varying flow velocity and fractions of solid.

The experimental results can be explained by the stability map for semi-solid processing generated by Alexandrou (Alexandrou, 2001). Alexandrou (Alexandrou, 2001) investigated the filling of a 2-D cavity geometry, where the effects of inertial, viscous and finite yield stress of semi-solid materials on filling were considered, as illustrated in Figure 9. In the simulations, the conservation of mass, momentum and energy equations are solved using a three-dimensional (3-D) finite volume numerical method. The computational code has been modified by Alexandrou et al (Alexandrou and Bardinet, 1999) and extended to fluids with yield. Specifically, to deal with the discontinuity in the constitutive relation, the regularized model introduced by Papanastasiou (Papanastasiou, 1987) was employed,

$$\tau = \left[\eta + \tau_o \frac{1 - \exp(-m\dot{\gamma})}{\dot{\gamma}}\right]\dot{\gamma} \qquad (1)$$

where τ is the shear stress, τ_0 is the yield stress, η is the effective viscosity, $\dot{\gamma}$ is the shear rate, $\dot{\gamma}$ is the second invariant of $\dot{\gamma}$, and the parameter m, which has dimensions of time, controls the exponential rise in the stress at low rates of strain. The material parameters, τ_0 and η, are determined from experimental data. The ideal Bingham-plastic behavior can be approximated by relatively large values of m.

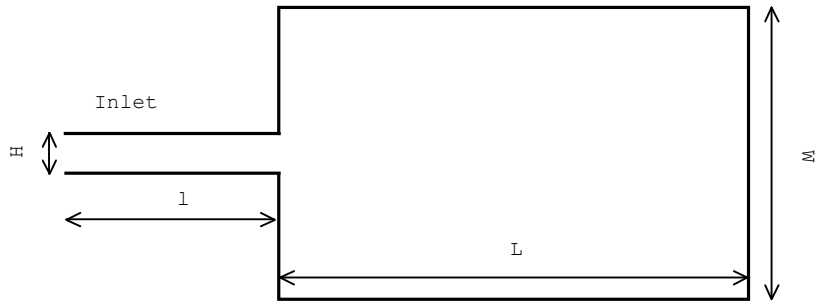

Fig.9: Geometry of the two dimensional cavity: (H=2 cm; l=7.8 cm; L=20cm and W=10 cm) (Alexandrou, 2001).

Dimensional analysis shows that filling depends on two-dimensionless parameters, the Reynolds number, and the Bingham number; Reynolds number representing flow velocity and Bingham number representing resistance to shear stress (or yield strength). These parameters are:

$$\mathrm{Re} = \frac{\rho\ U_0\ H}{\eta} \quad \text{and} \quad \mathrm{Bi} = \frac{\tau_o\ H}{\eta\ U_0} \qquad (2)$$

where ρ is the density and U_0 is the average inlet velocity.

A complete map of filling patterns has been developed in a wide range of Reynolds and Bingham numbers experienced in semi-solid processing (see Figure 10). Specifically, five distinct flow patterns have been identified (Alexandrou, 2001). These are:

Shell: is a filling of the cavity by a Newtonian fluid at a relatively high Reynolds number, where inertia force dominates the flow. The jet emanating from the inlet section reaches the end of the cavity, and splits into two layers along the upper and lower walls of the cavity. This pattern is a typical die filling in liquid metal casting. For SSP process, this type of filling is undesirable as a large volume of gas is entrapped.

Mound: is a filling at a lower Re number (i.e. lower inertia forces), where viscous effect is dominant. The higher viscous stress prevents the flow from splitting into two parts, and filling proceeds with growth and slow spreading of a central column or mound, as shown in Figure 10. For semi-solid processing, this filling pattern is desirable since no gas is entrapped.

Disk: is a filling under large Reynolds and Bingham numbers, where inertia and plastic drag prevail over viscous force. The initial jet splits into two layers, very similar to shell filling. However, these layers are sufficiently thick, and do not propagate backwards along the side-walls; instead, they form a disk front moving from the closed-end to the front of the cavity. In disk filling, the effects of the yield stress balance the inertia, a large part of the material comes to rest, and flow is confined near the advancing front.

Bubble: is a filling under a relatively low Reynolds number, but rather high Bingham number where yield stress is dominant. The filling pattern in this case is different from the previous cases. Once the jet hits the end of the cavity, the main growth of a single "solid-like" core occurs first at the end of the jet, and then moves upstream like a wave, and it eventually reaches the entrance of the cavity. After the wave reaches the entry, the filling proceeds primarily as a growing "bubble" at the open-end of the cavity.

Transition: is an intermediate flow pattern between mound and bubble. Filling in this case starts as disk, where the slurry spreads along the wall at the closed-end of the cavity, but it finally develops into a bubble-like filling pattern. At the moment the bubble starts to develop, the extent of the stagnant region remains constant indicating a local balance of inertia force and yield stress.

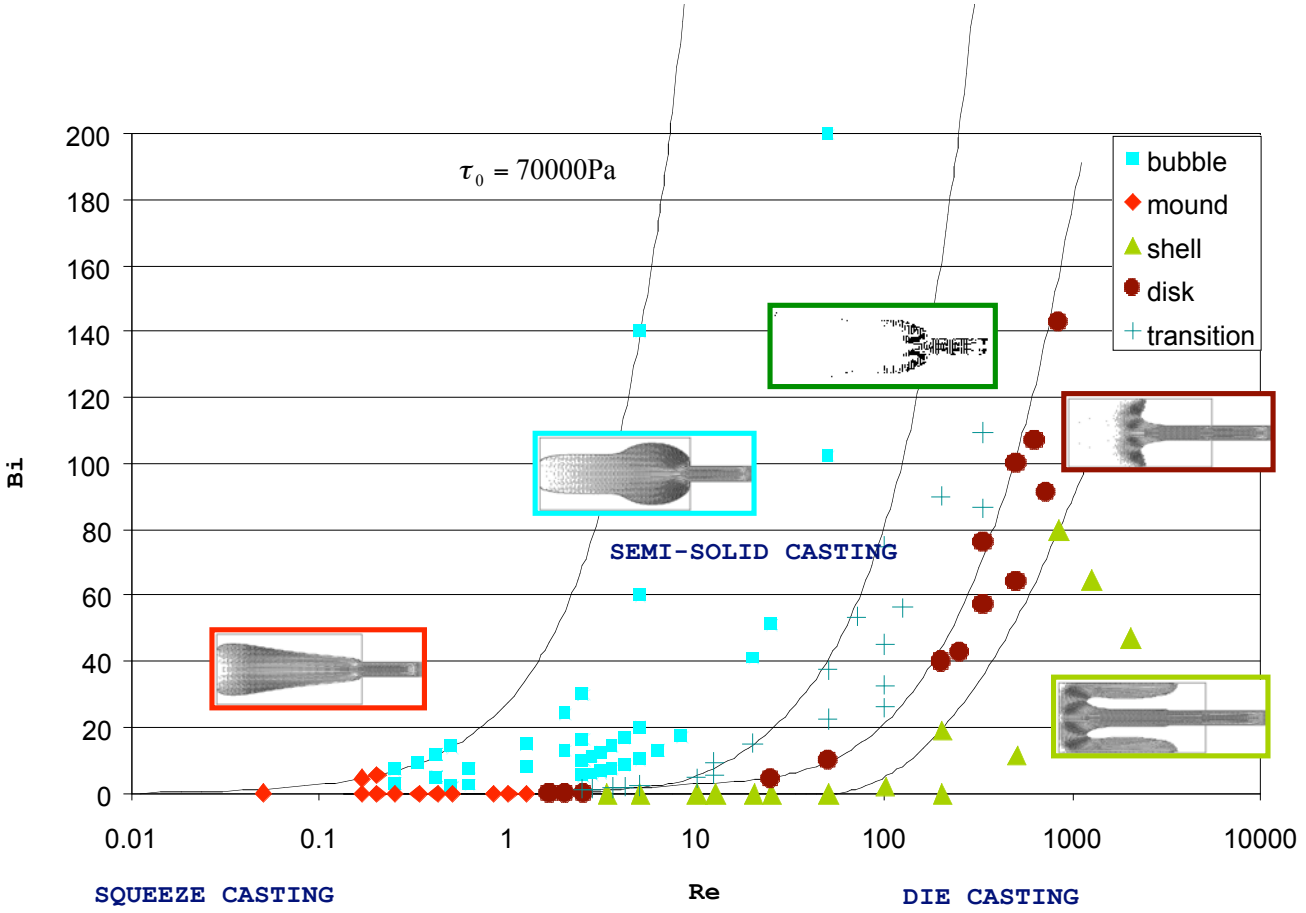

Fig. 10: Flow patterns as a function of Bingham number, Bi and Reynolds number, Re. The figure illustrates five distinct filling patterns (bubble, mound, shell, disk and transition) in semi-solid casting (Alexandrou, 2001).

The simulations highlight the significant role of the finite yield stress in Bingham type flows. Particularly, the bubble filling cannot be identified if the constitutive relation does not take into account the yield stress of the slurry. In fact, the five flow patterns have been confirmed through experimental observations carried out by various different researchers (Midson, et al, 2000; Paradies and Rappaz, 1998).

To understand flow instabilities encountered in semi-solid processing, Alexandrou (Alexandrou, 2001) analyzed the flow under the aforementioned geometry using "exact" finite element simulations along with a moving mesh scheme. The simulations are considered "exact" since the mesh of the finite element method follows the motion of the fluid, and the boundary conditions are satisfied exactly. Figure 11 gives a complete stability map. Depending on Re and Bi values considered, there are two distinct regions defined as "stable" and "unstable." It is clear that the instabilities are indeed the results of the finite yield stress and the way yielded and unyielded regions interact with each other. From a processing point of view, the simulations indicate that instabilities can be avoided by properly selecting operating conditions.

From Figure 11 and equation 2, one can see that:

- For a given alloy, the slurry flow instability depends on Re number, which is a function of inlet velocity, and Bi number, which is a function of yield stress and inlet velocity.

- Figure 12 gives Bingham yield stress of a semi-solid A356 alloy as a function of fraction solid in the two-phase region determined experimentally by Pan et al (Pan, et al, 2004). It can be seen that Bingham yield stress is a strong function of fraction solid/temperature, thus it has a significant impact on the flow front during die filling. A high fraction solid (thus a high yield stress) can accommodate high velocities without changing Bi number remarkably (see Equation 2). As a result, the slurry can still remain a smooth flow front even at relatively high flow velocities during die filling, which will result in less gas entrapment and porosity in the casting. Our x-ray examination results show a good correlation between velocity and the amount of porosity in SSM castings with high solid fractions.

- Also, from Figure 12, one can see that yield stress of a semi-solid slurry can change by 3-4 orders of magnitude in the fraction solid range between 0.1-0.5. For low solid fraction forming, where the effect of yield stress on flow front becomes negligible, and the filling patter depends solely on ingate flow velocity. Apparently, increasing velocity will make the die filling process move into unstable area. As a result, a turbulent flow front will occur, leading to more gas entrapment and porosity. Again, our x-ray examination results show a good correlation between velocity and the amount of porosity in SSM castings with low solid fractions.

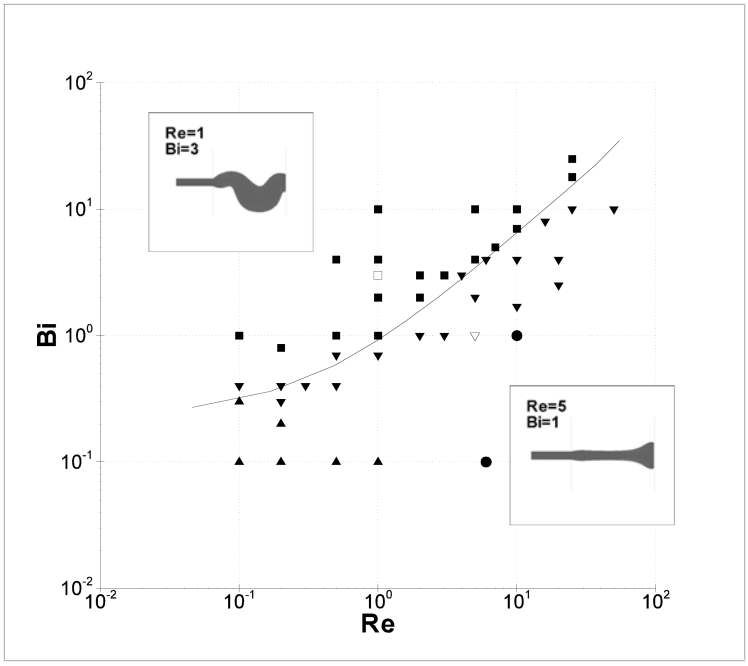

Fig. 11: Stability of the jet as a function of Re and Bi. The symbols indicate various flow patterns: ▲mound pattern; ● disk pattern; ■ bubble pattern; ▼ transition pattern (Alexandrou, 2001).

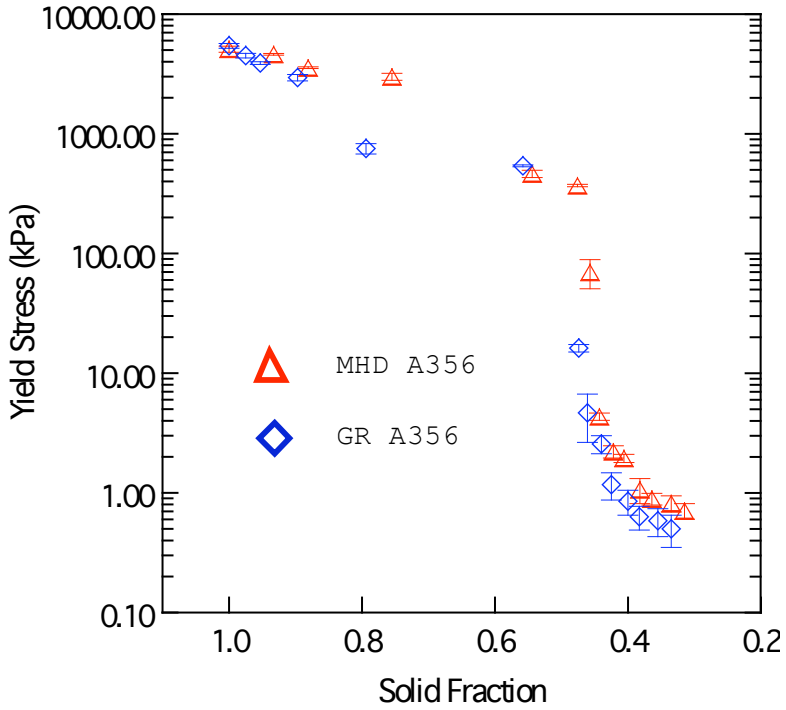

Fig. 12: Yield stress of GR A356 and MHD A356 alloys as a function of solid fraction (Pan, et al, 2004).

CONCLUSIONS

Experimental results have illustrated a valuable asset of semi solid processing; that is, the ability to fill die cavities at relatively high velocities while maintaining a stable flow front. This feature enables accomplishing thins sections and details, akin to those of high pressure die casting, without encountering turbulence-related porosity and oxides that impair properties and prevent heat treating without blistering.

The thixocasting (billet) semi solid route naturally required processing at near-maximum fractions of solid, thus little emphasis was placed on the effects of fraction solid on favorable flow stability. Rheocasting (the slurry route) has no natural requirement for high fractions of solid; processing can be accomplished over a broad fraction-solid range, thus the demonstrated importance of high fraction solid to flow stability is a finding important to rheocasting practitioners. These results both confirm and are supported by theoretical models of semi solid processing.

ACKNOWLEDGEMENTS

Sincere thanks to Mike Thiemen, CEO of THT Presses, Inc., for continuous encouragement and support and for making available the equipment and human resources needed to conduct the experiments described herein and to the staff of the Metals Processing Institute at Worcester Polytechnic Institute for their test analyses and relating results to process models.

REFERENCES

Alexandrou, A.N., "Science and Technology of Semi-Solid Metal Processing", published by NADCA, Rosemont, IL (2001).

Alexandrou, A.N. and Bardinet, F., J. Materials Processing Technology, vol. 96, pp. 59-72 (1999).

Jorstad, J. L. and Thieman, M., "Filling Mold Cavities at High Flow Velocities without Turbulence", TMS, Transactions of the Special John Campbell Symposium, San Francisco, CA (2005).

Jorstad, J. L. and Pan, Q.Y., "Interaction of Key Variables During Rheocasting: Importance of Microstructure, Fraction Solid and Flow Velocity", 9th S2P Conference, Solid State Phenomena Vols 116-117, pp24-33 (2006).

Jorstad, J. L. and Pan, Q.Y., "Interaction of Key Variables During Rheocasting: Importance of Microstructure, Fraction Solid and Flow Velocity", Die Casting Engineer, NADCA (November, 2006).

Jorstad, J., "SLC™ , The Low-Cost Alternative for SSM Processing". Transactions, NADCA Casting Congress, Rosemont, IL (2002).

Midson, S.P. Minkler, R.B. and Brucher, H.G., Proceedings of the 6th International Conference on Semisolid Processing of Alloys and Composites, Turin, Italy, pp. 67-71 (2000).

Pan, Q.Y. Apelian, D. and Alexandrou, A.N., Metallurgical and Materials Transactions B, Vol. 35B, pp. 1187-1202 (2004).

Papanastasiou, T.C., J. of Rheology, vol. 31, pp. 385-404 (1987).

Paradies, C.J. and Rappaz, M., Proceedings of the 8th International Conference on Modeling of Casting and Welding Processes, San Diego , pp. 933-940 (June 7-12, 1998).

Date: _____ Express Mail Label No._____

Inventors: Anacleto M. de Figueredo, Diran Apelian, Matt M. Findon, and Nicholas Saddock

Attorney's Docket No.: 1021.2003-001

ALLOY SUBSTANTIALLY FREE OF DENDRITES AND METHOD OF FORMING THE SAME

RELATED APPLICATION

This application claims the benefit of U.S. Provisional Application No. 60/412,992, filed on September 23, 2002, the entire teachings of which are incorporated herein by reference.

GOVERNMENT SUPPORT

The invention was supported, in whole or in part, by grant DE-FC 36-02ID 14232 from the Department of Energy. The Government has certain rights in the invention.

BACKGROUND OF THE INVENTION

Semi-solid metal (SSM) processing is a technology that resulted from research in the early 1970's at the Massachusetts Institute of Technology. It was found that imposing a shear on a liquid metal before the solidification process began and continuing the shear while the liquid cooled below its liquidus resulted in a non-dendritic microstructure with a shear stress (and corresponding viscosity) nearly three orders of magnitude lower than that of the dendritic material. At rest, the non-dendritic metal slurry behaved as a rigid material in the two-phase region; that is, its viscosity was high enough that it could be handled as a solid. However, when a shear stress was applied, the viscosity decreased dramatically so that the material behaved more like a

liquid. Thus, the slurry could flow in a laminar fashion, with a stable flow front, as opposed to the turbulent flow characteristic of molten metal.

A property of semi-solid metal ("slurry") that renders it superior to conventional casting processes is the non-turbulent ("laminar" or "thixotropic") flow behavior that results when one enters the "two-phase" field of solid plus liquid. Specifically, shearing of semi-solid slurry leads to a marked decrease in viscosity, so that a partially frozen alloy can be made to flow like a non-Newtonian fluid. Thixotropic flow behavior arises from the ideal SSM microstructure of small, spherical particles (e.g., α-Al) suspended in a liquid matrix. In all semi-solid processes, it is imperative that this microstructure be produced consistently. Moreover, a uniform distribution of this microstructure throughout a volume of slurry is essential for production of high-quality components.

The benefits that semi-solid processing holds over conventional liquid metal casting result from the flow behavior of the partially solidified metal. The way in which a metal fills a mold (or die cavity) directly impacts the solidification of the metal; thus, the properties of the formed part can be enhanced with improved mold filling. Turbulent flow of liquid metal into a die or mold can lead to incorporation of air and mold gases into the melt. This in turn can lead to both macro- and micro-porosity in the final part, which negatively affect its mechanical properties.

There are several reasons that the laminar flow of semi-solid slurries is very advantageous from a casting standpoint. The first major reason is the elimination of gas entrapment, resulting in decreased porosity and oxide content in the formed part. Secondly, since semi-solid metal has lower heat content than superheated molten metal, there is less solidification shrinkage in the casting. Thus, molds can be filled more effectively and uniformly, and less post-casting machining is required. As a result, all semi-solid processes are potentially "near net-shape" processes. The reduced heat content also lowers the thermal stresses of the casting apparatus (typically a steel die) that contacts the metal, leading to longer tool life. Also, since the starting material has the thixotropic microstructure, the microstructure of any part formed with semi-solid processing is always equiaxed and non-dendritic. Therefore, the mechanical properties

of the final component are better than a similar part formed from a conventional casting process.

The net result of the above-described advantages is that semi-solid casting can be used to produce intricate components with superior mechanical properties. The typical defects associated with molten metal casting can be circumvented when the microstructure (and thus the flow behavior) of the slurry is controlled. From an economic standpoint, it is expected that due to improved tool life, shorter cycle times, reduced machining, and ability to use less expensive heat treatment schedules, semi-solid processes will ultimately become as cost-effective as conventional casting routes such as high pressure die casting. Perhaps the most attractive attribute of semi-solid forming, however, is that due to the laminar flow of the slurry, very complex shapes can be cast, with thin walled sections on the order of millimeters.

A number of processes have been designed to take advantage of the unique behavior of semi-solid metal slurries. These processes produce the thixotropic microstructure through some method of vigorous agitation during solidification. It was hypothesized that the induced agitation broke up (or facilitated the melting off of) dendrite arms, which then ripened and spheroidized to form a non-dendritic structure.

There are two routes for processing semi-solid metal, i.e. two different ways to arrive at the desired point within the solid-liquid, two-phase region. The first route starts from the solid state ("thixocasting"), and the second starts from the liquid state ("rheocasting").

Thixocasting processes start out with a solid precursor material ("feedstock") that has been specially prepared by a billet manufacturer, and then supplied to the casting facility. The feedstock metal has an equiaxed, non-dendritic microstructure. Small amounts or "slugs" of this alloy are partially melted by reheating into the semi-solid temperature range, leading to the thixotropic structure. In most applications, the slug is subsequently placed directly into a shot sleeve of a die casting apparatus, and the part is formed.

During the initial years of SSM process development, mechanical stirring was used in various ways to break up dendrites and produce thixotropic metal structures.

The combination of rapid heat extraction and vigorous melt agitation was effected by using different sizes, shapes, and velocities of stirring rods. Various researchers addressed the evolution of the "stircast" structure during this time. Although these methods worked well in that they effectively produced the desired metal structures, erosion of the stirrer became the "weak link" of the process.

Magnetohydrodynamic (MHD) casting process has been utilized to overcome the limitations associated with the use of stirrers. In this approach, dendrites are still formed and then broken from the nuclei by agitation. The source of the agitation is not a mechanical stirrer, but alternating electromagnetic fields. Induction coils are placed around a crucible to induce these forces. The crucible is equipped with a cooling system to initiate freezing in the alloy while the melt is exposed to the electromagnetic forces. Upon cooling down to ambient temperature, the alloy has an equiaxed, non-dendritic microstructure. However, the MHD stirring process requires complicated and expensive machinery.

Thixoforming processes comprise the majority of industrial semi-solid applications used today. Rather than producing a semi-solid slurry directly from a superheated melt, a specially prepared feedstock metal is heated to form the semi-solid slurry. This approach eliminates the need for melting equipment within the SSM casting facility. However, the special feedstock must be purchased from special manufacturers at a premium in the form of metal billets, therefore thixocasting processes are not economical compared to conventional processes. Furthermore, in thixocasting processes, scrap metal must be sent back to the billet manufacturer and cannot be recycled. Most importantly, process control is difficult in thixocasting, because solid fraction (and corresponding viscosity) is sensitive to temperature gradients in the reheated material. Thus, narrow temperature ranges must be achieved consistently for successful operations. This, combined with the time it takes (several minutes on average) to reheat the feedstock to the desired solid fraction, negatively affects productivity.

The development of ideal one-step rheocasting applications is highly preferable to the current two- or three-step applications associated with most thixocasting methods.

Current thixocasting approaches are inherently batch processes, in which only small amounts of slurry can be produced during each forming operation. This places limits on the sizes and shapes of parts produced in this manner. A continuous process would circumvent these hindrances, and could be used for a broader variety of applications.

To date, none of these processes has satisfactorily addressed the need for providing a continuous semi-solid casting route. The current need in the SSM field is a relatively simple, easy-to-implement, flexible process that can be used for a wide variety of processing applications. Such a process should use relatively simple methods of melt agitation to avoid the problems associated with the previously discussed approaches.

SUMMARY OF THE INVENTION

This invention includes methods and processes for forming a semi-solid slurry. In one embodiment, this invention includes a method for forming an alloy substantially free of dendrites, comprising the steps of cooling a superheated alloy to form a nucleated alloy, wherein the nucleated alloy includes a plurality of nuclei, wherein essentially all of said nuclei are substantially free of entrapped liquid; controlling the temperature of the nucleated alloy to prevent the nuclei from melting; mixing the nucleated alloy to distribute the nuclei throughout; and cooling the nucleated alloy with nuclei distributed throughout, thereby forming an alloy substantially free of dendrites.

In another embodiment, this invention includes a continuous process for forming an alloy substantially free of dendrites, comprising the steps of directing a superheated alloy stream into a reactor, wherein the superheated alloy stream is continuously cooled and mixed to form a nucleated alloy stream, wherein the nucleated alloy stream includes a plurality of nuclei distributed throughout, wherein essentially all of said nuclei are substantially free of entrapped liquid; and continuously controlling the temperature of the nucleated alloy stream to prevent the nuclei from melting and continuously mixing the nucleated alloy stream to distribute the nuclei throughout, thereby continuously forming an alloy substantially free of dendrites.

In yet another embodiment, this invention includes a method for forming an alloy substantially free of dendrites, comprising the steps of cooling a superheated alloy to form a nucleated alloy, wherein the nucleated alloy includes a plurality of nuclei substantially free of entrapped liquid; controlling the temperature of the nucleated alloy to prevent the nuclei from melting and passively mixing the nucleated alloy to distribute the nuclei throughout; and cooling the nucleated alloy with nuclei distributed throughout, thereby forming an alloy substantially free of dendrites.

In a further embodiment, this invention includes a method for forming an alloy substantially free of dendrites, comprising the steps of superheating a first metal; superheating a second metal; mixing the first and second metals to form a superheated alloy; cooling the superheated alloy to form a plurality of nuclei substantially free of entrapped liquid; mixing the superheated alloy to distribute the plurality of nuclei throughout the superheated alloy; controlling the temperature of the superheated alloy to prevent the nuclei from remelting; and cooling the superheated alloy while the nuclei are distributed throughout, thereby forming an alloy substantially free of dendrites.

In still further embodiments, this invention includes an alloy substantially free of dendrites formed by a method comprising the steps of cooling a superheated alloy to form a nucleated alloy, wherein the nucleated alloy includes a plurality of nuclei substantially free of entrapped liquid; controlling the temperature of the nucleated alloy to prevent the nuclei from melting; mixing the nucleated alloy to distribute the nuclei throughout; and cooling the nucleated alloy with nuclei distributed throughout, thereby forming an alloy substantially free of dendrites.

The present invention has many advantages. This invention provides for semi-solid metal production process simplicity, control over semi-solid metal structure evolution, and the fast adjustment of physical characteristics of the slurry produced (e.g., solid fraction and the size of nuclei). This invention allows for the production of semi-solid slurries without the need to break up dendrites through external stirring of the metal slurry. Hence, this invention eliminates the need to use, repair, replace, and maintain mechanical stirring rods or expensive and complicated electromagnetic stirring mechanisms.

Also, this invention allows for semi-solid applications that do not need expensive, specially produced feedstocks (e.g., billets) or the associated recycling of such feedstocks, which can be complicated, time consuming, and expensive. By eliminating the need for specialty feedstock, this invention eliminates the time consuming step of reheating such a feedstock. In addition, not only does this invention eliminate the rigors associated with returning scrap feedstock to a feedstock supplier, but it also allows a practitioner to immediately reuse waste materials.

This invention provides continuous processes for producing semi-solid metal slurries. These continuous processes allow semi-solid metal slurries to be used in a much broader range of applications and relax the size and shape limitations imposed by the use of batch processes.

BRIEF DESCRIPTION OF THE DRAWINGS

The foregoing and other objects, features, and advantages of the invention will be apparent from the following more particular description of preferred embodiments of the invention, as illustrated in the accompanying drawings in which like reference characters refer to the same parts throughout the different views. The drawings are not necessarily to scale, emphasis instead being placed upon illustrating the principles of the invention. All parts and percentages are by weight unless otherwise indicates. All temperatures are in degrees Centigrade unless otherwise indicated.

Figure 1 shows a schematic diagram of an apparatus for producing an alloy substantially free of dendrites.

Figure 2 is a side-view of a reactor portion of the liquid mixing apparatus constructed to perform various experiments relevant to this invention.

Figure 3A and 3B exhibit micrographs from the T1-2 experiment.

Figure 4A and 4B exhibit micrographs from the T1-3 experiment.

Figure 5A and 5B exhibit micrographs from the T1-4 experiment.

Figure 6A and 6B exhibit micrographs from the T2-4 experiment.

Figure 7A and 7B exhibit micrographs from the T2-5 experiment.

Figure 8A and 8B exhibit micrographs from the T2-6 experiment.

Figure 9A and 9B exhibit micrographs from the T2-8 experiment.

Figure 10A and 10B exhibit micrographs from the R1-1 experiment.

Figure 11A, 11B, 11C, and 11D exhibit micrographs from experiment R2-2.

Figure 12A, 12B, and 12C exhibit micrographs from experiments R2-5, R2-6, and R2-7.

Figure 13A, 13B, and 13C exhibit micrographs from experiments R2-5, R2-6, and R2-7.

Figure 14A, 14B, and 14C exhibit micrographs from experiments R2-5, R2-6, and R2-7.

Figure 15A and 15B exhibit micrographs from experiment R2-5.

Figure 16A and 16B exhibit micrographs from experiment R3-1.

Figure 17A and 17B exhibit micrographs from experiment R3-4.

Figure 18A and 18B exhibit micrographs from experiment R3-5.

Figure 19 is a graph of particle size in as-solidified structures as a function of cooling rate of the slurry after exiting the reactor.

Figure 20 is a graph of particle size in slurry structures at 590°C as a function of cooling rate of the slurry after exiting the reactor.

DETAILED DESCRIPTION OF THE INVENTION

It has been advantageously discovered that the copious nucleation of a primary phase during the early stages of solidification coupled with forced convection due to complex fluid flow can result in the formation of semi-solid metal (i.e., "SSM") slurries useful in applications where thixotropic flow behavior of a metal alloy is advantageous and/or necessary (e.g., semi-solid processing applications). By controlling the temperature distribution, it is possible to maximize effective nucleation rates in the solidifying bulk liquid and ensures nuclei "survival" (i.e., the nuclei do not remelt into the metal liquor). The nuclei are dispersed throughout the bulk liquid by convective currents, where they can act as further nucleation sites and contribute to a homogeneously thixotropic microstructure. When very high numbers of nuclei are formed and prevented from remelting, the growth in size of the individual particle is

limited, since there is a lack of space available for the particles to grow into. Moreover by limiting growth, this allows the initial morphologies of the nuclei to remain unaffected; therefore enough of the nuclei initially grow spherically and overall dendritic growth is suppressed throughout the alloy.

Generally, this invention includes a method for forming an alloy substantially free of dendrites. For example, this invention includes a method for forming a semi-solid slurry or a metal suitable for processing in an application that requires semi-solid slurries. Such a slurry can be used as a feed material for applications that require a supply of a semi-solid slurry (e.g., a rheocasting application) or be formed into billets for later use (e.g., in a thixocasting application).

In one embodiment, the method comprises the steps of cooling a superheated alloy to form a nucleated alloy, wherein the nucleated alloy includes a plurality of nuclei substantially free of entrapped liquid; controlling the temperature of the nucleated alloy to prevent the nuclei from melting; mixing the nucleated alloy to distribute the nuclei throughout; and cooling the nucleated alloy with nuclei distributed throughout, thereby forming an alloy substantially free of dendrites.

Initially, the materials comprising the superheated alloy are heated to a temperature sufficient to liquefy all of the constituent components of the alloy. Examples of suitable temperatures include 5°C, 10°C, 15°C, 25°C, 35°C, 45°C, 50°C, or more than 50°C above the temperature at which the materials that make up the alloy are entirely liquid.

In some embodiments, the superheated alloy includes two or more materials used to make metallic items. For example, the superheated alloy can comprise mixtures that include aluminum, lead, tin, magnesium, manganese, strontium, titanium, silicon, iron, carbon, copper, gold, silver, and zinc. In further embodiments, the superheated alloy includes grain refiners, such as borides of titanium (e.g., TiB_2), borides of aluminum (e.g., AlB_2), TiC, and Al_3Ti.

In some embodiments, one or more of the individual components that are to make up the superheated alloy are heated separately. For example, if the superheated alloy is to comprise aluminum and titanium, the aluminum and titanium can be liquefied

or partially liquefied before they are mixed together to form the superheated alloy. In yet more embodiments, the individual components of the superheated alloy are heated to different temperatures before they are mixed. For instance in the previous example, the titanium can be heated to a dissimilar temperature as the aluminum before the two are mixed to form the superheated alloy.

The superheated alloy is cooled to form a nucleated alloy, wherein the nucleated alloy includes a plurality of nuclei substantially free of entrapped liquid. Preferably, the temperature is sufficiently low so as to provide for the copious formation of nuclei, yet sufficiently high that the formation of dendrites is substantially prevented. The temperature that accomplishes this varies with the composition of the alloy and the demands of the given application. In some embodiments, the nucleated alloy is formed by reducing the temperature of the superheated alloy to the liquidus temperature or slightly below the liquidus temperature. For example, the superheated alloy may be cooled to 1°C, 2°C, 3°C, 4°C, 5°C, 7°C, 9°C, 10°C, or more than 10°C below the liquidus temperature. In other embodiments, during this nuclei-forming stage, the nucleated alloy comprises a solids volume fraction of about 1% or less.

The temperature of the nucleated alloy is controlled to prevent the nuclei from melting, and the nucleated alloy is mixed to distribute the nuclei throughout the alloy. The temperature control scheme used to prevent the nuclei from melting varies depending on the composition of the alloy and the demands of the given application. In some embodiments, controlling the temperature to prevent the nuclei from melting entails maintaining the nucleated alloy at the same temperature to which the superheated alloy was initially cooled to provide for the copious formation of nuclei. In other embodiments, controlling the temperature entails continuously cooling the nucleated alloy at some predetermined rate and/or in a predetermined manner.

While cooling, the nucleated alloy is mixed in order to distribute the nuclei throughout the alloy. The distributed nuclei act as further nucleation sites and contribute to a homogeneously thixotropic microstructure. In some embodiments, the nucleated alloy is mixed by a passive mixer or by directing it through a tortuous flow path that induces convection and/or turbulence in the nucleated alloy.

The temperature of the nucleated alloy with nuclei distributed throughout is reduced to form an alloy substantially free of dendrites. The cooling rate of the nucleated alloy with nuclei distributed throughout and temperature to which it is cooled depends on the composition of the alloy and the demands of the given application. For example, some applications may require the alloy to be cooled at a rate of at least 5°C per second. In other embodiments, the cooling rate is at least 15°C per second. Other applications may require the alloy to be cooled at a rate of between about 20°C per second and about 30°C per second. In some embodiments, during this stage of nuclei growth, the nucleated alloy attains a solids volume fraction of at least about 30%. In yet more embodiments, the nucleated alloy attains a solids volume fraction in the range of about 40% to about 60%.

In some embodiments, the temperature of the alloy substantially free of dendrites is above the solidus line and the alloy is in the form of a slurry. In such embodiments, the alloy substantially free of dendrites can be directed to a metal forming process (e.g., a reheocasting application) where it is further formed and cooled to make a metal component. In other embodiments, the temperature of the alloy substantially free of dendrites is lowered below the solidus line prior to use in a metal forming process. For example in some embodiments, the nucleated alloy is poured into a form for a metal billet that is used as a specialty feedstock for future processing procedures (e.g., a thixocasting application) and cooled (e.g., by quenching with a cooler material).

In some embodiments, the alloy substantially free of dendrites possesses a primary particle size of about 100 microns or less. In other embodiments, the alloy substantially free of dendrites has a primary particle size in the range of between about 50 microns and about 100 microns when fully solid. In yet further embodiments, the alloy substantially free of dendrites has a primary particle size in the range of between about 30 microns and about 70 microns when the alloy is a slurry with a solid fraction of about 50%. In some embodiments, the alloy substantially free of dendrites possesses an average shape factor of at least 0.5. In other embodiments, the alloy substantially

free of dendrites possesses an average shape factor in the range of between about 0.75 and about 0.95.

In some embodiments, this invention includes a continuous process for forming an alloy substantially free of dendrites, comprising the steps of directing a superheated alloy stream into a reactor, wherein the superheated alloy stream is continuously cooled and mixed to form a nucleated alloy stream, wherein the nucleated alloy stream includes a plurality of nuclei, wherein essentially all of said nuclei are substantially free of entrapped liquid distributed throughout; and continuously controlling the temperature of the nucleated alloy stream to prevent the nuclei from melting and continuously mixing the nucleated alloy stream to distribute the nuclei throughout, thereby continuously forming an alloy substantially free of dendrites.

In yet another embodiment, this invention includes a method for forming an alloy substantially free of dendrites, comprising the steps of cooling a superheated alloy to form a nucleated alloy, wherein the nucleated alloy includes a plurality of nuclei substantially free of entrapped liquid; controlling the temperature of the nucleated alloy to prevent the nuclei from melting and passively mixing the nucleated alloy to distribute the nuclei throughout; and cooling the nucleated alloy with nuclei distributed throughout, thereby forming an alloy substantially free of dendrites.

In a further embodiment, this invention includes a method for forming an alloy substantially free of dendrites, comprising the steps of superheating a first metal; superheating a second metal; mixing the first and second metals to form a superheated alloy; cooling the superheated alloy to form a plurality of nuclei substantially free of entrapped liquid; mixing the superheated alloy to distribute the plurality of nuclei throughout the superheated alloy; controlling the temperature of the superheated alloy to prevent the nuclei from remelting; and cooling the superheated alloy while the nuclei are distributed throughout, thereby forming an alloy substantially free of dendrites.

Figure 1 is a schematic of apparatus 10, which can produce alloy 12. Alloy 12 is an alloy substantially free of dendrites. Two metals 14, 16 are heated separately until they attain a superheated liquid state in melting furnaces 18, 20, respectively. After metals 14, 16 have attained the desired temperature, they are directed from melting

furnaces 18, 20 through runners 22, 24 and into reactor 26. Optionally, runners 22, 24 include heaters to mitigate heat loss from metals 14, 16 en route to reactor 26.

The two flows of metal 14, 16 mix within reactor 26, leaving as alloy 12, which is collected in crucible 28. Inside of reactor 26, the temperature of the combined flow of metals 14, 16 is reduced to below the liquidus line in order to induce the formation of nuclei. The combined flow follows a "tortuous path" defined by reactor 26. The tortuous path induces forced convection and/or turbulence in the metal flow, which distributes the nuclei throughout the flow.

In some embodiments, the reactor is heated or cooled to vary the rate of heat extraction. In other embodiments, the reactor includes a heating means (e.g., a heating element) and/or cooling means (e.g., a chiller or cooling stream). The heating and cooling means provide for increasing or decreasing the rate of heat loss from the flow to reactor 26. By removing or slowing the rate of heat loss from the flow, the rate of nucleation in the flow and/or the resulting volume fraction of solids in alloy 12 is manipulated.

Apparatus 10 can be incorporated into either a thixocasting or rheocasting application. For example, in one rheocasting embodiment, alloy 12 is directed into a molding die while the temperature of alloy 12 is still above the solidus line. Once in the die, alloy 12 is cooled to form a metal component. In a thixocasting embodiment, alloy 12 is formed into a billet for latter use in a semi-solid metal forming application.

In still further embodiments, this invention includes an alloy substantially free of dendrites formed by a method comprising the steps of cooling a superheated alloy to form a nucleated alloy, wherein the nucleated alloy includes a plurality of nuclei substantially free of entrapped liquid; controlling the temperature of the nucleated alloy to prevent the nuclei from melting; mixing the nucleated alloy to distribute the nuclei throughout; and cooling the nucleated alloy with nuclei distributed throughout, thereby forming an alloy substantially free of dendrites.

EXPERIMENTAL SETUP

A liquid mixing apparatus was constructed in a manner similar to the schematic of Figure 1 to perform various experiments relevant to this invention. Two melting furnaces were formed from two ~15.24 cm in diameter and ~30.48 cm high (~6 inches in diameter and ~12 inches high) resistance tube furnaces were placed in sheet steel housings and insulated. Within each of these furnaces, a crucible-holding setup was constructed. The crucible-holding setup included two top and bottom steel rings connected to two threaded rods that ran vertically through the furnaces. These rods connect to a beam above the furnaces, and were anchored to ~10.16 cm diameter (~4 inches) ring plates that were in contact with the bottoms of the furnaces. The steel rings clamped the crucible in place, and the rods were put in tension so that the crucibles did not contact the furnace element.

The bottoms of the clay-graphite crucibles included threaded ~2.54 cm (~1 inch) holes. A "spout" component was screwed into the holes and extended about an inch from the bottom of the crucible. The exit hole through which the superheated metal flowed was ~1.27 cm (~0.5 inches) diameter. About a ~1.27 cm (~0.5 inches) diameter stopper rod was used to plug the hole during melting and temperature stabilization of the metal feeds. The rod and the spout were both made from hot-pressed boron nitride (BN).

The stopper rods were connected to two pull-action solenoids that were connected to the overhead beam. Both of the solenoids were wired to a toggle switch so that when the switch was thrown, the plugs were pulled from the exit spout allowing the liquid metal to flow from the exit holes of each crucible at the same time. Since each crucible was in a separate furnace, the temperatures of each feed metal could be independently controlled and monitored so that the heat contents of the melts upon mixing were precisely known.

The space beneath the melting furnaces was comprised of heated runners that transported the melt streams to the reactor. These runners were ~2.54 cm (~1 inch) diameter steel conduit tubes with a straightaway length of ~38.1 cm (~15 inches) and an angled length of ~10.16 cm (~4 inches). Several coats of insulating BN coating were applied to the insides of the tubes. In order to prevent heat loss from the flowing melts

during transport, the runners were heated to ten degrees above the temperatures of the melts using coiled heating elements. These elements ensured a uniform temperature distribution along the entire lengths of the runners. Insulation was wrapped tightly around the tubes prior to an experiment and the temperature was controlled using a thermocouple placed in direct contact with the tube. It was experimentally determined that no heat was lost through the runners during the various experiments.

At the entrance of the reactor, a steel "boot" component was placed around the tubes in order to change the angle and diameter of incoming liquid to match that of the reactor passages and to prevent welding of the metal flows to the entrance bays of the reactor. The boot was coated with BN and placed in contact with the tube heaters in order to prevent premature solidification of the melts.

The reactor used during the various experiments was machined from a square copper block, ~7.62 cm (~3 inches) square and ~15.24 cm (~6 inches) in height. The diameter of the inner channels was ~1.27 cm (~0.5 inches). Figure 2 shows a cut-away view of the reactor. Reactor 30 includes first melt inlet 32 and second melt inlet 34 for receiving one or more liquid melts. First melt inlet 32 has first exit 36, which connects to first channel 38. Second melt inlet 34 has second exit 40, which connects to second channel 42. First channel 38 and second channel 42 intersect at point 44 to allow liquid melts to mix with each other. First channel 38 and second channel 42 separate and later intersect again farther down stream at second point 46 to combine and mix in exit conduit 46. The melts in each channel exit reactor 30 through conduit 48 to enter, for example, a crucible.

It was important to ensure that the reactor would produce sufficient convection to effectively mix the melt streams. Therefore, a similitude experiment was carried out in which two water streams containing different colored dyes were mixed within the reactors. A transparent plastic was placed over the face of the reactor and the experiment was recorded with a video camera. It was determined that adequate mixing took place within the reactor and that metal melts flowing through the reactor would experience forced convection due to interaction between the two liquid streams.

As seen in Figure 2, the copper block of the reactor was split in half along the vertical direction. The inner machining was done using a computer-guided end mill. Holes were tapped in the two faces so that the two halves of each block could be clamped together with hexagonal screws. The inner face of the reactor was coated with graphite spray to improve melt flow. Four small thermocouple holes were also endmilled at various points of the mixing channel in order to record the temperatures of the flowing melt streams at various points of the process. Finally, two support arms were constructed to connect to the top of the reactor, allowing for the reactor to be placed within a third preheating furnace. When the third preheating furnace was not used, the reactor sat on two parallel beams, set at an appropriate height to connect to the transport tubes. The receiving crucible was placed as close to the exit of the reactor as possible to minimize turbulence in the product slurry as it filled the receptacle.

Three alloys were used throughout the various experiments: A356.2 (with no grain refiners; hereafter referred to as "NGR"), A356.2 (with TiB_2 grain refiners; hereafter referred to as "GR"), and SiBloy® (Elkem Aluminium ANS, Oslo, Norway) which contains permanent grain refiners in the form of AlB_2 particles. Table 1 gives the chemical compositions (in wt %) and liquidus temperatures (T_L in °C) of each of these alloys. Chemical compositions were obtained with a spectrographic analysis machine. Liquidus temperatures were determined with the derivative method on data collected in cooling experiments using calibrated thermocouples.

Table 1

	T_L	Si	Fe	Mn	Mg	Ti	Sr	V	B	Al
NGR	616.2	6.82	0.07	0	0.324	<0.002	<0.001	0.006	0.001	Balance
GR	615.5	6.87	0.06	0	0.36	0.11	<0.001	0.008	0.0005	Balance
SiBloy®	616.0	6.83	0.08	0.02	0.291	0.003	0	0.001	0.016	Balance

NGR had a negligible Ti content, and thus was absent of grain refinement. The GR alloy included TiB_2 ("TiBor") grain refiners. SiBloy® is a permanently grain refined alloy containing AlB_2 particles in the molten state.

Example 1: Thixocasting Experiments T1

Thixocasting processes were simulated in a series of experiments. The slurry was solidified in air within a clay-graphite crucible, after which small samples were reheated into the semi-solid metal range and quenched.

Heat transfer conditions in the reactor were affected by varying two parameters: melt superheat and reactor temperature. In the first set of thixocasting experiments (denoted "T1"), the superheats of the precursor melts were varied from 1-64°C in order to gauge the heat extraction capability of the reactor. The reactor was kept at room temperature. Table 2 lists these experiments. "T_{IN}" refers to the temperature of each melt prior to mixing.

Table 2

Exp.	T_{IN} (°C)	Mass/melt (g)	Alloy	$T_{reactor}$ (°C)
T1-1	617	300	NGR	room temp.
T1-2	625	300	NGR	room temp.
T1-3	640	300	NGR	room temp.
T1-4	660	300	NGR	room temp.
T1-5	680	300	NGR	room temp.

Figures 3A, 3B, 4A, 4B, 5A, and 5B exhibit the representative micrographs from the T1-2, T1-3, and T1-4 experiments, respectively. The as-solidified micrographs are shown as Figures 3A, 4A, and 5A, while the micrographs on Figures 3B, 4B, and 5B show the microstructure obtained after reheating to 585°C and holding for 10 minutes, followed by immediate quenching in water. The microstructures in Figure 3B had a residence time of reheated slug in semi-solid metal range of about 38 minutes. The microstructures in Figure 4B had a residence time of reheated slug in

semi-solid metal range of about 25 minutes. The microstructures in Figure 5B had a residence time of reheated slug in semi-solid metal range of about 18 minutes.

Figures 3-5 show the effect of raising the superheat of the precursor melts on the resultant microstructures. Each of the above microstructures is highly refined compared to typical as-received ingots. The reheated samples show globular α-Al particles distributed in a liquid matrix, with very little entrapped liquid. It is clear that the entrapped liquid in these samples results from coarsening of irregular (i.e. semi-dendritic) particles during reheating. Most of the particles have a spherical morphology, but small portions of them are irregular in shape. Irregularly shaped particles are likely related to dendritic growth within the reactor. Although to a limited extent, small dendrites inevitably grow in parts of the flowing liquid and collisions of these particles may account for the observed shapes. Also evident in the micrographs is an appreciable level of particle agglomeration, which is common characteristic of the structures obtained with the current reactor. It is believed this is a combination of the collisions undergone as the melts flow through the reactor, and grain coalescence during reheating.

Table 3

Experiment	Avg. Particle Diameter, As-solidified (μm)	Avg. Particle Diameter, reheated (μm)	Avg. Shape Factor, reheated	Number of particles analyzed
T1-2	65.2	92.1	0.86	547
T1-3	76.7	96.8	0.88	409
T1-4	90.1	101.2	0.87	378

Table 3 summarizes the image analysis results for the micrographs of Figures 3A, 3B, 4A, 4B, 5A, and 5B. Increasing the superheat clearly results in larger particle size in both the as-solidified and reheated samples. Shape factor data show that increasing superheat does not affect the morphologies of the analyzed particles. Shape factor was determined from the relationship:

$$\textit{Shape Factor} = (4\pi * \textit{Area}) / \textit{Perimeter}^2$$

A shape factor value of one corresponds to a perfectly spherical particle, whereas values close to zero indicate dendrites or very irregularly shaped particles. In the reheated samples (and slurry samples shown later), only the more spherical particles were analyzed in order to avoid confusion arising from numerical contributions of irregular particles. This was achieved by defining a classification scheme in the analysis program in which particles with very low shape factor values were excluded. Finally, the number of particles analyzed gives an indirect quantification of the degree of particle irregularity in the samples. Although the micrographs chosen may not portray the exact fraction of irregular particles in the entire sample, it is noteworthy that this value decreases for increasing superheat.

In Figure 3B, the most uniform as-solidified structure is observed, with the highest level of grain refinement and non-dendritic morphology. Figure 4B exhibits a similar microstructure, but with a larger average particle diameter. There is still a high amount of non-dendritic particles, but a well-globularized semi-solid metal structure is obtained upon reheating. Figure 4B has the largest particle size, and shows the highest number of irregular particles. Even at this high superheat, the particles are for the most part non-dendritic. Despite the higher fraction of irregular particles, the reheated structure indicates a predominantly globular morphology. This is probably due to the long residence times of the reheated samples in the SSM range (due to the long time is took for the sample to reach 585°C). Longer residence times lead to coarsening of the particles; therefore initially irregular particles may become more spherical due to the driving force for these particles to reduce surface area. This also explains why for each experiment the particles in the reheated samples are larger than in the as-solidified ones.

It is concluded from the T1 experiments that globular structures can be obtained by mixing alloy melts having relatively high superheats. This indicates that the reactor is able to extract very large amounts of heat in a small amount of time. Therefore it is not necessary to have a precursor liquid very close to the liquidus temperature in order to obtain thixotropic structures with the processes of this invention. Finally in both the as-solidified and reheated samples, there is a clear trend of (a) increasing particle size

for increasing superheat and (b) increasing level of particle irregularity (or tendency to grow dendritically to small degrees) for increasing superheat.

Example 2: Thixocasting Experiments T2

In a second set of thixocasting experiments (denoted "T2"), three superheats and three reactor temperatures were chosen to observe the effects of different heat transfer conditions on the resultant structures. The reactor was placed within the third furnace, and four thermocouples were inserted into the thermocouple holes to monitor its temperature. An increase in reactor temperature decreased the heat extraction rate of the melts as they flowed through the reactor, thereby decreasing the nucleation rate of the combined melts. The receiving crucible was at ambient temperature upon collection of the slurry. A thermocouple placed in the exit channel recorded the slurry's exit temperature. Table 4 lists the experiments carried out with this configuration.

Table 4

Exp.	T_{MIX} (°C)	$T_{reactor}$ (°C)	Alloy	Mass/melt (g)
T2-1	625	130		300
T2-2	625	315	NGR	300
T2-3	625	500		300
T2-4	640	130		300
T2-5	640	315	NGR	300
T2-6	640	500		300
T2-7	655	130		300
T2-8	655	315	NGR	300

For T2-4 through T2-6, the superheat was kept the same while the temperature of the reactor was varied. T2-8 had the lowest heat extraction conditions, thus the temperature of the exiting slurry was above the liquidus.

The temperature of the reactor was increased in order to decrease its heat extraction capability. The purpose was to vary the processing conditions to give a wide range of particle morphologies, as well as to establish relationships between the

variables and the resultant microstructures. In doing so, the limits of the reactor's heat extraction capability were gauged. Figures 6A, 6B, 7A, 7B, 8A, 8B, 9A, and 9B show the micrograph results from some of the experiments listed above.

Figure 6A shows the micrograph for the as-solidified structure of experiment T2-4, and Figure 6B shows the reheated micrograph that had a 24-minute residence time in the SSM temperature range. Figure 7A shows the micrograph for the as-solidified structure of experiment T2-5, and Figure 7B shows the reheated micrograph that had a 25-minute residence time in the SSM temperature range. Figure 8A shows the micrograph for the as-solidified structure of experiment T2-6, and Figure 8B shows the reheated micrograph that had a 16-minute residence time in the SSM temperature range. Figure 9A shows the micrograph for the as-solidified structure of experiment T2-8, and Figure 9B shows the reheated micrograph that had a 2-minute residence time in the SSM temperature range.

The particle size in the as-solidified samples increases slightly from T2-4 to T2-5 due to the lower heat transfer within the reactor. In the reheated samples, it is observed that both experimental conditions lead to highly globular structures of similar particle size. Figure 7B shows roughly the same number of irregular particles as shown in Figure 6B, and the majority of both structures is globular. In these two experiments, the product slurry exited the reactor at a temperature just below the liquidus temperature of the alloy, resulting in a very low solid fraction, highly fluid slurry. This indicates that most of the particles seen in any given sample are formed at or just below the liquidus temperature; therefore it is only necessary to cool the liquid to one or two degrees below the liquidus temperature.

Table 5

Experiment	Avg. Particle Diameter, As-solidified (μm)	Avg. Particle Diameter, reheated (μm)	Avg. Shape Factor, reheated	Number of particles analyzed
T2-4	67.6	96.8	0.89	393
T2-5	76.8	98.5	0.9	387
T2-6	105.3	116.7	0.71	235

Table 5 lists the image analysis results for the T2 experiments. As used herein, the term "average" in relation to shape factor values refers to the mean value taken from the entire data set of all particles analyzed by the classification scheme.

The micrographs show that particle shape irregularity reaches a maximum when the reactor temperature is highest. Numerically, shape factor values are about the same in T2-4 and T2-5, but change noticeably in experiment T2-6. Also, the number of particles analyzed drops in T2-6, which suggests that more irregular particles were excluded by the classification scheme. Moreover, in T2-6 the presence of non-spherical particles in both the as-solidified and reheated samples is more evident than in the previous experiments. The exiting slurry was just above the liquidus temperature of the alloy, therefore the thermal conditions of the reactor led to a lower level of nucleation. The decrease in nucleation rate led to a larger particle size in T2-6, since grain growth was promoted by the presence of fewer particles. On reheating, a significant amount of liquid was entrapped by the coarsening particles, as seen in Figure 8B.

Figure 9B reinforces the reasoning presented above concerning the requirement of a small solid fraction of the slurry upon exit. The exit temperature was 618°C, and these microstructures show the highest degree of dendritic growth. This is because the majority of nuclei formed within the receiving crucible rather than the reactor; therefore there was a lower cooling rate through the alloy's liquidus temperature. Upon reheating and quenching, the dendrites in the as-solidified structure coarsened, but did not approach the level of sphericity observed in the previous reheated samples.

It is concluded from the T2 experiments that the goal of forming a distinct range of particle morphologies was met by heating the reactor to various temperatures. Particle size increased and shape factor decreased when the reactor was hottest (providing less heat extraction), which suggests less effective heat extraction in the reactor. A higher reactor temperature led to more dendritic morphologies, whereas lower reactor temperatures produced spherical, thixotropic slurry structures. The extent to which the metal is cooled below its liquidus temperature dictates how globular the overall structure becomes.

Example 3: Rheocasting Experiments R1

Rheocasting processes were simulated in another series of experiments. In these experiments, the slurry was collected and quenched into water at various temperatures within the two-phase range of the alloy. Three distinct methods of collecting the rheocast slurry were used in the rheocasting set of experiments. In the first method, slurry was quenched immediately into water without entering a crucible. In the second technique, a heated receiving crucible was employed from which small amounts of the slurry were removed at various times and quenched in water. In the third approach, the entire slurry crucible was quenched in water at a single temperature in the two-phase field. By changing the temperature of the receiving crucible, the cooling rates of the received slurry were varied.

Two experimental runs were conducted using the first method (denoted as "R1"). A large reservoir of cold water was used as a receptacle. This resulted in a very high cooling rate in the collected slurry. The experiment was conducted at a temperature of 625°C. All other conditions were identical to those in experiment T1-2 (see Table 3).

In the R1 experiments, the slurry went from the reactor's exit directly into the large volume of water. Therefore the sample was immediately quenched and the microstructure was frozen in place. In the experiment presented below, the temperature of the precursor melts was 625°C, giving a superheat of about 9°C. The reactor was at room temperature, as was the water used for quenching. The cooling rate and temperature of the slurry upon exit was not measured due to the experimental setup, but the conditions were the same as those in experiment T2-2. Figures 10A and 10B show two micrographs from this experiment.

Two micrographs for Experiment R1-1 are shown in Figures 10A and 10B and the observed microstructures are much different than those seen in the thixocasting experiments. The primary particles are a great deal smaller, which is to be expected since there is very little time allowed for growth. The fine structure of eutectic phase shows that the cooling rate during quenching was very fast. The smallest particle seen above is about 13.6 μm in diameter, and the largest one is about 34μm. The average

particle diameter is about 19.7 μm and the average shape factor is about 0.79. Also, there are many more irregularly shaped particles (as well as some rosettes) observed here than in the thixocasting experiments.

Two major factors contribute to the morphologies of Experiment R1-1. First, the higher heat transfer undergone within the water bath results in very little particle growth after nucleation. Secondly, the additional convection that is typically experienced by the slurry as it fills the receiving crucible is absent here. Since the slurry is highly fluid on exit, convection from crucible filling may contribute to breaking up of dendrites and spheroidization of the irregular particles. It should be noted that Figure 10B is not representative of the entire sample; rather, the dendrites only formed in a particular section of the quenched sample. It is possible that the dendrites did not form in the reactor, but instead nucleated as the liquid phase was exposed to the air in the short distance between the reactor and the water.

When low solid fraction semi-solid slurry is quenched into water, it is expected that large amounts of eutectic be quenched from the liquid phase; therefore the density of the primary particles should be low. However the micrographs in Figures 10A and 10B dispute this expectation, since a large number of particles was present in the slurry as it exited the reactor. The solid fraction observed in the micrographs, which were from a slurry at ~610°C, are much higher than one would expect. This evidence suggests that additional nuclei form during the water quench, and then grow to a very small degree. These nuclei were most likely formed on particles that were present in the slurry as it exited the reactor.

It is concluded from these experiments that very fine-grained structures are obtained when the slurry is immediately quenched and not collected in a crucible. This finding directly shows that there is a very high density of nuclei in the exiting slurry, which further indicates that copious nucleation takes place in the reactor. Also, the convection/turbulence undergone by the slurry as it fills a receiving crucible may play a role in the mechanisms leading to SSM structure formation.

Example 4: Rheocasting Experiments R2

The second method involved the direct collection of semi-solid slurry. Using the third furnace, the receiving crucible was preheated to various temperatures. After slurry collection, small amounts were scooped out from the receptacle and quenched in water. The reactor was kept at ambient temperature for each of these experiments. The first phase of these experiments, denoted "R2," is listed in Table 6.

Table 6

Exp.	T_{MIX} (°C)	T_{cruc} (°C)	Alloy	Samples taken at (°C)
R2-1	640	585	GR	597, 590, 585, 575, RT
R2-2	655	585	GR	605, 597, 590, 585, 575, RT
R2-3	625	585	GR	610, 605, 597, 590, 585, 575, RT
R2-4	670	585	GR	610, 597, 590, 585, 575, RT
R2-5	625	450	GR	610, 600, 590, RT
R2-6	625	450	SiBloy®	610, 600, 590, 580, RT
R2-7	625	450	NGR	600, 590, 580, RT

Since two different crucible temperatures (585°C and 450°C) were used in the experiments, different cooling rates of the slurry through the two-phase field resulted. In all experiments the mass of each charge was approximately 300g.

In the first experiment, a very slow cooling rate though the SSM range occurred due to a high receiving crucible temperature. In the other three experiments, the cooling rate was higher, and was kept nearly constant. In these higher cooling rate experiments, the variable of grain refinement additions was also investigated. For each of these experiments, the reactor was kept at room temperature ("RT").

Figures 11A, 11B, 11C, and 11D show a collection of micrographs from experiment R2-2. The cooling rate for R2-2 was approximately –0.7 °/sec. Figure 11A is a micrograph of a sample taken at 4.2 minutes and 605°. Figure 11B is a micrograph of a sample taken at 9.6 minutes and 597°. Figure 11C is a micrograph of a sample taken at 14.5 minutes and 590°. Figure 11D is a micrograph of a sample taken at room temperature.

The structures illustrated in Figures 11A, 11B, 11C, and 11D are superior to those obtained with the thixocasting method. Particle sizes are much smaller using this technique, and size distributions do not vary to an appreciable extent. The presence of dendrites in isolated regions of the samples is an interesting feature, but the majority of these structures are of a globular nature. These dendrites probably resulted from small volumes of liquid that were deposited into the receptacle just above the liquidus temperature. These results give direct evidence that the liquid mixing methods of this invention lead to highly globular semi-solid slurries of fine particle size. Upon entry of these slurries into the heated receptacle, a relatively large amount of time was spent in the SSM range due to the slow cooling rate resulting from a high receptacle temperature. Nonetheless, whatever amount of growth occurred did not result in a significant increase in particle size. The solid fractions suggested by Figures 11A, 11B, 11C, and 11D, however, are in contradiction with theoretical values. That is, one would expect to see more liquid phase at a temperature of 605°C. Table 7 summarizes the image analysis results for the samples of R2-2.

Table 7

Slurry temperature (°C)	**Avg. Particle Diameter (μm)**	**Avg. Shape Factor**	**Number of particles analyzed**
605	68.8	0.83	745
597	84.2	0.82	377
590	85.7	0.87	459
As-solidified (RT)	103.2	-	87

It is concluded from these results that using a heated crucible and collecting slurry during its residence time in the SSM range observe even better refined thixotropic structures. The particle sizes are much smaller when compared to the reheated structures of the thixocasting experiments. As seen in Table 7, particle size gradually increases as the slurry is solidified. Average shape factor data do not vary appreciably.

Figures 12A, 12B, 12C, 13A, 13B, 13C, 14A, 14B, 14C, 15A, and 15B compare micrograph results from experiments R2-5, R2-6, and R2-7 which all had substantially higher cooling rates (~-0.22°C/sec, ~-0.23°C/sec, and ~-0.18°C/sec, respectively) than experiment R2-2. The purpose of these experiments was twofold: first, to compare the presence of two different kinds of grain refiners to the non-grain-refiner-containing A356.2 alloy; and secondly, to study the effect of a higher cooling rate through the semi-solid temperature range.

Figures 12A, 12B, 12C, 13A, 13B, 13C, 14A, 14B, and 14C show that the presence of grain refiners in an alloy only modifies the resultant structures to a small degree. Figure 12A shows the micrograph of a sample from experiment R2-5 which was quenched at 600°C and 1.8 minutes, 12B shows the micrograph of a sample from experiment R2-6 which was quenched at 600°C and 2.0 minutes, and 12C shows the micrograph of a sample from experiment R2-7 which was quenched at 600°C and 2.3 minutes. Figure 13A shows the micrograph of a sample from experiment R2-5 which was quenched at 590°C and 2.3 minutes, 13B shows the micrograph of a sample from experiment R2-6 which was quenched at 590°C and 2.8 minutes, and 13C shows the micrograph of a sample from experiment R2-7 which was quenched at 590°C and 2.3 minutes. Figure 14A shows the micrograph of a sample from experiment R2-5 taken at room temperature, 14B shows the micrograph of a sample from experiment R2-6 taken at room temperature, and 14C shows the micrograph of a sample from experiment R2-7 taken at room temperature. "Quenching time" refers to the amount of time a metal stays in the two-phase range before quenching.

The two types of grain refiners used in the experiments both lead to a similar particle size. The micrographs also clearly indicate that when a non-grain refined alloy is used, the average particle size becomes slightly coarser; however, they still have highly refined structures in comparison to most commercial SSM processes. It should be noted that the cooling rate of the slurry after exiting the reactor in experiment R2-7 was slightly lower than in experiments R2-5 and R2-6, which may have contributed to this observed trend.

The structures shown in Figures 12A, 12B, 12C, 13A, 13B, 13C, 14A, 14B, and 14C indicate that the level of nucleation obtained with the reactor with no inoculants present is sufficient for the formation of equiaxed, non-dendritic structures. They also show that when inoculants are present prior to mixing within the reactor, even finer structures can be produced. Quantitative verification of these statements is presented in Table 8, which shows the general trend of increasing particle size in the three experiments.

Table 8

Sample	Avg. Particle Diameter (μm)	Avg. Shape Factor	Number of particles analyzed
GR A356.2 - 600°C	41.4	0.88	446
GR A356.2 - 590°C	55.3	0.88	127
GR A356.2 - As-solidified	66.4	-	203
GR SiBloy - 600°C	47.6	0.86	305
GR SiBloy - 590°C	54.2	0.88	241
GR SiBloy - As-solidified	65.9	-	231
NGR A356.2 - 600°C	60.5	0.88	561
NGR A356.2 - 590°C	67.9	0.9	458
NGR A356.2 - As-solidified	81	-	167

When comparing the above results to those shown in Table 7, it becomes clear that the increased cooling rate led to a much finer particle size than in experiment R2-2. Values for shape factor are about the same in all four runs.

Figures 15A and 15B show two additional microstructures from a sample taken during experiment R2-5. This sample was quenched at 610°C (~50 seconds after collection), corresponding to a low solid fraction. Figure 15A is at 50X magnification, while 16(b) is at 200X magnification. Figures 15A and 15B indicate that more

nucleation events occur during the slurry quenching technique. Image analysis results of these micrographs are shown below in Table 9. The very small particles nucleated as the scooping utensil (thimble) was used to transfer the sample from the crucible to the water. These nucleation events were likely facilitated by the presence of TiB_2 inoculants in the liquid phase of the slurry. Therefore, if this additional nucleation event had not occurred, then the structures would be comprised of the larger particles seen above, combined with quenched eutectic in the regions where the smaller particles are observed. This structure would better reflect the low solid fraction of the slurry at this temperature. The higher magnification micrograph of Figure 15B shows that these secondary α-Al particles nucleate on the previously formed particles.

Table 9

Sample	Avg. Particle Diameter (μm)	Avg. Shape Factor	Number of particles analyzed
R2-5 - 610°C	Large particles (primary nucleation event): 36.1 Small particles (secondary nucleation event): 10.5	0.85	150

It is concluded from these experiments that a higher cooling rate through the two-phase range leads to more refined SSM structures. Also, it is clear that the presence of grain refiners in the alloys used does not significantly affect the particle size and shape of the structures; that is, nucleation rate is not enhanced to an appreciable extent when inoculants are present. The level of equiaxed, non-dendritic growth observed in non-grain-refined A356.2 is high enough to conclude that the reactor design is the major contributor to the observed structures.

Example 5: Rheocasting Experiments R3

In an alternative approach, different preheat temperatures in the receiving crucible were used to attain different cooling rates of the product slurry through the

two-phase region. Furthermore, the entire slurry crucible was quenched in a large volume of water at a single temperature in the SSM range, rather than removing small amounts at iterated times. This gave a more accurate sense of the temperature of the sample upon quenching. The volume of slurry quenched here is much larger than the volumes of "slugs" reheated in the thixocasting experimental set. Two variables were explored in these experiments. First, the effect of a higher cooling rate than the ones in the R2 experiments was investigated. Secondly, instead of using two separate melts, in experiment R3-4 only one melt was used, in order to compare forced convection levels. These experiments, denoted "R3," are summarized in Table 5.

Table 10

Exp.	T_{MIX} (°C)	$T_{crucible}$ (°C)	*Alloy*	Mass/melt (g)	Sample(s) taken at (°C)
R3-1	625	100	GR	300	588
R3-2	625	200	GR	300	585
R3-3	620	200	GR	300	585
R3-4*	625	500	GR	300	585
R3-5	625	500	GR	300	585

As seen in Table 10, the main variable was the receiving crucible temperature, which led to different cooling rates of the slurry through the two-phase field. R3-4 is marked with an asterisk because only one melt was used in order to observe the theoretical effect of less convection (due to less liquid mixing) on the resultant structures.

Figures 16A and 16B illustrate a micrograph from the R3-1 experiment. Figure 16A is at 50X magnification, while Figure 16B illustrates a 100X magnification. Among the rheocasting experiments, experiment R3-1 underwent the highest cooling rate through the SSM range (~-0.70°C/sec); thus its residence time within the two-phase field was the lowest (~0.5 min). This explains the small particle size observed in Figures 16A and 16B.

Figures 16A and 16B show primary particles in the range of 30-50μm in diameter with a majority of the particles have a spherical shape. This is an important result because it shows that when a suitable receptacle temperature is chosen, the cooling rate through the two-phase field can be optimized, thus limiting grain growth and forming better SSM structures.

Experiments R3-4 and R3-5 were carried out in order to see the effect of using only one melt rather than two. All other experimental conditions were similar. Figures 17A and 17B illustrate a micrograph for experiment R3-4 (at 25X and 50X magnification, respectively) and Figures 18A and 18B show a micrograph for experiment R3-5 (at 25X and 50X, respectively).

Although the processing conditions for R3-4 and R3-5 were similar, the cooling rates (and hence residence times in the SSM range) were not the same. R3-4 had a cooling rate of about –0.24 C/sec and a residence time of about 1.5 minutes. R3-5 had a cooling rate of about –0.14 C/sec and a residence time of about 3.5 minutes. This explains the slightly larger overall particle size in the micrograph of Figure 17B, since this sample was within the SSM range for about 2 minutes longer than in R3-4. Also, the temperature of the two slurries was about 586°C, which corresponds to a solid fraction of about 0.5. Figures 16A and 16B depict this solid fraction. It should be recalled that in experiment R2-2, the reported slurry temperatures and the observed solid fractions did not seem to match well. The results obtained with this alternate collection technique suggest that this was at least in part due to temperature variations between the thermocouple area and the extracted slurry area. The image analysis results from these three experiments are shown below in Table 11.

Table 11

Experiment	Avg. Particle Diameter (μm)	Avg. Shape Factor	Number of particles analyzed
R3-1	35.2	0.83	155
R3-4	49.5	0.85	308
R3-5	63.1	0.75	269

It is concluded from these experiments that the third rheocasting approach, wherein the entire crucible's contents were quenched, led to globular slurry structures of even finer size. Using a higher cooling rate, particle size was minimized. The use of one melt rather than two does not noticeably affect the structures, although there should theoretically be less forced convection. This suggests that the level of forced convection in the reactor using one melt is sufficient for the formation of non-dendritic slurries.

Example 6: Particle Size as a Function of Cooling Rates

Figures 19 and 20 illustrate data from selected rheocasting experiments showing particle size as a function cooling rates. Slower cooling rates through the SSM temperature range result in structures having larger particle diameters, while higher cooling rates lead to finer particle sizes. These results imply that in the rheocasting approach, an optimum cooling rate can be experimentally determined in order to yield highly refined and globular structures in the processed slurry. Such an optimum cooling rate, however, while leading to fine particle sizes, must be applied uniformly throughout the bulk of any given sized slurry bath. The data also suggest that the solid fraction of the processed slurry can be quickly adjusted prior to subsequent forming. From an industrial standpoint, this is highly desirable because uniform slurry structures, which directly impact the uniformity of thixotropic flow in a volume of slurry, can be realized. Furthermore, higher productivity can be achieved because shorter production times can result from faster thermal adjustment of the slurry prior to forming.

These experimental results clearly show that a high nucleation rate combined with turbulence and forced convection leads to (a) copious nucleation of the primary phase, (b) dispersal of nuclei throughout the bulk liquid, and (c) survival of nuclei due to a homogeneous temperature distribution. The high level of grain refinement observed in the as-solidified samples can be explained by numerous nucleation events within the reactor. The uniformity of these structures throughout the samples (as well as the degree of particle agglomeration) shows that these nuclei were dispersed effectively by the fluid flow in both the reactor and the receptacle. Survival of the

majority of these nuclei "seeds," though difficult to verify quantitatively, is strongly suggested by the high nuclei densities seen in the microstructures.

EQUIVALENTS

While this invention has been particularly shown and described with references to preferred embodiments thereof, it will be understood by those skilled in the art that various changes in form and details may be made therein without departing from the scope of the invention encompassed by the appended claims.

CLAIMS

What is claimed is:

1. A method for forming an alloy substantially free of dendrites, comprising the steps of:
   a. cooling a superheated alloy to form a nucleated alloy, wherein the nucleated alloy includes a plurality of nuclei, wherein essentially all of said nuclei are substantially free of entrapped liquid;
   b. controlling the temperature of the nucleated alloy to prevent the nuclei from melting;
   c. mixing the nucleated alloy to distribute the nuclei throughout; and
   d. cooling the nucleated alloy with nuclei distributed throughout, thereby forming an alloy substantially free of dendrites.

2. The method of Claim 1, wherein the superheated alloy is cooled at a rate of at least 15°C per second to form the nucleated alloy.

3. The method of Claim 2, wherein the superheated alloy is cooled at a rate in the range of about 20°C per second to about 30°C per second to form the nucleated alloy.

4. The method of Claim 1, wherein the superheated alloy includes at least one of the materials selected from the group consisting of aluminum, lead, tin, magnesium, manganese, strontium, titanium, silicon, iron, carbon, copper, gold, silver, and zinc.

5. The method of Claim 1, further includes the step of using the alloy substantially free of dendrites in at least one application selected from the group consisting of a thixocasting application and a rheocasting application.

6. The method of Claim 1, wherein the mixing of the nucleated alloy is accomplished by directing the nucleated alloy through a passive mixer.

7. The method of Claim 1, wherein the alloy substantially free of dendrites includes a primary particle size of about 100 microns or less.

8. The method of Claim 7, wherein the alloy substantially free of dendrites includes a primary particle size of about 70 microns or less.

9. The method of Claim 1, wherein the alloy substantially free of dendrites includes a shape factor value in the range of about 0.75 and about 0.95.

18. The method of Claim 1, further includes the step of quenching the nucleated alloy to form the alloy substantially free of dendrites.

11. The method of Claim 1, wherein the superheated alloy includes at least one grain-refining agent.

12. The method of Claim 11, wherein the grain-refining agent includes at least one of the materials selected from the group consisting of borides of titanium and borides of aluminum.

13. The method of Claim 11, wherein the grain-refining agent includes at least one of the materials selected from the group consisting of TiB_2, AlB_2, TiC, and Al_3Ti.

14. The method of Claim 1, wherein the superheated alloy is heated to at least about 5°C above the liquidus temperature.

15. The method of Claim 14, wherein the superheated alloy is heated to a temperature in the range of between about 10°C to about 15°C above the liquidus temperature.

16. The method of Claim 1, further includes the step of forming a billet from the alloy substantially free of dendrites.

17. The method of Claim 1, wherein at least a portion of the superheated alloy includes a metal recycled from a metal-forming process.

18. The method of Claim 1, further includes the step of directing the alloy substantially free of dendrites to a metal-forming process.

19. The method of Claim 18, wherein the alloy substantially free of dendrites directed to a metal-forming process includes a volume fraction of solids of at least about 30%.

20. The method of Claim 19, wherein the alloy substantially free of dendrites directed to a metal-forming process includes a volume fraction of solids in the range of from about 40% to about 60%.

21. A continuous process for forming an alloy substantially free of dendrites, comprising the steps of:

a. directing a superheated alloy stream into a reactor, wherein the superheated alloy stream is continuously cooled and mixed to form a nucleated alloy stream, wherein the nucleated alloy stream includes a plurality of nuclei distributed throughout, wherein essentially all of said nuclei are substantially free of entrapped liquid; and

b. continuously controlling the temperature of the nucleated alloy stream to prevent the nuclei from melting and continuously mixing the nucleated

alloy stream to distribute the nuclei throughout, thereby continuously forming an alloy substantially free of dendrites.

22. A method for forming an alloy substantially free of dendrites, comprising the steps of:

a. cooling a superheated alloy to form a nucleated alloy, wherein the nucleated alloy includes a plurality of nuclei, wherein essentially all of said nuclei are substantially free of entrapped liquid;

b. controlling the temperature of the nucleated alloy to prevent the nuclei from melting and passively mixing the nucleated alloy to distribute the nuclei throughout; and

c. cooling the nucleated alloy with nuclei distributed throughout, thereby forming an alloy substantially free of dendrites.

23. A method for forming an alloy substantially free of dendrites, comprising the steps of:

a. superheating a first metal;

b. superheating a second metal;

c. mixing the first and second metals to form a superheated alloy;

d. cooling the superheated alloy to form a plurality of nuclei, wherein essentially all of said nuclei are substantially free of entrapped liquid;

e. mixing the superheated alloy to distribute the plurality of nuclei throughout the superheated alloy;

f. controlling the temperature of the superheated alloy to prevent the nuclei from remelting; and

g. cooling the superheated alloy while the nuclei are distributed throughout, thereby forming an alloy substantially free of dendrites.

24. The method of Claim 23, wherein the fist metal comprises a dissimilar composition from the second metal.

25. The method of Claim 23, wherein each of the at least two metals are heated to nonequal temperatures.

26. The method of Claim 23, wherein the first metal is heated to a temperature in a range of between about 1°C and about 50°C above the liquidus temperature of the second metal.

27. The method of Claim 23, wherein the second metal is heated to a temperature in a range of between about 1°C and about 50°C above the liquidus temperature of the second metal.

28. An alloy substantially free of dendrites formed by a method comprising the steps of:

a. cooling a superheated alloy to form a nucleated alloy, wherein the nucleated alloy includes a plurality of nuclei, wherein essentially all of said nuclei are substantially free of entrapped liquid;

b. controlling the temperature of the nucleated alloy to prevent the nuclei from melting;

c. mixing the nucleated alloy to distribute the nuclei throughout; and

d. cooling the nucleated alloy with nuclei distributed throughout, thereby forming an alloy substantially free of dendrites.

ALLOY SUBSTANTIALLY FREE OF DENDRITES AND METHOD OF FORMING THE SAME

ABSTRACT OF THE DISCLOSURE

Described herein are alloys substantially free of dendrites. A method includes forming an alloy substantially free of dendrites. A superheated alloy is cooled to form a nucleated alloy. The temperature of the nucleated alloy is controlled to prevent the nuclei from melting. The nucleated alloy is mixed to distribute the nuclei throughout the alloy. The nucleated alloy is cooled with nuclei distributed throughout.

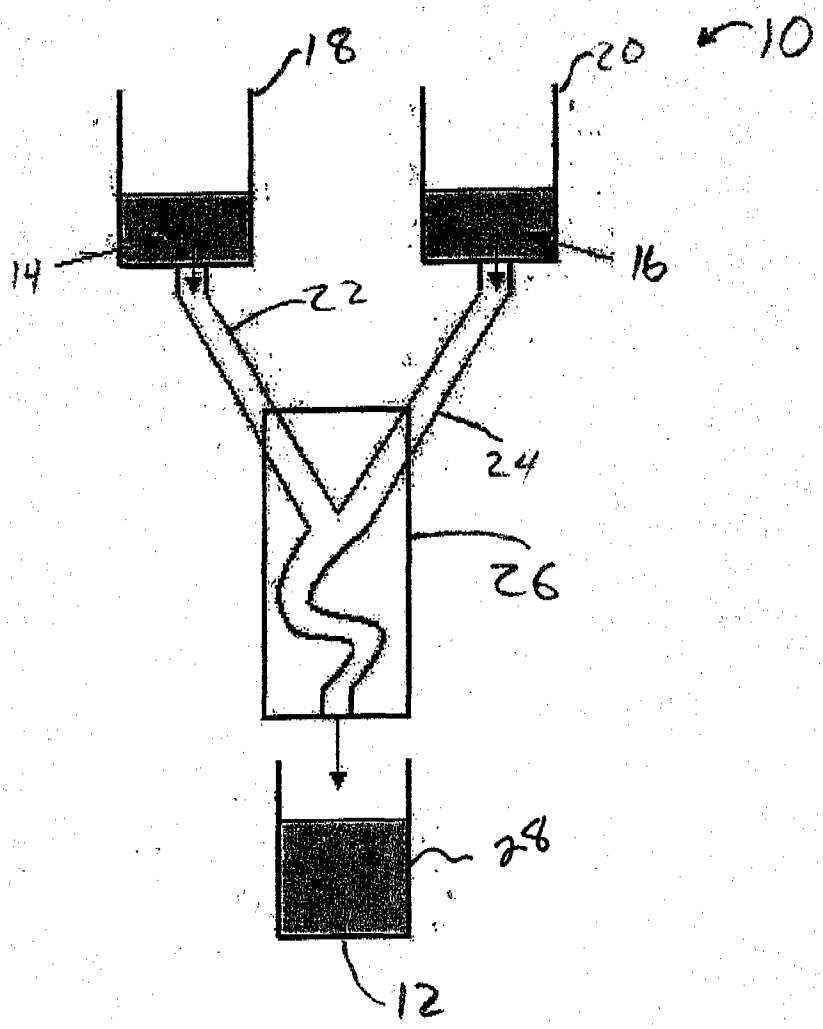

Fig. 1

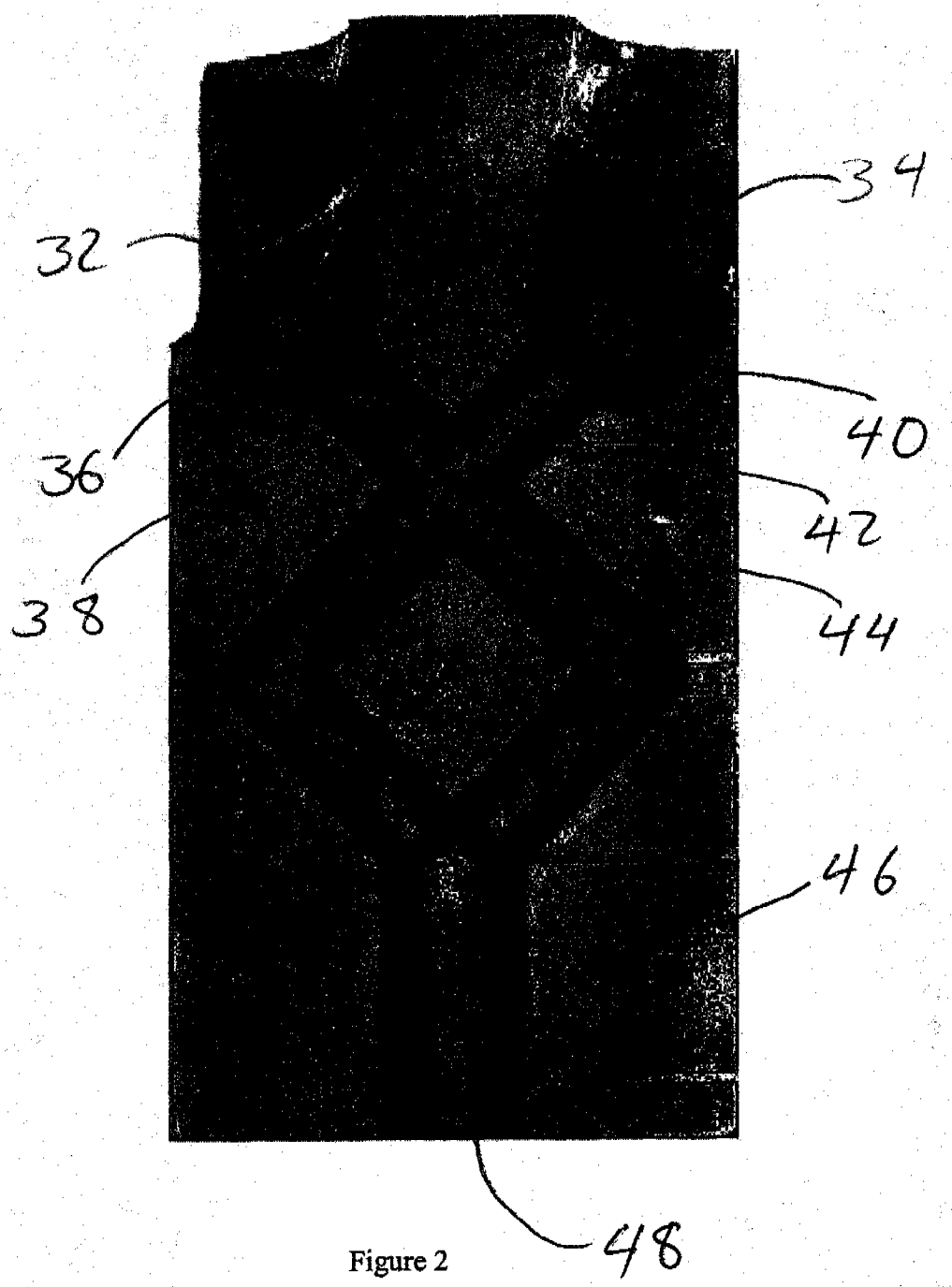

Figure 2

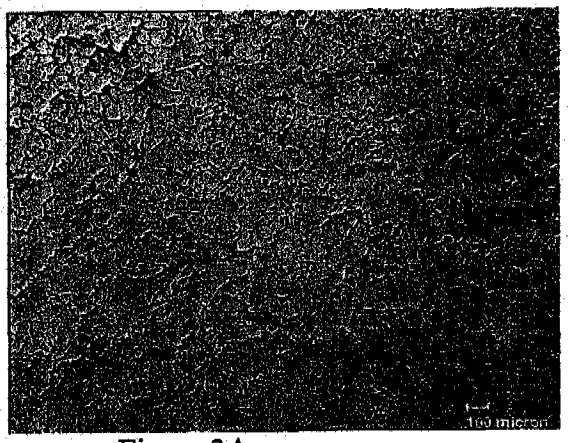

Figure 3A

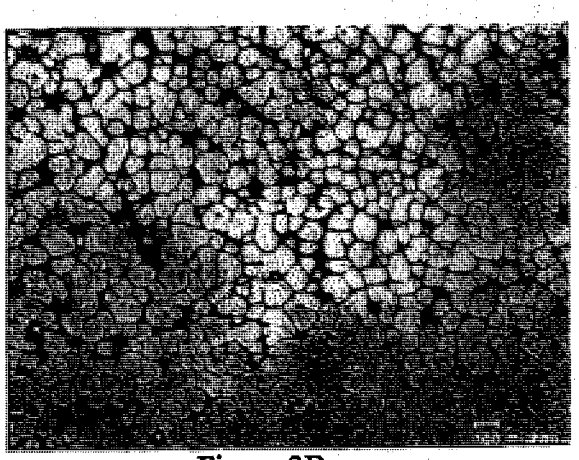

Figure 3B

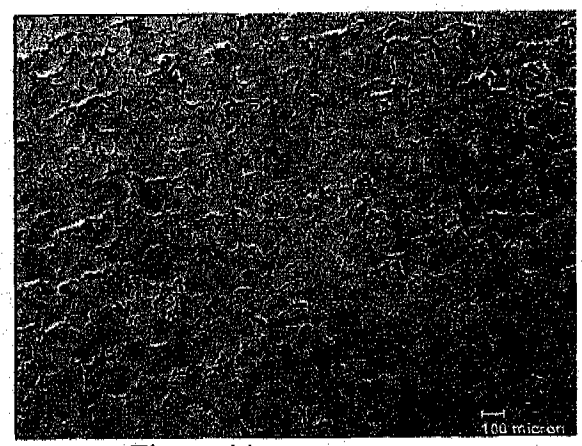

Figure 4A

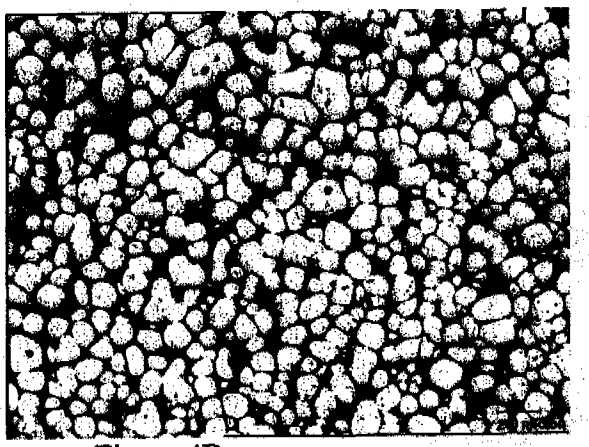

Figure 4B

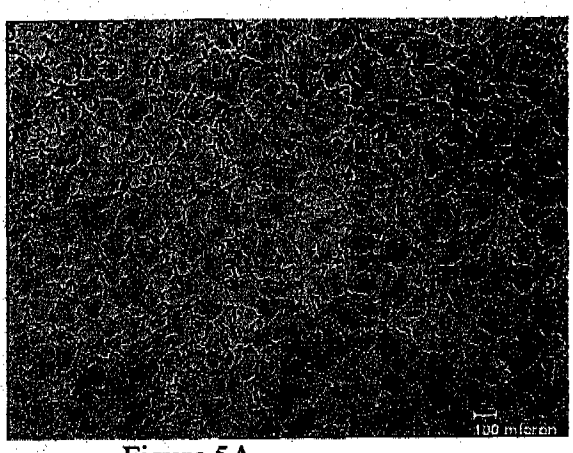

Figure 5A

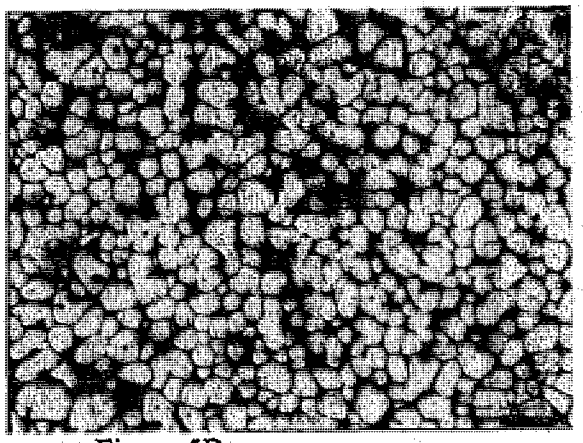

Figure 5B

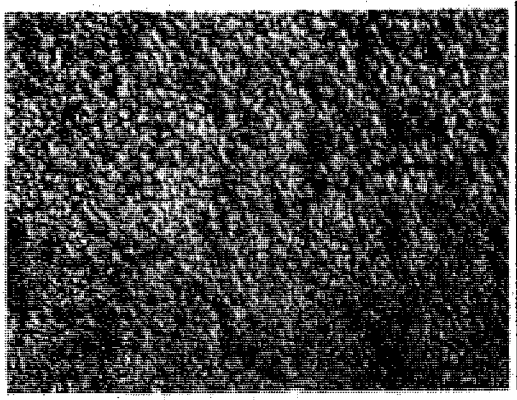

Figure 6A

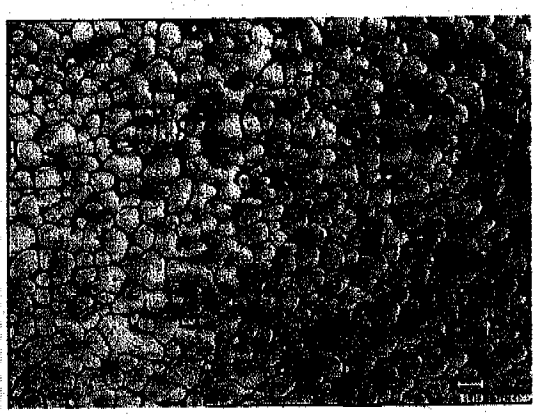

Figure 6B

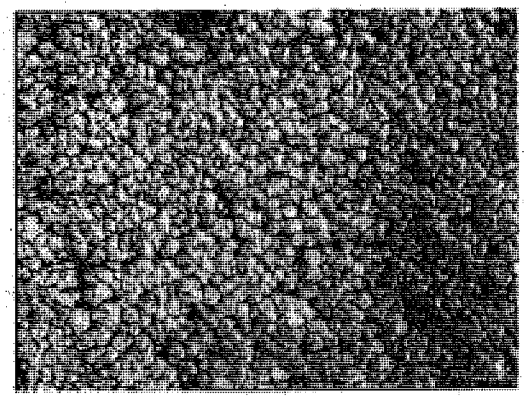

Figure 7A

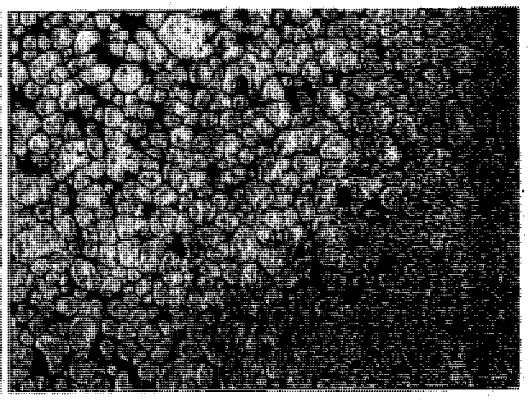

Figure 7B

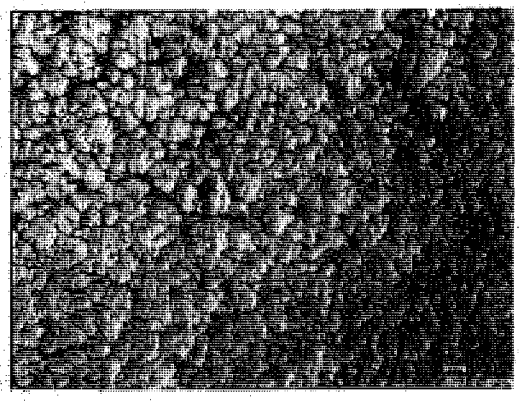

Figure 8A

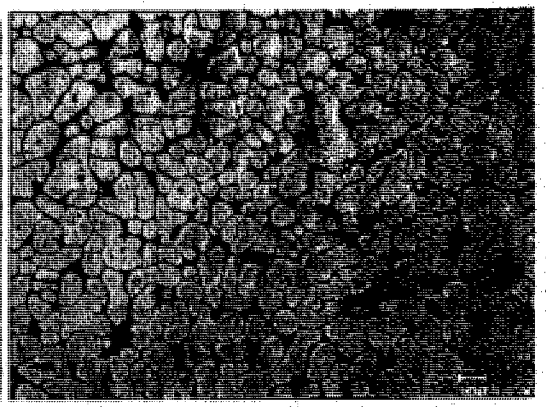

Figure 8B

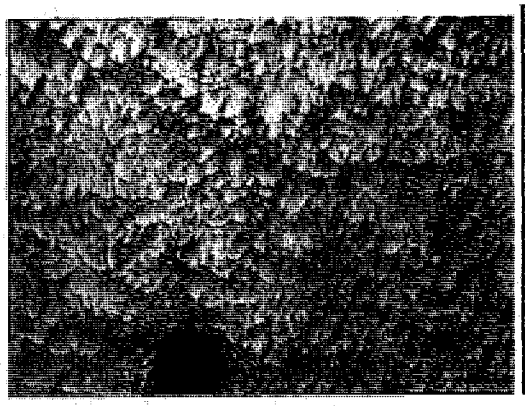

Figure 9A

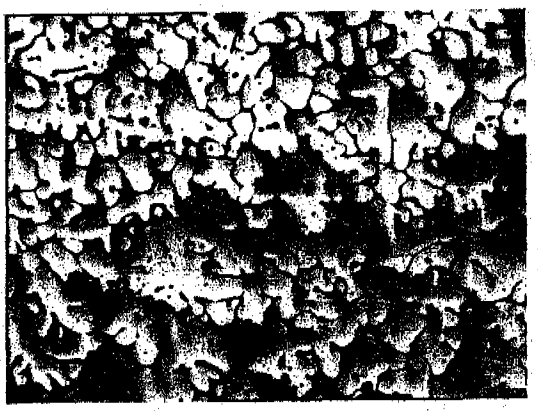

Figure 9B

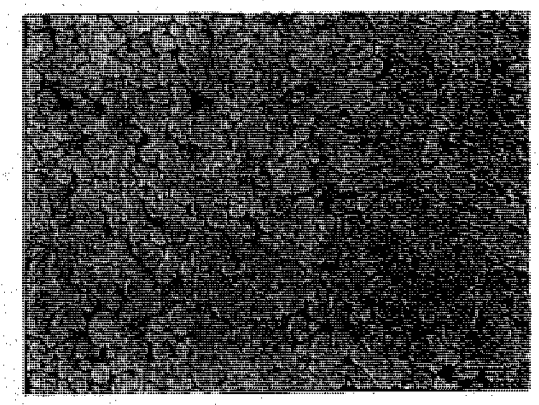

Figure 10A

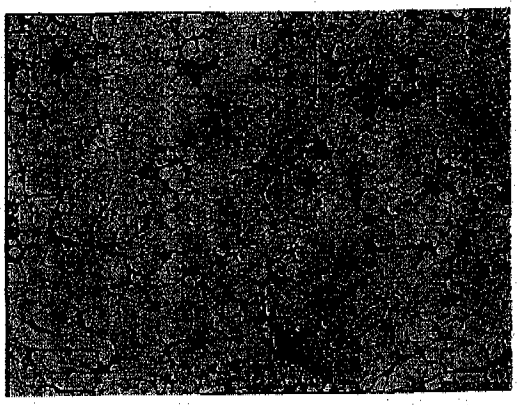

Figure 10B

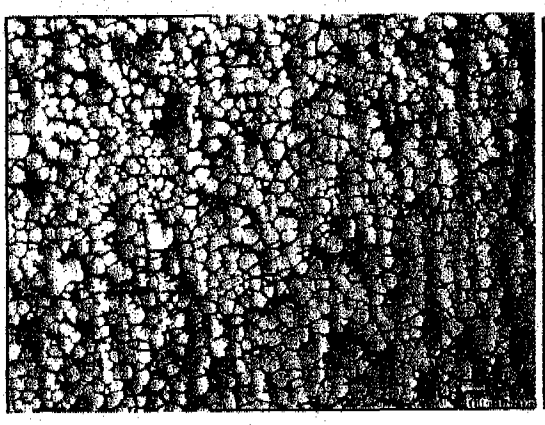

Figure 11A

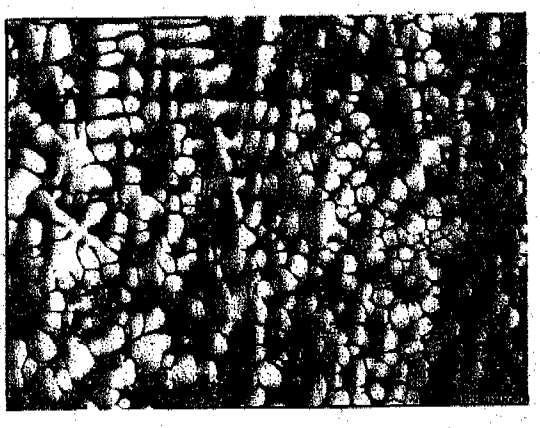

Figure 11B

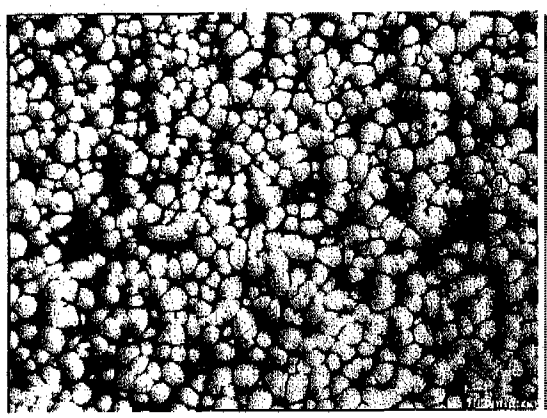

Figure 11C

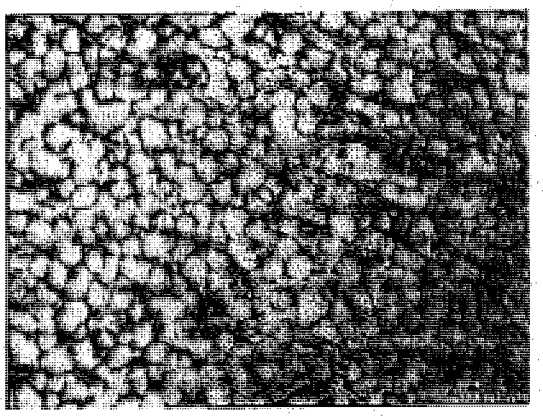

Figure 11D

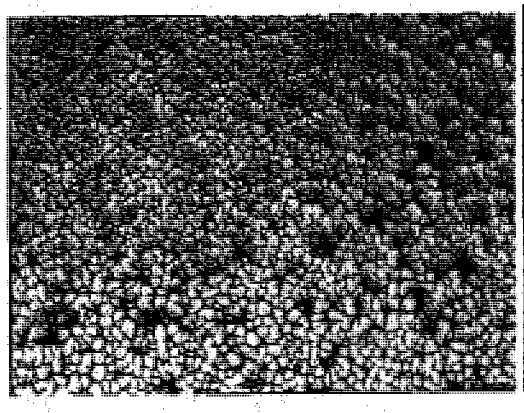

Figure 12A

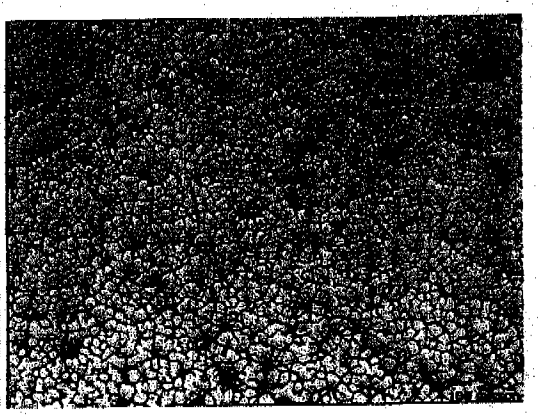

Figure 12B

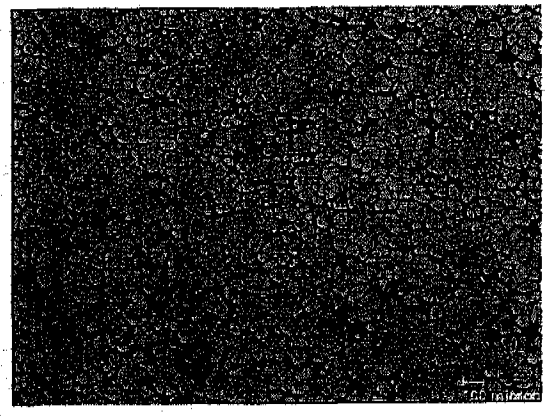

Figure 12C

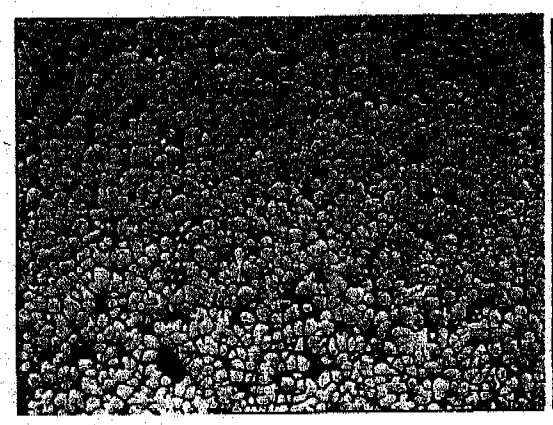

Figure 13A

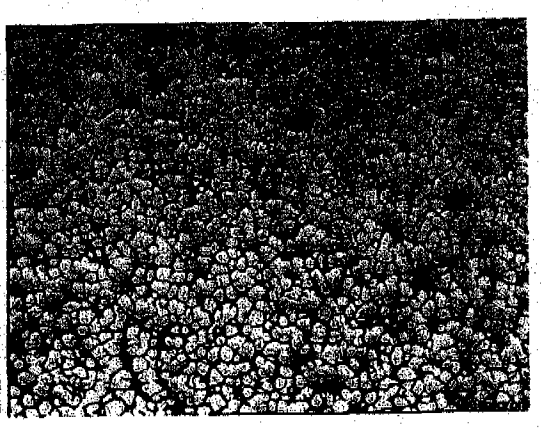

Figure 13B

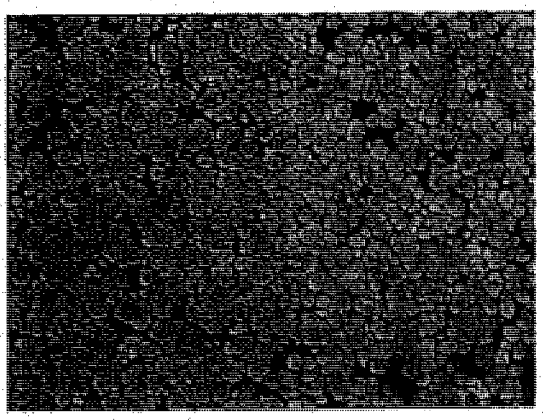

Figure 13C

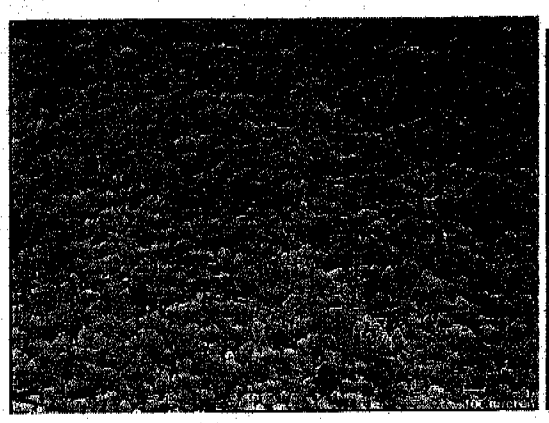

Figure 14A

Figure 14B

Figure 14C

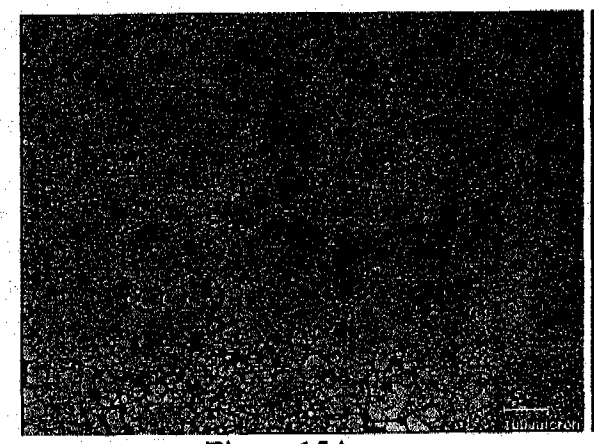

Figure 15A

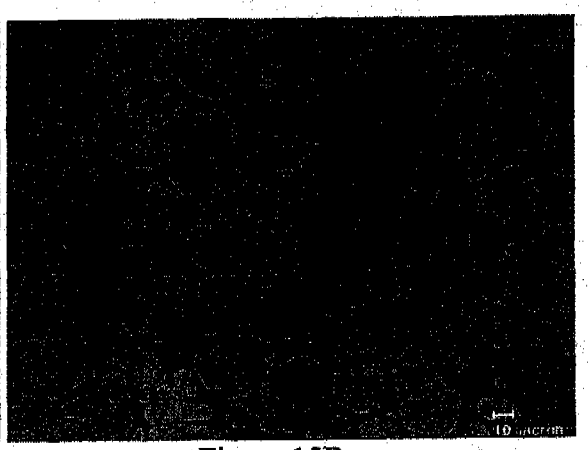

Figure 15B

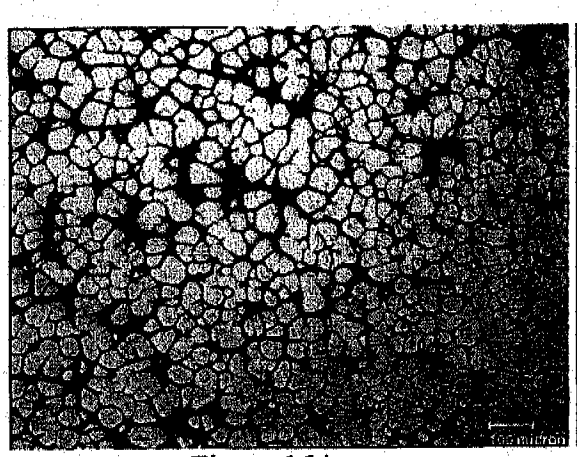

Figure 16A

Figure 16B

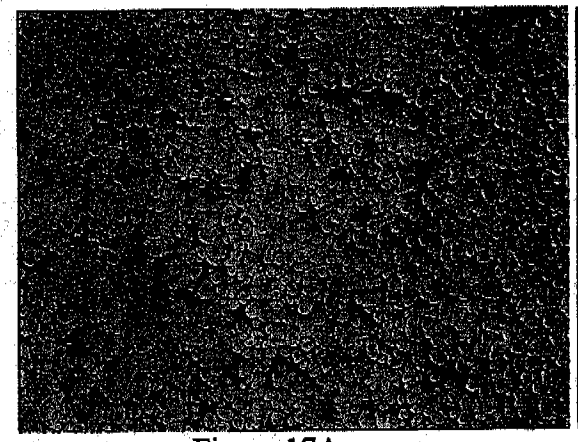

Figure 17A

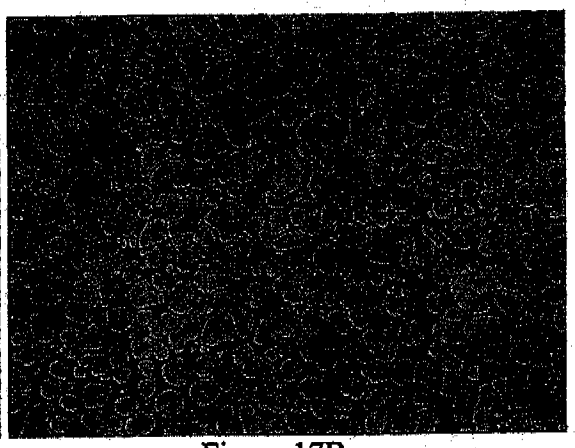

Figure 17B

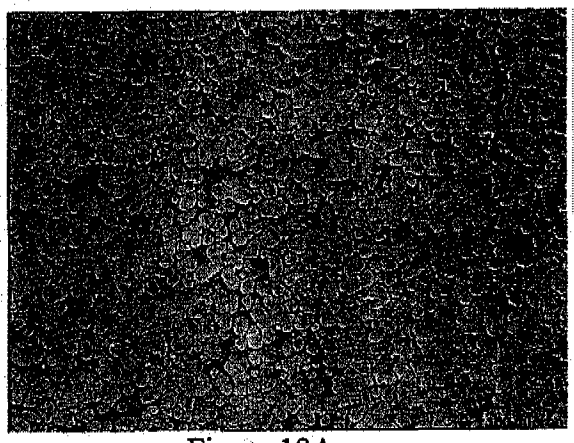

Figure 18A

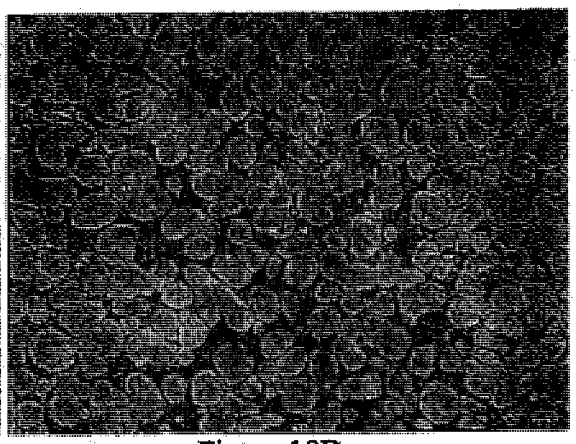

Figure 18B

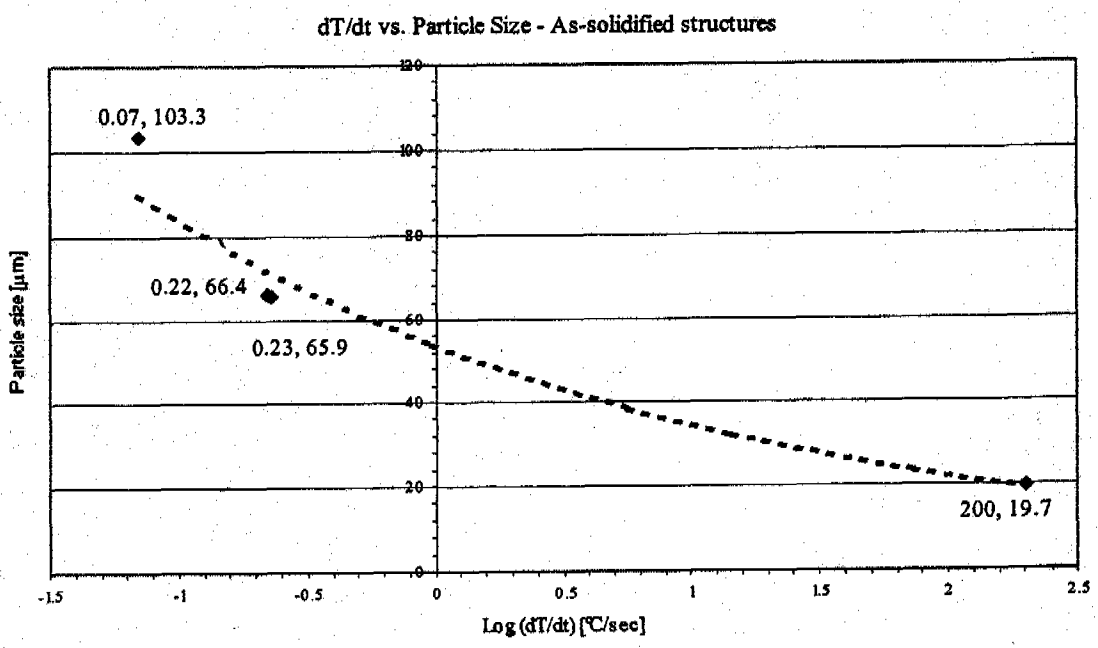

Figure 19

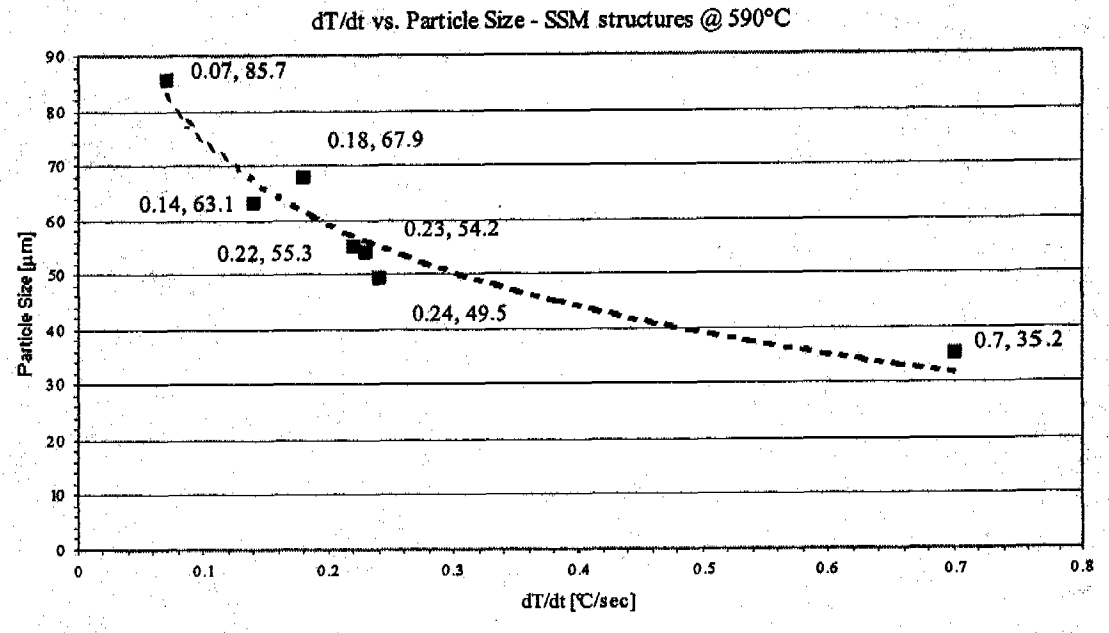

Figure 20

APPENDIX B

SSM Processing of AlB_2 Grain Refined Al-Si Alloys

Q.Y. Pan, M. Arsenault, D. Apelian and M.M. Makhlouf
Advanced Casting Research Center (ACRC)
Metal Processing Institute (MPI)
WPI, Worcester, MA 01609 USA

ABSTRACT

As part of the U.S. Department of Energy's program on ***"Low Cost and Energy Efficient Methods for the Manufacture of Semi-Solid (SSM) Feedstock"***, AlB_2 grain refined material has been evaluated as a candidate billet material, as well as an alloy for the slurry-on demand route. AlB_2 grain refined-SiBloy® is an emerging technology, which circumvents some critical problems encountered during conventional chemical grain refining in metal casting. These include the lack of grain size uniformity, the fading of nucleating agents, and the agglomeration and settling of insoluble nucleating particles in the melt. Through AlB_2 grain refinement, the grain-refining additions containing silicon and boron promote the formation of AlB_2 particles (grain nuclei) just above the liquidus temperature of the melt. In this manner, grain refinement is decoupled from the thermal history of the melt. In this study, the SiBloy® technology has been tailored for SSM applications (thixocasting route). Systematic experiments have been conducted to optimize both billet casting and reheating processes for AlB_2 grain refined alloys, and an optimal processing window has been established. It is found that billet casting parameters play an important role in the formation of high quality semi-solid structure. The optimized semi-solid structure of AlB_2 grain refined alloys is characterized by small, non-dendritic alpha particles with a small amount of entrapped liquid. Results from thixocasting experiments will be reviewed and discussed; the results point out that AlB_2 grain refined alloy is an excellent candidate for SSM processing.

1. INTRODUCTION

Semi-solid processing offers many benefits over traditional near-net shaping technologies such as reduced turbulence in the die cavity, reduced defects and entrained oxides, and the ability to produce components with better mechanical properties compared to high-pressure die castings. In addition, the process has other ancillary advantages such as reduced die wear, reduced energy consumption, and is also environmentally friendly. Currently, there are two major semi-solid processing routes: (1) thixocasting, and (2) rheocasting, as illustrated in Figure 1 (de Figueredo and Apelian, 2001). Thixocasting route starts from a solid precursor material that is specially prepared by primary aluminum manufacturers using continuous casting methods. Upon reheating the material into the mushy zone, a thixotropic slurry is formed, which becomes the feed for the casting operation. Commercially, semi-solid aluminum billets are cast using magneto-hydrodynamic (MHD) stirring or grain refinement methods. Whereas, in the rheocasting route one starts from the liquid state, wherein a thixotropic slurry is formed directly from the melt via special thermal treatments.

Currently, the thixocasting route comprises the majority of industrial semi-solid applications. The main reason for this is that the forming does not require melting equipment within the SSM casting facility, and the process can be highly automated using approaches similar to those employed in forging (Flemings, 2001). However, there are also some disadvantages with thixocasting. For instance, billets possess non-homogeneities with respect to structure and composition. There is also a certain amount of metal loss during the reheating process. Scrap metal such as gates and risers cannot be recycled within the forming facility, and must be sent back to the billet supplier. Therefore, there is a premium for casters, and the process is often deemed non-competitive with traditional casting processes (Jorstad, 2000).

In recent years, great efforts have been dedicated to improving current commercial techniques and to developing novel rheocasting methods to make semi-solid processing more *"cost-effective"*. Several new promising rheocasting processes have emerged. These include UBE's new rheocasting (NRC) process (UBE Industries, Ltd., 1996), the Semi-Solid Rheocasting (SSR) process (MIT/WPI, 2000); the SLC® (sub-liquidus casting) process (THT Presses, Inc., 2002); the "Continuous Rheoconversion Process" (CRP) (WPI, 2002), etc.

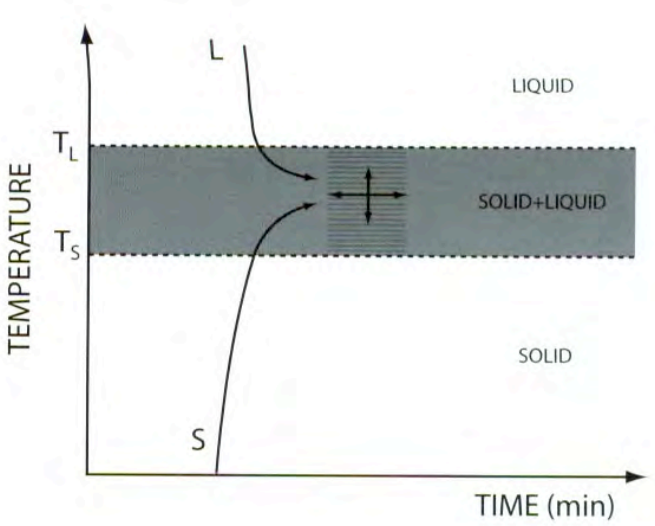

Figure 1. Schematic of the two major semi-solid processing routes (de Figueredo and Apelian, 2001).

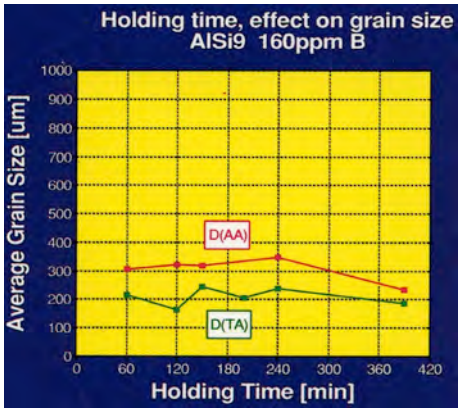

Figure 2(a)

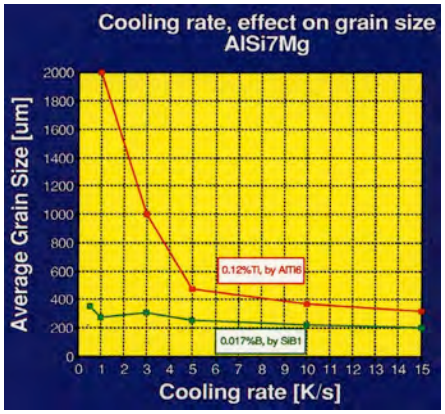

Figure 2(b)

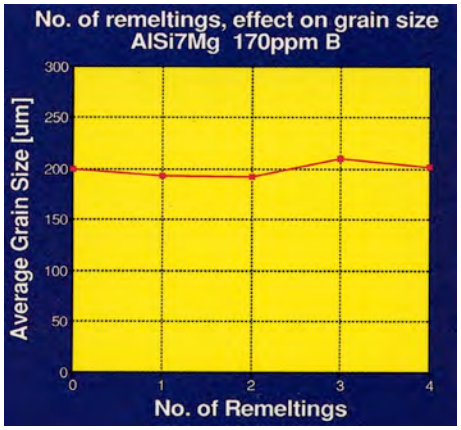

Figure 2(c)

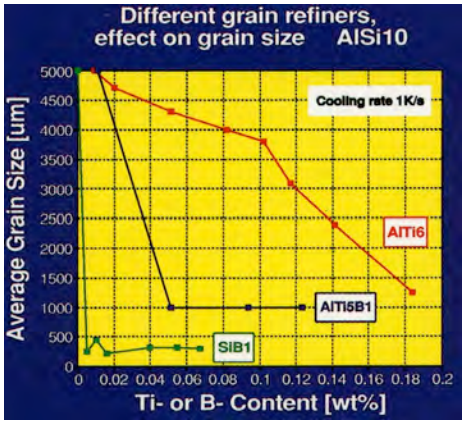

Figure 2(d)

Figure 2. Grain size of Si-1B grain refined alloys as a function of: (a) holding time; (b) cooling rate; (c) remelting number, and (d) grain refiner. (Tondel, 1994).

Compared to MHD techniques, the grain refinement approach is more flexible and is relatively cost-effective. Therefore, grain refined aluminum billets are being employed for thixocasting by many die casters. However, there are some drawbacks inherent to the current Al-Ti/Al-Ti-B/Al-Ti-C grain refined materials such as lack of grain size uniformity, the fading of nucleating agents, and the agglomeration and settling of insoluble nucleating particles in the melt. These can negatively affect the quality and productivity of SSM castings and the operation.

In the recent past, a permanent grain refining technology has emerged. This new technology is termed SiBloy®, and has been patented by Elkem Aluminum. Unlike traditional grain refining techniques, the grain refining effect of SiBloy® is achieved by adding Si-B master alloy into the melt. During cooling, fresh AlB_2 particles (instead of insoluble TiB_2, $TiAl_3$ etc.) precipitate out from the melt just above the liquidus temperature, which, in turn, serve as potent nucleating agents, and thus grain refining the melt. Extensive experiments with Al-Si cast alloys were carried out by Per-Arne Tondel (Tondel, 1994) which showed that the Si1B additive gives rise to the finest grain structure with a small boron addition level (~0.015wt%B) in contrast to traditional grain refiners such as Al6Ti, Al5Ti1B, Al5Ti0.2B and Al4B. Moreover, the grain refining effect is found to be: 1) independent of holding time (no fading); 2) unaffected by remelting treatments (permanent effect), 3) almost independent of cooling rate in the range between 0.5 and 15°C/s, and 4) effective for Al-Si alloys with Si content between 5 and 11%, as illustrated in Figure 2. Specifically, research performed here at WPI (Alem, 2002) has further confirmed the significant efficiency and the permanent grain refining effect of Si-1B grain refiner for A356 alloy. More importantly, it has been found that by mixing two separate melts--SiBloy and A356 (with or without Ti), an extremely fine structure that is excellent for semi-solid processing can be obtained under optimized mixing conditions.

As part of the U.S. Department of Energy's program on ***"Low Cost and Energy Efficient Methods for the Manufacture of Semi-Solid (SSM) Feedstock",*** AlB_2 grain refined material has been evaluated as a candidate billet material, as well as an alloy for the slurry-on demand route. In this study, the SiBloy® technology has been tailored for SSM applications (thixocasting route). Systematic experiments have been conducted to optimize both billet casting and reheating processes for AlB_2 grain refined alloys, and an optimal processing window has been established. Results from thixocasting experiments are reviewed and discussed below.

2. EXPERIMENTAL

In phase I of this study, critical processing parameters in billet casting and reheating processes (thixocasting route) were optimized for AlB_2 grain refined alloys. In phase II, a new AlB_2 grain refined alloy was cast using the optimized parameters at Elkem's production unit. The new alloy was then validated through extensive billet reheating and quenching experiments.

2.1 Materials

Two AlB_2 grain refined alloys provided by Elkem Aluminum were used in this study. SiBloy #1 is a commercial alloy that was optimized for shaped casting (*it should be emphasized that these billets were not cast for SSM processing*). SiBloy #2 is a new alloy that was cast specifically for SSM processing using the optimized processing parameters established in Phase I. For comparison, a commercial grain refined SSM A356 alloy was also used. Table 1 gives the composition of the three alloys. It should be pointed out that the SiBloy alloys used in the study have the same composition/alloy designation as A356. Simply stated, the difference between SiBloy and A356 alloys is the grain refiner utilized (Si-1B *vs.* Al-5Ti-1B).

Table 1. Chemical Composition of the Alloys Investigated

Alloy #	Composition, wt.%								
	Si	Fe	Mn	Mg	Na	Sr	Ti	B	Al
SiBloy 1	6.86	0.08	0.016	0.28	0.0001	0.0	<0.001	0.0179	bal.
SiBloy 2	7.38	0.08	0.017	0.28	0.0031	0.0	<0.001	0.0173	bal.
GR A356	6.87	0.09	<0.0005	0.33	0.0013	0.005	0.12	0.0065	bal.

2.2 Processing Conditions

Two critical parameters were investigated during billet casting: casting temperature and cooling rate; while for billet reheating process, only heating rate was considered in the experimental matrix. The reason for this is that the effect of reheating temperature and isothermal holding time on the semi-solid structure of SiBloy alloys has been fully characterized by the authors in their previous studies (Pan and Apelian, 2002). Figure 3 illustrates the processing parameters investigated. These include four different casting temperatures (720°C, 680°C, 650°C and 625°C), two different cooling rates (42°C/s and 20°C/s) at each casting temperature, as well as two different reheating rates (0.65°C/s and 0.07°C/s).

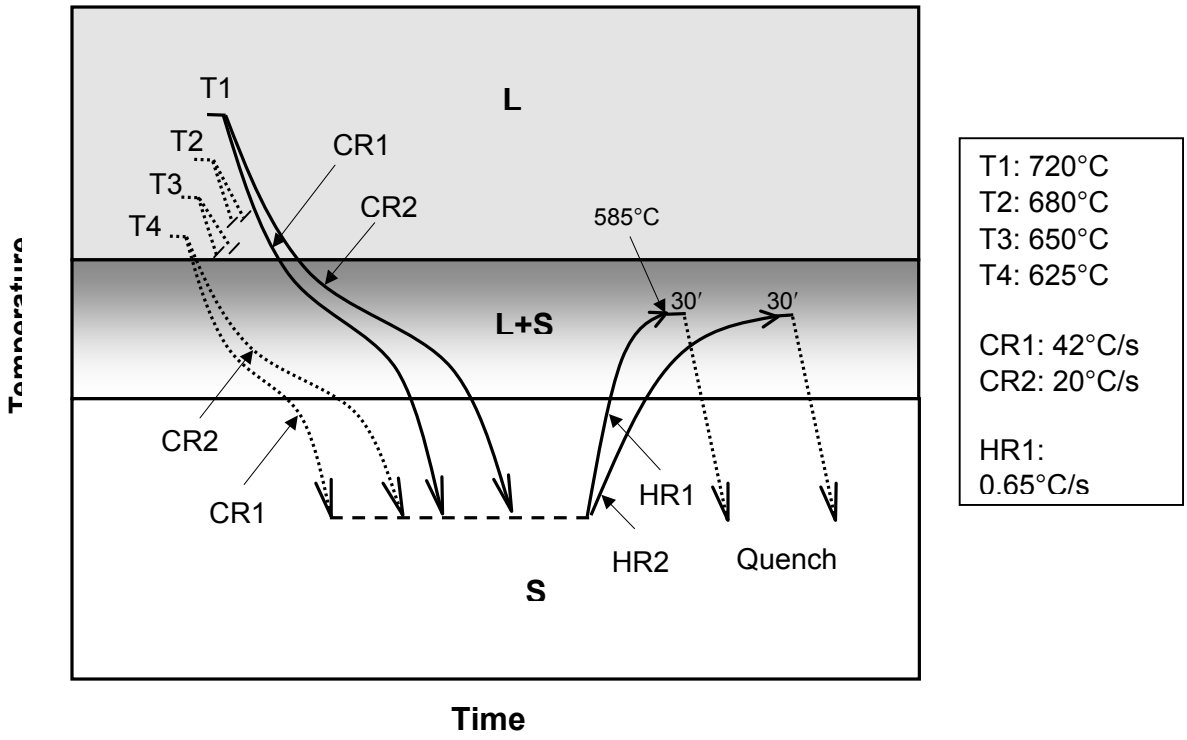

Figure 3: Schematic diagram of the processing parameters evaluated, which include four casting temperatures (T1-T4), two different cooling rates (CR1-CR2) at each casting temperature, and two different heating rates (HR1-HR2). In the study, cooling rate (CR) is defined as (T_{Melt}-$T_{Liquidus}$)/time elapsed; and heating rate (HR) is defined as (585°C-$T_{Ambient}$)/reheating time.

Experimentation involved remelting SiBloy billets using a 35KW induction furnace. The melt was degassed and then poured into a cylindrical permanent mold (3 inches in diameter) at different pouring temperatures. By changing mold temperature, different cooling rates at each casting temperature were obtained. Followed by casting experiments, samples were cut from the cast cylinders, and then reheated to 585°C at different heating rates. After isothermally holding at 585°C for about 30 seconds, the semi-solid samples were quenched in water for metallographic observation and image analysis.

2.3 Microstructure Characterization

Grain structure characterization was carried out using two different methods. Electro-etching and polarized light were used to examine grain structure, while ASTM standard methods were used to determine grain size.

Microstructure analyses were performed using optical microscopy and image analysis software (microGOP2000/S). Three specific microstructural parameters were measured to quantitatively characterize the semi-solid structure. They are

1. Average particle size of the alpha phase, *D*
2. Shape factor of the alpha particles, *SF*
3. Entrapped liquid content within the alpha particles, V_f

The average particle size (*D*) is determined by

$$D = 2 \times \sqrt{\frac{A}{\pi}} \qquad (1)$$

Where *A* is the area of the particle. The average particle size is the mean value of the total number of particles measured.

The shape factor *(SF)* is defined as

$$SF = \frac{P^2}{4\pi A} \qquad (2)$$

Where P is the perimeter of the particle. For a perfectly globular shape, SF is equal to 1. The more irregular the particles, the higher are shape factor values. The shape factor values reported here are the mean values of the total number of particles measured.

The entrapped liquid content (V_f) is defined as

$$V_f = \frac{A_{EL}}{A_{Liquid}} \times 100\% \quad (3)$$

Where A_{EL} is the area of the entrapped liquid, A_{Liquid} is the area of the entire liquid phase.

In order to obtain results of statistical significance, more than twelve images were analyzed for each sample.

3. RESULTS & ANALYSES

In sections 3.1-3.3, we analyze and discuss the effect of critical processing parameters such as billet casting temperature, cooling rate as well as reheating rate on the semi-solid structure of AlB_2 grain refined billets (SiBloy #1). Based on experimental results, an optimal processing window is given in section 3.4. Followed by the process optimization, a new SiBloy alloy was cast using the optimized parameters for further evaluation, and validation results are presented in section 3.5.

3.1 Effect of Billet Casting Temperature on Semi-solid Structure

Figure 4 shows typical as-cast microstructures of SiBloy billets (SiBloy #1) as a function of casting temperature. It can be seen that casting temperature has a significant influence on the morphology of the as-cast microstructure. With decreasing pouring temperature from 720°C to 625°C, the morphology of the as-cast microstructure changes from a highly dendritic structure (Figure 4a) to a rosette-like structure (Figure 4d).

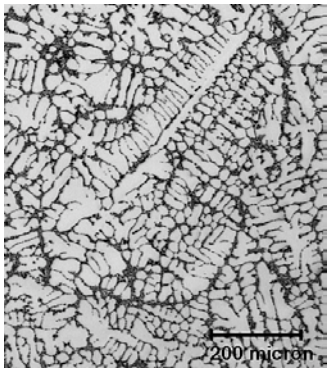

720°C

Figure 4(a)

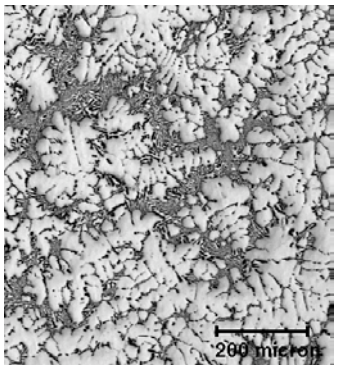

680°C

Figure 4(b)

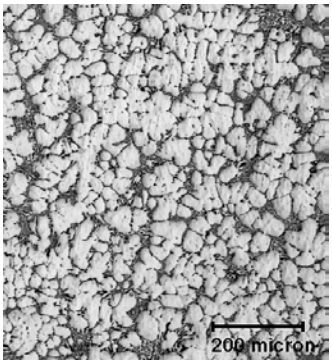

650°C

Figure 4(c)

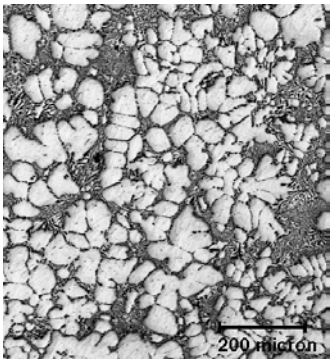

625°C

Figure 4(d)

Figure 4: Evolution of as-cast microstructure as a function of billet casting temperature (SiBloy #1; cooling rate: 42°C/s).

It is well known that the resultant SSM structure is very much influenced by the as-cast billet microstructure (thixocasting route). Figure 5 compares semi-solid structures of reheated billets cast at different temperatures. All semi-solid samples were obtained at 585°C and isothermally held for 30 seconds. From Figure 5, one can see significant differences among the partially remelted billets. The billet cast at 720°C shows the largest alpha particle size, most irregularly shaped, as well as having the highest entrapped liquid content. With deceasing billet casting temperature, a significant number of small alpha particles having a more spherical shape and much less entrapped liquid are formed (compare Figure 5a with Figures 5c and 5d). Specifically, image analysis clearly shows that:

- Billet casting temperature significantly changes both the size and the morphology of the alpha phase in semi-solid structures. With decreasing casting temperature from 720°C to 625°C, the average alpha particle size decreases from 140-160μm to 90-100μm, and the shape factor value decreases from 1.8 to 1.36, as shown in Figures 6a and 6b. Many small, globular alpha particles can be observed in the semi-solid structures of the reheated billets cast at 650°C and 625°C (see Figures 5c and 5d).

- More importantly, casting temperature shows a significant influence on entrapped liquid content (see Figure 6c). With decreasing billet casting temperatures (from 720°C to 625°C), the entrapped liquid content drops from 24-34% to 6-8%. This is a significant improvement.

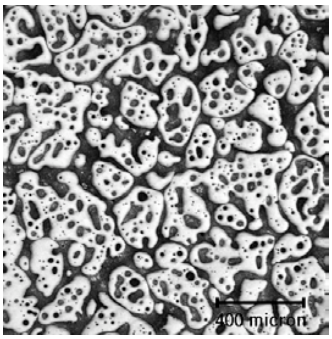

Figure 5(a)

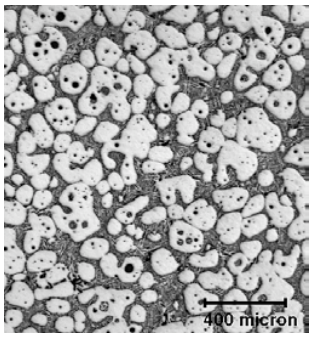

Figure 5(b)

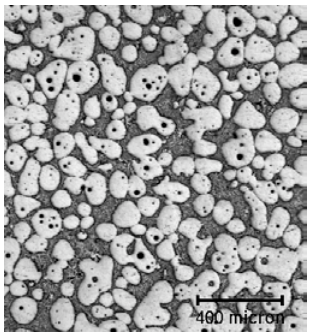

Figure 5(c)

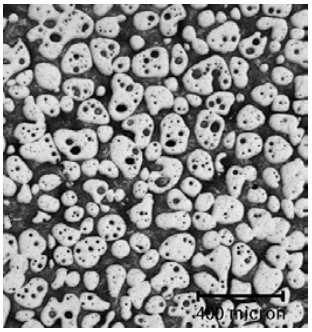

Figure 5(d)

Figure 5. Semi-solid structures of reheated billets (SiBloy #1) cast at different temperatures: (a) 720°C, (b) 680°C, (c) 650°C, and (d) 625°C (cooling rate: 42°C/s). All the billets were partially remelted at 585°C, and isothermally held for 30 seconds (heating rate: 0.65°C/s).

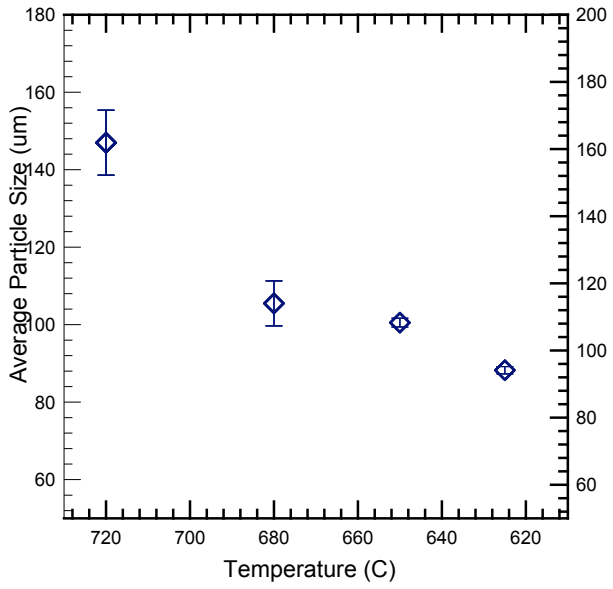

Fig. 6(a)

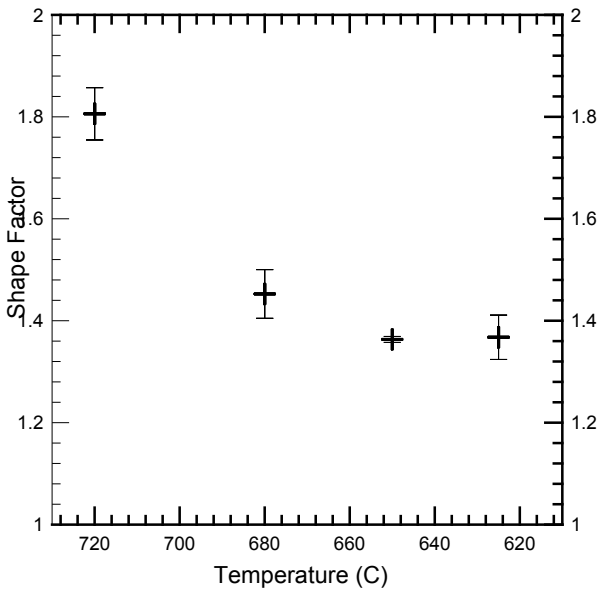

Fig. 6(b)

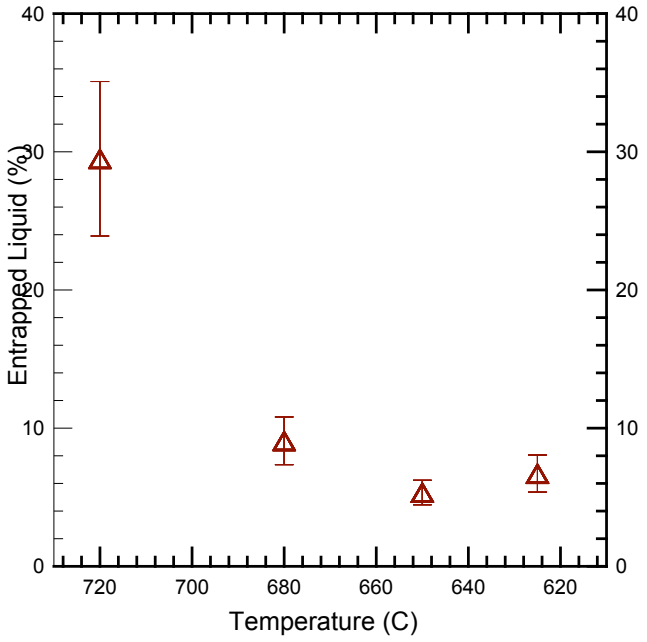

Fig. 6(c)

Figure 6. Image analysis results of the samples given in Figure 5, showing the effect of billet casting temperature on: (a) average Alpha particle size; (b) shape factor of the Alpha phase, and (c) entrapped liquid content.

3.2 Effect of Cooling Rate on Semi-solid Structure

Figure 7 shows the evolution of semi-solid structure of SiBloy billets as a function of billet casting temperature and cooling rate. The samples shown in Figures 7a-7d were obtained under a relatively high cooling rate compared to those shown in Figures 7e-7h (42°C/s versus 20°C/s). By comparing Figures 7a-7d with Figures 7e-7h, one can see that the cooling rate has a significant influence on the semi-solid structure. Obviously, high cooling rate tends to reduce entrapped liquid content of the partially remelted billets. From image analysis results given in Figure 8, we concluded that:

- Cooling rate affects not only the alpha particle size, but also the morphology of the alpha phase. Low cooling rate tends to slightly increase alpha particle size in the cooling rate range investigated (see Figure 8a). Moreover, low cooling rate increases the shape factor value remarkably, signifying that alpha particles with a more irregular shape are formed in the reheated billets cast using a relatively slow cooling rate. This effect is more pronounced in the casting temperature range between 650°C and 720°C, as shown in Figure 8b.

- In addition, cooling rate has a significant effect on entrapped liquid content (see Figure 8c). Increasing cooling rate decreases entrapped liquid content dramatically. This finding is in very good agreement with what we have found in other SSM alloys such as 356, 357 etc. (Pan and Apelian, 2001). Therefore, in order to improve the quality of SSM feedstock, a high cooling rate is highly recommended.

Cooling Rate: 42°C/s

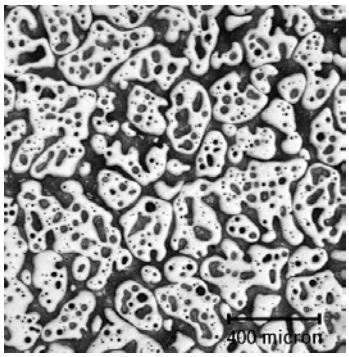

CT: 720°C

Figure 7(a)

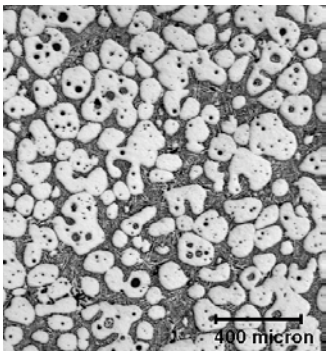

CT: 680°C

Figure 7(b)

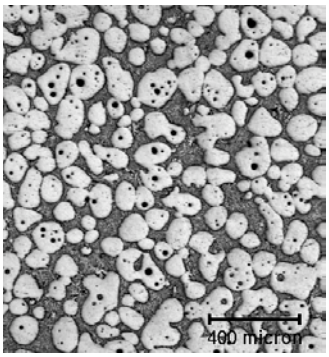

CT: 650°C

Figure 7(c)

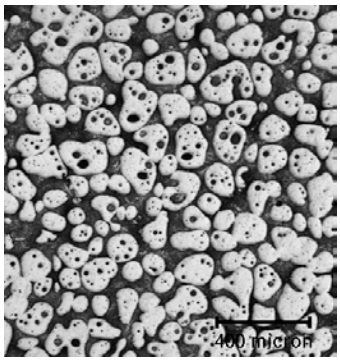

CT: 625°C

Figure 7(d)

Cooling Rate: 20°C/s

CT: 720°C

Figure 7(e)

CT: 680°C

Figure 7(f)

CT: 650°C

Figure 7(g)

CT: 625°C

Figure 7(h)

Figure 7. Evolution of semi-solid structure of SiBloy billets as a function of billet casting temperature and cooling rate. All samples were reheated at the same conditions (heating rate: 0.65°C/s; heated temperature: 585°C). Note the billets shown in Figures 5a-5d were cast under a relatively high cooling rate compared to those shown in Figures 7e-7h (42°C/s vs. 20°C/s). CT: casting temperature.

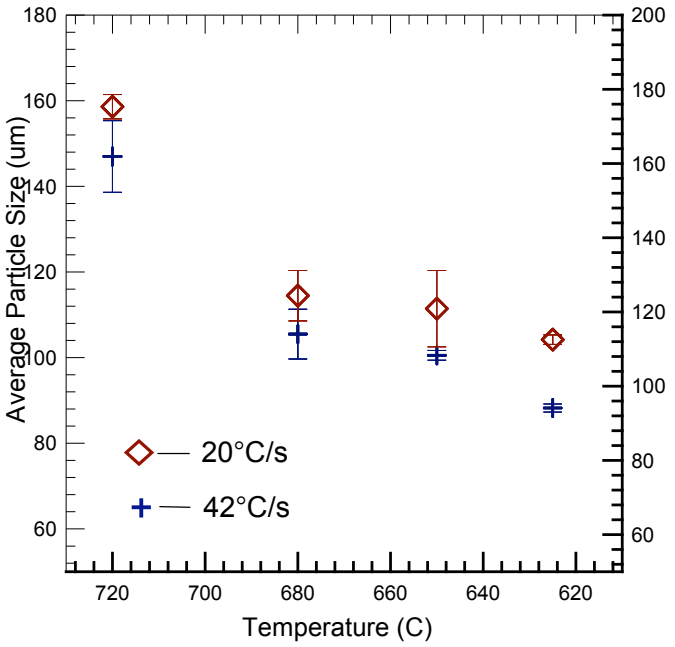

Fig. 8(a)

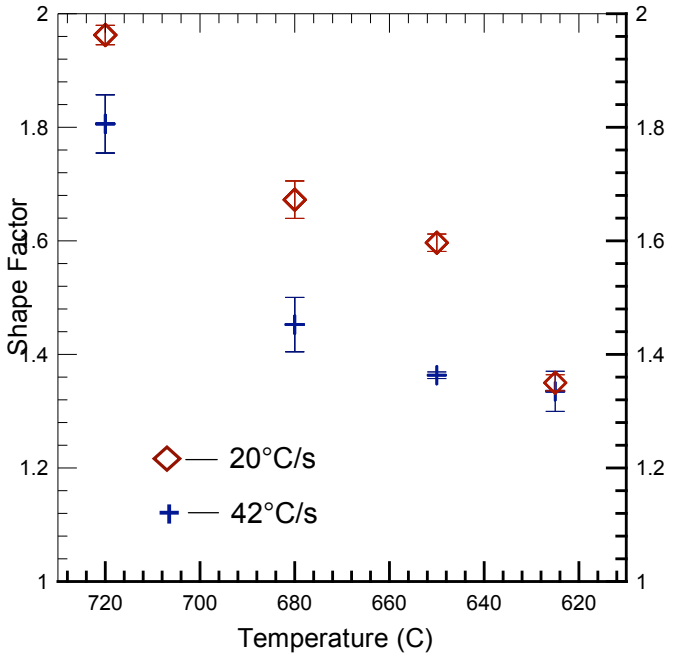

Fig. 8(b)

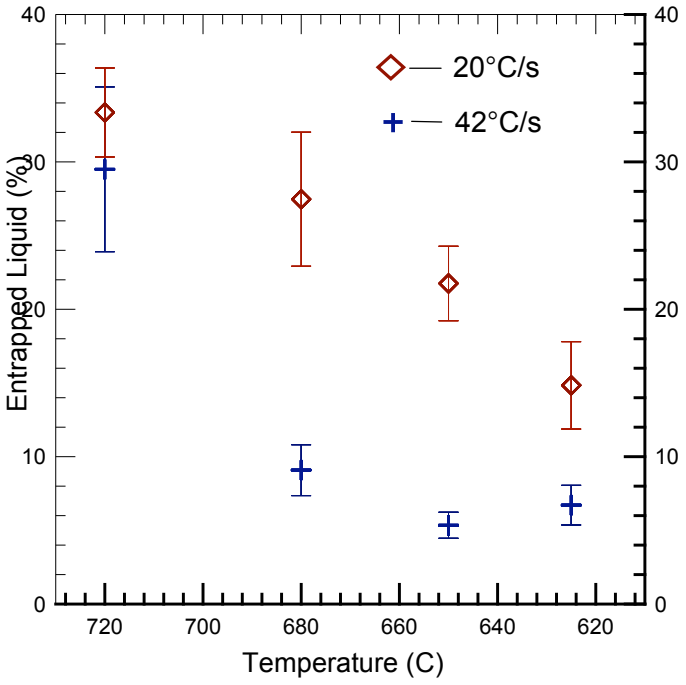

Fig. 8(c)

Figure 8. Image analysis results of the samples given in Figure 7, showing the effect of cooling rate and casting temperature on: (a) average Alpha particle size; (b) shape factor of the Alpha phase, and (c) entrapped liquid content.

3.3 Effect of Billet Reheating Rate on Semi-solid Structure

Figure 9 compares semi-solid structures of SiBloy billets reheated to 585°C at two different heating rates (0.65°C/s versus 0.07°C/s). The billets were cast at four different pouring temperatures (720°C, 680°C, 650°C, and 625°C) using a similar cooling rate (~42°C/s). It can be seen that heating rate does not change the semi-solid structure of SiBloy billets in a significant way. This is further verified from image analysis results.

Heating Rate: 0.65°C/s

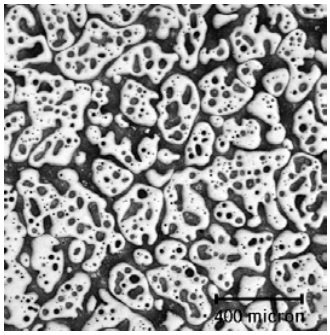

CT: 720°C

Figure 9(a)

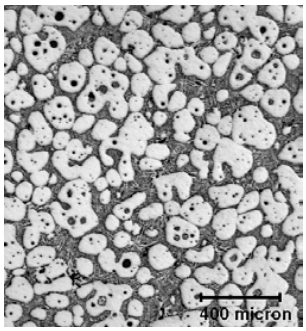

CT: 680°C

Figure 9(b)

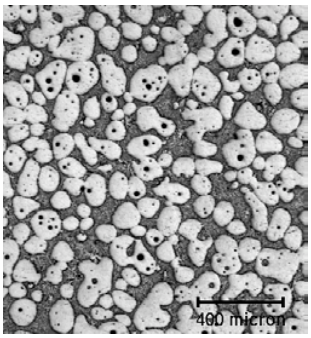

CT: 650°C

Figure 9(C)

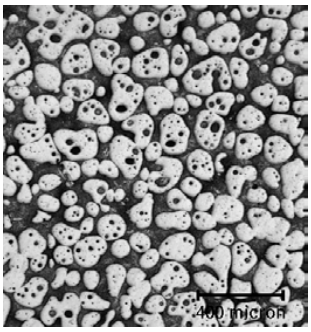

CT: 625°C

Figure 9(d)

Heating Rate: 0.07°C/s

CT: 720°C

Figure 9(e)

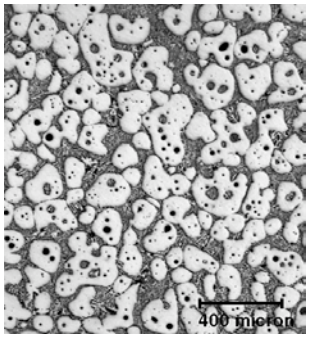

CT: 680°C

Figure 9(f)

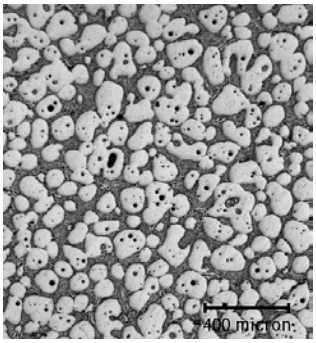

CT: 650°C

Figure 9(g)

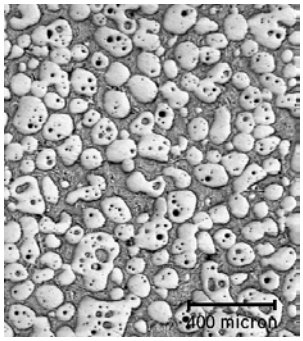

CT: 625°C

Figure 9(h)

Figure 9. Effect of heating rate on the semi-solid microstructures of SiBloy billets. The billets were cast using four different temperatures under a similar cooling rate (~42°C/s), and then reheated to 585°C using two different heating rates (0.65°C/s and 0.07°C/s). CT: casting temperature.

3.4 Optimization of Processing Parameters

From a rheological standpoint, an "ideal" semi-solid microstructure is composed of small, round alpha particles containing no entrapped liquid and homogeneously distributed in a eutectic phase. The small size of the alpha particles is beneficial for the casting of thin-walled parts, while a more spherical shape, and the absence of entrapped liquid are critical for the improvement of slurry rheological properties such as flow, filling behavior, etc. The relationship between various semi-solid structures and slurry rheological properties has been established and well documented by the authors (Pan and Apelian, 2000; Pan, et. al., 2002).

Based on the above experimental results and those from previous studies (Pan and Apelian, 2001-2002), an optimal processing window for SiBloy billets (thixocasting route) can be outlined as follows:

- *Billet casting temperature: 640-660°C*
- *Billet cooling rate: ≥ 40°C/s (as high as possible)*
- *Reheated temp.: 585°C*
- *Isothermal holding time: 2-5 min.*
- *Reheating rate: flexible*

3.5 Validation Experiments

Based on the optimal process window established in Phase I, a new AlB_2 grain refined alloy (SiBloy #2) was cast using Elkem's production unit for further evaluation. Specifically, a low casting temperature and a relatively high cooling rate were used. In addition, a certain amount of convection was induced during billet casting. Validation results of the new alloy are presented and discussed below.

3.5.1 Grain Structure

Figures 10(a)-10(c) show typical grain structures of the three alloys. From microstructure observations and grain size measurements, we found that:

- Optimized SiBloy billets (SiBloy #2) have the smallest grain size compared to SiBloy #1 and GR A356 alloys (see Table 2). Moreover, AlB_2 grain refined billets have a more uniform grain size distribution on the billet's cross-section than Ti-B grain refined semi-solid A356 billets.

- The homogeneity in grain size distribution of AlB_2 grain refined billets is related to its unique grain refining mechanism. Unlike traditional grain refining techniques, the grain refining effect of SiBloy arises from an in-situ chemical reaction that takes place just above the liquidus temperature during cooling, wherein fresh nuclei, *i.e.* AlB_2 particles (instead of insoluble nuclei such as TiB_2, $TiAl_3$ etc.) precipitate out from the melt. In this manner, the grain refining effect of SiBloy is decoupled from the thermal history of the melt, and the grain refining effect is more efficient. As a result, small grains with a uniform grain size distribution are formed in SiBloy billets.

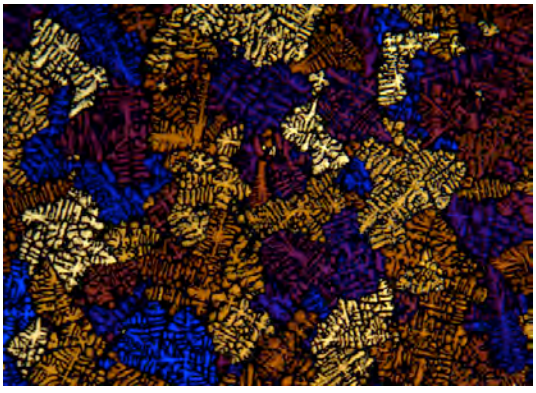

Figure 10(a)

100 μm

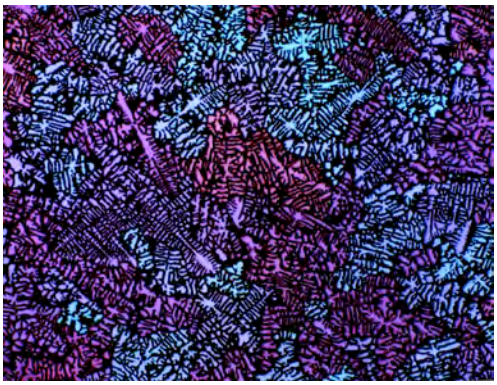

Figure 10(b)

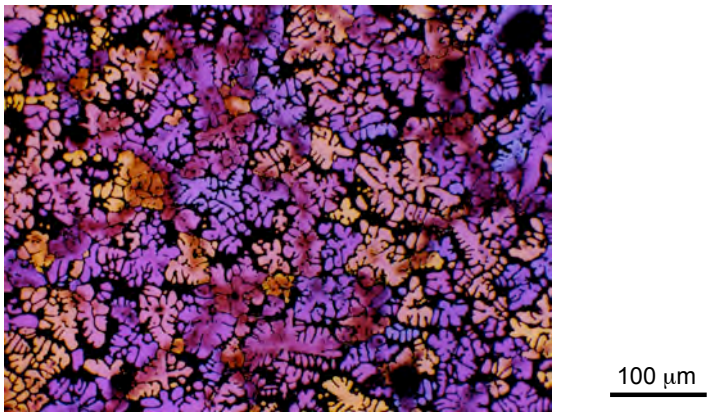

Figure 10(c)

Figure 10. Typical grain structures of the alloys investigated, (a) SiBloy #1; (b) SiBloy #2; and (c) GR A356.

Table 2. Grain size measurement results of the alloys investigated

Alloy/Billet #	Grain Size (μm)		
	Billet Center	Billet Periphery	Average
SiBloy 1	200	180	190
SiBloy 2	150	130	140
GR A356	220	130	175

Note: SiBloy #1 is a commercial alloy optimized for shaped casting (not for SSM); SiBloy #2 is a new alloy optimized for SSM.

3.5.2 Semi-Solid Structure

Figure 11 compares typical semi-solid microstructure of SiBloy #1 (not optimized for SSM) with that of SiBloy #2 (optimized for SSM). It can be seen that the semi-solid structure has been greatly improved through process optimization. A good number of small, globular alpha particles with much less entrapped liquid are formed in the optimized SiBloy alloy (see Figure 11b). Image analyses point out that the entrapped liquid content in the optimized billets is reduced by 3-4 times compared to those not optimized for SSM (from 18% to 5%). Shape factor value decreases from 1.75 to 1.35 and alpha particle size decreases from 120μm to 90μm (see Figure 12). This is a significant improvement in the semi-solid structure of SiBloy alloys.

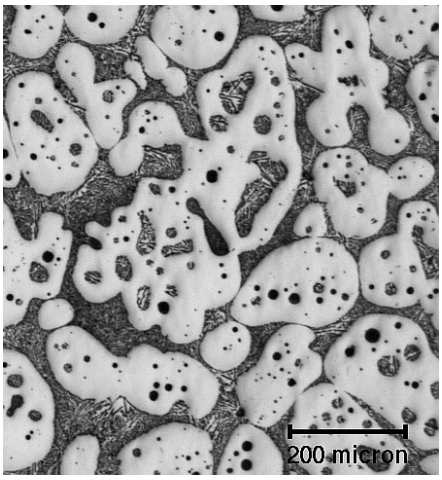

Figure 11(a)

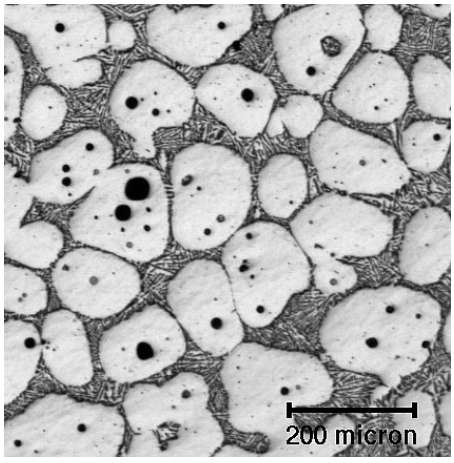

Figure 11(b)

Figure 11: A comparison of semi-solid structures of commercial SiBloy billets (NOT optimized for SSM) (Figure 11a) with those of the SiBloy billets optimized for SSM (Figure 11b). (Reheated Tempreature: 585°C).

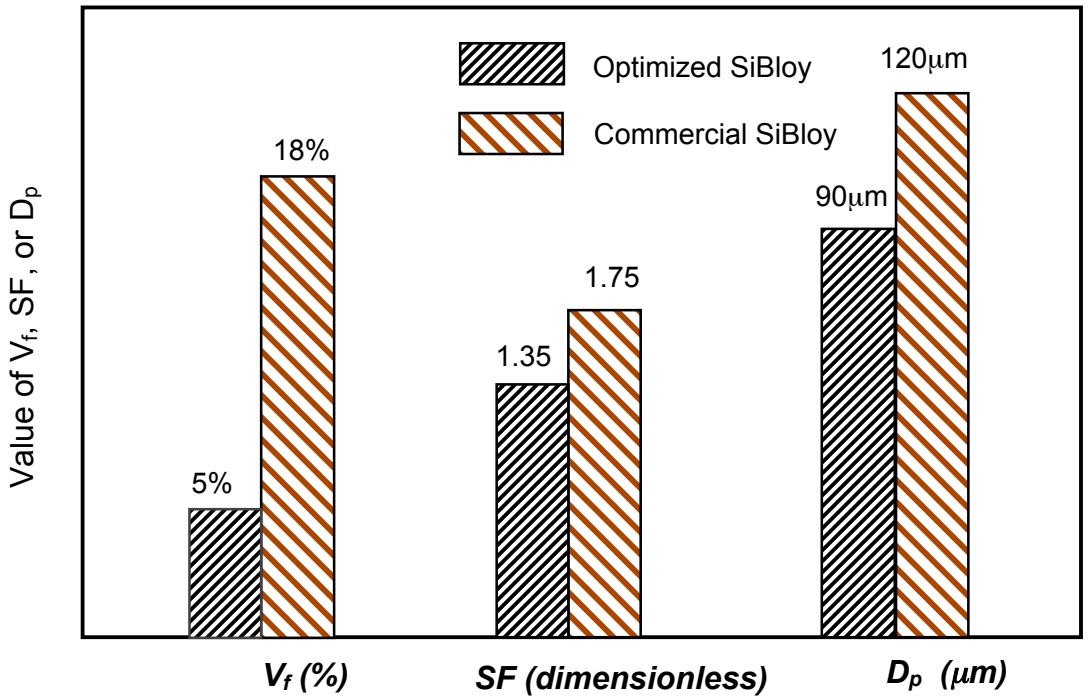

Figure 12. Image analysis results of the samples shown in Figure 11. V_f: entrapped liquid content, SF: shape factor of the Alpha phase, and D_p: Alpha particle size.

Figure 13 compares typical semi-solid structures of optimized SiBloy billets (SiBloy #2) with those of commercial semi-solid GR A356 billets. One can see that the structure of optimized SiBloy billets shows much less entrapped liquid content, smaller alpha particles and a more spherical alpha phase as compared to that of commercial GR billets. Image analysis results indicate that the entrapped liquid content in the optimized SiBloy billets is about 4 times less than that in the commercial GR billets. Moreover, the optimized structure has a smaller alpha particle size (90μm versus 128μm), and a slightly lower shape factor value (1.35 versus 1.40). It can be concluded from the quantitative data that the optimized SiBloy alloy is an excellent candidate billet material for SSM processing.

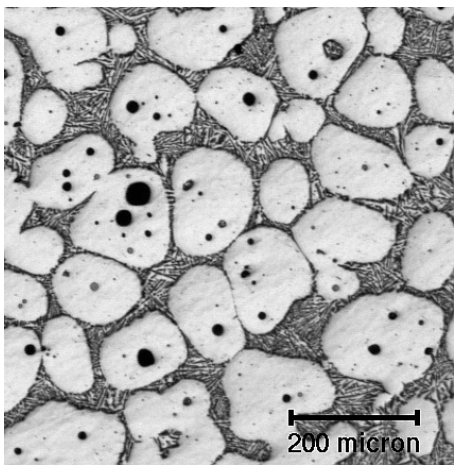

SiBloy

Figure 13(a)

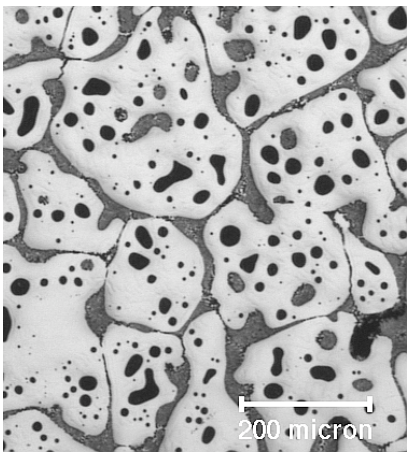

GR A356

Figure 13(b)

Figure 13. A comparison of semi-solid structures of SiBloy billets optimized for SSM (Figure 13a) with those of commercial grain refined A356 semi-solid billets. (Reheated Temperature: 585°C).

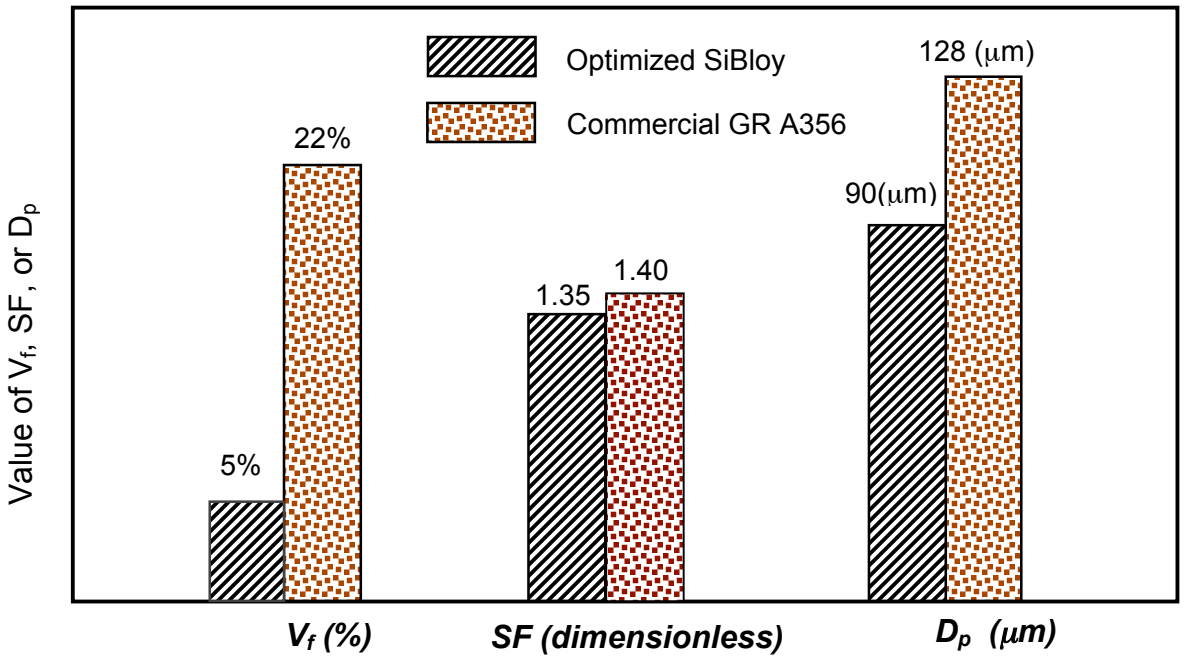

Figure 14. Image analysis results of the samples shown in Figure 13. V_f: entrapped liquid content, SF: shape factor of the Alpha phase, and D_p: Alpha particle size.

Lastly, it should be emphasized that processing parameters play a very important role in the formation of high quality semi-solid structures. Semi-solid structures of AlB_2 grain refined alloys can be greatly improved using the optimal process window established in this study. Currently, we are evaluating the optimized SiBloy billets in several industrial semi-solid forming facilities through close collaborations with ACRC consortium members.

CONCLUSIONS

Based on the above results, the following conclusions are drawn:

- Si-1B master alloy is an effective grain refiner for Al-Si alloys. Optimized Si-1B grain refined alloys show smaller grain size, and much more uniform grain size distribution compared to commercial Ti-B grain refined semi-solid A356 alloys.

- The grain refining effect of SiBloy alloys comes from an in-situ chemical reaction that occurs above the liquidus temperature during cooling, wherein fresh nuclei, *i.e.* AlB_2 particles (instead of insoluble nuclei such as TiB_2, $TiAl_3$ etc.) precipitate out directly from the melt. This ensures an efficient grain refining effect, more importantly, the refining effect is decoupled from the thermal history of the melt.

- Both billet casting temperature and cooling rate play a very important role in the formation of high quality semi-solid structures. Low casting temperature and high cooling rate can significantly reduce entrapped liquid content, and improve the size and morphology of the alpha phase. An optimal process window for SiBloy alloys (thixocasting route) has been established.

- The semi-solid structure of SiBloy alloys can be greatly improved using the optimal process window. The optimized semi-solid structure of SiBloy billets consists of small, round Alpha particles with a small amount of entrapped liquid.

- The optimized SiBloy alloy is an excellent candidate billet material for thixocasting applications.

Acknowledgements

This work was financially supported by the US Department of Energy under contract number DE-FC07-021D14232; the authors would acknowledge the support and guidance of the ACRC member companies on this project. Special thanks are due to Dr. Per-Arne Tondel for the stimulating discussions and for supplying the SiBloy alloys. In addition, the authors thank Mr. Jared Holland who worked as an intern and contributed to the image analysis work.

REFERENCES

Alem, N., M.S. Thesis, Worcester Polytechnic Institute, Worcester, MA (2002).

de Figueredo, A. and Apelian, D., *Science and Technology of Semi-Solid Metal Processing,* Chapter 2, edited by A. de Figueredo, published by NADCA, Rosemont, IL (2001).

Flemings, M.C., *Science and Technology of Semi-Solid Metal Processing,* Chapter 1, edited by A. de Figueredo, published by NADCA, Rosemont, IL (2001).

Jorstad, J., "Semi-Solid Metal Processing: A Cost-competitive Approach for High Integrity Aluminum Components" *Proceedings of the 6th International Conference on Semi-Solid Processing of Alloys and Composites,* Turin, Italy, pp.227-234 (2000).

Jorstad, J., Thieman, M., and Kamm, R., "SLC®, the Newest and Most Economical Approach to Semi-Solid Metal (SSM) Casting," *Proceedings of the 7th International Conference on Semi-Solid Processing of Alloys and Composites,* Tsukuba, Japan, pp.701-706 (2002).

UBE Industries, Ltd.: *European Patent EP 0 745 694 A1* (1996).

Pan, Q.Y. and Apelian, D., "Quantitative Microstructure Characterization of Commercial Semi-Solid Aluminum Alloys", *Proceedings of the 7th International Conference on Semi-Solid Processing of Alloys and Composites,* Tsukuba, Japan, pp.563-568 (2002).

Pan, Q.Y. and Apelian, D., "Yield Stress of Al Alloys in the Semi-Solid State", *Proceedings of the 6th International Conference on Semi-Solid Processing of Alloys and Composites,* Turin, Italy, pp.399-404 (2000).

Pan, Q.Y., Apelian, D. and DasGupta, B., "Yield Stress Of Commercial Semi-Solid Billets: *Processing Effects And The Role Of Microstructure", Proceedings of the 7th International Conference on Semi-Solid Processing of Alloys and Composites,* Tsukuba, Japan, pp.737-742 (2002).

Pan, Q.Y., and Apelian, D., ACRC Internal Reports, 2001-2002.

Tondel, P.A., Ph.D. Thesis, The University of Trondheim, Trondheim, Norway (1994).

Yurko, J.A., Martinez, R.A., and Flemings, M.C., "Development of the Semi-Solid Rheocasting (SSR) Process," *Proceedings of the 7th International Conference on Semi-Solid Processing of Alloys and Composites,* Tsukuba, Japan, pp.659-664 (2002).

Semi Solid Processing of Hypereutectic Alloys

Deepak Saha, D. Apelian
Metal Processing Institute, WPI, Worcester, MA, USA

R. DasGupta
SPX Contech, Michigan, USA

ABSTRACT

Semi-solid metal (SSM) processing of hypereutectic Al-Si alloys has been limited to the thixocasting route, where a billet (MHD cast) containing extremely fine primary Si (< 15 microns) particles is re-heated to the SSM temperature, emplaced in the die cavity and then cast. Conventional casting of these high silicon alloys, have shown primary Si refinement, however the silicon size distribution in the final part is not desirable for high integrity parts. Rheocasting or Slurry-on-Demand approach offers cost advantages over thixocasting in terms of alleviating billet premiums, reheating costs, recycling, etc. Rheocasting of hypereutectic Al-Si alloys has been hampered by the growth of the primary Si phase to an unacceptable range (> 100 microns). Ironically, a large solidification range, which is believed to be ideal for SSM processing, in this instance (i.e., 390 alloys) causes accelerated growth of the primary Si phase as the alloy cools from the liquidus to the SSM processing temperature. The possibilities of refining primary Si via rheocasting are limited to: ***a)*** breaking of primary Si (using external forces), and/or ***b)*** use of growth restrictors, and/or ***c)*** rapid heat extraction within the shot sleeve, without the formation of a chill zone. In this paper we present various experiments performed at SPX Contech and MPI, wherein we utilize diffusion solidification as a means to extract heat within the slug. The novel concepts introduced in this paper are: (i) mixing of a low temperature hypoeutectic alloy with a high temperature hypereutectic alloy, and (ii) cooling of the liquid hypereutectic alloy via chips having the same/or different composition. The paper presents laboratory results carried out at MPI and industrial trials performed at SPX Contech.

INTRODUCTION

Hypereutectic Al-Si alloys have gained much attention in the recent past due to their superior properties (low coefficient of thermal expansion, high yield strength and high wear resistance). Some of the most common applications are: engine blocks, cylinder heads, cylinder sleeves, clutch input housing, clutch assembly, brake cylinders, etc. The hard primary silicon in a soft matrix of Al-Si eutectic provides the requisite wear resistance. The final properties in the cast component are dictated by the distribution and size of the primary silicon phase. Work to date (Matsuura K, 2003) has established that an increase in the volume fraction of primary silicon (or reduced size) increases the resultant mechanical properties. With commercial interests in SSM processing burgeoning in the early to mid 90's, casting 390 type alloys via thixocasting and/or rheocasting has become of great interest. Unfortunately, the work to date in SSM processing of 390 type alloys has been stymied by the growth of the primary silicon to unacceptable ranges (> 100 microns).

In this paper we will review the impedances and technical challenges that arise when hypereutectic Al-Si alloys are processed through the SSM route; review existing SSM processing routes for hypereutectic alloys, and lastly present two novel approaches for casting hypereutectic Al-Si alloys.

HYPEREUTECTIC AL-SI ALLOYS: *SSM PROCESSING CHALLENGES*

Processing of hypereutectic Al-Si alloys is a challenge because of the heat associated during the solidification of primary Si. Figure 1 shows the heats evolved per mole of a hypereutectic Al-Si alloy (A356) and a hypereutectic Al-Si alloy (A390). The data were obtained by PANDAT software (using non-equilibrium solidification assumptions/Scheil equation). It can be seen from Figure 1 that the heat associated during the cooling of a hypereutectic alloy is at least 2-3 times that of an equivalent solid fraction of the hypoeutectic alloy. The same heat provides the required fluidity of these alloys. In traditional castings of hypoeutectic alloys, to remove the exothermic energy released during solidification, excessive use of chills is made. The high heat released in hypereutectic Al-Si alloys is attributed to the high entropy of fusion that is released during solidification.

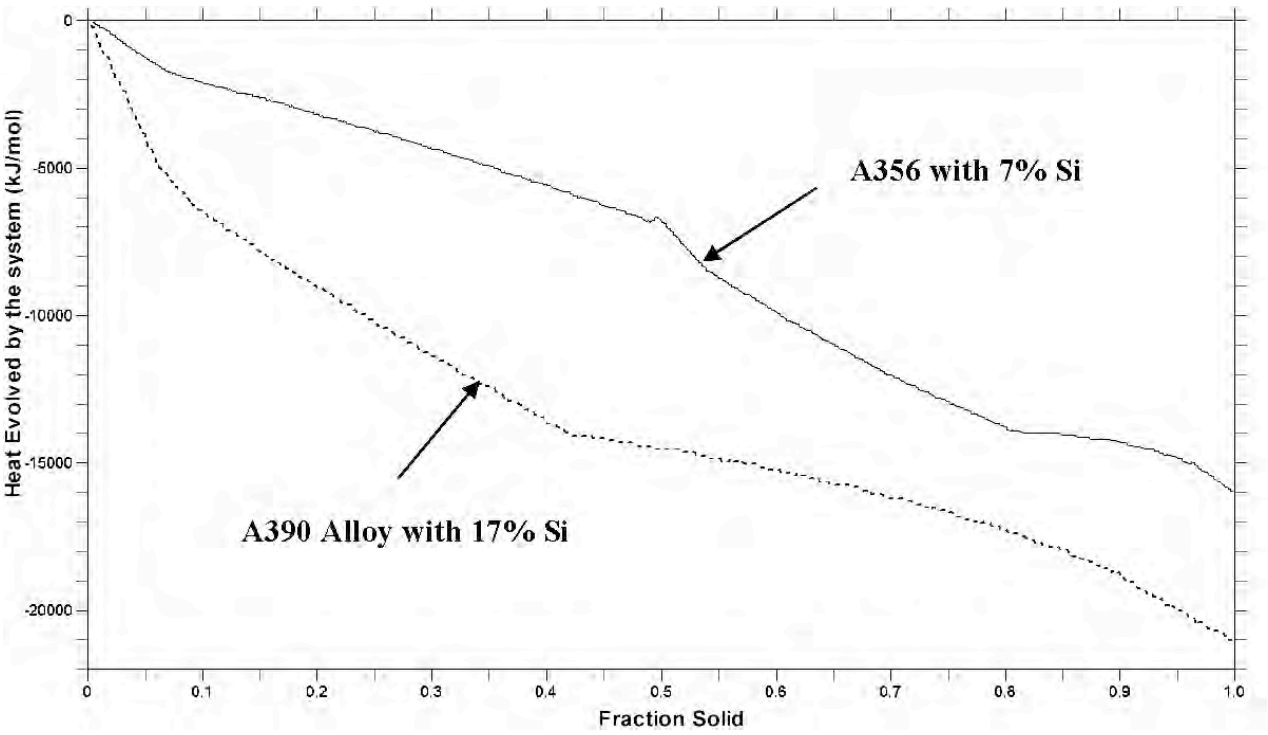

Figure 1: Heat released during the solidification of a hypereutectic Al-Si alloy (dashed) and a hypoeutectic Al-Si (continuous line) with respect to fraction solid.

The heats of fusion and the enthalpy of formation of one mole of Al (in hypoeutectic alloy) and Si (in hypereutectic alloy) are listed below:

$$\Delta S^{Si}_{Trans} = \frac{\Delta H_{trans}}{T_m}$$

$$\Delta S^{Si}_{Trans} = \frac{50{,}200}{1685} = 29.79 J/K$$

$$\Delta S^{Al}_{Trans} = \frac{10{,}700}{934} = 11.45 J/K$$

$$\frac{\Delta S^{Si}_{Trans}}{\Delta S^{Al}_{Trans}} = \frac{29.79}{11.45} = 2.6$$

Equation 1

Equation 1 shows that the energy released during the transformation of a mole of Si is at least 2 – 3 times that of Al. The high heat of fusion associated with Si accounts for the exothermic nature of this transformation. This can be seen by the ratio of the heats of fusion of Si with that of Al:

$$\frac{\Delta H^{Si}_{Trans}}{\Delta H^{Al}_{Trans}} = \frac{50{,}200}{10{,}700} = 4.7$$

Another problem associated with casting of hypereutectic Al-Si alloys is the role undercooling plays on the size of the primary Si. Figure 2 shows the salient results from a study performed by (Wang, 1999) on the growth mechanism of primary silicon as a function of undercooling.

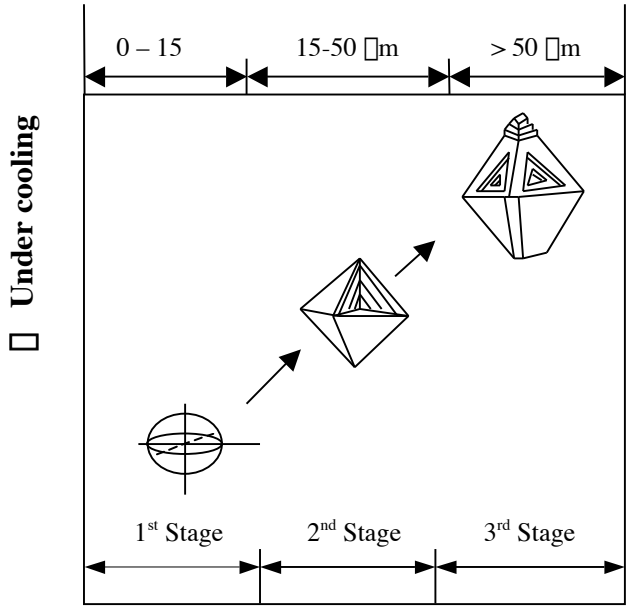

Figure 2: The three stages of growth of primary silicon as a function of undercooling (Wang, 1999).

The ideal microstructure of hypereutectic Al-Si alloys should consist of primary Si, which is small in size and evenly distributed throughout the matrix. The regions labeled as the 1st and 2nd stage give rise to the most desired primary Si microstructures. The transition from the un-faceted (1st stage) to faceted (2nd stage) is due to the crystal structure of primary Si. Jackson (Jackson, 1958) related crystal faceting to the entropy of melting and the crystal structure. Table 1 lists the values and conclusions from his studies.

Table 1. Jackson Criterion for the Morphology of Silicon Phase (Wang, 1999).

Plane	Ns / Nv	□	Growth Mode
111	3/4	2.67	Faceted
100	2/4	1.78	Non-Faceted
110	1/4	0.89	Non-Faceted

Where: Ns = No. of atoms on the surface and Nv = No. of atoms in the cell and alpha equals the ratio (Ns/Nv) multiplied by the entropy change divided by the transformation temperature ($\Delta S/T_E$), i.e., alpha = (Ns/Nv) x ($\Delta S/T_E$). The transition from continuous to faceted growth was analyzed by Sun et al (after Wang, 1999), and is shown in Figure 3. The shaded region shows the region relevant to primary silicon. It can be seen that the driving force (which is directly proportional to the under cooling) determines the growth mode of primary silicon – i.e., faceted / un-faceted structures. Traditional castings have employed high undercooling (use of chills, etc.) to precisely prevent the coarsening of the primary silicon (regions marked 1st / 2nd stage in Figure 2). These studies lay the essential foundation for the motivation for the rheocasting of hypereutectic Al-Si alloys. Primary silicon refinement and distribution is a direct function of the under cooling achieved during the solidification of a hypereutectic alloy.

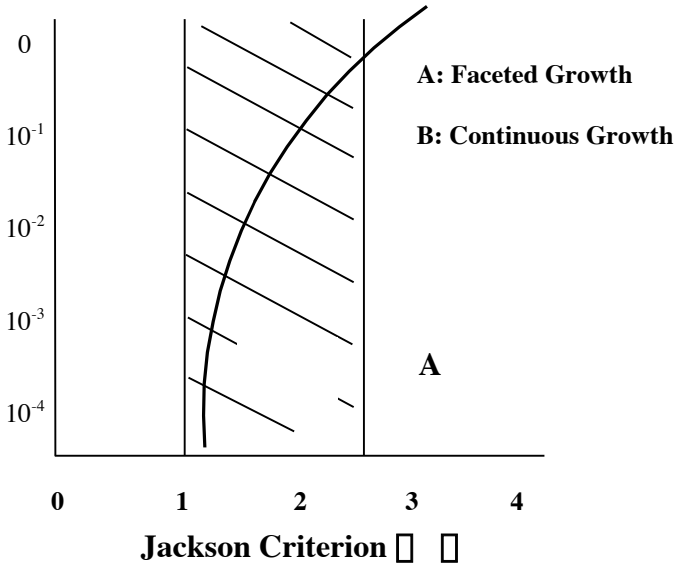

Figure 3: The variation in the driving force of transition from faceted to continuous growth. The shaded region corresponds to the values for Silicon (Wang, 1999).

SSM PROCESSING ROUTES FOR HYPEREUTECTIC AL-SI ALLOYS

In the recent past several rheocasting approaches have been developed, and have been commercially implemented. To establish context, prior to describing and reviewing the two novel approaches we have developed, existing processes will be briefly reviewed.

New Rheocasting Process, (UBE Industries) (UBE, 1996) where the liquid melt is held at relatively low superheats is poured in a cold mould, the natural convection during the pouring being utilized for the dispersion of nuclei.

A quick and initial mechanical stirring of the liquid metal in the early stages of solidification, known as SSR process, or the new MIT process (Matinez, 2001) leads to the nucleation of the primary phase and the dispersion of nuclei throughout the melt. In this process, it is important that the superheat is minimal, and controlled.

AEMP process (Flemings, 2003), which utilizes electromagnetic stirring to break up the dendrite arms to create a semi-solid slurry.

Sub-Liquidus Casting (SLC/THT process) (Anacleto, 2001), which utilizes pouring at very low or near close, liquidus temperatures giving rise to semi-solid structures.

CRP^{TM} (Continuous Rheocasting Process) developed by the ACRC-MPI team wherein liquid from two different reservoirs are fed into a reactor to produce a slurry. The reactor aids in the formation of the nuclei, and dispersing them throughout the bulk (DOE report).

Slurry-on-Demand and rheocasting processing routes (UBE-NRC, SSR, AEMP, SLC, CRP and etc.) for Al-Si alloys (hypoeutectic alloys) utilize the concept of nucleation and dispersion of nuclei (nucleated during the early stages of solidification) to achieve a semi-solid slurry state. Applying the above processing routes to hypereutectic Al-Si alloys has significant challenges (high heats of fusion and rapid growth of the primary Si phase), and the currently available processes may not be applicable for hypereutectic Al-Si alloys. Accordingly, two novel approaches both based on diffusion solidification concepts were explored to balance the release of the high heat of fusion in hypereutectic Al-Si alloys, and to control the growth of the primary silicon phase.

DIFFUSION SOLIDIFICATION

Diffusion solidification, introduced by Apelian and Langford (Langford, 1980) is a novel approach wherein solidification is controlled by mass flow rather than heat flow. During conventional solidification processing, when an alloy is

solidified, the temperature is reduced as one moves down an iso-concentration line. Partitioning takes place, and two phases are formed: primary alpha phase and enriched liquid phase. Moreover, the heat released by the liquid phase flows in the direction opposite to the motion of the liquid/solid interface, and solidification time is controlled by heat flow. In diffusion solidification, two phases – a solute enriched liquid phase and a solute poor solid phase (held at the same temperature – on an isothermal line) are brought into intimate contact, and solute diffusion from the liquid to the solid phase takes place. As the liquid loses solute, solidification proceeds via mass flow. Moreover, solidification times are independent of the size of the casting.

Originally, Apelian and Langford utilized diffusion solidification to die cast steels. In their pioneering experiments, they infiltrated a die filled with pure iron powder heated to a temperature in the Austenite region, T_1 with cast iron liquid phase also heated to the same temperature, T_1 (Figure 4). Carbon diffused away from the liquid into the iron powder, and since carbon diffuses interstitially, the diffusion rate is relatively high, and the liquid phase became solute (carbon) poor at T_1, and solidified. They produced a variety of cast components using diffusion solidification; commercially, the concept is utilized to make high-speed steels, and also dental amalgams.

The diffusion solidification approach has been applied to Al-Si alloys, both Hypo and Hypereutectic alloys. Specifically, we mixed solid particles with liquid metal, both phases having the same composition prior to mixing, however not at the same temperature. The central idea behind this concept is to utilize the excess superheat from the liquid metal (latent heat of solidification), as well as the heat released during the growth of the primary Si phase in melting the solid particles. This approach ensured that the heat released is internally consumed in the dissolution/melting of the solid pieces, as the hotter metal solidified. The turbulence generated during pouring of the metal was used in dispersing the nuclei throughout the melt. The process is rapid, and the amount of solid particles added into the system determined the final temperature of the slug.

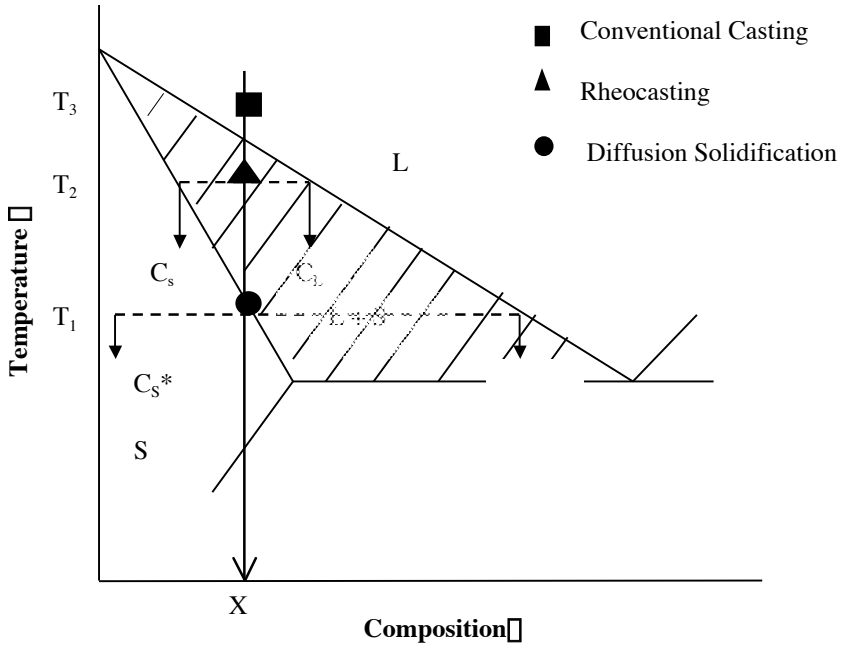

■ Conventional casting at temperature T_3

▲ Rheocasting: alloy X is cooled to T_2 and isothermally agitated. The solid-liqiud mixture consists of liquid phase of composition C_L of an amount f_L and solid phase of composition C_S and amount f_S, such that $f_S C_S + f_L C_L = X$

● Diffusion solidification: f_S amount of solid particles of composition C_S* and at temperature T_1 are infiltrated by f_L amount of liquid of Composition C_L* such that $f_S C_S^* + f_L C_L^* = X$

Figure 4: Schematic diagram illustrating the concept of diffusion solidification [9].

DIFFUSION SOLIDIFICATION: ***MIXING OF TWO LIQUIDS***

We addressed the challenge of rheocasting Al-Si alloys by mixing two melts of two different compositions, each held at different temperatures. Specifically, we mixed two Al-Si alloys, one a hypoeutectic melt (6-7% Si, A356), and the other a hypereutectic alloy (25% Si). The 25% Si alloy was held above its liquidus temperature, whereas the 6-7% Si alloy was held in the semi-solid range (two phase range) - see Figure 5. The purpose of adding the hypereutectic alloy to the cooler A356 alloy was to rapidly extract thermal energy from the hypereutectic melt, and to lower its temperature to the SSM casting temperature. The weight ratio of the two starting melts is 1:1, and the resultant alloy composition (based on a mass balance) is that of A390. The conceptual framework is to increase diffusion of heat from the hypereutectic alloy by the dissolution of the primary aluminum phase of the hypoeutectic alloy. The thermal imbalance leads to two advantages:

- heat from the higher Si alloy is absorbed by the cooler alloy, and concomitantly
- rapid chilling prevents the growth of primary silicon to unacceptable ranges.

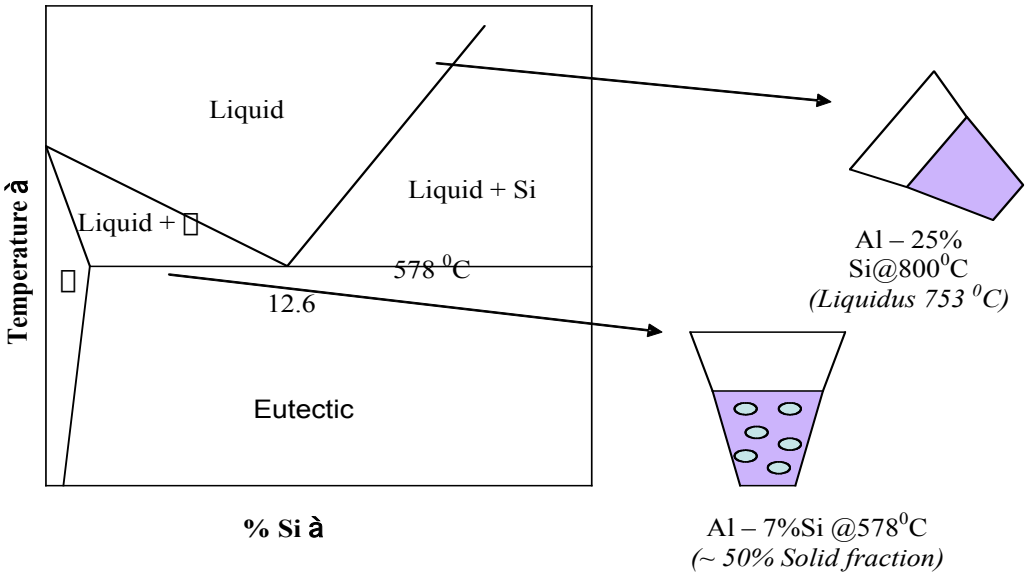

Figure 5: Diffusion Solidification concept of mixing liquid Al-Si at 800 ^{0}C, and A356 (7% Si) at 578 ^{0}C (semi-solid state).

A 100 grams sample of hypoeutectic alloy (A356) was heated in a furnace and cooled slowly to 577 ^{0}C. The schematic diagram illustrating the experimental approach is shown in Figure 5. The temperature of the bulk was continuously measured during the duration of the experiment; Figure 6 shows the time-temperature curve obtained by the mixing of the two entities. It can be seen that the temperature at the interface rises and subsequently drops to 615 ^{0}C. Microstructures were examined at various locations from the resultant cast samples. Figure 7 summarizes the microstructures obtained at various positions in the resultant cast product.

It can be seen from Figure 7, that the primary aluminum dissolves due to temperature and compositional variations. Precise experiments performed at WPI to study the thermal history of both the hypoeutectic and the hypoeutectic side is shown schematically in Figure 8.

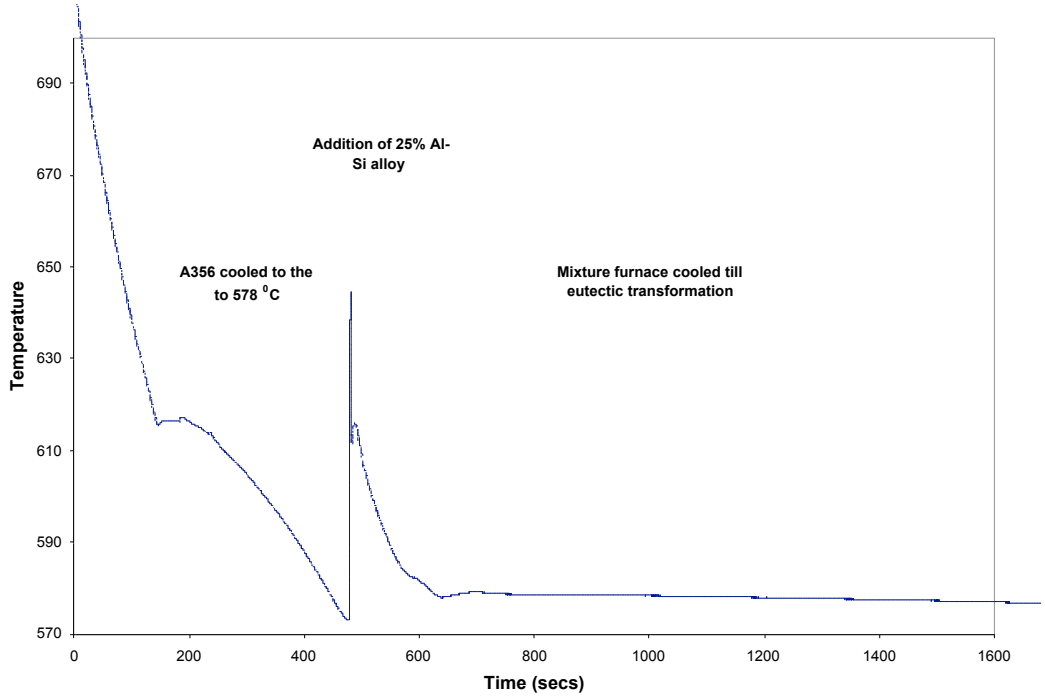

Figure 6: Time - Temperature plot at the interface during mixing of the two entities.

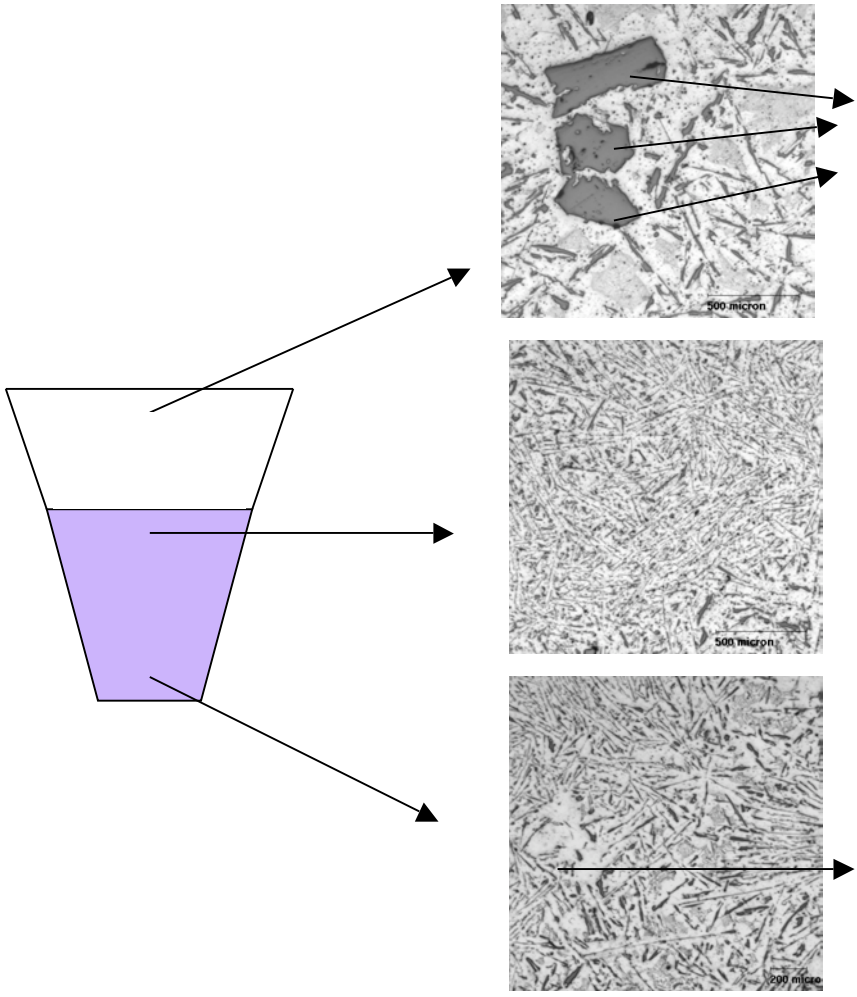

Figure 7: Microstructures of the resultant hypereutectic alloy at various positions in the mixture.

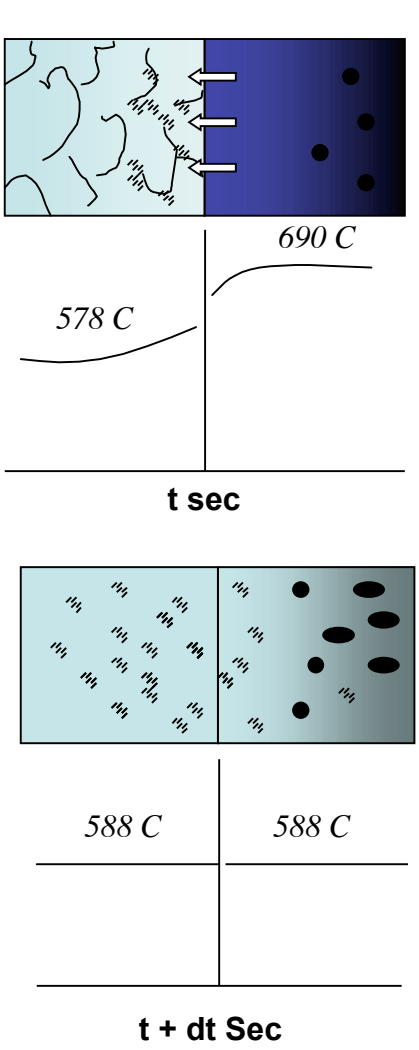

•Instantaneous precipitation of primary Si at the far end due to thermal drop to below liquidus
•Diffusion of Si / Al across the interface due to compositional imbalance/ heat imbalance
•Compositional balance between Si in the hypereutectic Al-Si alloy and the eutectic liquid of the Al- 50% Si hypoeutectic alloy

•The growth of primary Silicon at the far end is limited because of the chemical potential of Al/Si across the interface
•Conversion of 50% fraction solid to liquid of eutectic composition by diffusion solidification
•The final mixture has primary Si (due to chilling at the far end) and liquid eutectic

Figure 8: Schematic diagram of diffusion solidification between the liquid hypereutectic and the 50% hypoeutectic Al-Si alloys.

As these experiments were performed to ascertain the microstructural evolution across the interface (without the intention of controlling the primary Si size and distribution), experiments were also performed by physically mixing the liquids – i.e., the 25% Si liquid was poured into the A356 alloy. Figure 9 shows the resultant microstructure.

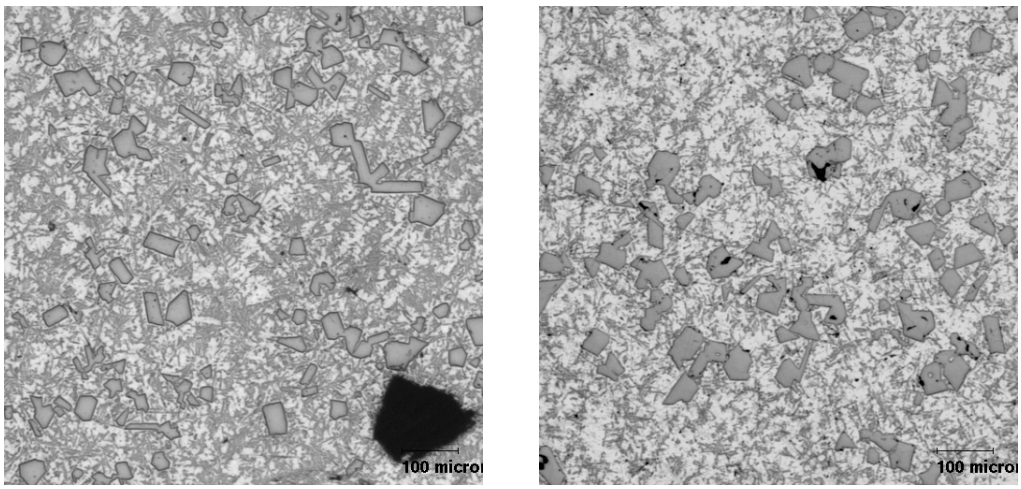

Figure 9: Microstructures obtained by stirring the mixture as the 25% Al-Si alloy was poured into the semi-solid hypoeutectic A356 alloy.

The mixing of two liquids held at different compositions and temperatures shows positive results in the rheocasting of hypereutectic Al-Si alloys. Figure 9 clearly shows the dissolution of the primary aluminum of the hypoeutectic alloy

(A356) that was achieved due to heat absorption and by diffusion solidification. The reactions can be broadly classified (experiment is schematically shown in Figure 8) as follows:

Liquid Hypereutectic Alloy (Al-25%Si): L → Primary Si and Eutectic

Semi-solid Hypoeutectic Alloy (Al-7%Si): L + Primary Al → Eutectic

Experiments are underway at WPI to ascertain the diffusion dynamics/kinetics and the interface motion during the dissolution of primary aluminum (in the hypoeutectic alloy) to a liquid that solidifies as a eutectic alloy.

DIFFUSION SOLIDIFICATION: *MIXING OF SOLID PARTICLES AND LIQUID METAL*

Another variation of the above discussed diffusion solidification approach was developed. In this process, solid particles/chunks of hypereutectic alloy were added into a liquid melt of hypereutectic Al-Si alloy (the alloy investigated being commercial 390 alloy). The addition of particles was performed to remove the heat from the liquid at a very rapid rate (to initiate nucleation of primary Si) and, to utilize the turbulence generated by the pouring liquid as a source for nuclei dispersion. Experiments were performed in two steps, schematically shown in Figures 10 and 11, respectively.

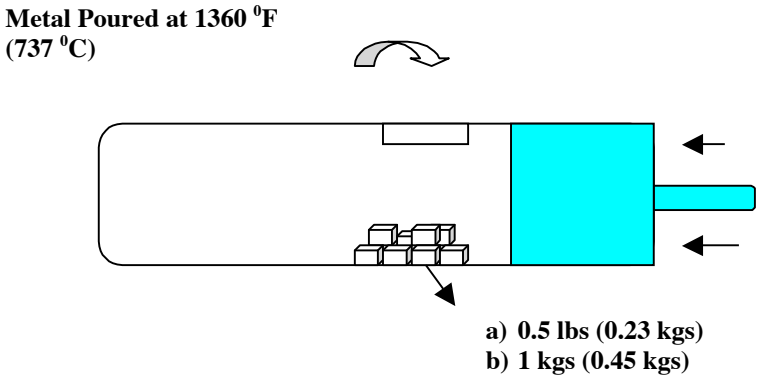

Figure 10: Schematic diagram illustrating the concept of solid particle addition into the shot sleeve.

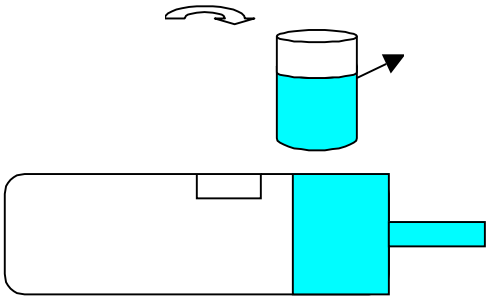

Figure 11: Schematic diagram illustrating the concept of solid particle addition into the ladle.

Table 2 lists the experiments performed in the plant trials at SPX Contech; details of the experiments are also given. The final part was cut and sections (thick and thin) were metallographically analyzed and compared to conventional die cast parts (baseline) from the same die-casting machine.

Table 2. Details of Various Experiments Performed at SPX Contech.

Experiment	Weight of solids added	Metal Temperature
Solids added into the shot sleeve		
a	0.5 lbs, 0.23 kgs (1.7% total weight)	1360 ^{0}F / 737 ^{0}C
b	1 lbs, 0.45 kgs (3.3% total weight)	
Solids added into the ladle		
c	2lbs, 0.91 kgs (6.7% total weight)	1360 ^{0}F / 737 ^{0}C
d	3lbs, 1.36 kgs (10% total weight)	

The cut samples (thick and thin) were analyzed for the primary Si size and distribution; 2-3 micrographs were taken at 100 X (to visually ascertain the special distribution of primary Si), and 4-5 micrographs (approximately 1 cm2) were taken at 200 X (to determine the size distribution of primary Si). The Dmax (shown in Figure 12) was used to estimate the silicon size. Dmax is the maximum length of primary size particle in the matrix. The primary Si are polygonal in nature, and their size distribution has a vast range; therefore the measurement of equivalent diameter is not representative, and it will be erroneous to utilize it as an index to reflect process parameter changes. The resulting microstructures are shown in Figures 13 – 16 for experiments a – d, respectively (see Table 2).

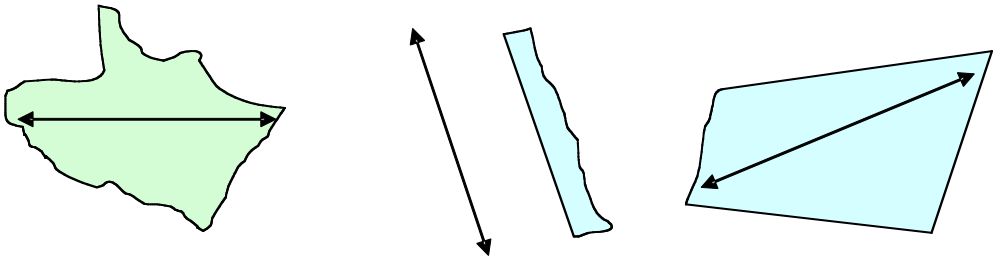

Figure 12: Schematic diagram of D_{max} for various primary Si shapes observed in the microstructure.

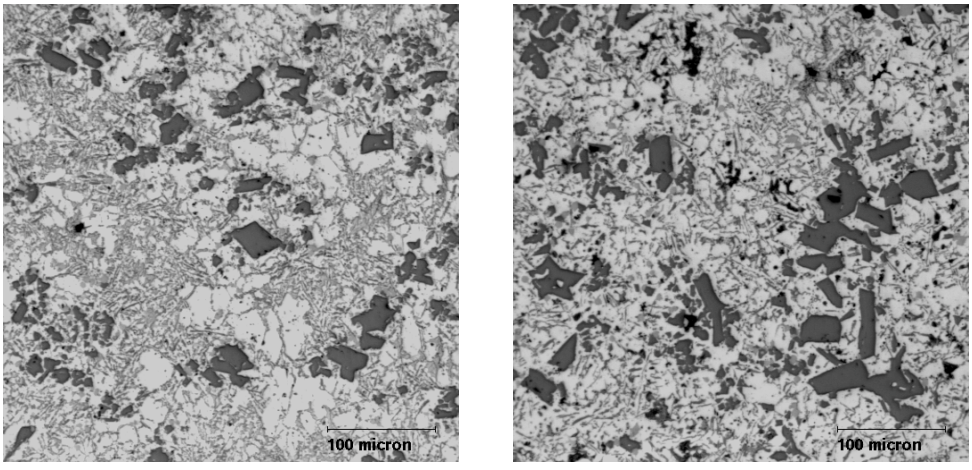

Figure 13: Representative microstructures from experiment a; thick section (left) and thin section (right).

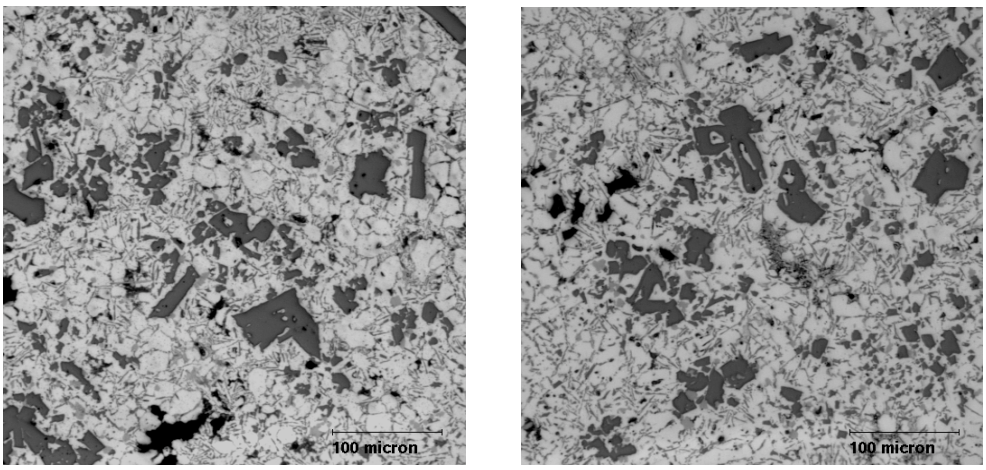

Figure 14: Representative microstructures from experiment b; thick section (left) and thin section (right).

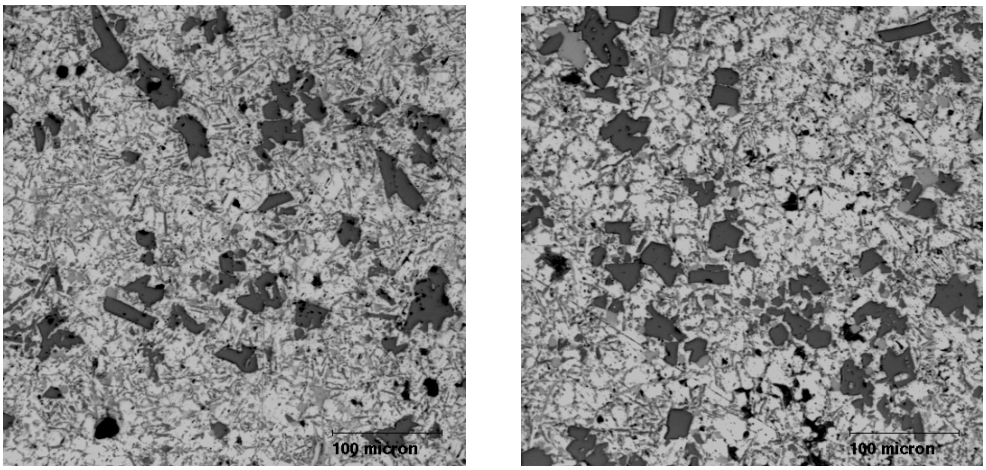

Figure 15: Representative microstructures from experiment c; thick section (left) and thin section (right).

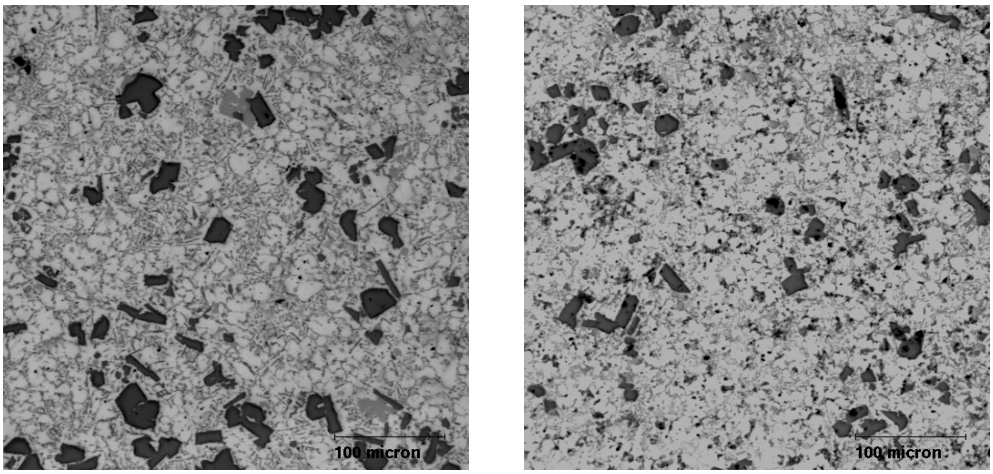

Figure 16: Representative microstructures from experiment d; thick section (left) and thin section (right).

Figure 17 lists the values of Dmax obtained for the set of experiments performed (Table 2). An average value from 4-5 micrographs was calculated, and these are given in Figure 17.

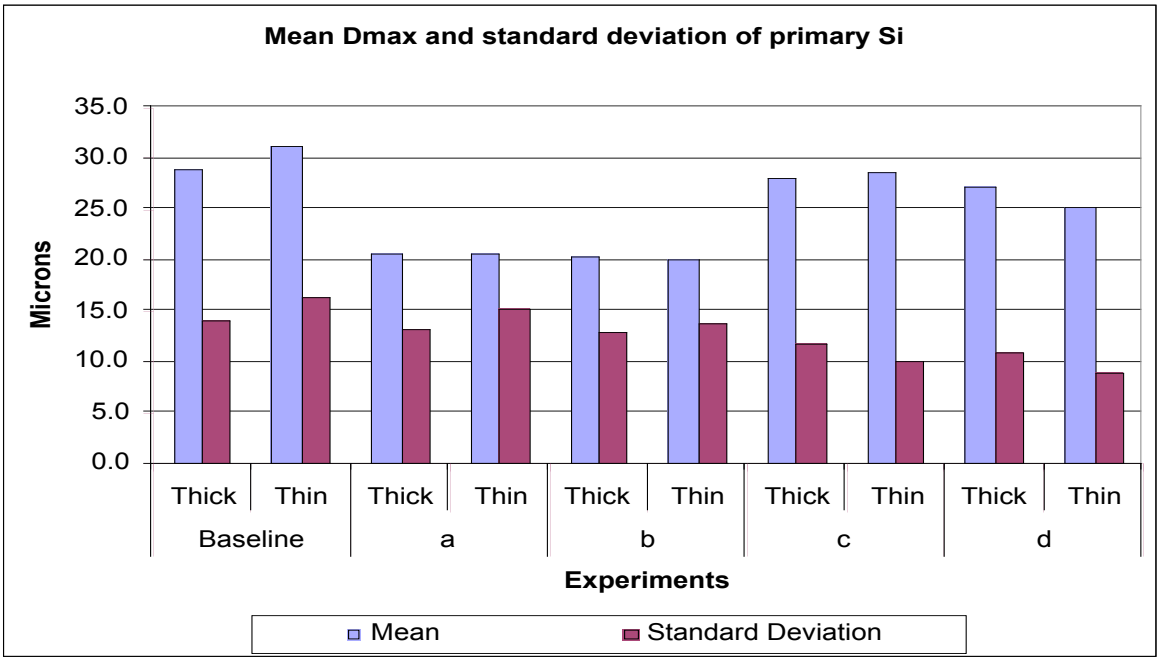

Figure 17: D_{max} and standard deviation of primary Si for the set of experiments carried out by the two novel diffusion solidification processes.

CONCLUSIONS

Hypereutectic Al-Si alloys have been a challenge to cast via semi-solid processing because of the growth of the primary silicon phase, which gives rise to unacceptable morphologies, and thus unacceptable mechanical properties. In this work we have developed two novel processing methods that utilize the concept of diffusion solidification to control the growth of the primary silicon.

Diffusion solidification is controlled by mass flow rather than heat flow. During conventional solidification processing, when an alloy is solidified, the temperature is reduced as one moves down an iso-concentration line. Partitioning takes place, and two phases are formed: primary alpha phase and enriched liquid phase. Moreover, the heat released by the liquid phase flows in the direction opposite to the motion of the liquid/solid interface, and solidification time is controlled by heat flow. In diffusion solidification, two phases – a solute enriched liquid phase and a solute poor solid phase (held at the same temperature – on an isothermal line) are brought into intimate contact, and solute diffusion from the liquid to the solid phase takes place. As the liquid loses solute, solidification proceeds via mass flow.

Specifically, two novel diffusion solidification processes have been developed: one where a liquid hypereutectic alloy is mixed with a hypoeutectic alloy that is held in the semi-solid state; the second process solid particles/chunks are added to the melt.

Experiments with both approaches, both at the laboratory state and in plant trials resulted in excellent microstructures of hypereutectic alloys. Results indicate that via these approaches one can control the size of the primary silicon phase in hypereutectic alloys to less than 25 microns.

ACKNOWLEDGMENTS

The authors would like to thank SPX Contech for providing the financial support for this work, use of die casting machines at the plant, and the needed man power for the successful conduction of these trials. We would also to thank Dayne Killingsworth, and Zach Brown of SPX Contech for their invaluable contributions during the trails.

REFERENCES

Anacleto Figueredo, Science and Technology of Semi-Solid Metal Processing, Published by the North American Die Casting Association, Rosemont, IL, page 2-12, (2001).

DOE Report number DE-FC07-98ID13618.

Flemings M.C, “Semi-Solid Processing – The Rheocasting Story”, Test Tube to Factory Floor: Implementing Technical Innovations, In the proceedings of the Spring Symposium May 22, 2002 published by Metal Processing Institute, Worcester Polytechnic Institute, Worcester MA 01609, (2003).

Jackson K.A , Liquid Metals and Solidification, ASM, Ohio, pp 17 (1958).

Langford. G and Apelian. D, "Diffusion Solidification", Journal of Metals, 32, No. 9, page. 28-34 (1980).

Martinez R. , Figueredo A.M, Yurko. and Flemings M.C, “Efficient Formation Structures Suitable for Semi-Solid Forming”, Transactions of the 21st International Die Casting Congress and Exposition, Oct 29 – Nov 1, Cincinnati, Ohio, page 47 – 54 (2001).

Matsuura K, Kudoh M, Kinoshita H , Takahashi H, “Precipitation of Si particles in a super-rapidly solidified Al-Si alloy”, Materials Chemistry and Physics, Volume 81, pp 393 – 395 (2003).

UBE Industries Ltd, European Patent No. EP 0 745 694 A1 (1996).

Wang Ru-yao, Lu Wei-hua, Logan L.M , “Growth morphology of primary Silicon in cast Al-Si alloys and the mechanism of concentric growth”, Journal of Crystal Growth, Volume 207, pp 43 -54 (1999).

Optimization of 380 Alloy for Semi-Solid Processing

Q.Y. Pan, L. Wang, D. Apelian and M.M. Makhlouf

Advanced Casting Research Center (ACRC)
Metal Processing Institute (MPI)
WPI, Worcester, MA 01609 USA

Abstract

Often newly developed manufacturing processes are evaluated with existing alloys rather than optimizing a special alloy that can take advantage of the unique attributes of the new process. Currently, conventional cast aluminum alloys, such as 356 and 357, are used for SSM processing. Process inconsistencies and excessive liquid metal loss during reheating (thixocasting) arising from the use of these alloys are mainly due to a high temperature sensitivity of fraction solid in the temperature range of commercial operations. SSM alloy development remains a significant issue in SSM processing.

In this study, thermodynamic simulations have been performed in order to optimize the composition of 380 alloy for SSM applications. Specifically, the effects of various alloying elements in 380 alloy on the alloy's solidification behavior and the fraction solid vs. temperature curve, as well as on the temperature sensitivity of the fraction solid have been characterized. Subsequently, recommendations are made to allow the optimization of 380 alloy composition for SSM applications.

Keywords: Thermodynamic simulation, alloy design, semi-solid processing, 380 alloy.

1. Introduction

Semi-solid metal (SSM) processing offers many benefits over conventional near-net shaping technologies. These include reduced turbulence in the die cavity, reduced defects and entrained oxides, and the ability to produce components with better mechanical properties compared to conventional high-pressure die castings. In principle, SSM slurries can be produced from any material system where liquid and solid phases coexist over a freezing range. An important drawback of conventional SSM processes is that the fraction solid, and consequently, the viscosity of the melt in the semi-solid state are strongly dependent on temperature. Therefore, process control is relatively difficult due to the necessity of a close control of temperature and temperature gradients in

reheated billets (thixocasting). Efforts are currently underway to overcome these problems by developing new SSM processes, and equally important, alloy systems that are better suited for semi-solid processing.

Often newly developed manufacturing processes are evaluated with existing alloys rather than optimizing a special alloy that can take advantage of the unique attributes of the new process. Currently, conventional cast aluminum alloys such as 356 and 357 are being used for SSM processing [1]. Process inconsistencies and excessive liquid metal loss during reheating (thixocasting) arising from the use of these alloys are caused mainly by a relatively high temperature sensitivity of fraction solid in the temperature range of commercial operations. SSM alloy development remains a significant issue in SSM processing

Historically, the trial-and-error method has been employed for alloy development. This approach has been proven to be cost-intensive and time-consuming. With the development of robust aluminum alloy databases, a new approach based on ***thermodynamic simulations*** has emerged. This approach provides a powerful tool for alloy design. In this approach, the Gibbs free energy of individual phases is calculated as a function of alloy composition, temperature and pressure, and then collected in a thermodynamic database that enables calculation of multi-component phase diagrams. The calculation results provide critical information for alloy design such as the phase formation and transformation temperatures, and the solidification characteristics of the alloy.

Using thermodynamic simulations, Han and Viswanathan [2] investigated tailoring the composition of A356/357 alloy to render it more suitable for SSM processing. Similarly, based on calculations of temperature sensitivity of the fraction solid, Liu and Fan [3] studied the suitability of commercial alloys in the Mg-Al-Zn and Mg-Al-Mn systems for SSM processing, and they identified several alloys that have great potential for thixo- and rheocasting applications. Recently, a great deal of effort has been devoted to wrought alloys [4-8], and several alloys in the 2xxx and 7xxx series have been evaluated and optimized for thixoforming [4-8].

In this contribution, we present preliminary work on the optimization of 380 die cast alloy for SSM applications. Specifically, we characterize the effects of various alloying elements in 380 alloy on the alloy's solidification behavior and the fraction solid vs. temperature curve, as well as on the temperature sensitivity of the fraction solid. In addition, recommendations are made to optimize the composition of 380 alloy for SSM applications.

2. Criteria for SSM Alloy Design

Several factors need to be considered for SSM alloy design. They are outlined as follows:

1) ***Solidification range (ΔT):*** is defined as the temperature range between the solidus and the liquidus lines of the alloy. Pure metals and eutectic alloys are not suitable for SSM processing, whereas, alloys with too wide a solidification range experience poor resistance to hot tearing. It is therefore suggested that the solidification range of an SSM alloy be between 40-130K [7].

2) ***Temperature sensitivity of the fraction solid:*** As illustrated in Figure 1, for a given alloy composition, temperature sensitivity of the fraction solid (fs) is defined as the slope of the fs vs.T curve, *i.e.,* it is dfs/dT. In order to obtain stable and repeatable processing conditions, the temperature sensitivity of the fraction solid should be as small as possible in the fraction solid range of commercial operations (ideally fs should be 0.3-0.5 for rheocasting, and 0.5-0.7 for thixocasting/thixoforging).

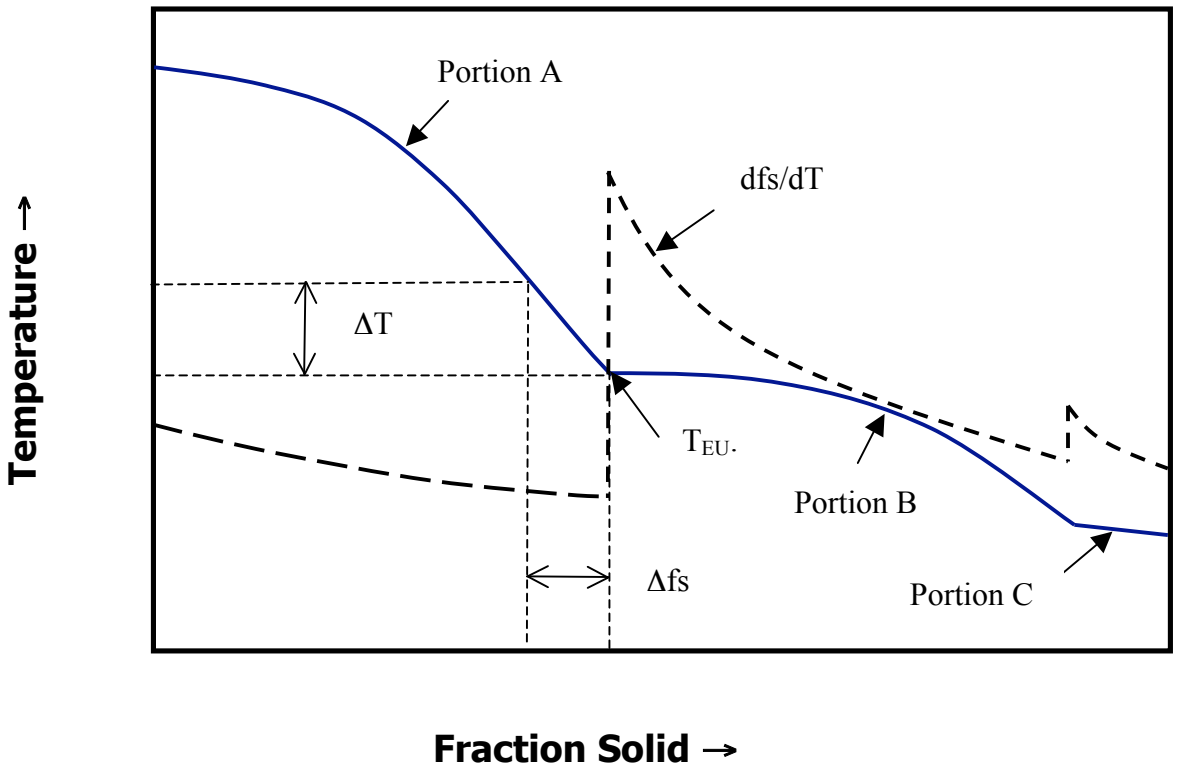

Figure 1: Typical fraction solid vs. temperature curve of cast Al alloys.

3) ***Potential for age hardening:*** In order to achieve high strength, the alloys designed for SSM processing need to have high potential for age hardening. During a T5 temper, SSM parts ejected from the die are quenched immediately in water and then artificially aged at a relatively low temperature. Therefore, the potential for age hardening of a phase can be gauged by the concentration difference (ΔC) of the major alloying elements in the α-phase between the quenching and ageing temperatures.

4) ***Rheological properties in the semi-solid state:*** It is the unique rheological properties of SSM slurries that give SSM processing its advantages over conventional casting methods. Usually, the rheological properties of semi-solid slurries are evaluated by developing shear stress vs. shear rate curves under various shearing conditions and temperatures.

5) ***Morphology of the solid phase:*** An ideal SSM slurry consists of small ($\leq$100μm), round α particles that are uniformly distributed in a liquid matrix. This slurry structure ensures smooth mold filling, and a high quality of SSM castings.

Among the above factors, the rheological properties of SSM slurries and the morphology of the solid phase are controlled by process conditions, and cannot be predicted using thermodynamic simulations. In this study, thermodynamic calculations are used as the first step in evaluating the effects of alloy composition on solidification behavior and developing the fraction solid vs. temperature curve, and characterizing the temperature sensitivity of the fraction solid in 380 alloy.

3. Simulation Results & Analyses

In section 3.1, we present phase equilibra and highlight the typical phase transformations in 380 alloy. In section 3.2, we analyze the effects of various alloying elements in 380 alloy on the temperature vs. fraction solid curve and on the temperature sensitivity of the fraction solid. Finally, in section 3.3, we present recommendations for optimizing the composition of 380 alloy for SSM processing.

3.1 Phase Equilibria

Table 1 gives the chemical composition of 380 alloy as specified by ASTM. Phase diagram calculations under non-equilibrium conditions (i.e., using the Scheil equation) show complicated phase equilibria. With decreasing temperature from the liquidus to the solidus, typical phase transformations occur as outlined in Table 2.

Table 1: Chemical Composition of 380 Alloy

Si	Fe	Cu	Mg	Mn	Ni	Zn	Sn	Al
7.5-9.5	2.0	3.0-4.0	0.1	0.5	0.5	3.0	0.35	Bal.

Note: All single values are maximum composition percentage

Table 2: Phase Equilibria in 380 Alloy

T (°C)	fs	Phase
596.5	0	L+β(AlFeSi)
587.5	0.0058	L+β(AlFeSi)+α(Al)
576.4	0.166585	L+β(AlFeSi)+α(Al)+ $Al_{15}FeMn_3Si_2$
563.3	0.298	L+β(AlFeSi)+α(Al)+ $Al_{15}FeMn_3Si_2$+Si
526.2	0.864435	L+β(AlFeSi)+α(Al)+ $Al_{15}FeMn_3Si_2$+Si+Al_3Ni
508.2	0.918131	L+β(AlFeSi)+α(Al)+ $Al_{15}FeMn_3Si_2$+Si+Al_3Ni+δ(AlCu)
447.1	0.9909	L+β(AlFeSi)+α(Al)+ $Al_{15}FeMn_3Si_2$+Si+δ(AlCu)
444.7	0.991416	L+β(AlFeSi)+α(Al)+Si+δ(AlCu)+$Al_5Cu_2Mg_8Si_6$
415.0	0.996467	L+β(AlFeSi)+α(Al)+δ(AlCu)+$Al_5Cu_2Mg_8Si_6$
405.5	1.0	β(AlFeSi)+α(Al)+δ(AlCu)+$Al_5Cu_2Mg_8Si_6$

3.2 Thermodynamic Simulations

In order to understand the role of each alloying element and in order to simplify the analysis, alloying elements other than the one under investigation are kept at a constant value (as given in Table 1). Also, in order to amplify the effect of each alloying element on the solidification behavior, the fs vs. T curve, and the temperature sensitivity of the fraction solid, the concentration of the alloying elements is varied within a range that extends outside the limits specified by ASTM.

A. Effect of Silicon

Figure 2 gives the T-fs curves of 380 alloy as a function of Si content. Apparently, Si has a significant influence on the solidification behavior and consequently on the SSM processablility of the alloy. Table 3 shows (dfs/dT) values as a function of Si content and fraction solid. From Figure 2 and Table 3, one can see that:

- Si does not change the shape of the fraction solid vs. temperature curve of 380 alloy, but it affects the location of the binary eutectic point. With decreasing Si content, the fs vs. T curves shift towards the right, indicating that the temperature of the binary eutectic reaction is decreased, and more α phase is formed (segment A in the fraction solid vs. temperature curves that corresponds to the formation of the α phase is extended).

- For rheocasting (fs: 0.3-0.5), in order to enhance process control, the Si content should be less than 8.5% if the slurry is processed at a low fraction solid (e.g., 0.3); however, the Si content should be less than 6.5% if the slurry is processed at a fraction solid of 0.5.

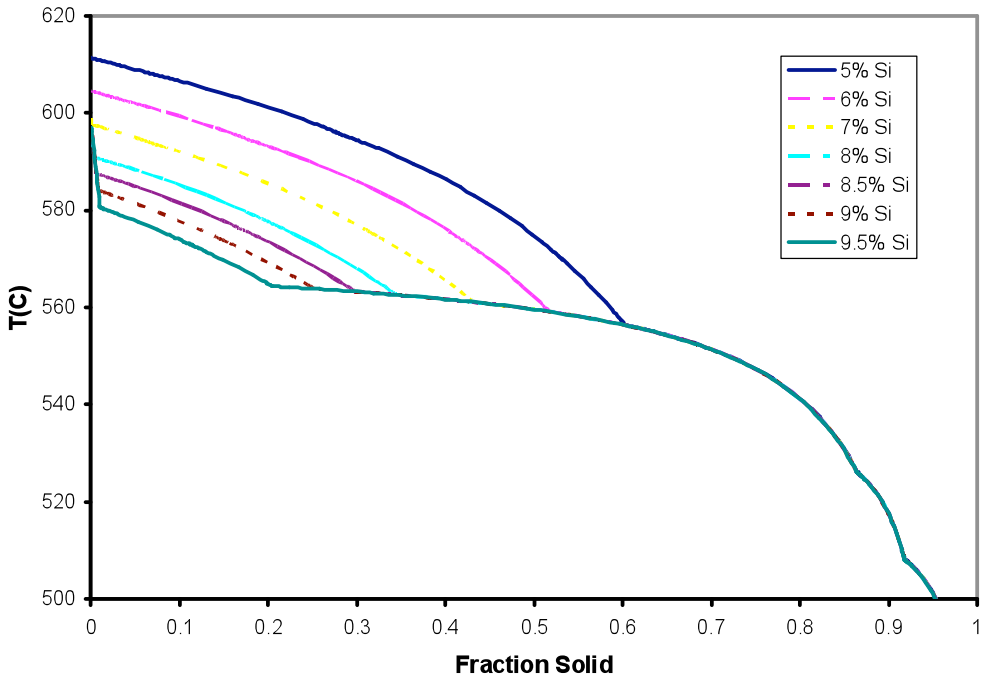

Fig. 2: Effect of Si content on fraction solid vs. temperature curves of 380 alloy.

Table 3: dfs/dT values of 380 alloy as a function of Si content and fraction solid

Si Content	$(dfs/dT)_{fs=0.3}$	$(dfs/dT)_{fs=0.4}$	$(dfs/dT)_{fs=0.5}$	$(dfs/dT)_{fs=0.6}$	$(dfs/dT)_{fs=0.7}$
5%	0.014	0.010	0.007	0.004	0.012
6%	0.011	0.008	0.006	0.023	0.014
7%	0.010	0.007	0.036	0.024	0.014
8%	0.009	0.050	0.036	0.023	0.014
8.5%	0.073	0.051	0.035	0.023	0.013
9%	0.069	0.049	0.034	0.022	0.014
9.5%	0.069	0.047	0.037	0.024	0.014

B. Effect of Copper

Figure 3 gives the T vs. fs curves for 380 alloy as a function of Cu content. It is found that Cu increases the slope of the T vs. fs curves in the fraction solid range typical to commercial SSM practices. This indicates that Cu reduces the temperature sensitivity of the fraction solid of the alloy. Therefore, in order to create a relatively large SSM process window, it is recommended to use the upper limit of Cu specified by ASTM. Table 4 shows (dfs/dT) values as a function of Cu content and fraction solid.

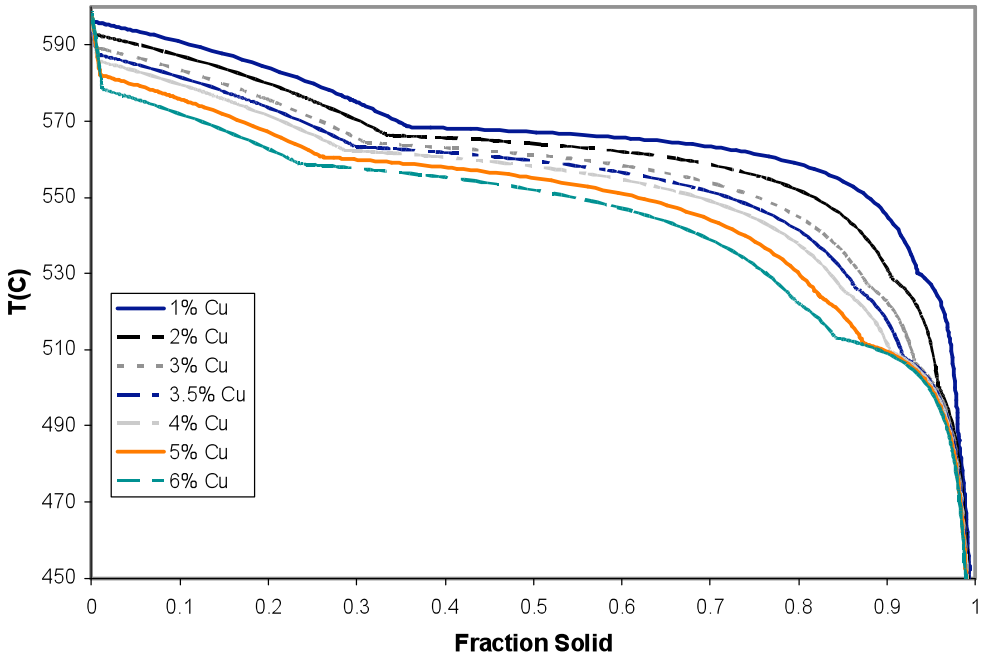

Fig. 3: Effect of Cu content on fraction solid vs. temperature curves of 380 alloy.

Table 4: dfs/dT values of 380 alloy as a function of Cu content and fraction solid

Cu Content	$(dfs/dT)_{fs=0.3}$	$(dfs/dT)_{fs=0.4}$	$(dfs/dT)_{fs=0.5}$	$(dfs/dT)_{fs=0.6}$	$(dfs/dT)_{fs=0.7}$
1%	0.010	0.103	0.066	0.044	0.023
2%	0.008	0.067	0.050	0.032	0.020
3%	0.008	0.053	0.040	0.025	0.015
3.5%	0.073	0.051	0.035	0.023	0.013
4%	0.065	0.044	0.031	0.021	0.012
5%	0.054	0.037	0.028	0.018	0.010
6%	0.043	0.033	0.024	0.015	0.008

C. Effect of Nickel

Ni is a strengthening element in 380 alloy. It improves hardness and strength at elevated temperatures and reduces the coefficient of thermal expansion. Figure 4 gives the T vs. fs curves for 380 alloy as a function of Ni content. It is quite clear that Ni has a significant effect on the shape of the temperature vs. fraction solid curves. With the increase of Ni content, the slope of the temperature-fraction solid curves in the fraction solid range of commercial forming operations increases remarkably, thus leading to a small dfs/dT value, and a large process window. Based on the calculation results (see Table 5), a Ni content of no less than 1wt.% is recommended.

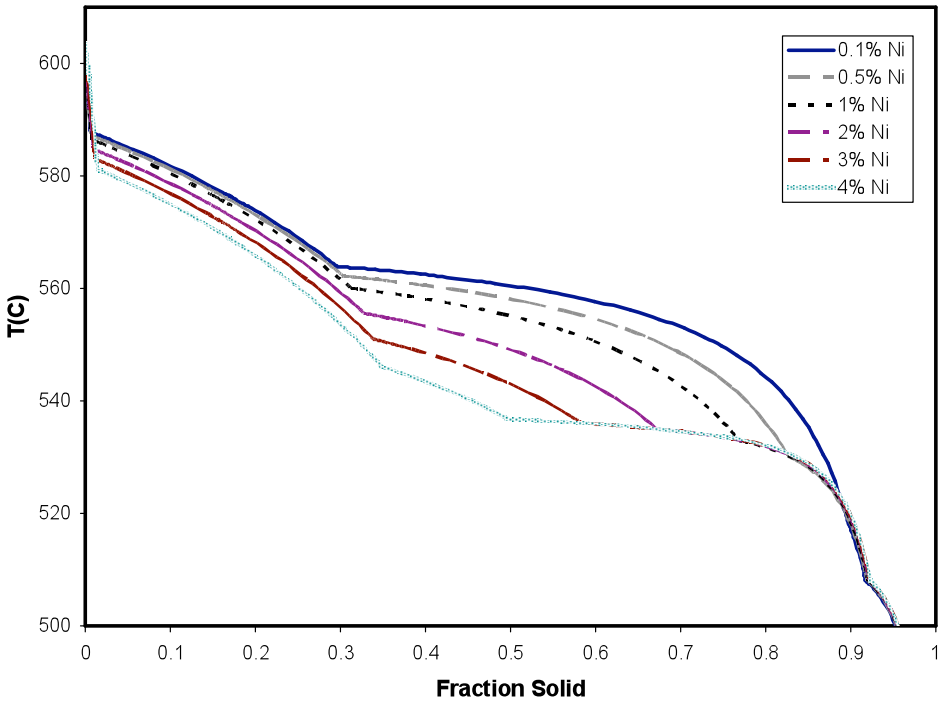

Fig. 4: Effect of Ni content on fraction solid vs. temperature curves of 380 alloy.

Table 5: dfs/dT values of 380 alloy as a function of Ni content and fraction solid

Ni Content	$(dfs/dT)_{fs=0.3}$	$(dfs/dT)_{fs=0.4}$	$(dfs/dT)_{fs=0.5}$	$(dfs/dT)_{fs=0.6}$	$(dfs/dT)_{fs=0.7}$
0.1%	0.080	0.054	0.037	0.026	0.015
0.5%	0.008	0.041	0.029	0.020	0.011
1%	0.008	0.035	0.026	0.016	0.009
2%	0.007	0.027	0.019	0.012	0.055
3%	0.007	0.020	0.014	0.091	0.046
4%	0.006	0.017	0.013	0.078	0.047

D. Effect of Magnesium and Zinc

Mg and Zn affect the temperature vs. fraction solid curve in a similar way as does Ni, but their effect is not as significant as the effect of Ni. The thermodynamic calculation results are summarized in Figures 5-6 and Tables 6-7.

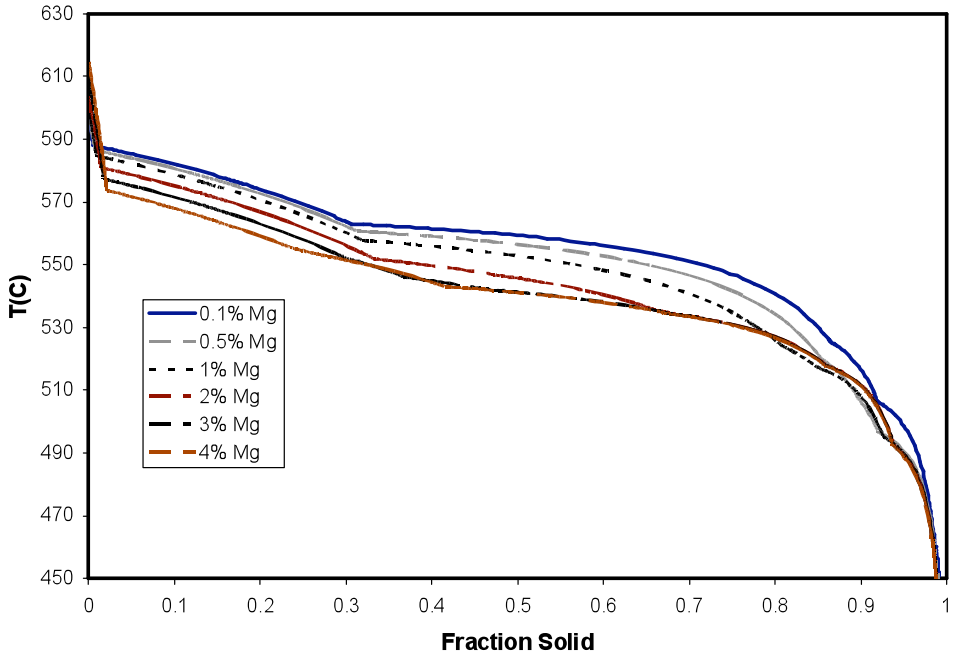

Fig. 5: Effect of Mg content on fraction solid vs. temperature curves of 380 alloy.

Table 6: dfs/dT values of 380 alloy as a function of Mg content and fraction solid

Mg Content	$(dfs/dT)_{fs=0.3}$	$(dfs/dT)_{fs=0.4}$	$(dfs/dT)_{fs=0.5}$	$(dfs/dT)_{fs=0.6}$	$(dfs/dT)_{fs=0.7}$
0.1%	0.008	0.049	0.034	0.023	0.013
0.5%	0.008	0.037	0.029	0.020	0.011
1%	0.008	0.034	0.024	0.017	0.009
2%	0.008	0.027	0.024	0.014	0.023
3%	0.014	0.024	0.036	0.024	0.023
4%	0.017	0.011	0.034	0.024	0.019

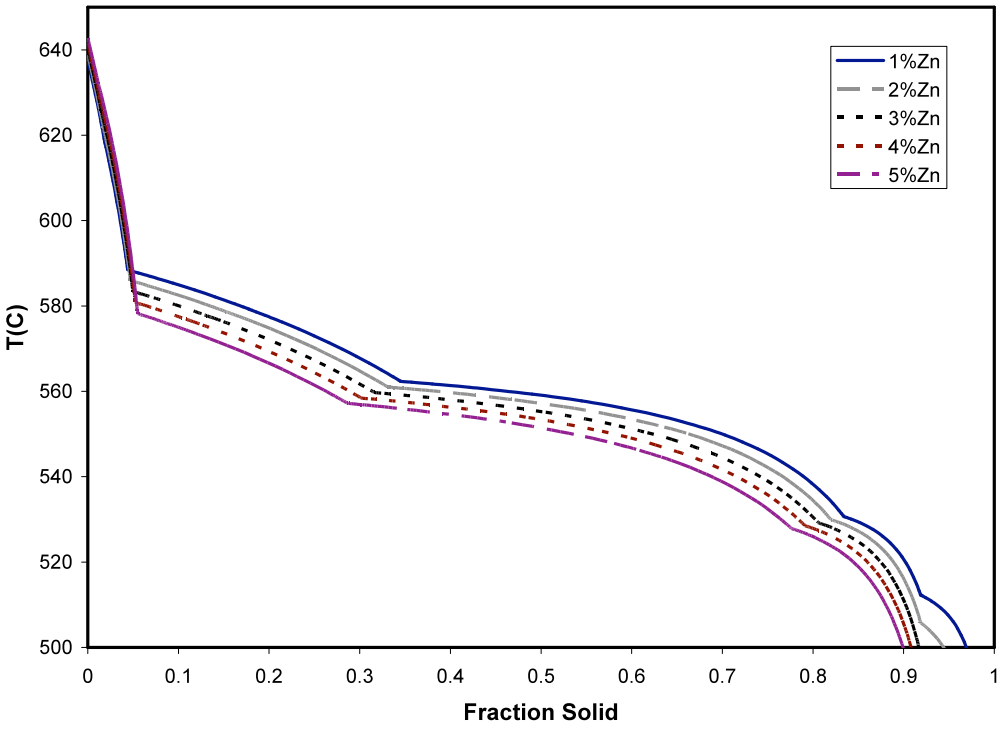

Fig. 6: Effect of Zn content on fraction solid vs. temperature curves of 380 alloy.

Table 7: dfs/dT values of 380 alloy as a function of Zn content and fraction solid

Zn Content	$(dfs/dT)_{fs=0.3}$	$(dfs/dT)_{fs=0.4}$	$(dfs/dT)_{fs=0.5}$	$(dfs/dT)_{fs=0.6}$	$(dfs/dT)_{fs=0.7}$
1%	0.009	0.052	0.034	0.021	0.012
2%	0.008	0.042	0.030	0.019	0.011
3%	0.008	0.040	0.027	0.017	0.010
4%	0.008	0.035	0.027	0.017	0.009
5%	0.005	0.033	0.023	0.015	0.008

E. Effect of Iron, Manganese, and Tin

These three elements do not have a significant effect on the temperature vs. fraction solid curves of 380 alloy as illustrated in Figures 7-8. However, an excess of these elements affects the formation of intermetallic phases. It is found that:

- Increasing Fe content promotes the formation of β-(Al,Fe,Si) and $Al_{15}FeMn_3Si_2$ phases, and since these are solid phases, the overall fraction solid is increased.

- Increasing Mn content suppresses the formation of the β-(Al,Fe,Si) phase, and the $Al_{15}FeMn_3Si_2$ phase (instead of the β-(Al,Fe,Si)) becomes the initial phase when Mn content of the alloy is in excess of 1 wt.%.

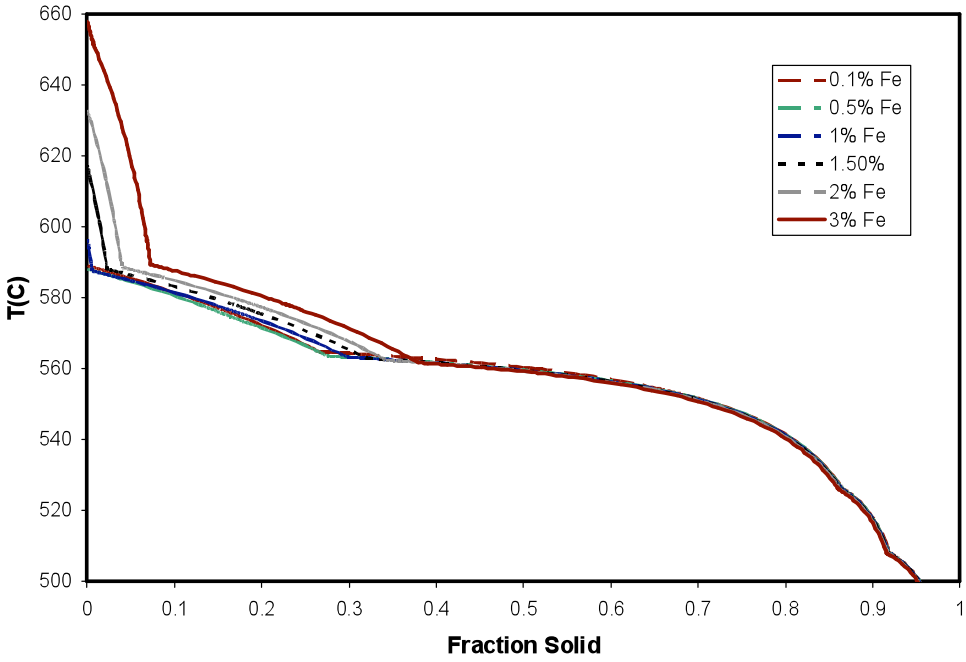

Fig. 7: Effect of Fe content on fraction solid vs. temperature curves of 380 alloy.

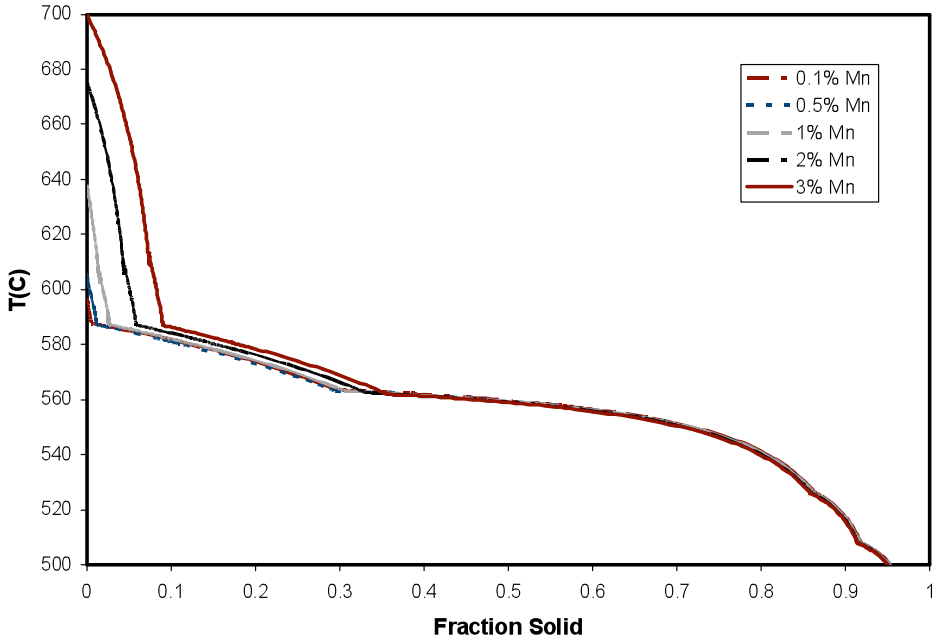

Fig. 8: Effect of Mn content on fraction solid vs. temperature curves of 380 alloy.

3.3 Optimization of 380 Alloy Composition for SSM Processing

The thermodynamic simulations point out that Si, Cu, Mg, Ni and Zn are important alloying elements that have a significant effect on the SSM processability of 380 alloy, and therefore should be optimized for SSM applications. Specifically, Si affects the length of segment A (see Figure 1) and the location of the binary eutectic point, therefore, it has the most significant effect on the processability of the alloy. Based on the calculation results for 380 alloy, a slight decrease in Si content (6.5%-8.5%) is recommended, depending on the targeted processing temperature (fraction solid).

Cu, Ni, Mg, and Zn change the shape of the temperature vs. fraction solid curves of 380 alloy. Among these elements, Ni has the most remarkable effect on the slope of the temperature vs. fraction solid curves of the alloy. Increasing Ni opens up the SSM process window significantly. Based on the calculation data, a Ni content of no less than 1wt.% is recommended. Whereas, increasing Cu, Mg and Zn content shows a similar effect, but not as significant as Ni.

Our simulation work to date has shed light on the effects of various alloy elements on the solidification behavior and SSM processablibity of 380 alloy. Experiments are currently underway at the Advanced Casting Research Center (ACRC) to validate the thermodynamic simulation results presented in this paper and to further optimize the composition of 380 alloy for SSM applications.

4. Conclusions

The following conclusions are drawn based on the thermodynamic simulations that have been performed to date:

- Si, Ni, Cu, Mg, and Zn are important alloying elements in 380 alloy and should be optimized for successful SSM processing.

- Si does not change the shape of the temperature vs. fraction solid curves of 380 alloy, but it changes the location of the binary eutectic point on the curves. Simulation results indicate that in order to enlarge the SSM process window, a Si content of 6.5-8.5 wt.% is recommended depending on the targeted fraction solid.

- Ni, Cu, Mg, and Zn increase the slope of the temperature vs. fraction solid curves of 380 alloy thus leading to a relatively large process window. Among these four alloying elements, Ni has the most significant effect. Based on the calculation results, a Ni content of no less than 1wt.% is recommended.

Currently, extensive validation experiments and thermodynamic calculations are going on at the Advanced Casting Research Center (ACRC) to further optimize the composition of 380 alloy for SSM processing.

Acknowledgements

The authors are grateful to the ACRC Consortium Members for their engagement and active participation in our work on SSM processing. This work was supported by the Department of Energy, Contract No. DE-FC36-04GO14230.

References

1. de Figueredo, A. and Apelian, D. (2001). Science and Technology of Semi-Solid Metal Processing, Chapter 2, edited by A. de Figueredo, published by NADCA, Rosemont, IL.

2. Han, Q. and Viswanathan, S. (2004). "", Mat. Sci.& Eng., vol A364, p48-54.

3. Liu, Y.Q., and Fan, Z.. (2002). "Magnesium Alloy Selections for Semi-Solid Metal Processing", Proceedings of the 7th International Conference on Semi-Solid Processing of Alloys and Composites, Tsukuba, Japan, p.587-592.

4. Atkinson, H.V., Kapranos, P., and Kirkwood, D.H. (2000). "Alloy Development for Thixoforming," Proceedings of the 6th International Conference on Semi-Solid Processing of Alloys and Composites, Turin, Italy, p.443-450.

5. Atkinson, H.V., and Liu, D. (2002). "Development of High Performance Aluminum Alloys for Thixoforming," Proceedings of the 7th International Conference on Semi-Solid Processing of Alloys and Composites, Tsukuba, Japan, p.51-56.

6. Camacho, A.M., Atkinson, H.V., Kapranos, P., and Argent, B.B. (2003). "Thermodynamic Predictions of Wrought Alloy Compositions Amenable to Semi-Solid Processing", Acta Mater., 51, p. 2319-2330.

7. Liu, D., Atkinson, H.V., and Jones, H. (2004). "MTDATA Thermodynamic Prediction of Suitability of Alloys for Thixoforming", Proceedings of the 8th International Conference on Semi-Solid Processing of Alloys and Composites, Limassol, Cyprus, September 2004, published by NADCA, Wheeling, Illinois, Paper # 08-3.

8. Azpilgain, Z., et al. (2004). "Development of Aluminum Alloys for the Thixofoming Process", Proceedings of the 8th International Conference on Semi-Solid Processing of Alloys and Composites, Limassol, Cyprus, September 2004, published by NADCA, Wheeling, Illinois, Paper # 24-4.

Solid State Phenomena Vols. 116-117 (2006) pp 64-67
Online available since 2006/Oct/15 at www.scientific.net

doi:10.4028/www.scientific.net/SSP.116-117.64

Application of the Continuous Rheoconversion Process (CRP™) to Low Temperature HPDC-Part II: Alloy Development & Validation

S. Wiesner[1, a], Q.Y. Pan[2, b] and D. Apelian[2, c]

[1]Bühler Druckguss AG CH-9240, Uzwil, Switzerland

[2]Advanced Casting Research Center (ACRC), Metal Processing Institute (MPI), WPI, Worcester, MA, USA

[a]stuart.wiesner@buhlergroup.com, [b]qypan@wpi.edu, [c]dapelian@wpi.edu

Keywords: Semi-Solid Processing, The Continuous Rheoconversion Process, Alloy Development

Abstract: The continuous rheoconversion process (CRP™) is a novel slurry-on-demand process that was developed at MPI/WPI in 2002. The process is based on a passive liquid mixing technique in which the nucleation and growth of the primary phase are controlled using a specially designed "reactor". The reactor provides heat extraction, copious nucleation, and forced convection during the initial stage of solidification, thus leading to the formation of globular structures. This paper presents our recent work on the scale-up of the CRP™ for industrial applications. In Part II of this paper, we present salient results on alloy optimization via thermodynamic simulations, as well as validation results obtained from industrial Beta trials.

Introduction

Recent work on the scale-up of the CRP™ for industrial applications was covered in Part I; specifically application of the CRP™ to low temperature (low fraction solid) HPDC was shown. It was found that CRP™ processed castings have much finer eutectic and smaller intermetallic phases as compared to conventional liquid die castings, which is beneficial for the casting quality. In Part II, we present salient results on optimizing the composition of a European standard die cast alloy--EN AC-46000 (similar to 383 alloy) for rheocasting/CRP™ applications via thermodynamic simulations, as well as validation results obtained from industrial Beta trials.

Criteria for SSM Alloy Design/Optimization

Several important factors need to be considered for SSM alloy development/optimization. These include: 1) solidification range; 2) temperature sensitivity of fraction solid; and 3) SSM temperature process window. A detailed description of these parameters is given in Ref. [1].

In this study, thermodynamic calculations were used as the first step in evaluating SSM processability of EN AC-46000 alloy. The effects of various alloying elements on the solidification behavior, the temperature sensitivity of fraction solid, as well as the SSM temperature process window of the alloy were characterized. Based on simulation results, a modified/optimized EN AC-46000 alloy was produced and validated through Beta casting trials using the CRP™ reactor.

Simulation Results & Analyses

Table 1 gives the chemical composition of the standard EN AC-46000 alloy and the modified/optimized EN AC-46000 alloy used in this study. Figure 1 gives the fraction solid (fs) vs temperature (T) curves of the standard EN AC-46000 alloy, and the modified/optimized EN AC-46000 alloy. For comparison, the fs-T curve of an SSM A356 is also included in the Figure. Table 2 gives important simulation results of the three alloys. From Figure 1 and Table 2, one can see that compared to SSM A356, the SSM temperature process window of standard EN AC-46000 is quite small. In addition, due to its relatively high Si content (10.58wt.%), the maximum volume fraction of the primary alpha phase (SSM structure) that can be achieved is about 13%. It can be noted that

the alloy is not an ideal candidate material for semi-solid processing. To improve the SSM processability of the alloy, the alloy composition has to be modified/optimized.

Table 1: Chemical Composition of the Standard and the Modified/optimized EN AC-46000 Alloys Used in This Study.

Alloy	Si	Fe	Cu	Mn	Mg	Cr	Ti	Ni	Zn
EN AC-46000	10.58	0.72	2.0	0.19	0.21	0.04	0.06	0.06	0.77
Mod. EN AC-46000	8.1	0.85	3.4	0.35	0.42	0.02	0.03	0.82	0.89

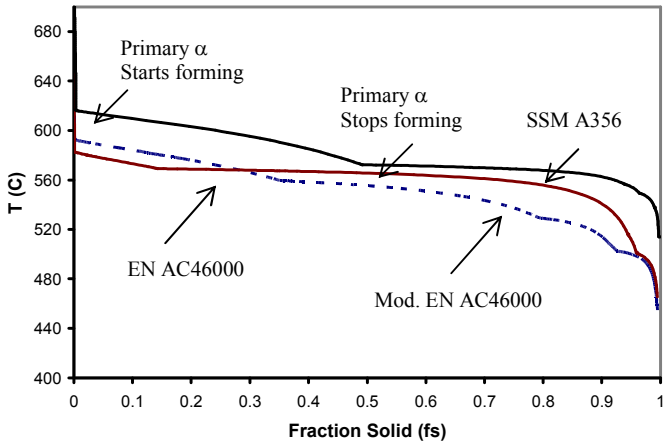

Figure 1: Fraction solid vs temperature curves of the EN AC-46000, the modified/optimized EN AC-46000, and SSM A356 alloys.

Table 2: Important Thermodynamic Simulation Results.

Alloy	**T@fs=0.5**	**ΔT@ fs:0.3-0.5**	**Primary α @ fs=0.5**	**(dfs/dT) @fs=0.4**	**(dfs/dT) @fs=0.5**	**(dfs/dT) @fs=0.6**
EN AC46000	566°C	3°C	0.13	.122	.070	.020
Mod. EN AC46000	555°C	10°C	0.33	.035	.021	.014
SSM A356	*575°C*	*23°C*	*0.48*	*.008*	*.112*	*.070*

In order to understand the effect of various alloying elements on the SSM processability of EN AC-46000 alloy, extensive thermodynamic simulations have been performed. Specifically, to simplify the analysis, alloying elements other than the one under investigation are kept at a constant value (as given in Table 1). Also, in order to amplify the effect of each alloying element on the solidification behaviour, the fs vs. T curve, and the temperature sensitivity of the fraction solid, the concentration of the alloying elements is varied within a range that extends outside the specified limits.

Thermodynamic simulation results point out that Si, Ni, Cu, Mg, and Zn are important alloying elements that have an impact on the SSM processability of the alloy. Specifically, it was found that:

- Si has a significant influence on the solidification behaviour, and consequently on the SSM processablility of EN AC-46000 alloy (as illustrated in Figure 2a). Si does not change the shape of the temperature vs. fraction solid curves of the alloy, but it changes the location of the binary eutectic point on the curves, *i.e.* the volume fraction of the primary alpha phase and the dfs/dT value. With decreasing Si content, the fs vs. T curves shift towards the right, indicating that more primary α phase is formed, and a relative large SSM temperature process window is resulted.

- Ni, Cu, Mg, and Zn increase the slope of the temperature vs. fraction solid curves of EN AC-46000 alloy, thus leading to a relatively large SSM temperature process window, and relatively small dfs/dT values (see Figure 2b). As a result, the SSM processability of the alloy is improved. Among these four alloying elements, Ni has the most significant effect.

- Fe, Mn and Sn do not show any significant effect on the SSM processability of the alloy.

Based on simulation results, a modified EN AC-46000 alloy (SSM version) was made and evaluated (see Table 1).

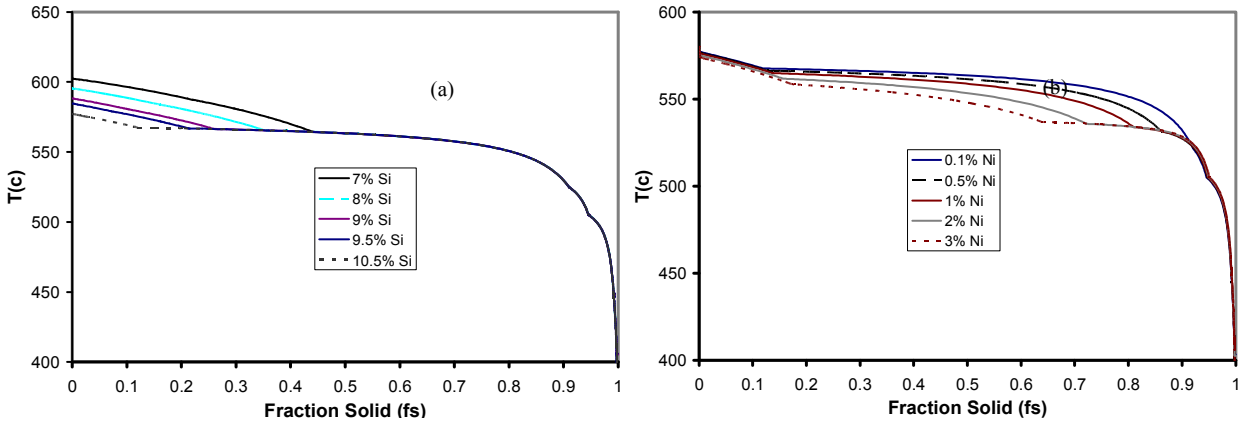

Figure 2: Effect of Si and Ni on the fraction solid vs temperature curve of EN AC-46000 alloy.

Validation Trials

To validate the thermodynamic simulation results, industrial Beta trials have been carried out using the scaled-up CRP^{TM} reactor and a 840T Bühler die casting machine. Experimental details are given in [2]. SSM forming experiments show that the modified/optimized EN AC-46000 alloy has much better SSM formability than standard EN AC-46000 alloy. Figures 3 and 4 show typical SSM slugs and microstructure obtained from the modified EN AC-46000 alloy, whereas, no slug-type SSM slurry can be produced using the standard EN AC-46000 alloy. Analysis on casting diagrams (piston stroke, speed, hydraulic pressure and the pressure of three cavity sensors as a function of time) shows that there is no significant difference between the two alloys under standard liquid die casting or low fraction solid (slurry-on-demand) casting conditions. However, it does show some differences in hydraulic pressure while die casting modified EN AC-46000 alloy using slug type slurries (relatively high fraction solids). The hydraulic pressure increased from 150 bars (during standard or low fraction solid trials) to 200 bars. In addition, there was no significant dynamic impact at the end of die filling, meaning the slurry has a higher viscosity and smoother filling than in other series.

Fig. 3: SSM slugs of mod. EN AC-46000 alloy.

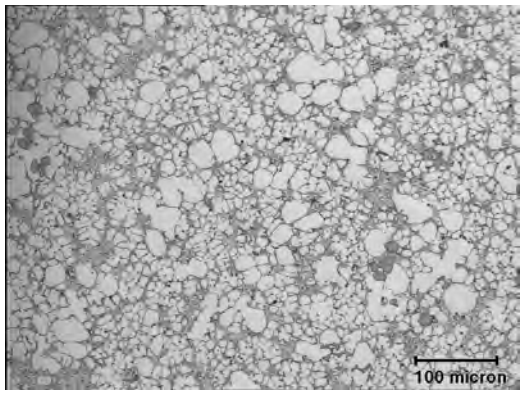

Fig. 4: Typical microstructure of mod. EN AC-46000 SSM castings.

Concluding Remarks

Thermodynamic simulation is a powerful tool for alloy development and optimization. The modified/optimized EN AC-46000 alloy shows much better SSM processability than standard EN AC-46000 alloy. The modified alloy coupled with CRP^{TM} reactor offers an opportunity to make low-cost, high quality SSM castings.

References

[1] Q.Y. Pan, P. Hogan and D. Apelian: Optimization of Commercial Alloys for Semi-Solid Processing, 110th Metalcasting Congress, Columbus, OH 43215, April 18-21 (2006)

[2] Q.Y. Pan, S. Wiesner, and D. Apelian: Application of the Continuous Rheoconversion Process (CRP) to Low Temperature HPDC-Part I: Microstructure, the 9th International Conference on Semi-Solid Processing of Alloys and Composites, Busan, South Korea, September (2006)

Semi-Solid Processing of Alloys and Composites
10.4028/www.scientific.net/SSP.116-117

Application of the Continuous Rheoconversion Process (CRP^{TM}) to Low Temperature HPDC-Part II: Alloy Development & Validation

10.4028/www.scientific.net/SSP.116-117.64

Optimization of Commercial Alloys for Semi-Solid Processing

Q.Y. Pan, P. Hogan, and D. Apelian

Listing of Authors:

(1)
Q.Y. Pan
Research Associate Professor
Advanced Casting Research Center (ACRC)
Metal Processing Institute (MPI)
WPI, Worcester, MA 01609 USA

(2)
P. Hogan
Undergraduate Student
Advanced Casting Research Center (ACRC)
Metal Processing Institute (MPI)
WPI, Worcester, MA 01609 USA

(3)
D. Apelian
Professor
Advanced Casting Research Center (ACRC)
Metal Processing Institute (MPI)
WPI, Worcester, MA 01609 USA

Abstract

Often newly developed manufacturing processes are evaluated with existing alloys rather than optimizing a special alloy that can take advantage of the attributes of the new process. Currently, conventional cast aluminum alloys such as 356 and 357 are being used for SSM processing, which limits the full potential of this new technology. SSM alloy development/optimization remains a significant issue in SSM processing.

Recently, several other commercial cast alloys such as 380, 319, and 206 have been of great interest by the industrial sector, and are emerging as candidate SSM alloys due to the economic or property benefits associated with these alloys. In this study, thermodynamic simulations have been performed to evaluate the SSM processability of 380, 319 and 206 alloys. Specifically, the effects of various alloying elements on the alloy's solidification behavior, the fraction solid vs. temperature curve, as well as the temperature sensitivity of fraction solid have been characterized. Subsequently, based on simulation results, recommendations are made to allow the optimization of 380/319/206 alloy composition for SSM applications.

Keywords: Thermodynamic simulation, alloy development, semi-solid processing.

1. Introduction

Semi-solid metal (SSM) processing has emerged as a preferred manufacturing method due to the superior quality associated with semi-solid castings. In principle, slurries for semi-solid processing can be produced from any material system where liquid and solid phases coexist over a freezing range. An important drawback of conventional SSM processes is that the fraction solid, and consequently, the viscosity of the melt in the semi-solid state are strongly dependent on temperature. Therefore, process control is somewhat difficult due to the necessity of close control of temperature and temperature gradients in reheated billets (thixocasting). Efforts are currently underway to overcome these problems by developing new SSM processes, and equally important, alloy systems that are better suited for semi-solid processing.

Often newly developed manufacturing processes are evaluated with existing alloys rather than optimizing a special alloy that can take advantage of the unique attributes of the new process. Currently, conventional cast aluminum alloys such as 356 and 357 are being used for SSM processing [1], which limits the full potential of this new technology. SSM alloy development/optimization remains a significant issue in SSM processing.

Historically, the trial-and-error method has been employed for alloy development. This approach has been proven to be cost-intensive and time-consuming. With the development of robust aluminum alloy databases, a new approach based on thermodynamic simulations has emerged. This approach provides a powerful tool for alloy design. In this approach, the Gibbs free energy of individual phases is calculated as a function of alloy composition, temperature and pressure, and then collected in a thermodynamic database that enables calculation of multi-component phase diagrams. The calculation results provide critical information for alloy design such as the phase formation and transformation temperatures, the solidification characteristics of the alloy, etc.

Using thermodynamic simulations, Han and Viswanathan [2] investigated tailoring the composition of A356/357 alloy to render it more suitable for SSM processing. Similarly, based on calculations of temperature sensitivity of the fraction solid, Liu and Fan [3] studied the suitability of commercial alloys in the Mg-Al-Zn and Mg-Al-Mn systems for SSM processing, and they identified several alloys that have great potential for thixo- and rheocasting applications. Recently, a great deal of effort has been devoted to wrought alloys [4-8], and several alloys in the 2xxx and 7xxx series have been evaluated and optimized for thixoforming [4-8].

In addition to the above mentioned alloys, recently, a few commercial cast alloys such as 380, 319, and 206 have been of great interest by the industrial sector and are emerging as candidate SSM alloys due to the economic or property benefits associated with these alloys. In this study, thermodynamic simulations

have been performed to evaluate the SSM processability of these alloys. Specifically, we investigated the effect of various alloying elements on the solidification behavior and SSM processability of the alloys. Based on simulation results, recommendations are made to allow the optimization of 380/319/206 alloy composition for SSM applications.

2. Criteria for SSM Alloy Design/Optimization

Several important factors that need to be considered for SSM alloy development/optimization are outlined below:

1) ***Solidification range (ΔT):*** is defined as the temperature range between the solidus and the liquidus lines of the alloy. Pure metals and eutectic alloys are not suitable for SSM processing, whereas, alloys with too wide a solidification range experience poor resistance to hot tearing. It is therefore suggested that the solidification range of an SSM alloy be between 40-130K [7].

2) ***Temperature sensitivity of fraction solid:*** As illustrated in Figure 1, for a given alloy composition, temperature sensitivity of the fraction solid (fs) is defined as the slope of the fs vs.T curve, i.e., dfs/dT. In order to obtain stable and repeatable processing conditions, the temperature sensitivity of the fraction solid should be as small as possible in the fraction solid range of commercial operations (ideally fs should be 0.3-0.5 for rheocasting, and 0.5-0.7 for thixocasting/thixoforging).

INSERT FIGURE 1 HERE

3) ***Temperature process window (ΔT):*** Depending on the application, for rheocasting, ΔT is defined as the temperature difference between 0.3-0.5 fraction solid, whereas, for thixoforging, ΔT is defined as the temperature difference between 0.5-0.7 fraction solid. Considering temperature variations during commercial forming operations, a relatively large temperature window is expected.

4) ***Potential for age hardening:*** In order to achieve high strength, the alloys designed for SSM processing need to have high potential for age hardening. During a T5 temper, SSM parts ejected from the die are quenched immediately in water and then artificially aged at a relatively low temperature. Therefore, the potential for age hardening of a phase can be

gauged by the concentration difference (ΔC) of the major alloying elements in the α-phase between the quenching and ageing temperatures.

In this study, thermodynamic calculations are used as the first step in evaluating the SSM processability of 380, 319 and 206 alloys. This is followed by detailed analyses on the effect of various alloying elements on the solidification behavior, the temperature sensitivity of the fraction solid, as well as the SSM temperature process window of these alloys. Subsequently, recommendations are made to allow the optimization of 380/319/206 alloy composition for semi-solid processing.

3. Simulation Results & Analyses

3.1 SSM Processability of 380/319/206 alloys

Table 1 gives 380/319/206 alloy compositions specified by ASTM. Figure 2 compares the fraction solid (fs) vs temperature (T) curves of the three alloys with nominal composition. For comparison, the fs-T curve of SSM A356 alloy is also included in the figure. Table 2 gives important simulation results. From Figure 2 and Table 2, one can see that:

- 319 alloy has a similar SSM temperature process window for rheocasting as SSM A356 (24°C vs. 23°C), and a much larger temperature window for thixocasting/thixoforging (12°C vs. 3°C). Moreover, the alloy has very small dfs/dT values in the fraction solid range of commercial forming. Thus, from semi-solid processing point of view, it is an excellent candidate material.

- Compared to SSM A356, the SSM temperature process window of 380 for rheocasting is somewhat narrow. In addition, its relatively high Si content (7.5-9.5%) limits the maximum volume fraction of the primary alpha phase (SSM structure) that can be achieved during commercial forming (for 380 alloy with nominal composition, about 40% primary alpha phase can be formed at the fraction solid of 0.5). The SSM processability of the alloy can be improved by optimizing/modifying the alloy composition. This will be discussed in Sections 3.2 and 3.3.

- 206 alloy has a fairly poor SSM processability. The alloy has a quite small SSM temperature process window, and a high temperature sensitivity of fraction solid for rheocasting applications. Moreover, a large two-phase region makes the alloy susceptible to hot-tearing.

INSERT TABLES 1-2 HERE

INSERT FIGURE 2 HERE

3.2 Effect of Alloying Elements on SSM Processability of 380/319/206 Alloys

In order to understand the effect of various alloying elements on the SSM processability of the three alloys, extensive thermodynamic simulations have been performed, and salient simulation results are presented and discussed in this section. Specifically, to simplify the analysis, alloying elements other than the one under investigation are kept at a constant value (as given in Table 1). Also, in order to amplify the effect of each alloying element on the solidification behavior, the fs vs. T curve, and the temperature sensitivity of the fraction solid, the concentration of the alloying elements is varied within a range that extends outside the limits specified by ASTM.

3.2.1 380 Alloy

Thermodynamic simulation results point out that Si, Ni, Cu, Mg, and Zn are important alloying elements that have an impact on the SSM processability of the alloy and should be optimized for successful SSM processing. Figures 3 through 5 illustrate the effects of different Si, Cu, and Ni contents on the fs vs T curves of the alloy. Table 3 summarizes the SSM processability of 380 alloy as a function of Si/Ni/Cu/Mg/Zn content. From Table 3 and Figures 3 through 5, it can be seen that:

- Si has a significant influence on the solidification behavior, and consequently on the SSM processablility of 380 alloy. It does not change the shape of the temperature vs. fraction solid curves of the alloy, but changes the location of the binary eutectic point on the curves, *i.e.* the relative location of segment A and segment B (see Figure 1). With decreasing Si content, the fs vs. T curves shift towards the right, indicating that more primary α phase is formed (segment A corresponds to the formation of the primary α phase). Also, due to a relatively large slope of segment A (thus, small dfs/dT values), the processing temperature is preferred to locate in this segment. Based on simulation results, a slight decrease in Si content (6.5%-8.5%) is recommended, depending on the targeted processing temperature (fraction solid).

- Ni, Cu, Mg, and Zn increase the slope of the temperature vs. fraction solid curves of 380 alloy, thus leading to a relatively large SSM temperature process window, and relatively small dfs/dT values. As a result, the SSM processability of the alloy is improved. Among these four alloying elements, Ni has the most significant effect.

- Fe, Mn and Sn do not show any significant effect on the SSM processability of the alloy.

INSERT FIGURES 3-5 HERE

INSERT TABLE 3 HERE

3.2.2 319 Alloy

Figures 6 and 7 illustrate the effect of different Si, and Cu contents on the fs vs T curves of the alloy, respectively. Table 4 summarizes the SSM processability of 319 alloy as a function of Si/Cu/Ni//Mg content. It is clear that:

- Si content (5.5-6.5%) of 319 alloy is at an optimal concentration range for SSM. A relatively large SSM temperature process window, as well as low dfs/dT values renders the alloy an excellent candidate material for semi-solid processing.

- Cu, Ni, Mg, and Fe can be slightly adjusted to improve the SSM processability of the alloy. Increasing the content of Cu, Ni, and Mg or decreasing Fe content opens up the SSM process window and reduces dfs/dT values. As a result, the SSM processability of the alloy is improved.

- Mn, Zn and Sn do not show any significant effect on the SSM processability of the alloy.

INSERT FIGURES 6-7 HERE

INSERT TABLE 4 HERE

3.2.3 206 Alloy

Compared to 319 or 356 alloy, 206 has a much smaller SSM temperature process window for rheocasting, and a higher temperature sensitivity of fraction solid, which could be a challenge for commercial forming operations. Moreover, a relatively large two phase region makes the alloy prone to hot-tearing. Extensive

simulation results show that the SSM processability can be improved to some extent by optimizing the content of Cu, Si and Mg. Specifically, it is found that:

- Increasing Cu content opens up temperature process window of the alloy. Moreover, increasing Cu content reduces temperature sensitivity of fraction solid, which is beneficial for semi-solid processing. This can be clearly seen from Figure 8 and Table 5.

- Si has the most significant impact on the SSM processability of the alloy. Increasing Si content can reduce temperature sensitivity of fraction solid, and open up temperature process window considerably. As a result, the SSM processability of the alloy is greatly improved (see Figure 9 and Table 5). Moreover, increasing Si content can improve the castability of the alloy, however, a too high Si content may affect the strengthening effect of the alloy. Thus the adjustment of Si content should be made with caution.

- Mg content does not show any effect on the SSM processability of the alloy in the concentration range (0.15-0.35%) specified by ASTM. However, when Mg content is above 0.35%, increasing Mg content increases SSM processability of the alloy slightly.

- Fe/Zn/Ni/Mn/Sn do not show any significant effect on the SSM processability of 206 alloy, even in a concentration range that extends far outside the limits specified by ASTM.

INSERT FIGURES 8-9 HERE

INSERT TABLE 5 HERE

3.3 Optimization of 319/380/206 Alloy Composition for SSM Processing

319 alloy is an excellent candidate material for SSM processing. The alloy has a fairly large SSM temperature process window (24°C for rheocasting, and 11°C for thixocasting/thixoforging**)**, and a low temperature sensitivity of fraction solid during the fraction solid range of commercial forming. Extensive thermodynamic simulations show that the Si content (5.5-6.5%) is at an optimal range for SSM. Moreover, the SSM processability of the alloy can be further improved by slightly tailoring the alloy composition. Based on simulation results, an optimal composition window is suggested below.

INSERT TABLE 6 HERE

As a typical die casting alloy, 380 has a potential for SSM applications by tailoring/optimizing its alloy composition. Thermodynamic simulations point out that Si, Ni, Cu, Mg, and Zn are important alloying elements and should be optimized for successful SSM processing. Specifically, Si affects the length of segment A (see Figure 1) and the location of the binary eutectic point, therefore, it has a predominant effect on the processability of the alloy. Whereas, Ni, Cu, Mg, and Zn increase the slope of the temperature vs. fraction solid curves of the alloy, thus leading to a relatively large process window. Among these four alloying elements, Ni has the most significant effect. Based on simulation results, an optimal composition window is given below.

INSERT TABLE 7 HERE

Compared to commercial SSM A356, 206 alloy has a small SSM temperature process window and a high temperature sensitivity of fraction solid for rheocasting applications. However, it does show a relatively good suitability for thixocasting/thixoforging. Specifically, Si has the most significant impact on SSM processability of the alloy; increasing Si content improves SSM processability considerably. Based on simulation results, a Si content of no less than 1% is recommended provided that the increase of Si content does not affect the strengthening effect of the alloy significantly.

To validate the thermodynamic simulation results, numerous industrial Beta trials have been carried out recently using the scaled-up Continuous Rheoconversion Process (CRP^{TM}) and commercial 319, SSM A356 alloys, as well as a modified 380 alloy (with an increased Ni content: ~0.82%). The Beta trial results show that 319 alloy has excellent SSM processability, while the modified 380 alloy illustrates noticeable improvement in SSM formability as compared to commercial 380 alloy. These confirm our simulation results. Specifically, using the scaled-up CRP^{TM} reactor, we have been able to consistently generate SSM auto components (weighing 5-20kg) with the three alloys. Figures 10 and 11 show typical SSM structures obtained from these auto components. It was found that compared to conventional HPDC, CRP^{TM} processed SSM castings have finer eutectic and much smaller intermetallic phases, which is beneficial for the casting quality. Detailed Beta trial results and analyses are presented and reviewed in Ref. [9].

INSERT FIGURES 10-11 HERE

4. Conclusions

The following conclusions are drawn based on the thermodynamic simulation results:

- 319 alloy is an excellent alloy for semi-solid processing. The alloy has a fairly large SSM temperature process window, and a low temperature sensitivity of fraction solid during the fraction solid range of commercial operations. SSM processability of the alloy can be further improved by tailoring the alloy composition slightly.

- 380 alloy, as a typical die cast material, has potential for SSM applications. To improve the SSM processability of the alloy, Si, Ni, Cu, Mg, and Zn are important alloying elements and need to be optimized for SSM processing; Si, and Ni have significant impact on SSM processability. Based on simulation results, a modified composition window for SSM applications has been established.

- 206 alloy is not an ideal candidate material for SSM processing. The alloy has a small SSM temperature process window, and fairly high dfs/dT values for rheocasting applications. However, it does show a relatively good suitability for thixocasting/thixoforging. Increasing Si content can improve the SSM processability of the alloy significantly. However, the adjustment of Si content should be made with caution as it may affect the strengthening effect of the alloy.

Acknowledgements

The authors are grateful to the ACRC Consortium Members for their engagement and active participation in our work on SSM processing. This work was supported by the Department of Energy, Contract No. DE-FC36-04GO14230.

References

1. De Figueredo, A. and Apelian, D. (2001). Science and Technology of Semi-Solid Metal Processing, Chapter 2, edited by A. de Figueredo, published by NADCA, Rosemont, IL.

2. Han, Q. and Viswanathan, S. (2004), Mat. Sci.& Eng., Vol A364, p.48-54.

3. Liu, Y.Q., and Fan, Z.. (2002). "Magnesium Alloy Selections for Semi-Solid Metal Processing", Proceedings of the 7th International Conference on Semi-Solid Processing of Alloys and Composites, Tsukuba, Japan, p.587-592.

4. Atkinson, H.V., Kapranos, P., and Kirkwood, D.H. (2000). "Alloy Development for Thixoforming," Proceedings of the 6th International Conference on Semi-Solid Processing of Alloys and Composites, Turin, Italy, p.443-450.

5. Atkinson, H.V., and Liu, D. (2002). "Development of High Performance Aluminum Alloys for Thixoforming," Proceedings of the 7th International Conference on Semi-Solid Processing of Alloys and Composites, Tsukuba, Japan, p.51-56.

6. Camacho, A.M., Atkinson, H.V., Kapranos, P., and Argent, B.B. (2003). "Thermodynamic Predictions of Wrought Alloy Compositions Amenable to Semi-Solid Processing", Acta Mater., 51, p. 2319-2330.

7. Liu, D., Atkinson, H.V., and Jones, H. (2004). "MTDATA Thermodynamic Prediction of Suitability of Alloys for Thixoforming", Proceedings of the 8th International Conference on Semi-Solid Processing of Alloys and Composites, Limassol, Cyprus, September 2004, published by NADCA, Wheeling, Illinois, Paper # 08-3.

8. Azpilgain, Z., et al. (2004). "Development of Aluminum Alloys for the Thixofoming Process", Proceedings of the 8th International Conference on Semi-Solid Processing of Alloys and Composites, Limassol, Cyprus, September 2004, published by NADCA, Wheeling, Illinois, Paper # 24-4.

9. Q.Y. Pan, S. Wiesner, and D. Apelian, "Application of the Continuous Rheoconversion Process (CRP) to Low Temperature HPDC-Part I: Microstructure", the 9th International Conference on Semi-Solid Processing of Alloys and Composites, Busan, South Korea, September 2006 (submitted).

Listing of Tables

Table 1: Chemical Composition of 380/319/206 Alloys Specified by ASTM

Alloy	Si	Fe	Cu	Mg	Mn	Ni	Zn	Sn	Ti
380	7.5-9.5	2.0	3.0-4.0	0.1	0.5	0.5	3.0	0.35	
319	5.5-6.5	1.0	3.0-4.0	0.1	0.5	0.35	1.0	0.35	0.25
206	0.1	0.15	4.2-5.0	0.15-0.35	0.2-0.5	0.05	0.1	0.05	0.15-0.3

Note: All single values are maximum composition percentage

Table 2: Simulation Results of 319/380/206/A356 Alloys with Nominal Composition

Alloy	T@fs=0.5	ΔT@ fs:0.3-0.5	ΔT@ fs:0.5-0.7	(dfs/dT) @fs=0.4	(dfs/dT) @fs=0.5	(dfs/dT) @fs=0.6
319	563°C	24°C	12°C	.009	.006	.020
380	556°C	10°C	13°C	.034	.025	.016
206	633°C	7°C	14°C	.027	.019	.013
SSM A356	*575°C*	*23°C*	*3°C*	*.008*	*.112*	*.070*

Table 3: Effect of Various Alloying Elements on SSM Processability of 380 Alloy

Content	T@fs=0.5	ΔT@ fs:0.3-0.5	ΔT@ fs:05-0.7	(dfs/dT) @fs=0.4	(dfs/dT) @fs=0.5	(dfs/dT) @fs=0.6
	Si					
5%	570°C	20°C	23°C	0.010	0.007	0.004
6%	560°C	25°C	14°C	0.008	0.006	0.023
7%	560°C	17°C	10°C	0.007	0.036	0.024
8%	560°C	16°C	9°C	0.050	0.036	0.023
9%	560°C	9°C	9°C	0.049	0.034	0.022
9.5%	560°C	5°C	9°C	0.047	0.037	0.024
	Cu					
2%Cu	564°C	5°C	6°C	0.067	0.050	0.032
3%Cu	561°C	5°C	8°C	0.053	0.040	0.025
3.5%Cu	559°C	5°C	9°C	0.051	0.035	0.023
4%Cu	558°C	5°C	10°C	0.044	0.031	0.021
5%Cu	555°C	5°C	12°C	0.037	0.028	0.018
	Ni					
0.1%Ni	560°C	4°C	7°C	0.054	0.037	0.026
0.5%Ni	558°C	5°C	10°C	0.041	0.029	0.020
1%Ni	555°C	7°C	13°C	0.035	0.026	0.016
2%Ni	549°C	10°C	15°C	0.027	0.019	0.012
3%Ni	543°C	14°C	10°C	0.020	0.014	0.091
	Mg					
0.1%Mg	559°C	4°C	9°C	0.049	0.034	0.023
0.5%Mg	557°C	6°C	10°C	0.037	0.029	0.020
1%Mg	554°C	6°C	14°C	0.034	0.024	0.017
2%Mg	546°C	9°C	13°C	0.027	0.024	0.014
	Zn					
1%Zn	558°C	7°C	9°C	0.052	0.034	0.021
2%Zn	556°C	6°C	12°C	0.042	0.030	0.019
3%Zn	553°C	6°C	12°C	0.040	0.027	0.017
4%Zn	551°C	7°C	13°C	0.035	0.027	0.017
5%Zn	549°C	7°C	14°C	0.033	0.023	0.015

Table 4: Effect of Various Alloying Elements on SSM Processability of 319 Alloy

Content	T@fs=0.5	ΔT@ fs:0.3-0.5	ΔT@ fs:05-0.7	(dfs/dT) @fs=0.4	(dfs/dT) @fs=0.5	(dfs/dT) @fs=0.6
			Si			
5%Si	575°C	22°C	24°C	0.008	0.007	0.004
5.5%Si	568°C	23°C	18°C	0.008	0.006	0.023
6%Si	563°C	24°C	12°C	0.008	0.005	0.022
6.5%Si	560°C	21°C	10°C	0.008	0.036	0.023
7%Si	559°C	18°C	9°C	0.007	0.035	0.023
			Cu			
2%Cu	572°C	22°C	14°C	0.009	0.006	0.033
3%Cu	566°C	23°C	13°C	0.008	0.006	0.025
3.5%Cu	563°C	24°C	13°C	0.008	0.005	0.022
4%Cu	559°C	25°C	11°C	0.008	0.005	0.021
5%Cu	555°C	25°C	12°C	0.007	0.002	0.018
			Ni			
0.1%Ni	564°C	23°C	10°C	0.008	0.005	0.027
0.35%Ni	563°C	24°C	11°C	0.008	0.005	0.022
0.5%Ni	562°C	24°C	12°C	0.008	0.005	0.021
1%Ni	560°C	25°C	16°C	0.008	0.005	0.017
2%Ni	556°C	27°C	22°C	0.007	0.005	0.011
			Mg			
0.05%Mg	563°C	24°C	11°C	0.009	0.006	0.024
0.1%Mg	563°C	24°C	13°C	0.008	0.006	0.022
1%Mg	557°C	26°C	16°C	0.008	0.006	0.016
2%Mg	551°C	27°C	22°C	0.008	0.005	0.012

Table 5: Effect of Various Alloying Elements on SSM Processability of 206 Alloy

Content	T@fs=0.5	ΔT@ fs:0.3-0.5	ΔT@ fs:05-0.7	(dfs/dT) @fs=0.4	(dfs/dT) @fs=0.5	(dfs/dT) @fs=0.6
	Cu					
2.0%Cu	645°C	5°C	8°C	0.047	0.032	0.024
3.0%Cu	640°C	6°C	10°C	0.035	0.026	0.018
4.0%Cu	636°C	7°C	14°C	0.030	0.022	0.015
5.0%Cu	631°C	8°C	17°C	0.024	0.019	0.012
6.0%Cu	625°C	9°C	19°C	0.021	0.015	0.010
7.0%Cu	621°C	10°C	24°C	0.019	0.014	0.009
	Si					
0.05%Si	633°C	7°C	15°C	0.035	0.019	0.013
1.0%Si	622°C	10°C	22°C	0.020	0.014	0.009
2.0%Si	609°C	14°C	29°C	0.014	0.011	0.007
3.0%Si	596°C	17°C	36°C	0.012	0.008	0.005
	Mg					
0.15%Mg	633°C	7°C	15°C	0.028	0.020	0.013
0.35%Mg	632°C	7°C	16°C	0.027	0.019	0.013
1.0%Mg	627°C	8°C	20°C	0.024	0.017	0.012
2.0%Mg	618°C	10°C	22°C	0.020	0.014	0.009

Table 6: Recommended Composition Window of 319 for Semi-solid Processing

Alloy	**Si**	**Fe**	**Cu**	**Mg**	**Mn**	**Ni**	**Zn**	**Sn**	**Ti**
319 (ASTM)	5.5-6.5	1.0	3.0-4.0	0.1	0.5	0.35	1.0	0.35	0.25
319 (Recommended)	5.5-6.5	1.0	3.0-4.0	0.1-0.5	0.5	0.35-1.0	1.0	0.35	0.25

Table 7: Recommended Composition Window of 380 for Semi-solid Processing

Alloy	**Si**	**Fe**	**Cu**	**Mg**	**Mn**	**Ni**	**Zn**	**Sn**
380 (ASTM)	7.5-9.5	2.0	3.0-4.0	0.1	0.5	0.5	3.0	0.35
380 (Recommended)	6.5-8.5	2.0	3.0-4.0	0.1-0.5	0.5	0.5-1.0	3.0	0.35

Listing of Figures with Captions

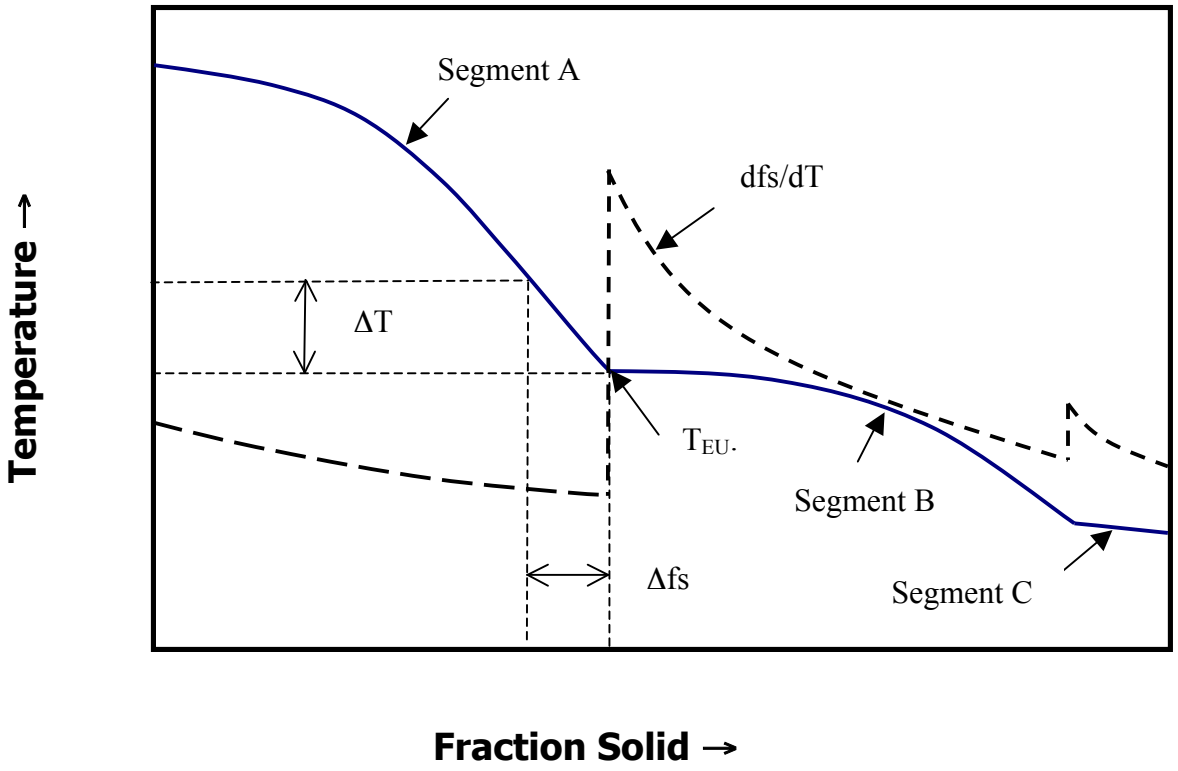

Figure 1: Typical fraction solid vs. temperature curve of cast Al-Si alloys.

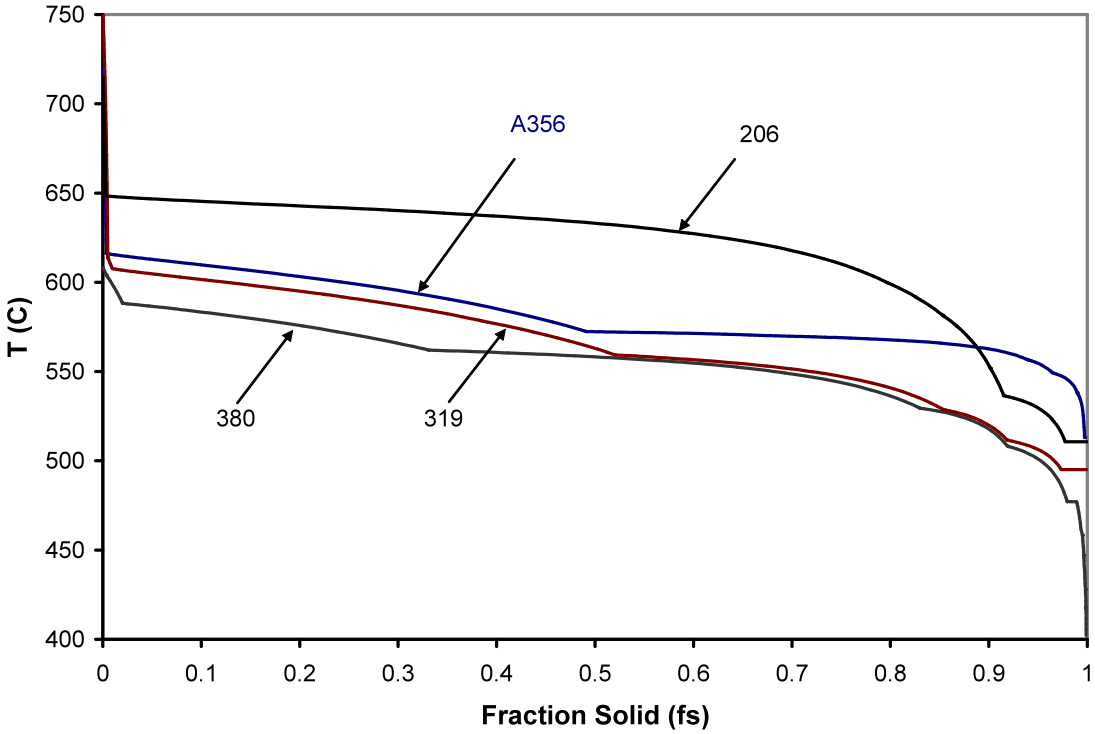

Figure 2: Fraction solid (fs) vs. temperature (T) curves of A356, 206, 380 and 319 alloys with nominal composition.

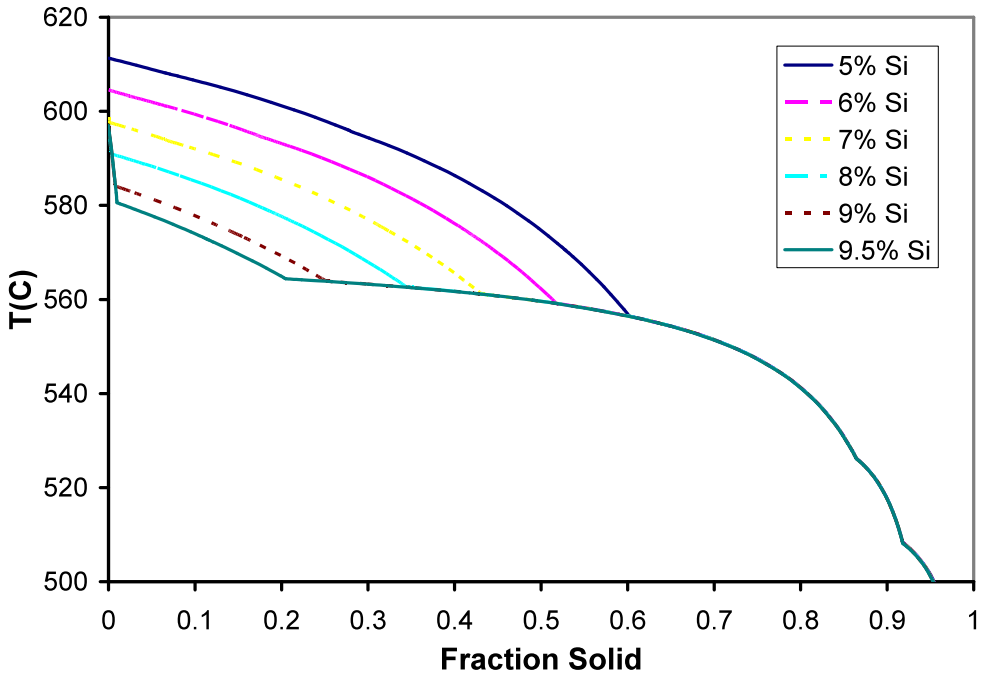

Figure 3: Effect of Si content on fraction solid vs. temperature curves of 380 alloy.

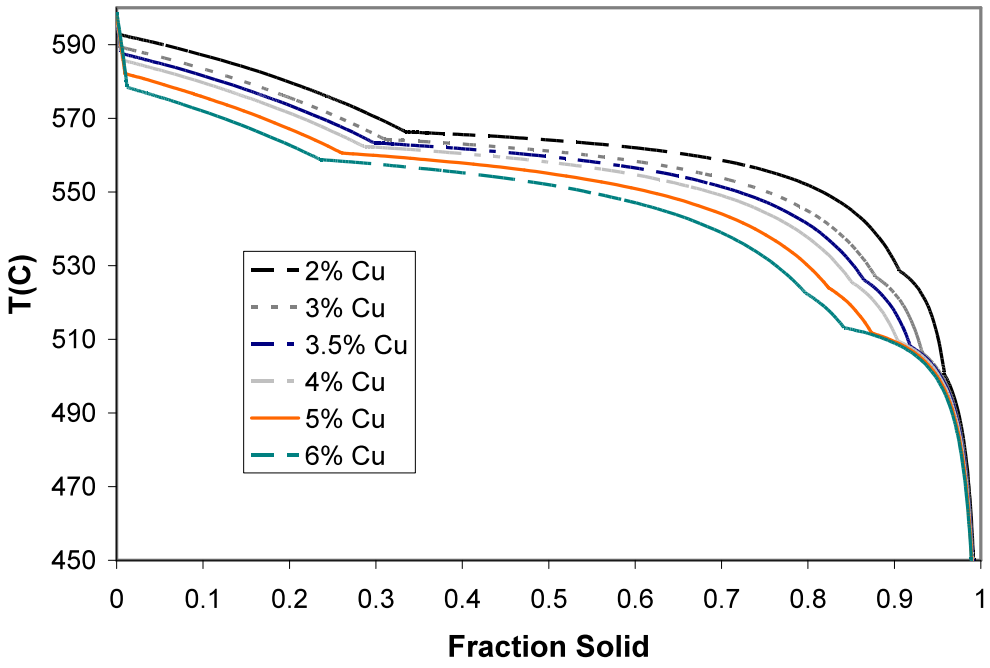

Figure 4: Effect of Cu content on fraction solid vs. temperature curves of 380 alloy.

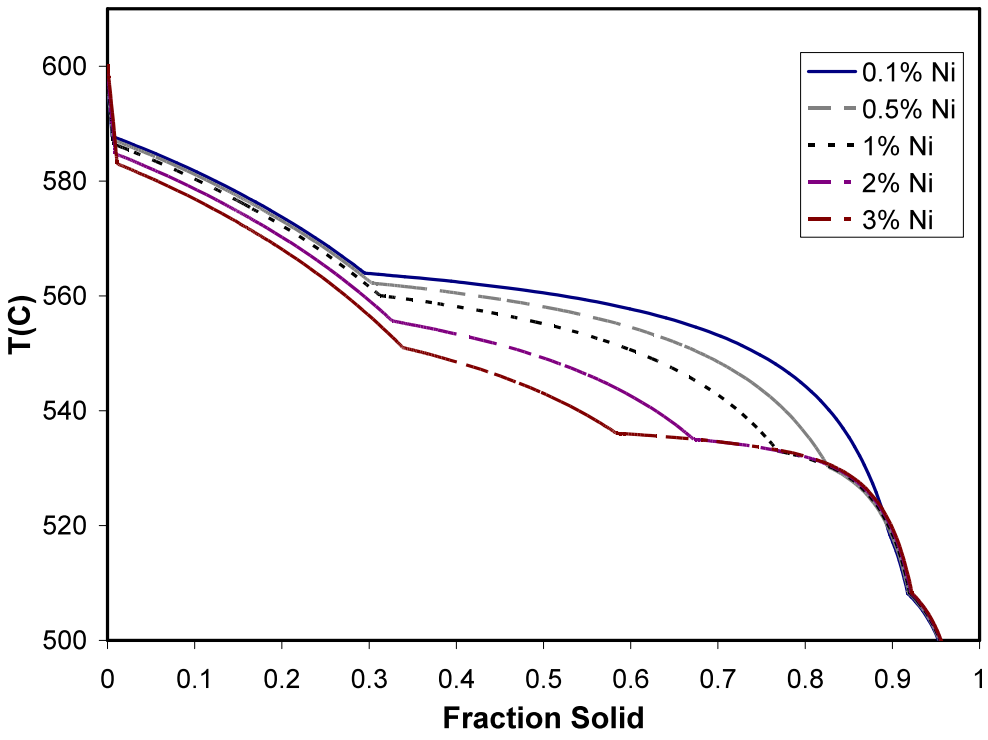

Figure 5: Effect of Ni content on fraction solid vs. temperature curves of 380 alloy.

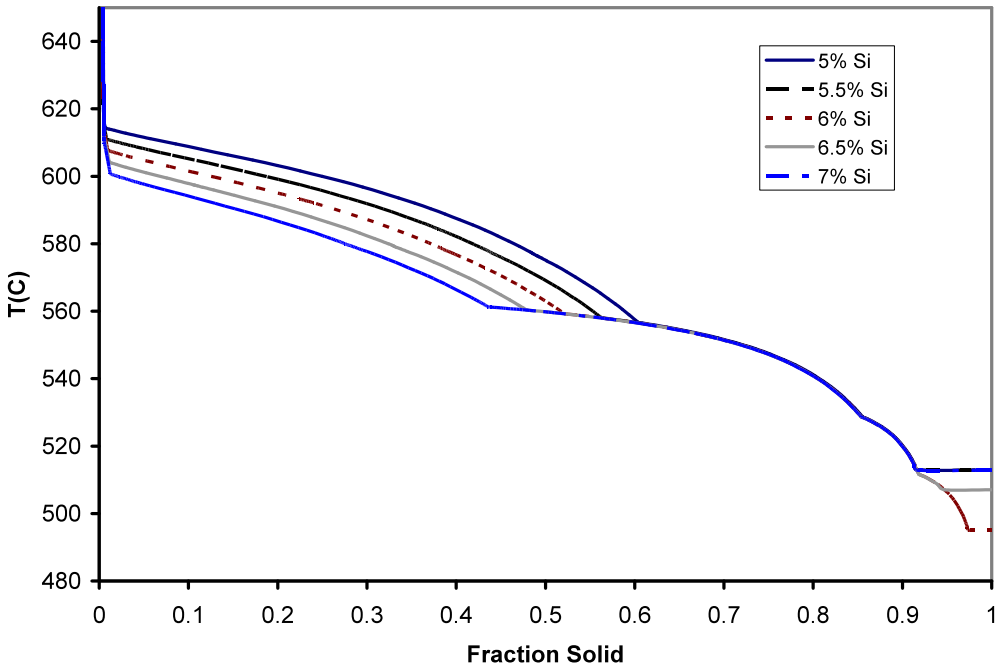

Figure 6: Effect of Si content on fraction solid vs. temperature curves of 319 alloy.

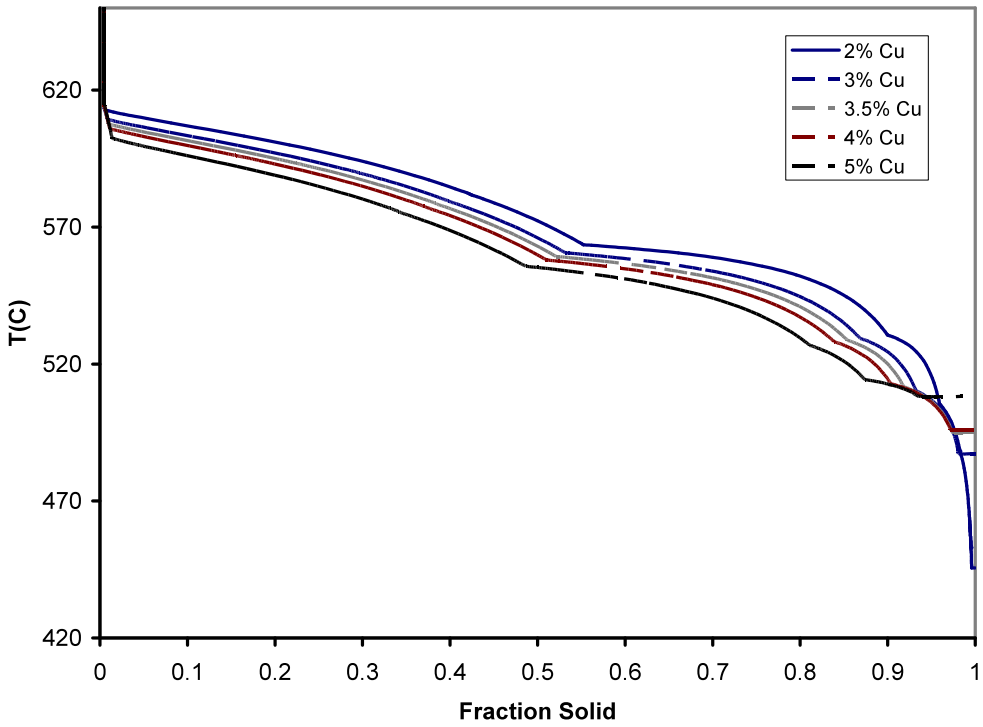

Figure 7: Effect of Cu content on fraction solid vs. temperature curves of 319 alloy.

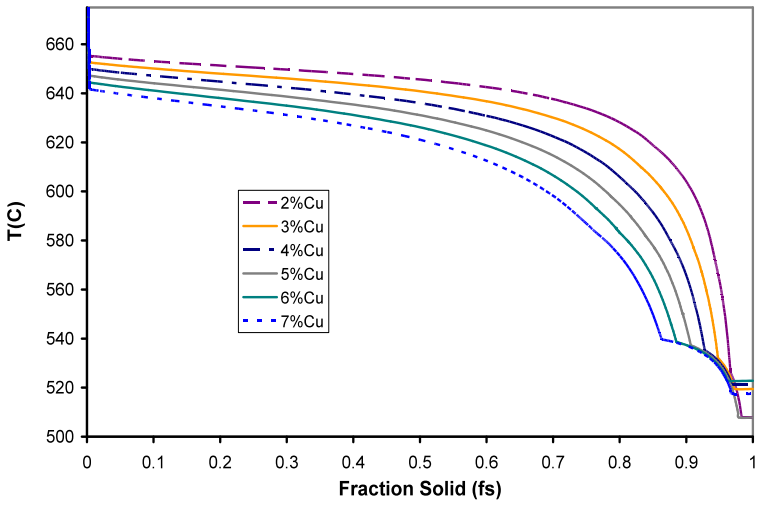

Figure 8: Effect of Cu content on fraction solid vs. temperature curves of 206 alloy.

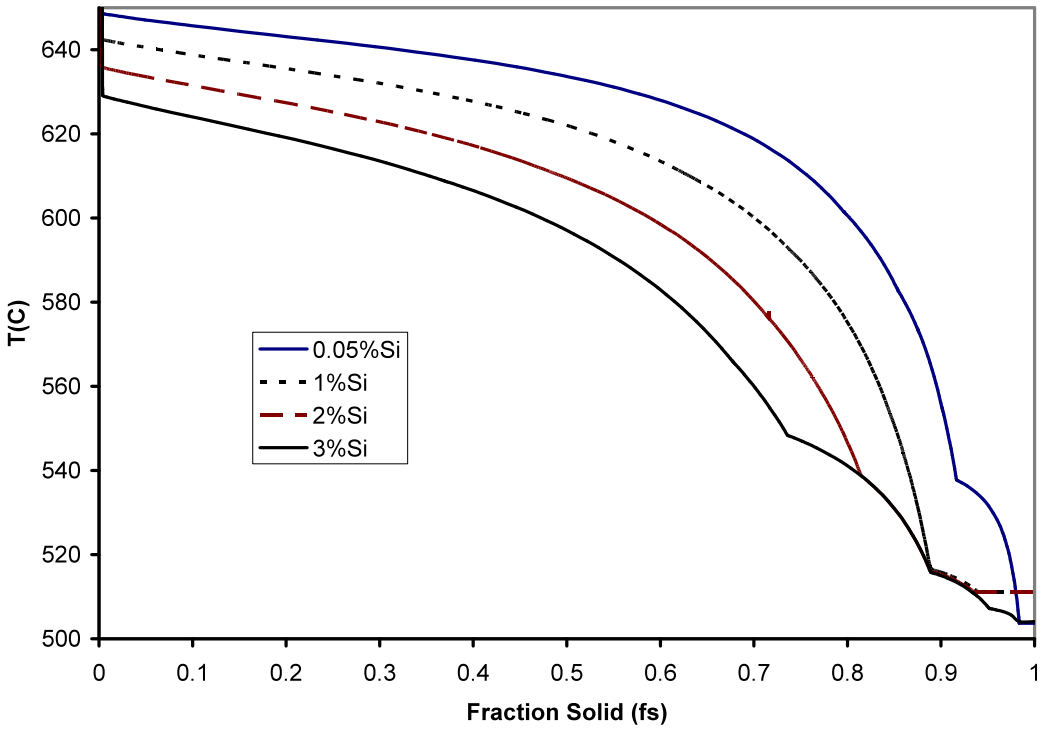

Figure 9: Effect of Si content on fraction solid vs. temperature curves of 206 alloy.

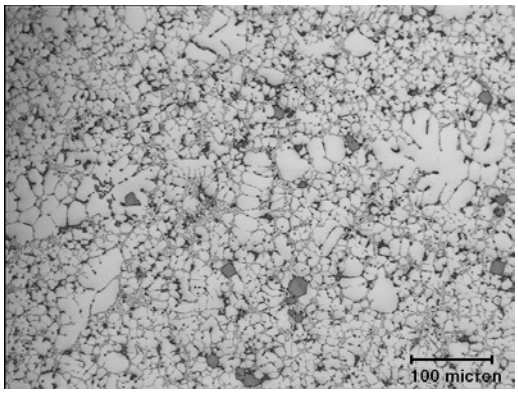

Figure 10 (a)

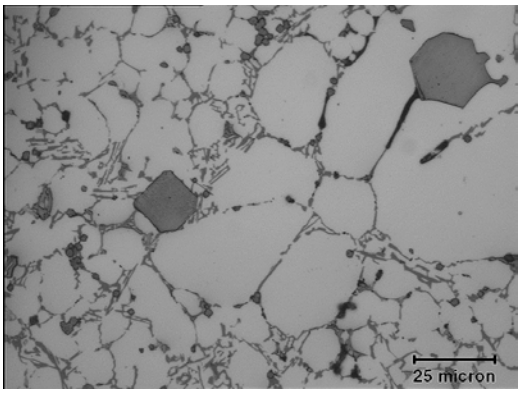

Figure 10 (b)

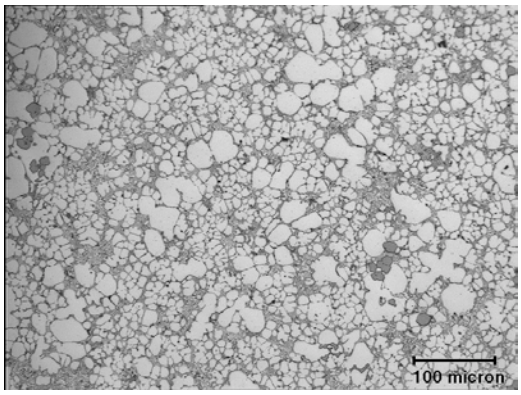

Figure 10 (c)

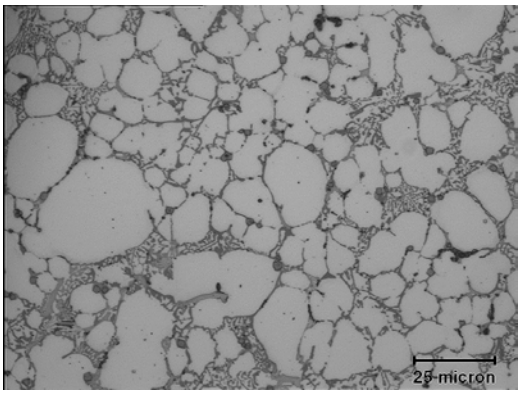

Figure 10 (d)

Figure 10: Microstructures of modified 380 standard HPDC (10a and 10b) vs. CRP processed SSM castings (10c and 10d). Finer eutectic Si and smaller intermetallic phases are seen in the CRP processed castings.

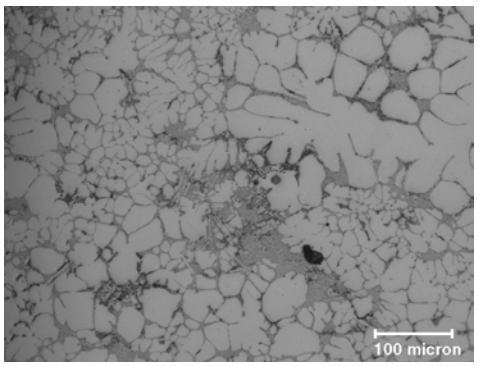

Figure 11 (a)

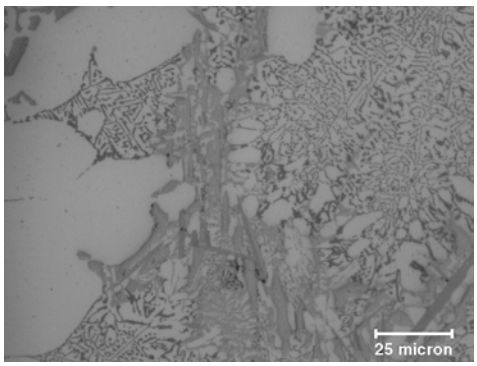

Figure 11 (b)

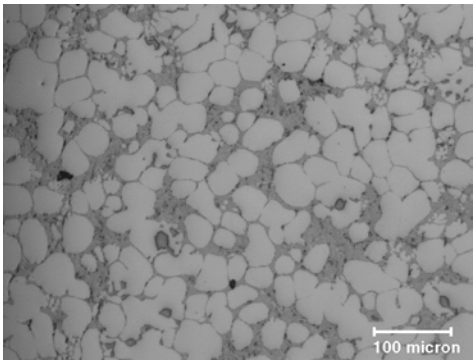

Figure 11 (c)

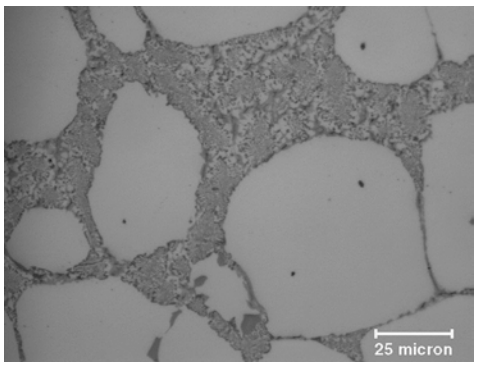

Figure 11 (d)

Figure 11: Microstructures of 319 squeeze castings (11a and 11b) vs. CRP processed SSM castings (11c and 11d), showing finer eutectic Si and much smaller secondary phase in the CRP processed castings.

APPENDIX C

FIRST PUBLISHED IN 2005 TRANSACTIONS DIE CASTING CONGRESS SESSIONS AND PRESENTED AT CASTEXPO'05.

Effect of Artificial Aging on Microstructure and Tensile Properties of Semi-Solid Processed A356 Castings

Brian Dewhirst, Doctoral Candidate
Diran Apelian, Professor, Director
Metal Processing Institute, Worcester Polytechnic Institute
Worcester, Massachusetts

J. Jorstad, Consultant
JLJ Technologies, Inc.
Richmond, Virginia

INTRODUCTION

As with all new processes, after the mechanisms for SSM heat treatment were commercialized, the first heat treatments applied to it were essentially those already in use for dendritic materials. As time passed, it was discovered that certain heat treatments in SSM produced desirable combinations of material properties. In the silver anniversary lecture at the 108th Metalcasting Congress in Chicago, John Jorstad pointed out the promise of SSM in the T5 heat treated condition to meet or exceed design specifications while reducing energy costs [1]. In particular, he discussed how quenched and then T5 aged SSM components retained their high as-cast ductility while improving yield strength and ultimate tensile strength to values just below the same material in the T6 condition. The mechanisms of this retention of ductility are still poorly understood. There are still questions regarding the generality of this behavior.

An examination of case studies of SSM parts from the 8th Biannual S2P conference shows a majority of the castings in the 356/357 family of Al Si Mg alloys are heat treated to the T5 temper [2]. Chief reasons for selecting SSM processing for these parts was the high toughness/ductility/strength and low porosity of SSM components. A357 is found most frequently for parts requiring the highest strength, as the additional magnesium increases precipitate hardenability.

It is hoped that through an understanding of the fundamental mechanisms, SSM processing can be optimized to provide key material properties with the least expenditures of time, energy, and money. This paper presents intriguing data which underscores the assertion that SSM heat treatment has the potential to save time, energy and money.

There are two main routes for producing semi-solid aluminum parts. These are thixocasting, and rheocasting. Thixocasting involves a specially-prepared billet of solid material that is subsequently heated into the semi-sold range. Due to the preparation of the billet, the final microstructure displays a series of spheroidal or rosette aluminum phases surrounded by a eutectic [3]. The other route involves taking liquid and cooling it into the semi-solid range, the rheocasting route. Measures are taken to provide copious nucleation and to retard grain growth. Once the part is cooled, the microstructure exhibits similar spheroidal structures to those found with thixocast materials. Two chief benefits of SSM processing include the presence of a stable flow front which helps prevent the entrapment of air in parts and a reduced processing temperature which helps to extend die life significantly. In this work, rheocast components were produced by THT Presses (Dayton OH, USA) using the sub liquidus casting (SLC) process.

In this paper, we discuss heat treatment characteristics of SSM 319 and A356 alloys prepared through the rheocasting route. Tensile properties of both T5 and T6 tempered alloy are evaluated, along with a detailed metallographic examination of the as-cast and heat treated microstructures.

METHOD

Materials properties and microstructures are only relevant in the context of the chemical makeup, processing history, and bulk geometry. Rheocast samples were supplied by THT from their SLC process. In some tests (indicated by "QT5") THT material was quenched from the die to retain as much of the elements in solution prior to precipitate hardening; however, the time required for manual part removal from the die, and thus the part temperature at the time of quenching, may have not have been optimized. Data from previous WPI research on the heat treatment of dendritic A356 alloy material will be compared to the data presented here.

Tensile specimens and testing conformed to ASTM specifications. Samples were heat treated prior to machining. An extensometer was used to measure bar extension with increased precision.

Table 1 – Heat treatment region for SSM tensile specimens.

	SHT °C	Age °C/hrs	bar size
P 319 F			0.125" round
P 319 T-5	x	170/4	
P 319 QT-5	x	170/4	
S B319 F			0.125" round
S B319 T-5	x	170/4	
S B319 QT-5	x	170/4	
S B319 T-6	525	185/4	
K A356 F			0.25" round
K A356 T-5	x	170/5	
K A356 T-6	532	170/5	
P A356 F			0.375" round
P A356 T-5	x	170/4	
P A356 QT-5	x	170/4	
PS A356 F			0.25" round
PS A356 T-5	x	172/4	
PS A356 QT-5	x	172/4	
PS A356 T-6	540	172/4	
Squeeze A356 F			0.25" round
Squeeze A356 T-5	x	155/4	
Squeeze A356 T-6	530	155/4	

Table 1, above, shows the heat treatment conditions of the tensile samples along with their respective bar sizes. "P" 319 refers to primary 319, that is, high purity 319 without Mg. "S" B319 is a secondary alloy which typically contains 0.3% Mg. "K" A356 refers to a primary alloy A356 component which was formed into the same steering knuckle geometry as the dendritic squeeze cast A356 component. Five parts were cut into 3 bars each, for a total of 15 tensile bars tested for these 319 "S" and "P" alloys in their various heat treatment conditions. The "K" data was produced from six bars. Both "P" and "SP" A356 refer to primary alloys, but their compositions differ slightly. Six bars were produced and tested for each of these A356 heat treatment conditions.

QT-5 refers to a T5 heat treatment of a part which was quenched from the die. The more familiar "F" refers to the as-cast condition, T-6 to a solutionizing heat treatment followed by quenching and artificial aging, and T-5 to artificial aging without prior solution treatment or quenching.

Since an off-site manufacturer provided samples, there were several months of natural aging time between casting and heat treatment for the micrographic specimens. Induction heated box furnaces were used for the micrographic samples. Blistering was not observed in any of the samples, tensile or micrographic.

SEM samples for microscopic analysis were cut from the grip sections of tensile bars. These samples were successively ground with finer grits of paper (240/ 320/ 600/ 4000 grit) on a water cooled wheel rotating at 240 rpm. Following grinding, the sample was carefully cleaned with wet cotton before being polished with 0.3 micron alumina and ultrasonically cleaned in acetone for at least five minutes. For final polishing, an electropolisher was used to polish and etch the sample simultaneously. The electrolyte contains 60% ethanol, 20% perchloric acid, and 20% ethyl glycol monobutyl ether. Samples are electropolished for 15-30 seconds and then subsequently rinsed in running tap water. A final acetone ultrasonic cleaning insures that there is no debris or dust on the sample when it is placed into the SEM. SEM analyses were performed using a JEOL JSM-840 scanning electron microscope with an EDX unit attached.

RESULTS

The presence of Ti and Sr indicates that all alloys were modified and grain refined. In the 319 alloys, $CuAl_2$ (or Al_2CuMg in B319) plays the main role in age hardening whereas in 356 alloys it is Mg_2Si which contributes to the strengthening. The "Micro A356" is the composition of the samples which were heat treated prior to being sectioned and polished for micrographic examination in the scanning electron microscope.

Table 2 – Chemical composition of alloys.

	Si	Fe	Cu	Mn	Mg	Zn	Ti	Sr
P 319	6.19	0.35	3.45	0.06	0.01	0.06	0.12	yes
S B319	6.39	0.58	3.61	0.25	0.31	0.47	0.14	yes
K A356	6.8	0.11	0.03	0.01	0.31	0.05	0.09	yes
P A35 6	6.91	0.13	0.07	0.01	0.42	0.08	0.12	yes
PS A356	7.03	0.08	0.03	0.01	0.37	0.02	0.11	yes
Squeeze A356	6.9	0.12	0.04	0.01	0.39	0.04	0.14	yes
Micro A356	7.01	0.09	0.05	0.01	0.41	0.02	0.15	yes

Table 3 – Tensile properties of SSM and dendritic permanent mold samples.

	UTS Mpa	YS Mpa	%El	BHN	QI Mpa	SSM
P 319 F Average	215	160	11	68	371	yes
Range	202-221	154-162	9-13			
P 319 T-5 Average	235	150	10	65	385	yes
Range	220-240	139-165	7-13			
P 319 QT-5 Average	265	180	10	74	415	yes
Range	250-269	165-190	9-12			
S B319 F Average	239	142	9	89	382	yes
Range	230-251	130-155	7-11			
S B319 T-5 Average	265	165	9	93	408	yes
Range	260-275	155-177	8-10			
S B319 QT-5 Average	285	205	8	100	420	yes
Range	280-293	193-215	7-9			
S B319 T-6 Average	305	223	9	110	448	yes
Range	290-320	210-250	6-11			
K A356 F Average	184	116	10		334	yes
Range	171-211	112-118	7-11			
K A356 T-5 Average	189	116	10		339	yes
Range	183-204	101-125	7-13			
K A356 T-6 Average	310	213	12		472	yes
Range	294-319	208-228	7-20			
P A356 F Average	220	130	12	58	382	yes
P A356 T-5 Average	265	160	12	78	424	yes
P A356 QT-5 Average	295	180	12	80	457	yes
PS A356 F Average	235	120	12		397	yes
Range	220-245	105-135	11.5-13			
PS A356 T-5 Average	280	190	12		442	yes
Range	265-295	175-210	11-13			
PS A356 QT-5 Average	310	220	12		472	yes
Range	290-325	190-235	11-14			
PS A356 T-6 Average	340	260	12		502	yes
Range	330-345	250-265	10-14			
Squeeze A356 F	170	123	11		326	no
Squeeze A356 T-5	174	126	5		279	no
Squeeze A356 T-6	315	232	11		471	no
Perm mold A356 F	169	101	4		259	no
Perm mold A356 T6	258	152	10		408	no

The most striking part of these data is the high elongation values through the different alloy systems. In all cases, while the range may vary slightly, the mean elongation retains its high as-cast value throughout heat treatment. In dendritic castings, the elongation values typically drop markedly after T5 heat treatments. The mechanism which allows yield stress to improve while retaining the as-cast ductility is not completely established. In the T6 condition, high elongation is known to result from the spherodization of the eutectic silicon during the solutionizing step, but both the low temperatures of T5 treatment and micrographic investigation indicate that this process is not taking place in either the simple T5 or in the quenched-from-die then T5 (QT5) case. It is worth noting that the temperatures of T5 heat treatment employed herein are higher than those typically used with the dendritic castings.

As one would expect, yield strength increases more for the QT5 and T6 conditions than the simple T5 case, which in turn is somewhat higher than the as-cast yield strength. This trend follows the increasing presence of dissolved age hardening constituents in the alloys. QT5 traps more in solution than T5 but less than T6. While T6 treatments of SSM parts do produce the highest yield strength values, the improvement between a QT5 and a T6 heat treatment is small compared to the increased energy and time costs, as noted in the introduction. Ultimate tensile strength and hardness increase in the same way and for the same reasons.

The Quality Index (QI) helps us to gauge the relative improvement brought about by a heat treatment. This parameter was developed by Drouzy et al. and applied in the optimization of heat treatments by Shivkumar et al. [4,5]. C.H. Caceres et al. have done further work to show the fundamental basis of the quality index [6].

Equation 1:

$$Q\ (MPa) = UTS\ (MPa) + 150 * \log(\%\ elongation) \quad (1)$$

Given what has already been noted regarding the elongation and strength of these alloys under heat treatment, it is not surprising that Quality Indices improves as strength improves. Since elongation is constant to well within the range of experimental variation, this is to be expected. It is the constancy of elongation itself which is unusual. The relatively small difference between QT5 and T6 heat treatments is again underscored by the small difference in their quality indices. The high as-cast elongation results in a high quality index for the as-cast material itself.

The entries listed as "Perm mold A356" F and T6 are dendritic permanent mold samples which have been included for the purposes of comparison. Quickly comparing the ultimate tensile strength, yield strength, and elongation of the dendritic T6 to the QT5 SSM results, we see that the SSM QT5 parts have much better properties with much less time and energy spent in heat treatment. By examining the Quality Indexes of the A356 dendritic and SSM heat treatments, it is immediately obvious that the SSM components have superior properties. It is also quite clear that the as-cast SSM properties start off much better than those of the dendritic permanent mold material.

The "Squeeze" A356 entries are similarly dendritic. An important fact to note when considering these data is that the aging temperature is lower than that for the SSM A356 components. Even so, the elongation in the T5 condition has decreased by half as compared to the as-cast and T6 conditions. The high ductility in the T6 is attributable to the spherodization of silicon, as previously discussed. While squeeze casting is another high integrity casting technique, it doesn't show the same high T5 ductility that has been seen in the T5 and QT5 treated SSM components. This may or may not present a clue as to the mechanism whereby the elongation of SSM T5 components is higher, as it clearly cannot be due to something which also occurs in squeeze casting. Again, similar trends are seen in Quality Index values. The decrease in quality index between F and T5 suggests that the heat treatment regime applied isn't necessarily optimal. In fact, dendritic A356 is normally aged to a T5 temper at 225°C for purposes of growth stability, not at lower temperatures for strength improvement.

Below are a number of SEM micrographs which were taken using the procedure described earlier. Discussion follows each set of micrographs.

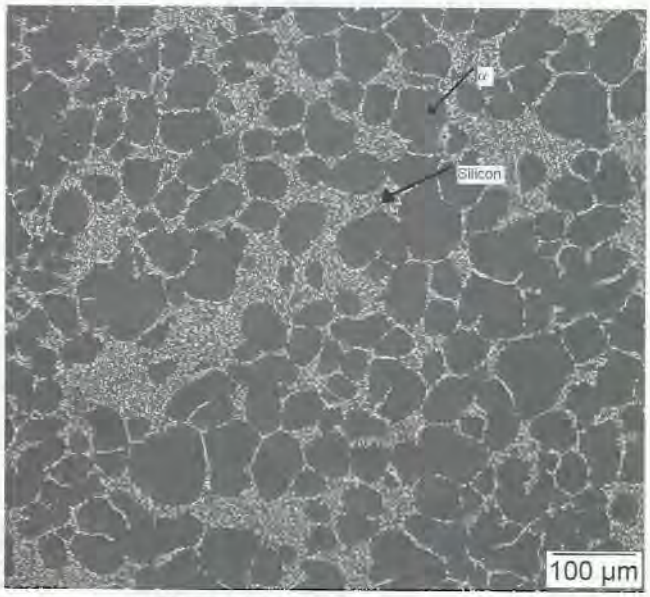

Figure 1 – A356 SSM T6, 540°C, 8 hr.

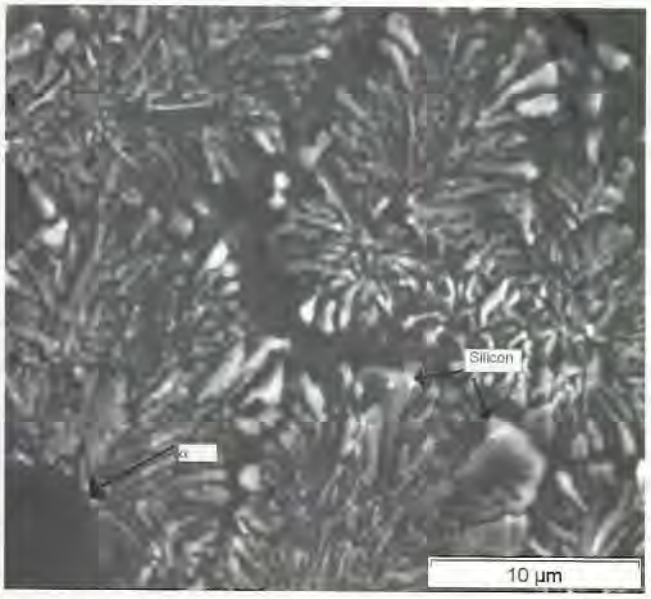

Figure 2 – A356 SSM F.

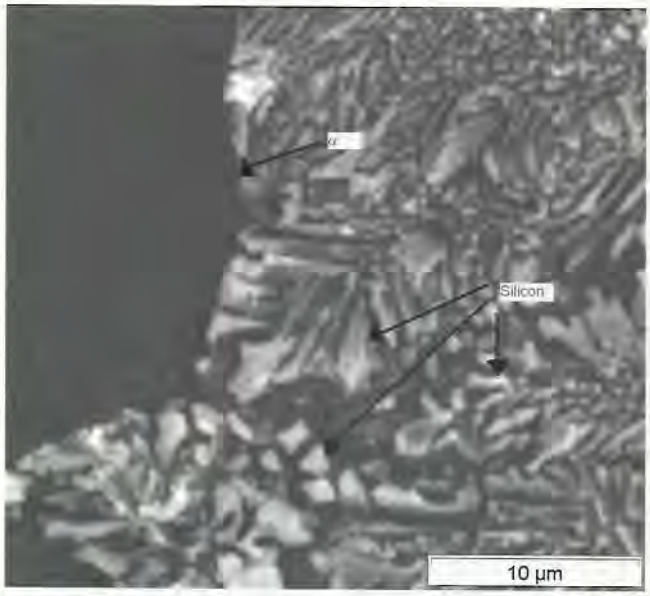

Figure 3 — A356 SSM T5, 160°C, 8 hr.

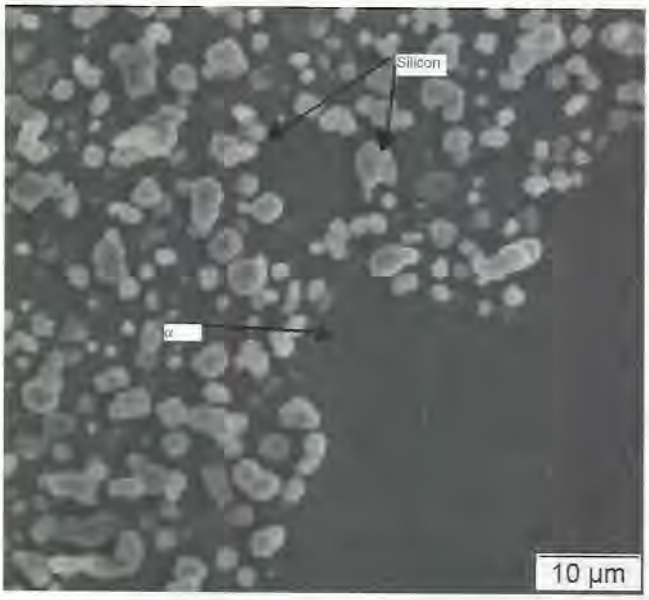

Figure 4 — Micrograph of A356 SSM in the T6 condition. Solutionized at 555°C for 2 hours and aged at 160°C for 5 hours.

In the SEM images given in Figures 1 through 4, the α-aluminum and silicon are identified. When Mg_2Si is present in the eutectic, it appears as a grey phase with a similar morphology to the silicon, however it isn't necessarily the case that a particular grey phase is Mg_2Si instead of silicon. Micron bars in the figures indicate the respective magnifications. In addition, some Fe rich phase was also observed. EDX analysis shows that it's a π phase (AlFeSiMg).

Since the visible changes are taking place in the eutectic whereas the primary phases are not visibly changed during heat treatment, one low magnification image is accompanied by a higher magnification picture for each heat treatment condition (F, T5, T6).

The as-cast (F) SSM components display a fine, fibrous network of eutectic silicon due to the effects of Sr additions and perhaps also to the unique solidification conditions encountered during semi solid processing. This same microstructure is retained in the T5 condition, as heat treatment temperatures were not high enough to modify the silicon. However, after T6 heat treatments, when much higher solutionizing temperature conditions were applied, the silicon network has transformed into a series of small discrete spheroids of silicon. These observations are not unique to SSM A356 components. Indeed, all hypoeutectic aluminum silicon alloys which have been modified with strontium show these kinds of structures before and after T6 treatment regardless of whether the casting process produces dendritic or SSM primary aluminum.

What is different here, however, is the retention of the high as-cast ductility in the T5 condition. Normally, the only way to improve yield and ultimate strength and maintain a high ductility via heat treatment is by performing a T6 heat treatment. The spheroidization of the Si is a mechanism known to improve ductility while precipitation hardening decreases it (at least in dendritic materials). Consequently, one mechanism decreases ductility as another increases it. When heat treatment times are chosen carefully, the net result is a cast part with a high yield stress and ductility without the cost of a lengthy solutionization treatment. Semi-solid components, on the other hand, do not show a decrease in their ductility as yield stress is increased. In other words, quality index is not conserved in SSM components which have been T5 heat treated.

DISCUSSION

As detailed in the introduction, it has been suggested that SSM components subjected to T5 conditions retain their high as-cast ductility [1]. Many commercial manufacturers who produce SSM components have found that they can obtain the desired material properties for their parts with only a T5 heat treatment [2]. Here, data are presented which support these claims with tensile and hardness results.

As can be seen from the tensile data, these phenomena are present for multiple alloy systems (A356 and 319). It occurs in both primary and secondary 319 alloys, with and without the presence of Mg and Zn. T5 properties are improved by quenching components from the die prior to T5 treatment to insure the maximum amount of hardening constituents are in solution at the time of hardening. SEM micrographic analysis shows that the mechanism whereby dendritic T6 elongation is retained or increased, silicon spherodization, is not taking place in T5 components. It is not seen in permanent mold or squeeze cast samples prepared with A356 alloys.

This work clearly shows that there is a definite phenomenon taking place during the T5 treatment of semi-solid formed components, the cause of this retention of the as-cast ductility is still being pursued to establish the operative mechanism. A series of experiments has already been planned to explore the boundaries and causes of these phenomena. In addition to tensile and hardness measurements of thixocast and rheocast A356 components produced by SAG (Salzburger Aluminium AG) and THT Presses (Dayton OH, USA), TEM examination of samples will allow examination of the actual hardening phases present. It may be that the artificial aging kinetics differs in SSM components in some manner which can explain the unusual retained ductility, and these TEM investigations will help us explore this factor.

Table 4 – Proposed experimental matrix.

MATERIAL	TEMPER	SOL'N TEMP [C]	SOL'N Time (hr)	AGING TEMP [C]	AGING Time (Hr).
THT (rheo.)	F	–	–	–	–
SAG (thixo.)	F	–	–	–	–
THT/SAG	T5	–	–	140	4 / 6 / 8
THT/SAG	T5	–	–	160	4 / 6 / 8
THT/SAG	T5	–	–	180	4 / 6 / 8
THT/SAG	T6	540	6	160	5

ACKNOWLEDGEMENTS

Although dozens of individuals have provided immense help throughout the course of this research, certain individuals and organizations stand out. Dr. Sujoy Chaudhury and Dr. Rathindra DasGupta have both provided critical advice on heat treatments, and Dr. Chaudhury also conducted the permanent mold dendritic testing. This work was funded by the Department of Energy as a part of an ongoing Energy SMARRT project, and their financial support is of course critical to this work.

REFERENCES

1. *Jorstad, John. (2004). Silver Anniversary Lecture, AFS/NADCA 108th Metal Casting Congress, Rosemont, IL, June 12-15.*
2. *DasGupta, R. (2004). Proc. 8th Int. Conf. "On Semi-solid Proc. Of Alloys and Composites", Limassol, Cyprus, September 21-23.*
3. *Kirkwood, D.H. (1994). "Semi-solid metal processing", International Materials Reviews, Vol. 39 (5), p.173-189.*
4. *Drouzy, M., Jacob, S., Richard, M. (1980). AFS International Cast Metals Research Journal, pp 43-50.*
5. *Shivkumar, S., Ricci S. Jr., Steenhoff, B., Apelian, D., Sigworth, G. (1989). "An Experimental Study to Optimize the Heat Treatment of A356 Alloy", AFS Transactions, vol. 138, 791-810.*
6. *Caceres, C.H., Wang, L., Apelian, D., Makhlouf, M.M., (1999). "Alloy Selection for Die Castings Using the Quality Index". AFS Transactions vol. 147, 239-247.*

APPENDIX D

113th METALCASTING CONGRESS
April 7-10, 2009 • Las Vegas, Nevada
NADCA

Numerical Modeling and Computer Simulation of the Continuous Rheoconversion Process

Qingyan Xu
Department of Mechanical Engineering, Tsinghua University, Beijing 100084, China
Advanced Casting Research Center, WPI, Worcester, MA, USA 01609

Diran Apelian, and Makhlouf M. Makhlouf
Advanced Casting Research Center, WPI, Worcester, MA, USA 01609

ABSTRACT

The Continuous Rheoconversion Process (CRP) is a novel slurry-on-demand process that was developed at the Advanced Casting Research Center of Worcester Polytechnic Institute. The process is based on passive liquid mixing in which nucleation and growth of the primary solid phase are controlled by a specially designed inclined plane. This inclined plane provides heat extraction from the melt, copious nucleation of the primary solid phase, and forced convection that efficiently distributes the solid nuclei in the melt during the initial stages of solidification. Thus castings that are manufactured by the CRP exhibit a globular microstructure and all the advantages of semi-solid processed materials. In this work, a numerical model was developed to simulate the CRP and the model was used to optimize the design and to develop relationships between the CRP parameters and outcomes. The mathematical model is based on the commercially available software and solves the interaction between fluid flow and heat transfer for a liquid aluminum alloy using a κ-ε turbulent fluid flow model coupled to the Reynolds-averaged Navier-Stokes equations and a 3D heat transfer equation.

INTRODUCTION

The Continuous Rheoconversion Process (CRP) is an energy-efficient, low cost metal casting process [1] that involves the flow of molten metal on a specially designed "reactor". The reactor is located just before the entry point into the die cavity of the die casting machine and allows the production of SSM slurry as needed directly from the melt [2]. The CRP reactor, which is shown in Figure 1, consists of an inclined steel plate with two longitudinal channels. Molten metal which is ladled onto the plate splits into two streams and then re-combines into one channel. Cold water flows underneath the melt through channels that are drilled in the bottom of the reactor. The high nucleation rate caused by contact with the cold steel surface combined with the mixing that happens as the two melt streams re-combine lead to: (1) copious nucleation of the primary solid phase in the liquid, (2) dispersion of the solid nuclei throughout the bulk of the liquid, and (3) survival of the nuclei in the homogeneous temperature field. The result is a thixotropic material that can be delivered to the die cavity in one processing step [3]. In addition to providing slurry-on-demand and allowing incorporation of scrap metal into the melt stream, the CRP has many advantages over traditional SSM processing methods. These include its relative simplicity, and its ability to allow tight control over the evolution of the SSM structure through control of the fraction solid in the liquid [4]. However, this control can only be attained through an understanding of the interdependency of the process parameters and their effect on the outcome of the process. Accordingly, a mathematical model has been developed to simulate the CRP, and in this paper the model is used to demonstrate the effect of *(i)* the angle of inclination of the CRP reactor, *(ii)* the flow rate of the cooling water, and *(iii)* the melt superheat on the temperature distribution and liquid mixing on the CRP reactor. The simulations are performed by the commercially available software Fluent® 6.3 and COMSOL multiphysics® 3.4.

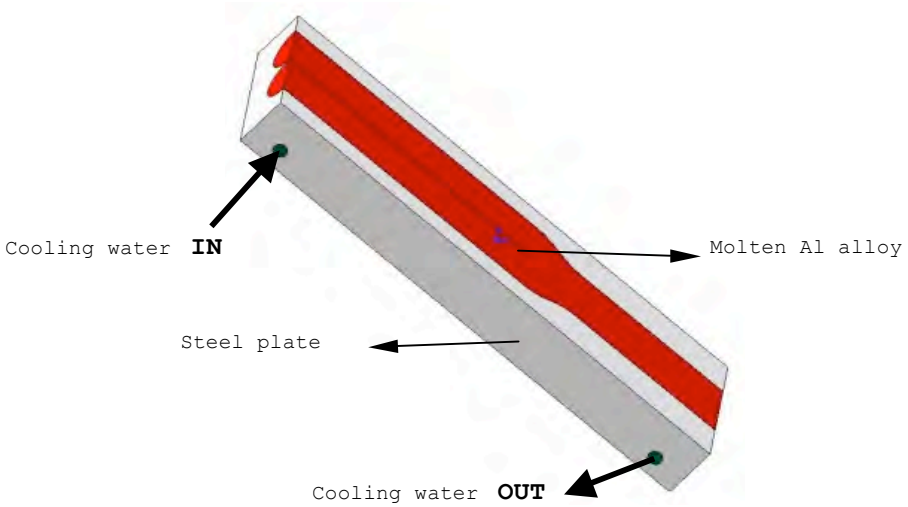

Figure 1- Schematic representation of the CRP.

MODEL CONSTRUCTION AND COMPUTER SIMULATIONS

The dimensions of the CRP reactor together with the 3-D geometry created and meshed by the COMSOL pre-processor are shown in Figure 2. The meshed geometry contained 182,228 elements and 34,900 nodes. A turbulent non-isothermal flow model was used to simulate the fluid flow and thermal interactions that occur in the liquid alloy as it flows over the CRP reactor. The thermo-physical parameters that are used in the simulation are listed in Table 1. They are for aluminum casting alloy A356 and a H13 tool steel CRP reactor.

Table 1- Thermo-physical parameters used in the simulation.

Thermo-physical parameter	Units	Magnitude
Density of liquid alloy	$kg \cdot m^{-3}$	2,340
Viscosity of liquid alloy	Pa·s	1.3×10^{-3}
Heat transfer coefficient	$W \cdot m^{-2} \cdot K^{-1}$	300-2,000
Thermal conductivity of liquid alloy	$W \cdot m^{-1} \cdot K^{-1}$	151
Heat capacity of liquid alloy	$J \cdot kg^{-1} \cdot K^{-1}$	963
Density of steel CRP	$Kg \cdot m^{-3}$	7,760
Thermal conductivity of steel CRP	$W \cdot m^{-1} \cdot K^{-1}$	28.6
Heat capacity of steel CRP	$J \cdot kg^{-1} \cdot K^{-1}$	475

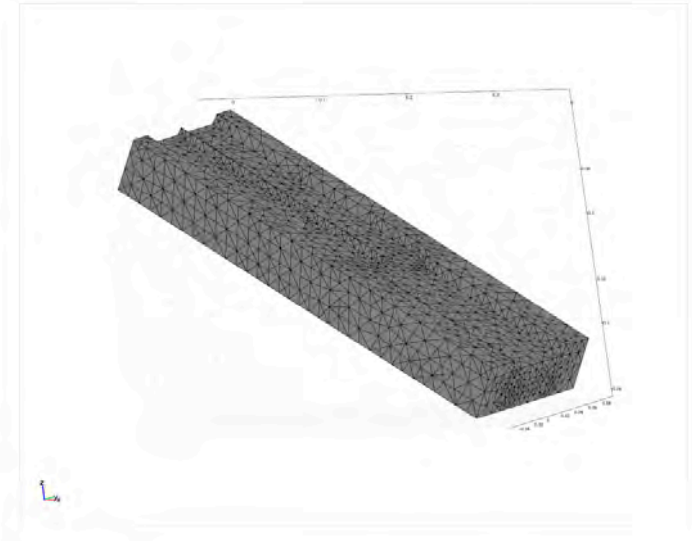

Figure 2- Geometry and mesh used in the model.

SOLUTION PROCEDURE AND BOUNDARY CONDITIONS

The boundary conditions employed in the simulation may be divided into the following:

BOUNDARY CONDITIONS FOR FLUID FLOW AT THE INLET TO THE CRP

Velocity - There are two possible ways for specifying the inlet velocity of the liquid alloy: (1) Set the velocity equal to a given vector, u0; i.e., $\mathbf{U}=\mathbf{U}_0$, or (2) specify a normal inflow velocity; i.e., $\mathbf{U}=-n\mathbf{U}_0$. For this simulation the following condition was used

$$u_x = 0.5\cos(\theta)$$
$$u_y = 0$$
$$u_z = 0.5\sin(\theta)$$

Where, θ is the inclination angle of the CRP. Inlet velocity of the liquid metal was set as 0.5 m/s according to the real case.

BOUNDARY CONDITIONS FOR FLUID FLOW AT THE OUTLET FROM THE CRP

A "Pressure outlet" boundary condition was employed at the outlet from the CRP. This boundary condition specifies a vanishing viscous stress and the pressure at the boundary will be calculated due to the effect of the body force--gravity.

OTHER CONDITIONS FOR FLUID FLOW

Two parameters were specified in order to adequately represent the turbulence that happens and causes liquid mixing on the CRP. These are: (1) the turbulent length scale, L_T, and (2) the turbulent intensity factor, I_T. Good wind tunnels can produce values of IT as low as 0.05%, while fully turbulent flows have intensities between 5 and 10%. The turbulent length scale is a measure of the size of eddies that are not resolved. For free-stream flows, these eddies are typically very small (i.e., in the order of centimeters). For this simulation the following conditions were used at the inlet of the liquid metal: L_T=0.001, I_T=0.01. In addition, the standard logarithmic wall function was used to represent the influence of the CRP's steel walls on the flow of the liquid alloy.

BOUNDARY CONDITIONS FOR HEAT FLOW AT THE INLET TO THE CRP

Dirichlet type boundary condition was used for this simulation:

$$T = T_{liquid}$$

Where, T_{liquid} is the pouring temperature of the liquid metal.

BOUNDARY CONDITIONS FOR HEAT FLOW AT THE OUTLET FROM THE CRP

For this simulation the following convective flux type conditions were used

$$q_0 = -\rho C_p \mathrm{u} T$$

where, q_0 is inward heat flux normal to the boundary.

OTHER BOUNDARY CONDITIONS FOR HEAT FLOW

Internal boundaries, i.e., boundaries between adjacent domains were specified such that the temperature profile is continuous across the internal boundary.

SIMULATION RESULTS

EFFECT OF ANGLE OF INCLINATION

Figure 3 shows the temperature variation on the CRP rector as a function of the angle of inclination of the CRP relative to the horizon. Only one half of the CRP is displayed due to its symmetric shape. In this case, the pouring temperature of the liquid alloy is 750°C, the temperature of the surrounded environment is 20°C. Figure 3 shows that the temperature at the interface of mold / liquid increases to a very high value, but decreases quickly from inside to the outside of the CRP reactor due to the cooling effect of the water. It is clear that the mold temperature increase becomes lower with increasing of the inclination angle of the CRP reactor. This is because the liquid metal can flow faster at large inclination angles - see Figures 5 and 6. Therefore, the contact time between mold and liquid metal would decrease greatly, which gives rise to lower mold temperature increases. Figure 4 shows the temperature profile within the liquid alloy at the exit of the CRP. It is clear from Figure 4 that the angle of inclination does have a significant effect on the temperature of the liquid alloy as it exits the CRP, and on the shape of the flowing liquid metal as well.

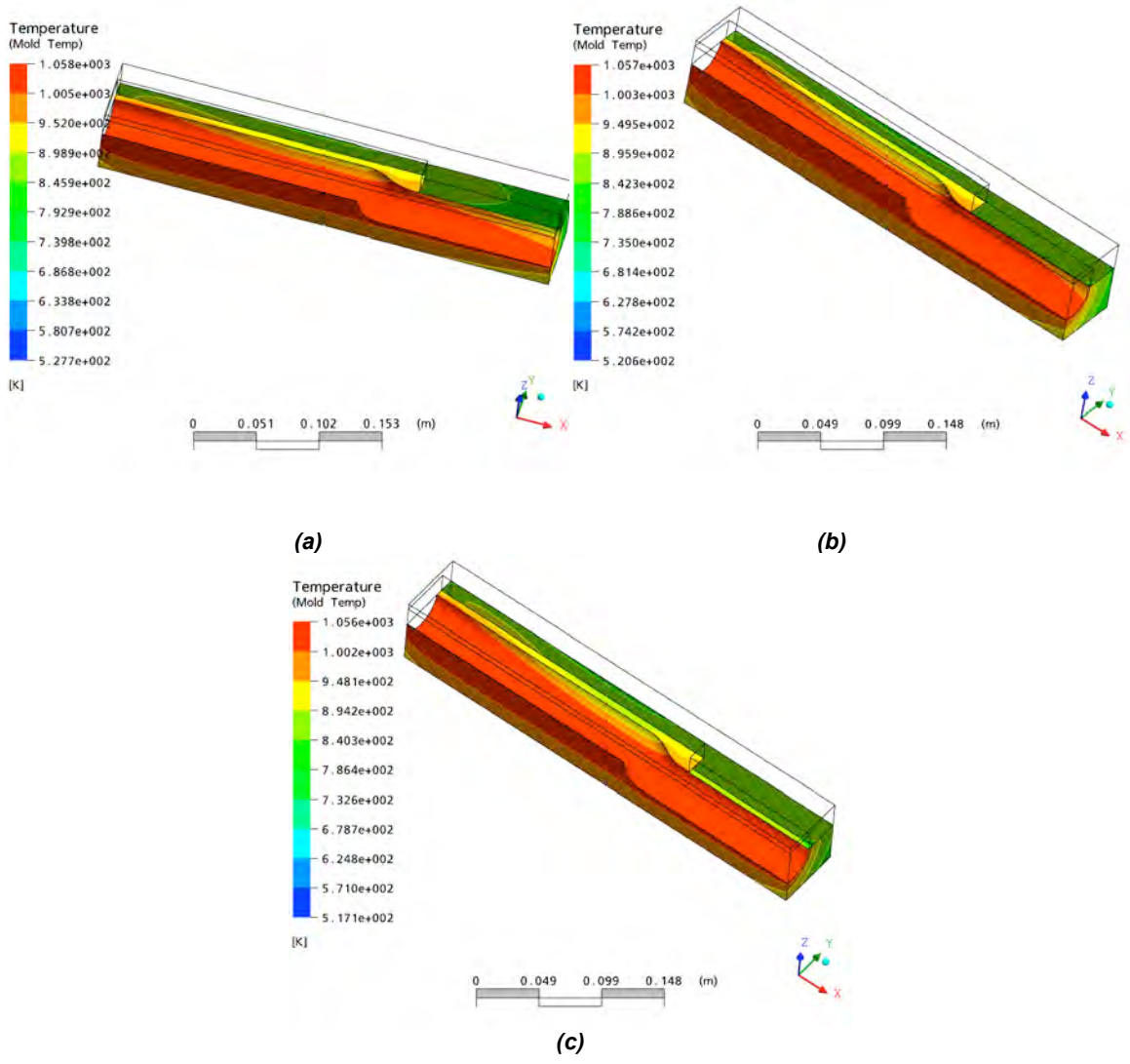

Figure 3- Temperature distribution on the CRP's steel plate as a function of inclination angle. Inclination angle is (a) 15°, (b) 30°, and (c) 45° to the horizon.

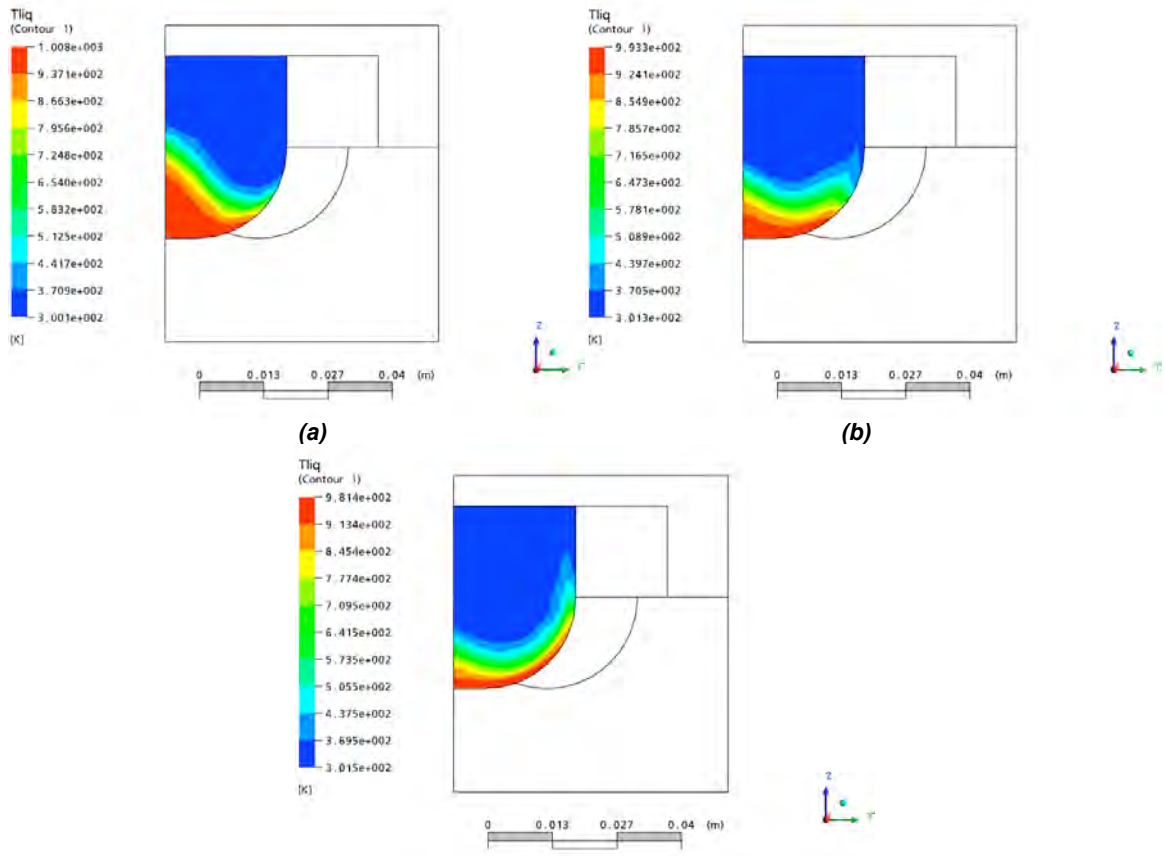

Figure 4- Temperature distribution in the liquid alloy at the exit from the CRP as a function of inclination angle. Inclination angle is (a) 15°, (b) 30°, and (c) 45° to the horizon.

Figure 5 shows the velocity distribution along the free moving surface of the liquid metal and Figure 6 shows the velocity distribution of the liquid alloy at the exit of CRP as functions of the angle of inclination of the mold relative to the horizon. Notice that the melt velocity increases from its relatively low value of 0.5 m/s at the inlet of the CRP to a maximum value of 1.8~3.0 m/s at the outlet from the CRP at different inclination angle of CRP. This increase in velocity is caused by the gravity force acted on the liquid metal and the constriction in cross sectional area at the point where the two alloy streams merge. It can be seen that the liquid metal impinges against the mold wall and changes its flowing direction toward the inside, which merged it into another flow and produced vortex and eddies. With the increasing of the inclination angle, the liquid metal flows faster and faster and adheres tightly on the mold wall. It is noted that the shape of the liquid metal during the flowing process changes greatly with the increasing of the inclination angle, and the thickness of the liquid metal decreases as well. The vortexes and associated eddies that form at merging location promote liquid mixing and enhance heat extraction from the liquid alloy, which in turn aid nucleation and distribution of the solid phase in the liquid alloy.

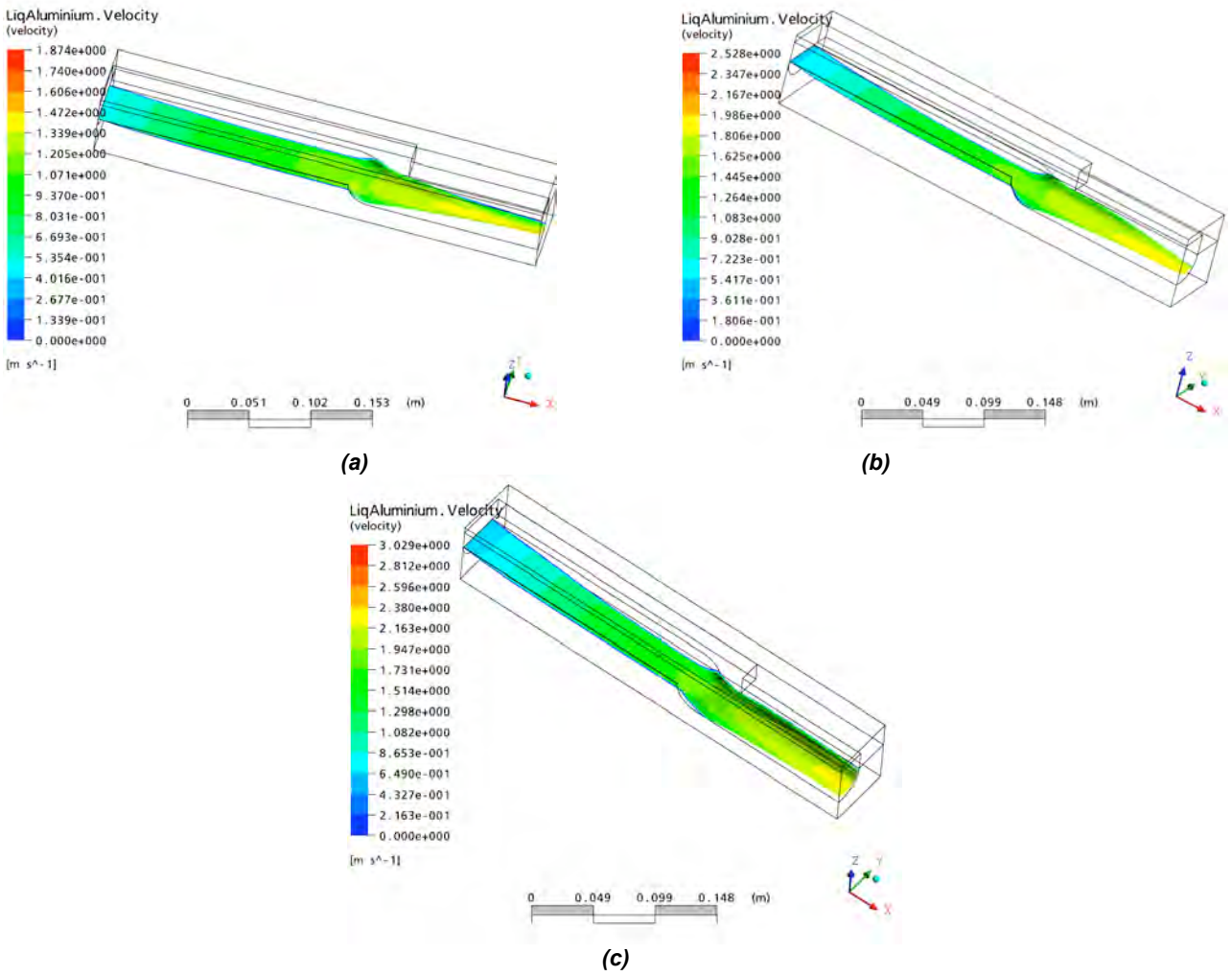

Figure 5- Velocity distribution in the liquid alloy as a function of inclination angle. Inclination angle is (a) 15°, (b) 30°, and (c) 45° to the horizon.

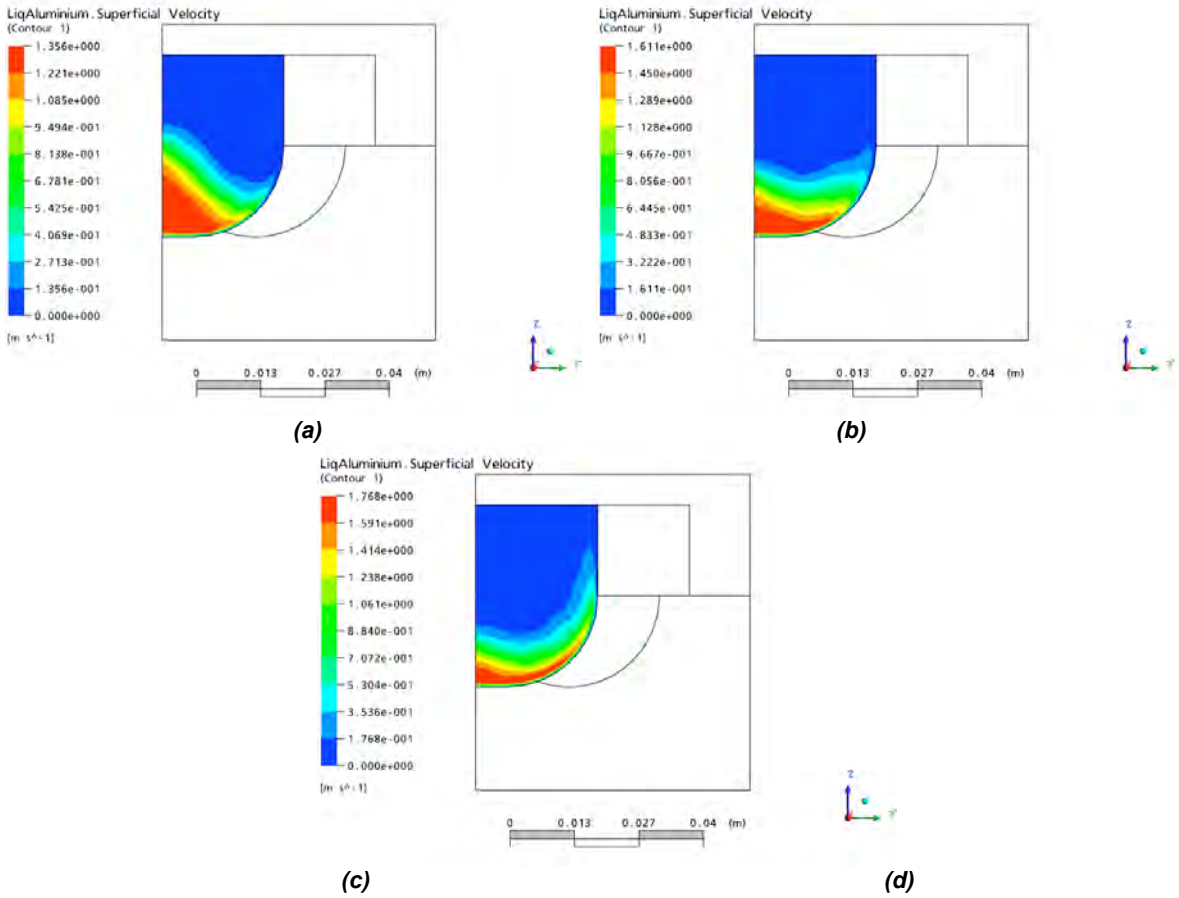

Figure 6- Velocity distribution in the liquid alloy at the exit from the CRP as a function of inclination angle. Inclination angle is (a) 15°, (b) 30°, and (c) 45° to the horizon.

EFFECT OF FLOW RATE OF COOLING WATER

Figure 7 shows the temperature distribution within the liquid alloy as a function of the flow rate of the cooling water. In this case, the pouring temperature of the liquid alloy is 720°C, the temperature of the cooling water is 20°C, and the angle of inclination of the CRP to the horizon is 30°. Similar to Figure 4, Figure 8 shows the temperature profile within the liquid alloy at the exit from the CRP. It is clear from Figure 8 that the flow rate of the cooling water does not have a significant effect on the temperature of the liquid alloy as it exits the CRP.

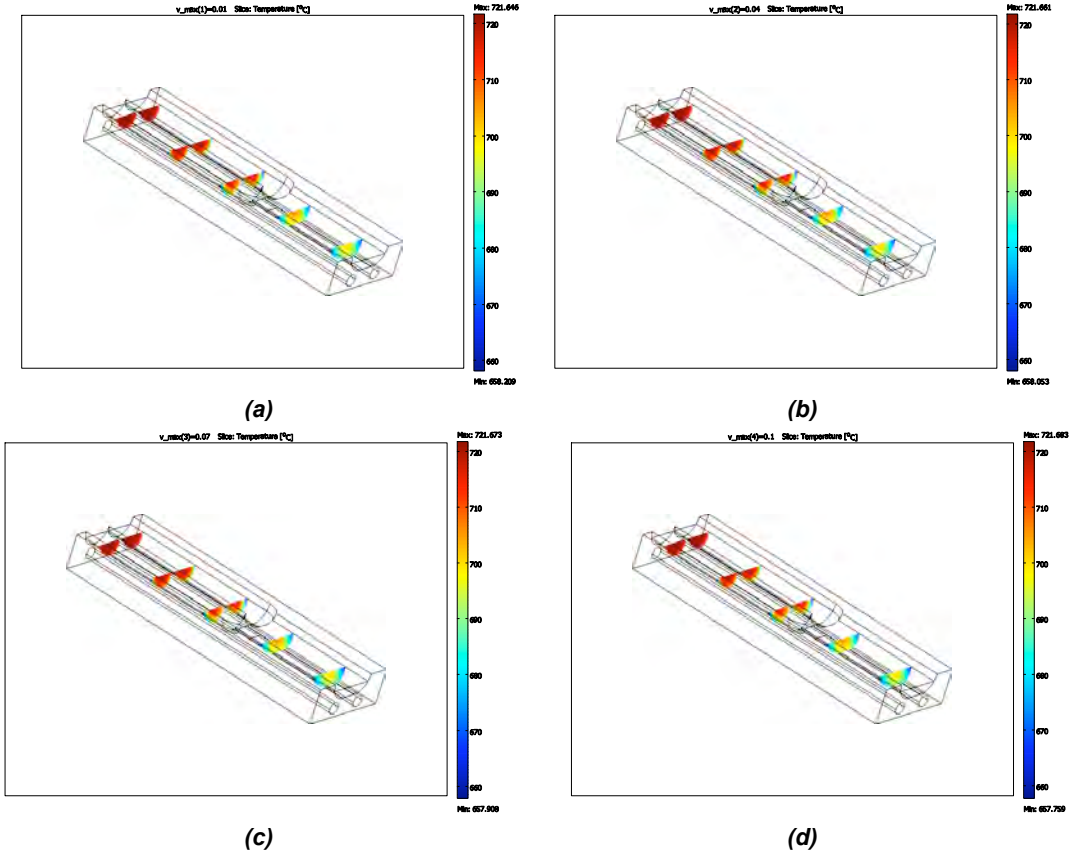

Figure 7- Temperature distribution within the liquid alloy as a function of the flow rate of the cooling water. Cooling water flow rate is (a) 0.01, (b) 0.04, (c) 0.07, and (d) 0.10 m/s.

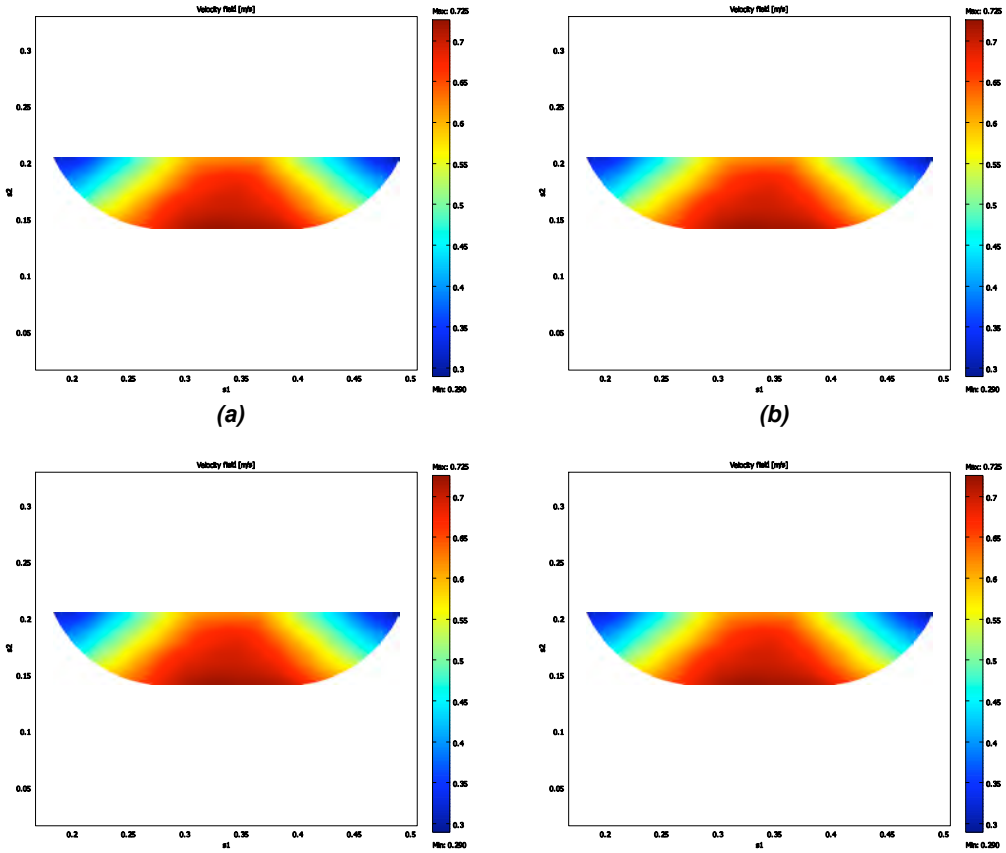

Figure 8- Temperature distribution in the liquid alloy at the exit from the CRP as a function of the flow rate of the cooling water. Cooling water flow rate is (a) 0.01, (b) 0.04, (c) 0.07, and (d) 0.10 m/s.

EFFECT OF LIQUID ALLOY SUPERHEAT

Figure 9 shows the temperature distribution within the liquid alloy as a function of the liquid alloy's superheat. In this case, the angle of inclination of the CRP to the horizon is 30°, the cooling water flow rate is 0.01m/s, and the temperature of the cooling water is 20°C. Similar to Figures 4 and 8, Figure 10 shows the temperature profile within the liquid alloy at the exit from the CRP. It is clear from Figure 10 that the liquid alloy's superheat has a very significant effect on the temperature of the liquid alloy as it exits the CRP and it is by far the process parameter that controls performance of the CRP. Table 2 shows the model-predicted temperature of the liquid alloy at the exit.

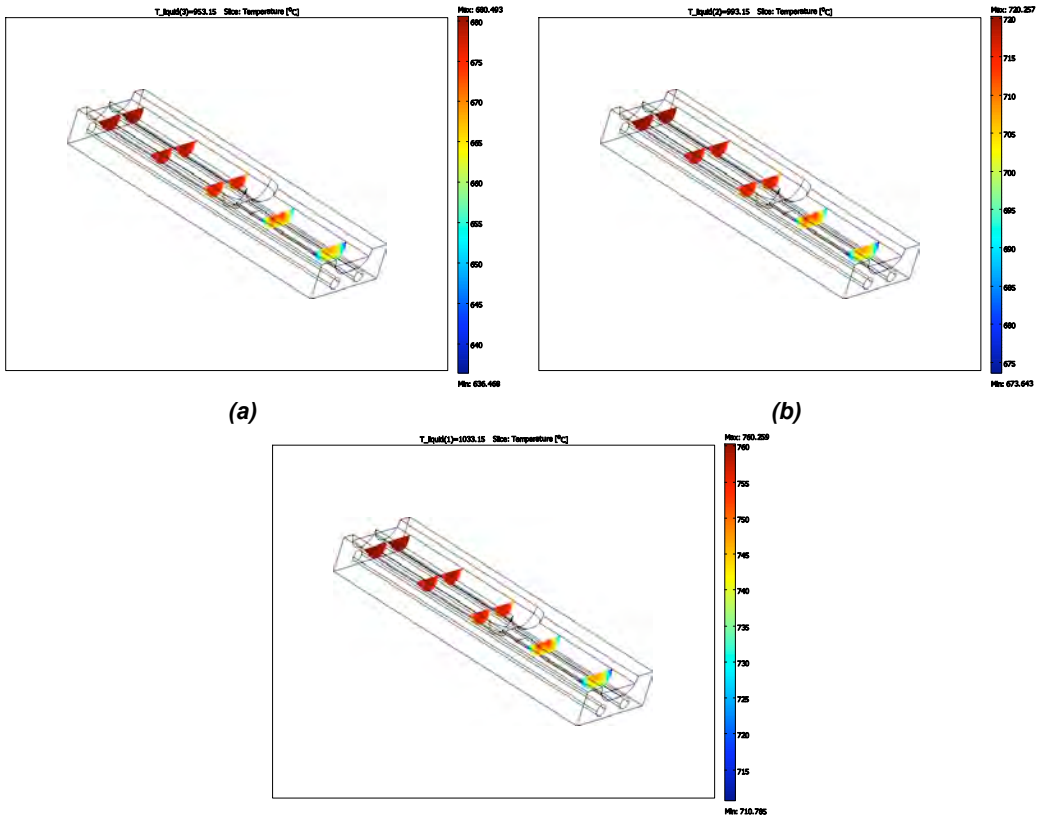

Figure 9- Temperature distribution within the liquid alloy as a function of liquid alloy superheat. Liquid alloy superheat is (a) 680, (b) 720, and (c) 760°C.

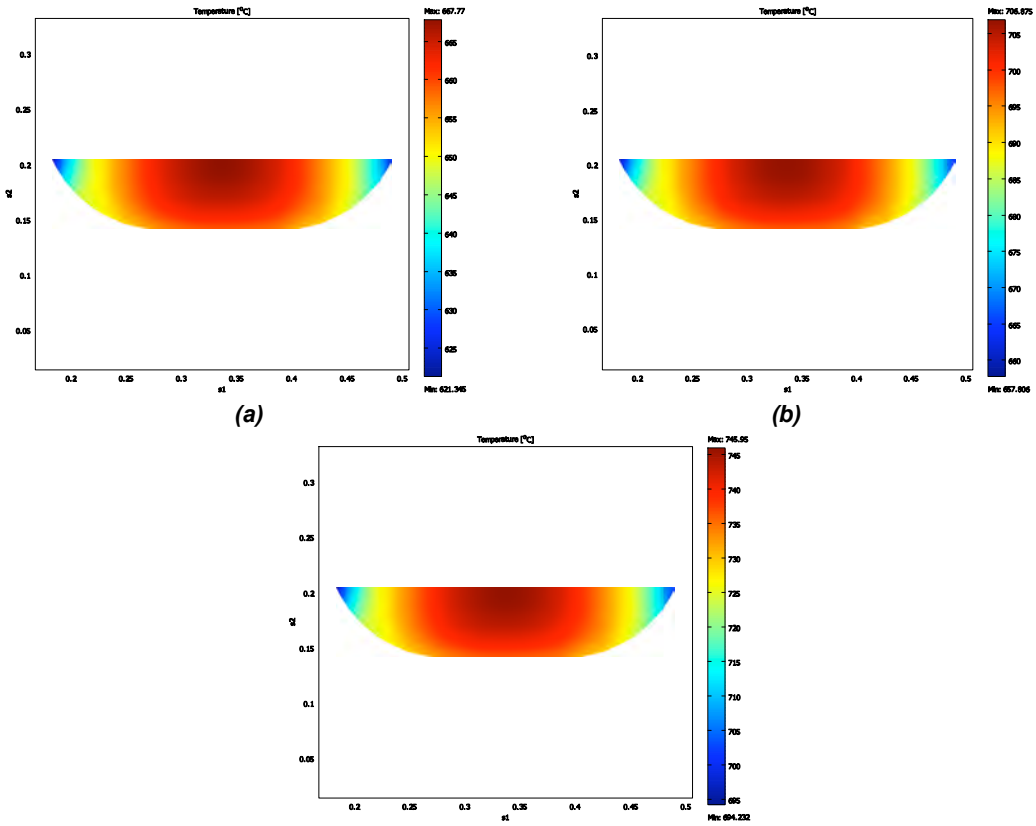

Figure 10- Temperature distribution in the liquid alloy at the exit from the CRP as a function of liquid alloy superheat. Liquid alloy superheat is (a) 680, (b) 720, and (c) 760°C.

Table 2- Model-predicted temperature of the liquid alloy as it exits from the CRP.

Pouring temperature T_p (°C)	**Temperature (T_{exit}) of the liquid alloy at the exit from the CRP (°C)**		
	Maximum	Minimum	T_p-T_{exit}
680	668	621	12 – 59
720	707	658	13 – 62
760	746	694	14 - 66

SUMMARY AND CONCLUSIONS

Control of copious nucleation of the solid phase during the production of semi-solid alloys by the CRP is critical. Accordingly, the effect of the CRP process parameters - namely the angle of inclination of the CRP reactor, the flow rate of the coolant water, and the melt superheat - on temperature distribution and melt mixing on the reactor were investigated using a commercially available computer software. It was found that the flow rate of the coolant water does not have a significant effect on the temperature distribution within the melt; and therefore it has little influence on nucleation of the solid phase. On the other hand, the melt superheat and the angle of inclination of the CRP reactor to the horizon have significant effect on the temperature distribution within the melt; and therefore, they control nucleation of the solid phase in the liquid. Moreover, it is found that the turbulence in the liquid alloy, which is created by the special design of the CRP in which two streams of melt combine into one stream, has a significant effect on liquid mixing as well as on heat extraction from the liquid by the CRP; therefore, it is a necessary design aspect of the CRP.

REFERENCES

1. Apelian D., Pan Q.Y., Findon M., "Low Cost and Energy Efficient Methods for the Manufacture of Semi-Solid (SSM) Feedstock," *Die Casting Engineer*, vol 48, No 1, pp 22-28 (2004)
2. Findon M., Apelian D., "The Continuous Rheoconversion Process for Semi-Solid Slurry Production", *AFS Transactions,* vol 112, pp 4-56 (2004)
3. Jorstad J. L., Pan Q. Y., Apelian D., "A Rheocasting Route: SLC + CRP, A Marriage of Unique Processes," *NADCA Transactions* 2006
4. Pan Q.Y., Findon M., Apelian D., "The Continuous Rheoconversion Process (CRP): A Novel SSM Approach," Paper No. 2-4 in the *Proceedings of the Eighth International Conference on Semi-Solid Processing of Metals and Alloys*, Limasol, Cyprus, September 2004

APPENDIX E

2010

10-05 Y. Li, D. Apelian, Y. Ma, and Y. Hao, "Commercial AM60 Alloy for Semisolid Processing: I - Alloy Optimization and Thermodynamic Analysis", Science Press, S2P Conference 2010, Transactions of Nonferrous Metals Society of China, Vol. 20, 2010 pp 1572-1578.

10-06 B. Xing, Y. Li, Y. Ma, Y. Hao and D. Apelian "Commercial AM60 Alloy for Semisolid Processing: II - Effects of CRP (continuous rheoconversion process) on Microstructure", Science Press, S2P Conference 2010, Transactions of Nonferrous Metals Society of China, Vol. 20 (2010), pp. 723-728.

2009

09-06 Q. Xu, D. Apelian, M.M. Makhlouf, "Numerical Modeling and Computer Simulation of the Continuous Rheoconversion Process", NADCA Congress Transactions, April 2009.

09-11 A. M. de Figueredo, D. Apelian, M. Findon, and N. Saddock, "Alloy Substantially Free of Dendrites and Method of Forming the Same", US Patent No. 7,513,962, April 7, 2009.

09-12 J. Jorstad and D. Apelian, "Pressure Assisted Processes for High Integrity Aluminum Castings – Part 1, Foundry Trade Journal International, Vol. 182, No. 3669, October 2009, pp.250-254.

09-13 J. Jorstad and D. Apelian, "Pressure Assisted Processes for High Integrity Aluminum Castings – Part 2, Foundry Trade Journal International, Vol. 182, No. 3669, November 2009, pp. 282-287.

2007

07-05 John L. Jorstad, Q. Y. Pan, Diran Apelian, " Interaction of Key Variables During Rheocasting: *Effects of Fraction Solid and Flow Velocity on Performance* ", NADCA Transactions 2007.

07-10 Q.Y. Pan, P. Hogan, D. Apelian, and M.M.Makhlouf, "The Continuous Rheoconversion Process (CRP™)", in the Proceedings of LMT – Light Metals Technology 2007, September 2007, Saint-Sauveur, Québec, CA, published by CANMET.

07-14 Q. Y. Pan, D. Apelian, "Semi-Solid Metal (SSM) Processing Methods: An Overview", in Proceedings of 2007 Xi'an International Symposium on Solidification, Northwestern Polytechnical University, May 29-31,2007.

07-15 D. Apelian and Q. Y. Pan, "Future Challenges and Opportunities Facing the Materials Science and Engineering Community", in Proceedings of 2007 Xi'an International Symposium on Solidification, Northwestern Polytechnical University, May 29-31, 2007.

07-19 J. L. Jorstad, D. Apelian, "Pressure Assisted Processes for High Integrity Aluminum Castings", International Journal of Metalcasting, Vol. 2, Issue 1, Winter 2008, pp 19-39.

07-21 Q.Y Pan, Diran Apelian & John Jorstad, "Semi-Solid Casting: Introduction and Fundamentals", ASM Vol. 15: Casting, published by ASM (2007), pp. 761-763.

07-22 Q.Y Pan, Diran Apelian & John Jorstad, "Rheocasting", ASM Vol. 15: Casting, published by ASM (2007), pp. 773-776.

07-26 Q.Y Pan, Diran Apelian & John Jorstad, "SemiSolid Metal Processing", ASM Vol. 15: Casting, published by ASM (2007), pp. 379-381.

2006

06-06 J. L. Jorstad, Q. Y. Pan, D. Apelian, "A Rheocasting Route: SLC^{TM} + CRP^{TM}, A Marriage of Unique Processes", NADCA Transactions (2006).

06-07 Q.Y. Pan, P. Hogan, and D. Apelian, "Optimization of Commercial Alloys for Semi-Solid Processing", NADCA Transactions (2006).

06-10 Q.Y. Pan, S. Wiesner, D. Apelian, "Application of the Continuous Rheoconversion Process (CRP) to Low Temperature HPDC-*Part I: Microstructure*, in the Proceedings of 9th International S2P, Busan, Korea, September 11-13, 2006, in Solid State Phenomena Vols. 116-117 (2006) pp. 402-405 Trans Tech Publications, Switzerland.

06-11 S. Wiesner, Q.Y. Pan, D. Apelian, "Application of the Continuous Rheoconversion Process (CRPTM) to Low Temperature HPDC-Part II: Alloy Development & Validation", in the Proceedings of 9th International S2P,

Busan, Korea, September 11-13, 2006, in Solid State Phenomena Vols. 116-117 (2006) pp 64-67 Trans Tech Publications, Switzerland.

06-12 D. Apelian, "SSM and Squeeze Casting: Principles & Opportunities", NADCA Transactions 2006.

06-15 Q.Y. Pan, D. Apelian, and P. Hogan, "The Continuous Rheoconversion Process (CRP^{TM}): *Optimization & Industrial Applications",* 3rd International Conference on High Tech Die Casting, Vicenza, Italy, 21-22 September 2006, paper 53, published in the CD-ROM of the conference proceedings by the Italian Association of Metallurgy (AIM), Milan, 2006; the paper also published in "Metallurgical Science and Technology", 2006, Vol. 24, n. 2, pp. 9-18 (2006), edited by Teksid Aluminum.

06-16 J.L. Jorstad and D. Apelian, "Pressure Assisted Processes for High Integrity Automotive Aluminum Castings – Part I: Principles and Fundamentals", 3rd International Conference on High Tech Die Casting, Vicenza, Italy, 21-22 September 2006, paper 54, published in the CD-ROM of conference proceedings by Italian Association of Metallurgy (AIM), Milan, 2006.

06-17 D. Apelian and J.L. Jorstad, "Pressure Assisted Processes for High Integrity Automotive Aluminum Castings – Part II: Recent Developments and Innovations", 3rd International Conference on High Tech Die Casting, Vicenza, Italy, 21-22 September 2006, paper 55, published in the CD-ROM of conference proceedings by Italian Association of Metallurgy (AIM), Milan, 2006.

06-23 A. Alexandrou, G. Georgiou, N. Tonmukayakul and D. Apelian, "Parameter Estimation for Semi-Solid Aluminum Alloys using Transient Experiments", Solid State Phenomena Vols. 116-117, (2006) pp 429-432, Trans Tech Publications, Switzerland

2005

05-03 Q.Y. Pan, L. Wang, D. Apelian and M.M. Makhlouf , "Optimization of 380 Alloy for Semi-Solid Processing", NADCA Transactions, #T05-143 (2005).

05-04 W. J. Bernard III, Q. Y. Pan, D. Apelian and M.M. Makhlouf, "The Continuous Rheoconversion Process (CRP): Modeling and Optimization", NADCA Transactions, #T05-141 (2005).

05-05 B. Dewhirst, J.L. Jorstad, and D. Apelian, "Effect of Artificial Aging on Microstructure and Tensile Properties of Semi-Solid Processed A356 Castings", NADCA Transactions, #T05-063 (2005) - Selected as the Best

Paper of the Congress. The paper was also published in Die Casting Engineer, May 2005, published by NADCA, pp 38-44, 2005

05-25 J. L. Jorstad, Q. Y. Pan, D. Apelian, " Solidification Microstructure Affecting Ductility in Semi Solid (SSM) Cast Products", Materials Science and Engineering A V 413-414 (2005) pp 186-191.

05-28 J. L. Jorstad, D. Apelian, "Pressure Assisted Processes for High Integrity Automotive Aluminum Castings – Part I: Principles and Fundamentals", in Proceedings of the International Conference on High Integrity Metal Castings, October 31 –November 1, 2005, Indianapolis, IN, published by AFS, Chicago, Ill. (2005).

05-29 J. L. Jorstad, D. Apelian, "Pressure Assisted Processes for High Integrity Automotive Castings – Part II: Recent Developments and Innovations", in Proceedings of the International Conference on High Integrity Metal Castings, October 31 –November 1, 2005, Indianapolis, IN, published by AFS, Chicago, Ill. (2005).

2004

04-1 Zachary Brown, Rathindra DasGupta, Dayne Killingsworth, Mark Musser, and Diran Apelian, "Semi-Solid Metal Casting Practices: Past, Present and Future", Proceedings of SAE 2004, Detroit, MI.

04-2 Q.Y. Pan, M. Arsenault, D. Apelian and M.M. Makhlouf, "SSM Processing of AlB2 Grain Refined Al-Si Alloys", AFS Transactions, Vol. 112, June 2004, pp 04-053.

04-3 M. Findon and D. Apelian, "The Continuous Rheoconversion Process for Semi-Solid *Slurry Production",* AFS Transactions, Vol. 112, June 2004, pp 04-056.

04-4 D. Saha and D. Apelian, *"Semi Solid Processing of Hypereutectic Alloys",* AFS Transactions, Vol. 112, June 2004, pp 04-057.

04-5 D. Apelian, Q.Y. Pan, M. Findon "Low Cost and Energy Efficient Methods for the Manufacture of Semi-Solid (SSM) Feedstock", Die Casting Engineer, V. 48, No. 1, January 2004, pp. 22-28.

04-6 Q.Y. Pan, D. Apelian and A.N. Alexandrou, *"Yield Behavior of Commercial Aluminum Alloys In The Semi-Solid State"*, Metallurgical and Materials Transactions (B), Vol. 35B, December 2004, pp 1187-1202.

04-7 D. Apelian, Q.Y. Pan, M. Findon and M. M. Makhlouf, *"Low Cost and Energy Efficient Methods for the Manufacture of Semi-Solid (SSM) Feedstock"*, in the Proceedings of HTDC (ISBN 88-86259-26-3), Brescia, Italy, published by Edimet, Brescia, Italy 2004, pp. 323-332.

04-8 Q.Y. Pan, M. Findon and D. Apelian, "The Continuous Rheoconversion Process (CRP): A Novel SSM Approach", Paper # 2-4 in the Proceedings of the Eighth International Conference on Semi-Solid Processing of Metals and Alloys, Limasol, Cyprus, September 2004; published by NADCA, Wheeling, Illinois.

04-9 Q.Y. Pan, D. Apelian and M. M. Makhlouf, " AlB_2 Grain Refined Al-Si Alloys: Rheocasting/Thixocasting Applications", Paper # 13-1 in the Proceedings of the Eighth International Conference on Semi-Solid Processing of Metals and Alloys, Limasol, Cyprus, September 2004; published by NADCA, Wheeling, Illinois.

04-10 A.N. Alexandrou, G.C. Florides, G.C. Georgiou and D. Apelian, "Rheological Effects of Structure Breakdown in Semisolid Slurries", Paper # 9-1 in the Proceedings of the Eighth International Conference on Semi-Solid Processing of Metals and Alloys, Limasol, Cyprus, September 2004; published by NADCA, Wheeling, Illinois.

04-11 D. Apelian, Q.Y. Pan and M. M. Makhlouf, "Low Cost and Energy Efficient Methods for the Manufacture of Semi-Solid (SSM) Feedstock", in NADCA Transactions, AFS/NADCA 108th Congress, June 2004, Session 3: Cast Materials, T01-033.